



UNIVERSITY of LIMERICK

O L L S C O I L L U I M N I G H

**BIOENERGETICS AT
EXTREME TEMPERATURE**

**Structural and functional studies of Complexes II and IV
of *Thermus thermophilus***

Mohamed Radzi Noor, B.Sc. (Hons.)

Ph.D. Thesis

University of Limerick

Supervisor: Dr. Tewfik Soulimane

Submitted to the University of Limerick, December 2012

ABSTRACT

While abundantly evident that thermophilic organisms are adapted to grow at high temperatures, the exact thermoadaptation mechanisms are often very subtle. Various membrane-bound respiratory oxidases have been characterised and their structures determined but questions on their proton and electron transfer pathways still remain. In this study, two such protein complexes from the extreme thermophile *Thermus thermophilus* were investigated. Multiple variants of Complex II (succinate:quinone oxidoreductase) were recombinantly produced to homogeneity through a homologous expression system, including a novel synthetic monomer. For the first time, the monomeric Complex II was shown to be functional and proves the hypothesis of an intraprotomer electron transfer. One of the variants was also crystallised. With a diffraction to 3.8 Å, a preliminary crystallographic analysis is reported here. The second complex is *caa*₃-oxidase, uniquely possessing a covalently-bound substrate cytochrome *c* and formed by ‘fused’ subunits. A recombinant protein expression and mutagenesis system is described along with circular dichroism and preliminary ultrafast spectroscopic studies. Together with analytical gel filtration chromatography, the wild type and mutant oxidases are shown to be homogeneous, well folded and suitable for future crystallisation trials. Preliminary femtosecond spectroscopy on wild type oxidase demonstrates a novel multiexponential NO binding kinetics at 140 and 930 ps. In addition, an oxidase subpopulation with a distinct spectrum is present after flash-photolysis of CO bound to the oxidase dinuclear centre that might represent molecules with an inaccessible Cu_B. Nonetheless, further mutagenesis studies, made possible by the expression system described here, would be required to confirm these findings.

PUBLICATIONS

Peer-reviewed publications

- I. Kolaj-Robin, O., **Noor, M. R.**, O’Kane, S. R., Baymann, F., Soulimane, T., Atypical features of *Thermus thermophilus* succinate:quinone reductase, PLoS One (accepted).
Contribution: MRN expressed and purified the recombinant proteins and performed some biochemical characterisations of the recombinant proteins.
- II. **Noor, M. R.**, Soulimane, T., (2012) Bioenergetics at extreme temperature: *Thermus thermophilus* *ba*₃- and *caa*₃-type cytochrome *c* oxidases. Biochim. Biophys. Acta – Bioenergetics, 1817, 638-649.
Contribution: The review article was written by MRN with contribution from TS.
- III. Soulimane, T., **Noor, M. R.**, Arese, M., Forte, E., McCarthy, M., Sarti, P., Giuffrè, A., Cytochrome *c*₅₅₂ mediates electron transfer between Complexes III and IV of *Thermus thermophilus*, (submitted).
Contribution: MRN contributed novel bioinformatic- and literature-based insights into the electron transfer kinetics between the Complexes III and IV, in addition to writing the paper.
- IV. Loullis, A., **Noor, M. R.**, Soulimane, T., Pinakoulaki, E., (2012). Observation of ligand transfer in *ba*₃ oxidase from *Thermus thermophilus*: simultaneous FTIR detection of photolabile heme *a*₃²⁺-CN and transient Cu_B²⁺-CN complexes. J. Phys. Chem. B., 116, 8955-8960.
Contribution: MR purified the protein for spectroscopic measurements and contributed to the scientific discussion leading to its publication.

Conference proceedings

- I. **Noor, M. R.**, Kolaj-Robin, O., O’Kane, S., Baymann, F., Soulimane, T., (2012). *Thermus thermophilus* Complex II – unique properties of a thermophilic enzyme. Biochim. Biophys. Acta – Bioenergetics. 1817, S158. (European Bioenergetics Conference 2012 Supplement).

DECLARATION

I declare that this work is the result of my own investigations and that this thesis has not been submitted previously in this form or any other form to this or any other university in candidature for a higher degree. Some materials have been previously published as listed in the Publications section and the candidate's contributions to each of them are indicated. Throughout the text, these are referred according to the number on the Publications section and cited as references.

This thesis is subject to an embargo until the end of December 2017.

Mohamed Radzi Noor

ACKNOWLEDGEMENTS

This thesis resulted from the constant guidance and scientific discussions with Drs. Tewfik Soulimane, as the research group leader, as well as Olga Kolaj-Robin and Sarah O’Kane. The contributions of other colleagues in the laboratory are also kindly appreciated. Local contacts at Diamond Light Source I24 and Swiss Light Source PXIII are acknowledged for their help in the data collection from Complex II crystals. The published papers have also benefited from the critical comments of the anonymous reviewers.

Scientific endeavours are often of collaborative nature. In this regard, the presented work is the result from the extensive collaborations with Alessandro Giuffrè (CNR Institute of Molecular Biology and Pathology, Rome, Italy), Eftychia Pinakoulaki (University of Cyprus, Nicosia, Cyprus), Frauke Baymann (CNRS Marseille, France) and Marten Vos (Ecole Polytechnique, Paris, France).

Funding towards the project was provided by the Science Foundation Ireland (SFI BICF685) to Tewfik Soulimane, the Irish Research Council (formerly Irish Research Council for Science, Engineering and Technology, IRCSET) EMBARK Scholarship and Ulysses Scheme for Travel France-Ireland. Synchrotron visits were funded by the European Community Seventh Framework Programme (FP7/2007-2013) under BioStruct-X (grant agreement number 283570).

TABLE OF CONTENTS

ABSTRACT	I
PUBLICATIONS	III
DECLARATION	IV
ACKNOWLEDGEMENTS	V
LIST OF TABLES	IX
LIST OF FIGURES	X
CHAPTER 1	1
INTRODUCTION	1
1.1 OVERVIEW OF BIOENERGETICS.....	3
1.1.1 Complex I – NADH:quinone oxidoreductase	6
1.1.2 Complex II – Succinate:quinone oxidoreductase.....	7
1.1.3 Complex III – Quinone:cytochrome <i>c</i> oxidoreductase	7
1.1.4 Complex IV – Cytochrome <i>c</i> oxidase	7
1.1.5 Proton motive force generation.....	9
1.2 OUTLINE OF THESIS	12
CHAPTER 2	13
SUCCINATE:QUINONE OXIDOREDUCTASE	13
2.1 INTRODUCTION.....	15
2.1.1 Succinate:quinone oxidoreductase superfamily (classification)	15
2.1.2 Succinate:quinone reductase	23
2.1.4 Oligomeric states of SQR and QFR.....	45
2.1.5 SQOR reaction mechanism	47
2.1.6 Crystallographic and spectroscopic investigations into Complex II to date.....	56
2.1.7 Activity measurements.....	56
2.2 SUMMARY OF PUBLISHED WORK	58
2.2.1 Materials and Methods.....	58
2.2.2 Results and Discussion.....	59
2.3 UNPUBLISHED WORK	61
2.3.1 Generation of mutagenesis system.....	61

TABLE OF CONTENTS

2.3.2 Crystallography.....	66
2.4 CONCLUSION.....	70
CHAPTER 3.....	73
CYTOCHROME C OXIDASES	73
3.1 INTRODUCTION.....	75
3.1.1 Classification.....	79
3.1.2 Subunit I.....	80
3.1.3 Subunit II	81
3.1.4 Supernumerary subunits.....	83
3.1.5 Catalytic cycle.....	87
3.1.6 Cytochrome <i>c</i>	88
3.2 MATERIALS AND METHODS	90
3.2.1 Recombinant protein production.....	90
3.2.2 Circular dichroism	91
3.2.3 Ultrafast spectroscopy.....	92
3.2.4 Computational analyses of CcO.....	92
3.3 RESULTS AND DISCUSSION.....	93
3.3.1 Protein purification	93
3.3.2 Folding of recombinant protein	98
3.3.3 Ultrafast spectroscopy.....	101
3.3.4 Computational analyses	107
3.4 CONCLUSION.....	108
CHAPTER 4.....	109
OVERALL CONCLUSION	
AND OUTLOOK	109
REFERENCES.....	113
APPENDIX.....	1333

LIST OF TABLES

Table 1. Proton translocation efficiency of respiratory complexes	6
Table 2. Structures of SQR and QFR in PDB.....	17
Table 3. Sequence-based classification of SQOR superfamily.....	21
Table 4. Conversion table for the Fe-S ligands of SQR and QFR.....	28
Table 5. Reduction potential of reactions occurring during the SQR and QFR catalysis	33
Table 6. Chemical structures of menaquinone and ubiquinone	41
Table 7. Primer sequences for Complex II	62
Table 8. Preliminary crystallographic analysis of Complex II crystals	69
Table 9. Available three-dimensional structures of haem-copper oxidases.....	77
Table 10. Primers for <i>caa</i> ₃ -oxidase expression.....	91

LIST OF FIGURES

Fig. 1. Current view of electron transport chain	5
Fig. 2. Mechanisms of proton motive force generation	10
Fig. 3. The L-aspartate oxidase oxidises L-aspartate to iminoaspartate	16
Fig. 4. Sequence and structural alignments of SQR, QFR and LASPO indicate evolutionary conservation of two different protein classes.....	19
Fig. 5. Chemical structures of FAD (top) and FMN (bottom).....	24
Fig. 6. Conservation of FAD-binding site in SQR and QFR flavoprotein subunit (SdhA/FrdA) from various organisms	25
Fig. 7. Various Fe-S clusters as identified crystallographically	26
Fig. 8. Ligands of Fe-S clusters located within the SdhB/FrdB subunit.....	29
Fig. 9. [2Fe-2S] cluster of <i>E. coli</i> SQR.....	30
Fig. 10. [4Fe-4S] cluster of <i>E. coli</i> SQR.....	31
Fig. 11. [3Fe-4S] cluster of <i>E. coli</i> SQR.....	32
Fig. 12. Multiple sequence alignment of the membrane anchor subunit SdhC	35
Fig. 13. Multiple sequence alignment of the membrane anchor subunit SdhD....	36
Fig. 14. Conserved His residues of dihaem SQOR in the SdhC subunit.....	37
Fig. 15. Haem <i>b</i> ligands in dihaem SQOR SdhC/D subunit.....	38
Fig. 16. Quinone binding site in the <i>E. coli</i> SQR	39
Fig. 17. Quinone binding site in the <i>E. coli</i> QFR	40
Fig. 18. Succinate oxidation.....	48
Fig. 19. Quinone binding sites in <i>E. coli</i> SQR.....	49
Fig. 20. Quinone reduction mechanism	51
Fig. 21. Transmembrane proton transfer coupled to the electron transfer.....	52
Fig. 22. Multiple sequence alignment of dihaem SQR and QFR	54
Fig. 23. Proposed E-pathway operating in the <i>W. succinogenes</i> dihaem QFR.....	55
Fig. 24. Oligomerisation states of recombinant Complex II variants	59
Fig. 25. Multiple sequence alignment of recombinant Complex II variants	63
Fig. 26. SDS-PAGE of recombinant Complex II with TEV protease sites	65
Fig. 27. Gel filtration chromatograms of recombinant Complex II with TEV sites	65
Fig. 28. Diffraction image of recombinant Complex II.....	69

Fig. 29. Oxygen channels in Types A and B CcO	78
Fig. 30. Crystallographic assemblies of two Type A oxidases	79
Fig. 31. Proton pumping pathways in CcO	80
Fig. 32. Conservation of a key Glu residue in the D-pathway of different CcO ..	81
Fig. 33. Family-specific loops in subunit II of CcO	82
Fig. 34. Sequence alignment of CcO subunits IV	85
Fig. 35. Structural alignment of subunit IV	86
Fig. 36. Various states during CcO catalysis	87
Fig. 37. Covalent attachment of haem <i>c</i> to protein residues	89
Fig. 38. Sequence alignment of <i>T. thermophilus</i> cytochromes <i>c</i>	89
Fig. 39. Purity and homogeneity of recombinant wild type and Y248F mutant <i>caa</i> ₃ -oxidases	94
Fig. 40. Chromatogram of recombinant wild type <i>caa</i> ₃ -oxidase plasmid	95
Fig. 41. Chromatogram of recombinant Y249F mutant <i>caa</i> ₃ -oxidase	96
Fig. 42. Absorption spectra of recombinant wild type <i>caa</i> ₃ -oxidase	97
Fig. 43. Dithionite reduced- <i>minus</i> -oxidised absorption spectrum of Y248F mutant <i>caa</i> ₃ -oxidase	97
Fig. 44. CD spectrum of wild type <i>caa</i> ₃ -oxidase	100
Fig. 45. Urea-induced denaturation of wild type <i>caa</i> ₃ -oxidase	100
Fig. 46. Spectra of fully-reduced wild type <i>caa</i> ₃ -oxidase excited with 590-nm laser pulse	104
Fig. 47. Excitation of CO-reduced <i>caa</i> ₃ -oxidase	105
Fig. 48. Excitation of NO-bound <i>caa</i> ₃ -oxidase	106

CHAPTER 1
INTRODUCTION

1. INTRODUCTION

The extremely-thermophilic eubacterium, *Thermus thermophilus*, has an optimum growth temperature of 70 °C. This bacterium, therefore, provides an attractive model to investigate the molecular basis of aerobic respiration at high temperatures compared to the well-studied mesophiles particularly in relation to oxygen solubility and protein thermostability. While the respiratory chain of *T. thermophilus* is not fundamentally different from other organisms, several key differences in the protein sequence-structure-function relationship have been noted. These include the enlarged oxygen cavity in the cytochrome *c* oxidases and the interaction between cytochrome *c* and the oxidase [reviewed in (Noor and Soulimane, 2012)] (**Paper II**). Furthermore, the succinate:quinone oxidoreductase (SQR) displays a temperature-dependent positive cooperativity. From the evolutionary perspective, *T. thermophilus* is a phylogenetically-ancient organism. Sequence comparison between *T. thermophilus* and other counterparts have revealed such interesting features. These are discussed separately in the Chapters 2 and 3. The different aerobic thermophilic electron transfer chains have been described in (Pereira *et al.*, 2004).

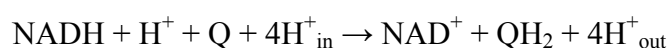
1.1 OVERVIEW OF BIOENERGETICS

Chemical and physical processes, including ion transport and motility, in living organisms can only be sustained by the ability to harness chemical and/or physical (light) energy. Prokaryotes exhibit an enormous capability not only to live in but also fully exploit their extreme surroundings. The myriad of prokaryotic physiology is a reminder of their long evolutionary history, when they first colonised Earth 3.6 billion years ago just a billion years after Earth formation. Large proton motive force in acidic environments aids the ATP synthesis in acidophiles but the simultaneous increased cytoplasmic acidity is prevented by several adaptations. Contrarily, alkaliphiles depend on Na⁺/H⁺ antiporter to maintain a sufficiently acidic cytoplasmic space relative to the high external pH as required for the ATP synthesis [see (Krulwich *et al.*, 2011) for a review]. Notwithstanding these adaptations, the ‘standard’ glycolysis, Krebs cycle and electron transport chain remain central to their very existence. The

impact of parallel pathways for respiration and fermentation (*i.e.* biochemical redundancy) are not similar. Respiration pathway efficiencies differ and directly determine growth rate, a phenomenon not observed for fermentation pathways [*cf.* (Bauchop and Elsdon, 1960; Calhoun *et al.*, 1993; Helling, 2002)]. The respiratory chain generates the bulk of ATP, yet details of the individual protein complex mechanism remain poorly understood. This is unsurprising given the inherent difficulties of studying membrane proteins. Moreover, heterologous membrane protein expression can be problematic if the lipid profile of overexpression host is dissimilar to the originating organism, given that lipids constitute a functional determinant of membrane proteins (Arias-Cartin *et al.*, 2011). A current view of respiratory complexes is given in Fig. 1.

1.1.1 Complex I – NADH:quinone oxidoreductase

Complex I forms the largest protein complex (~ 550 kDa, 14 subunits in prokaryotes and 980 kDa, 45 subunits in eukaryotes) within the respiratory chain. Detailed three-dimensional crystal structures of *Escherichia coli* and *T. thermophilus* complexes were only obtained recently (entire complex PDB ID: 3M9S), with a low-resolution structure of *Yarrowia lipolytica* complex at 6.3 Å (Hunte *et al.*, 2010). One of the most characteristic features of this complex is an amphipathic helix spanning the *parallel* of membrane, possibly acting as a piston. The oxidation of NADH results in the transfer of two electrons to quinone (see equation below), a lipid soluble electron carrier between Complexes I and III as well as Complexes II and III.



Three or four protons are then translocated (*i.e.* 1.5-2 H^+/e^-), generating about 40 % of the proton flux in the transmembrane proton gradient [(Efremov and Sazanov, 2011) *cf.* (Wikström and Hummer, 2012)]. A recent theoretical consideration of proton pumping stoichiometries based on experimental data is summarised in Table 1. Classical inhibitors used in Complex I studies are rotenone and amytal.

Table 1. Proton translocation efficiency of respiratory complexes. The values were based on the conversion of experimental ATP/2 e^- ratios obtained for rat-liver mitochondria. Table taken from (Wikström and Hummer, 2012).

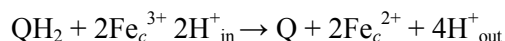
Complex	ATP/2 e^-	$\text{H}^+/\text{2e}^-$ (efficiency, %)
I + III + IV	2.27 ± 0.08	8.32 (92)
III + IV	1.48 ± 0.04	5.43 (91)
III	0.49 ± 0.02	1.80 (90)
IV	0.98 ± 0.09	3.59 (90)
I (I + III + IV <i>minus</i> III + V)	0.79	2.90 (97)
I (I + III + IV <i>minus</i> III <i>minus</i> IV)	0.80	2.90 (97)

1.1.2 Complex II – Succinate:quinone oxidoreductase

Complex II has several unique properties in the context of respiratory chain – (i) it consists of only four subunits in both prokaryotes and eukaryotes (*i.e.* no supernumerary/accessory subunits), (ii) it is the only complex participating in both the cytoplasmic Krebs cycle and membrane quinone reduction and, (iii) it does not pump protons. Details of Complex II are presented in Chapter 2. As-isolated SQR is inactive due to the tight association with inhibitor oxaloacetate; another inhibitor is thenoyltrifluoroacetone (TTFA).

1.1.3 Complex III – Quinone:cytochrome *c* oxidoreductase

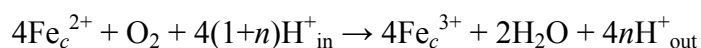
Linking the reduced quinol to its oxidation by Complex IV is the Complex III. This complex is not an obligatory component of aerobic respiration as quinol oxidases can directly transfer the electrons from quinol to molecular oxygen. The disadvantage of bypassing *bc*₁ complex through quinol oxidation lies in the reduced conserved energy. Two protons are translocated (vectorial protons) in addition to two protons from quinone oxidation (scalar protons):



A mechanistic approach to the study of Complex III is reviewed by (Crofts *et al.*, 2006). Complex III is inhibited by antimycin, myxothiazol and stigmatellin.

1.1.4 Complex IV – Cytochrome *c* oxidase

Cytochrome *c* oxidase is perhaps the most important member of respiratory chain in that it reduces molecular oxygen, the most electronegative electron acceptor (second only to the non-physiological fluorine on the Pauling scale), to water as illustrated in the equation below, where *n* is the H⁺/e⁻ stoichiometry (1 and 0.5 for A- and B-type oxidases, respectively).



Aerobic respiration is, hence, the most efficient metabolic pathway for organisms as long as no other limitations exist. While not immediately intuitive, aerobic respiration mechanisms have been suggested to have occurred prior to the availability of atmospheric oxygen produced by photosynthetic organisms (Castresana and Saraste, 1995; Gribaldo *et al.*, 2009). A direct consequence of the eventual existence of higher free oxygen concentration is the requirement for the then-existing redox enzymes, which were suited to low levels of oxygen, to rapidly evolve mechanisms to prevent the damaging properties of superoxide radicals (O_2^-) while retaining as much of catalytic efficiency as possible. The evolutionarily dictated measure was to use back-reactions, electron leaks and other wasteful pathways – “sacrifice-of-efficiency-for-protection” (Rutherford *et al.*, 2012).

Closely related to CcO are the quinol oxidases (QOX) that also act as terminal oxidases. Unlike CcO, not all QOX are members of the haem-copper oxidase (HCO) superfamily; the *bd* oxidase, for instance, lacks the copper redox centre and instead contains only a low-spin and a high-spin haem *b* (b_{558} and b_{595}) together with a modified ‘haem’ *d* (technically, a chlorin) (Miller and Gennis, 1983; Garcia-Horsman *et al.*, 1994). This type of oxidase has been used as a basis to question the need for copper centre in HCO superfamily. More recently, a dual functioning cytochrome *c* and quinol oxidising ba_3 -type terminal oxidase has been identified in *Aquifex aeolicus* (Gao *et al.*, 2012).

The branching in respiratory pathways has been more studied using terminal oxidases than any other complexes. The *in vivo* expression of these complexes correlates directly to the available oxygen concentration. In *E. coli*, three quinol oxidases bo_3 -, *bd*-I and *bd*-II types exist (Bekker *et al.*, 2009); interestingly, this organism is devoid of Complex III and soluble cytochrome *c* as an electron carrier. Similarly, *T. thermophilus* expresses ba_3 -oxidase in addition to caa_3 -oxidase only under low oxygen tension (see Chapter 3). Sequence analysis alone is sufficient neither to determine which oxidase(s) is expressed under a particular condition nor its proton pumping efficiency. CcO of Types A1, A2, B and C all mostly retain classical proton and electron transfer pathways but their oxygen cavities are not of similar volumes (Noor and Soulimane, 2012) (**Paper II**).

Cyanide and CO act as inhibitors of CcO; the latter is chemically similar to oxygen and being photodissociable, it is useful for time-resolved spectroscopic measurements to study ligand binding and electron transfer kinetics.

1.1.5 Proton motive force generation

For the ATP generation by ATP synthase to occur, protons must be translocated into the periplasmic space (or the mitochondrial intermembrane space). Two alternative mechanisms exist – the redox loop and the proton pump (Fig. 2). Classical examples are the Complex III and CcO, respectively. At its simplest level, the redox loop mechanism originally described by [(Mitchell, 1966) Rpt. in (Mitchell, 2011)] operates in the *E. coli* formate dehydrogenase N (Fdh-N)-nitrate reductase (Nar) system (Jormakka *et al.*, 2003). The release of electrons from the periplasmic formate oxidation to the quinone (MK) binding site of Fdh-N is concomitant with the uptake of two cytoplasmic protons required for MK reduction. MK is then oxidised by Nar with two protons released into the *periplasmic* space while two electrons are used to reduce nitrate on the cytoplasmic side, resulting in a net transmembrane proton translocation of 2 H⁺/e.

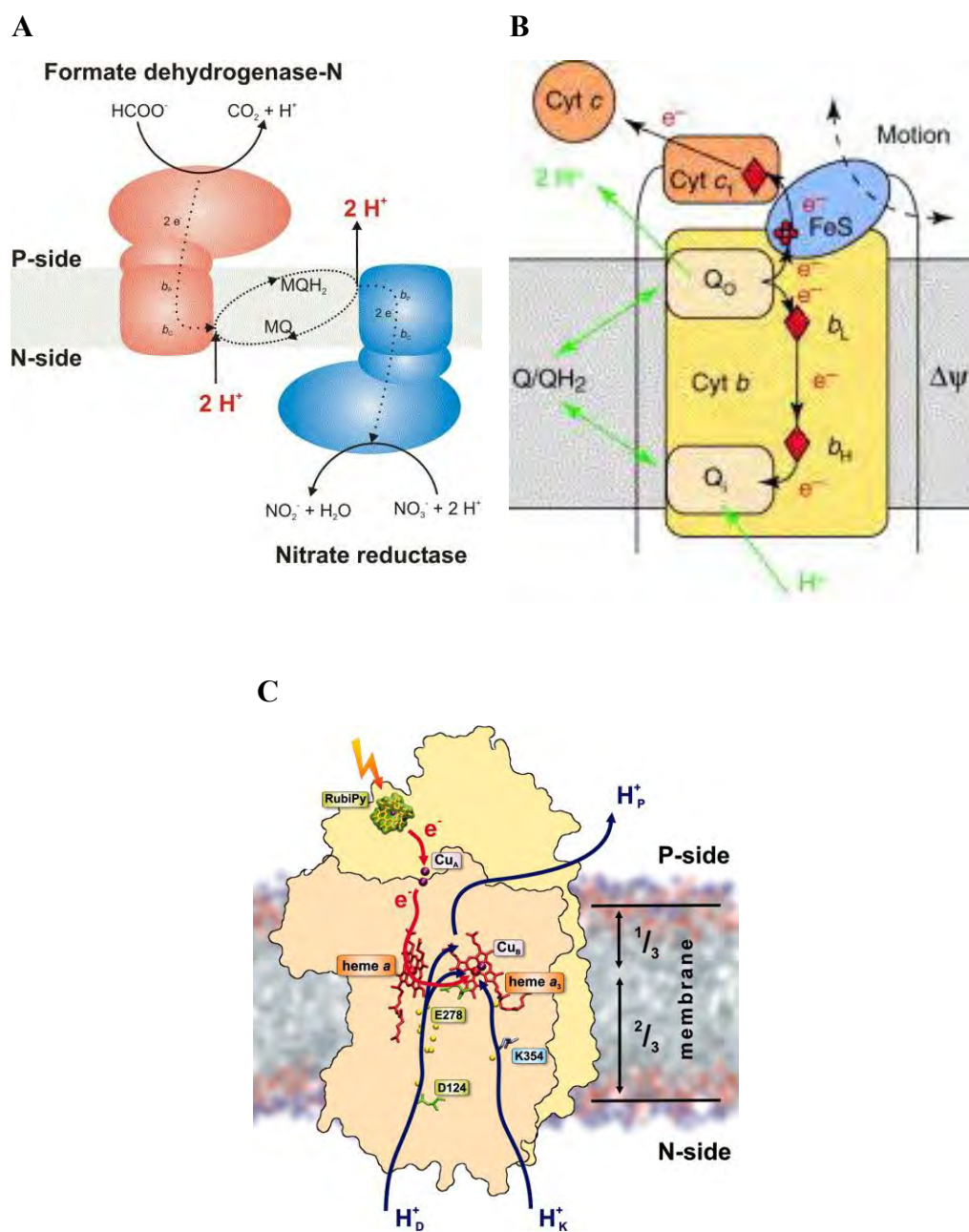


Fig. 2. Mechanisms of proton motive force generation. (A) Simple redox loop mechanism operating in formate dehydrogenase N-nitrate reductase system. **(B)** Proton translocation in Complex III is a more complicated example of (A). **(C)** Cytochrome *c* oxidase pumps protons by using ion channel-like pathways. Figures taken from (Cape *et al.*, 2006) (A), (Darrouzet *et al.*, 2001) (B) and (Belevich *et al.*, 2007) (C).

Far more complicated is the Q-cycle operating in Complex III (bc_1 complex) where the electron pathway bifurcates and two quinone binding sites are present; these sites are termed proximal (facing periplasmic space; Q_P) and distal (Q_D) sites. Four protons are released into the periplasmic space from the reduction of two quinol molecules. As each cytochrome c molecule can only be reduced by one electron, two cytochrome c are required to accept the two of four electrons from quinol reduction. Nature's ingenuity may have been responsible in evolving two haem b moieties (b_L and b_H , indicating low and high potential) to allow sequential transfer of the other two electrons in that order. Two further protons are taken up from the cytoplasmic space to complete the quinone reduction. The proposed concerted double-electron transfer avoiding the semiquinone formation (Osyczka *et al.*, 2004) has been refuted based on continuous wave and pulsed EPR spectroscopy (Cape *et al.*, 2007).

Protons can also be pumped into the periplasmic space via ion channel-like pathways as present in CcO . Fundamentally, this involves uptake of cytoplasmic protons and their eventual transfer through a series of protonable residues extending from the cytoplasmic to the periplasmic space. The current agreed view is that two proton pathways (D- and K-pathways) exist; the third H-pathway is controversial [see (Noor and Soulimane, 2012) and references therein] (**Paper II**).

1.2 OUTLINE OF THESIS

The thesis involved studies into the structure and function of two membrane-bound respiratory complexes, Complex II and cytochrome *c* oxidases from *T. thermophilus* as outlined below. Each is, therefore, treated separately in Chapters 2 and 3, respectively.

Complex II:

- i. Recombinant production of Complex II variants
- ii. Crystallisation and crystal analysis
- iii. Attempts to generate an expression system for site-directed mutagenesis

Cytochrome *c* oxidases:

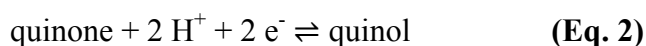
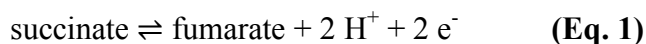
- i. Recombinant production of wild type *caa*₃-oxidase
- ii. Proof-of-concept site-directed mutagenesis
- iii. Preliminary ultrafast visible spectroscopy of *caa*₃-oxidase
- iv. Computational analyses of *caa*₃- and *ba*₃-oxidases

CHAPTER 2
SUCCINATE:QUINONE
OXIDOREDUCTASE

2.1 INTRODUCTION

2.1.1 Succinate:quinone oxidoreductase superfamily (classification)

The succinate:quinone oxidoreductase (SQOR) superfamily is divided into the classical succinate:quinone reductase (SQR) and quinone:fumarate reductase (QFR) [reviewed in (Lemos *et al.*, 2002)] families as well as the more unusual L-aspartate oxidase (LASPO) (Mortarino *et al.*, 1996; Tedeschi *et al.*, 1996). The general reaction for the former two is indicated below as Eq. 1 and 2 in which the electrons from the oxidation of succinate is passed to the electron carrier quinone; the reverse reaction is catalysed by the QFR. The nomenclature for a particular protein complex depends on the actual reaction catalysed *in vivo*, although both the forward and reverse reactions could be catalysed *in vitro* under the appropriate conditions. In addition, it is not possible to determine computationally from a particular protein sequence which reaction is physiological. One of the key features differentiating the two is the fact that the succinate oxidation with the concomitant reduction of quinone is part of aerobic respiration (tricarboxylic acid cycle or Krebs's cycle) whereas the fumarate is used during anaerobic respiration.



Of the different protein complexes constituting the membrane-bound electron transfer chain, only Complex II is not decorated with supernumerary subunits in eukaryotes compared to prokaryotes (*i.e.* all contain four subunits or three subunits with two being fused) [for comparisons of prokaryotic and eukaryotic complexes and possible functions of the accessory subunits, see (Berry, 2003; Mimaki *et al.*, 2012; Smith *et al.*, 2012; Soto *et al.*, 2012; Noor and Soulimane, 2012; Hong and Pedersen, 2004; Jonckheere *et al.*, 2012; Muench *et al.*, 2011; Dimroth *et al.*, 2006; Noji and Yoshida, 2001) and references therein]. An exception to this would probably be the *Trypanosoma cruzi* SQR with twelve subunits (Morales *et al.*, 2009). Nevertheless, “Complex II is complex too”, as aptly described by Matti Saraste (Hederstedt, 2003) and detailed below.

The LASPO enzyme, in contrast, catalyses the oxidation reaction of L-aspartate to iminoaspartate, forming the first step in the *de novo* bacterial NAD^+ biosynthesis, through the noncovalently-attached FAD prosthetic group (Griffith *et al.*, 1975; Nasu *et al.*, 1982) (Fig. 3). Interestingly, both oxygen and fumarate can act as electron acceptors for FAD oxidation and, thereby, providing the additional L-aspartate:fumarate oxidoreductase function. This has a physiological relevance as fumarate is a by-product during Krebs's cycle and could allow its functionality under both aerobic and anaerobic conditions (Tedeschi *et al.*, 1996; Mattevi *et al.*, 1999). This feature is not uncommon and has been described for haem biosynthesis (Jacobs and Jacobs, 1975; Möbius *et al.*, 2010). The key evolutionary link between the classical SQR/QFR and LASPO was only clear after the latter structure was determined to 2.2 Å (PDB ID: 1CHU) (Mattevi *et al.*, 1999). However, succinate cannot be oxidised as the associated FAD cofactor has a low midpoint potential of -216 mV (Tedeschi *et al.*, 1997).

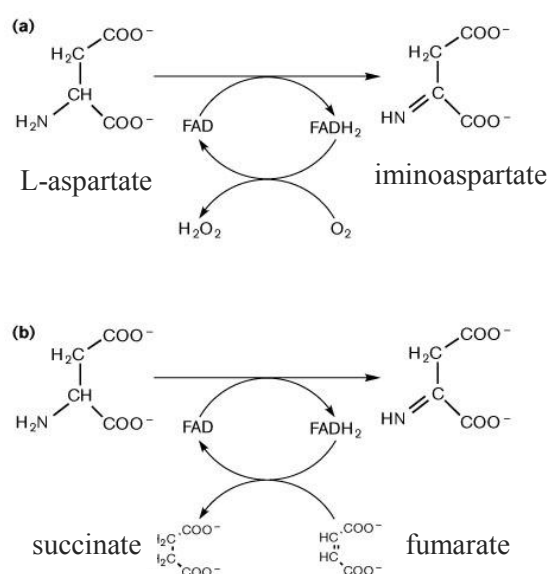


Fig. 3. The L-aspartate oxidase oxidises L-aspartate to iminoaspartate. Reoxidation of FAD occurs by either oxygen with the production of hydrogen peroxide (a) or by fumarate that is converted to succinate (b). Figure adapted from Mattevi *et al.* (1999).

A more comprehensive description between SQR, QFR and LASPO is given below (2.1.2.1 SdhA – flavoprotein subunit). The sequence and structural alignments of *E. coli* SQR, QFR and LASPO together with *T. thermophilus* SQR

and LASPO indicating conserved features are shown in Fig. 4. The other structurally known SQR and QFR enzymes are listed in Table 2. As the mitochondrial QFR from the parasitic nematode *Ascaris suum* (PDB ID: 3VR8) has high sequence identities to the SdhA and SdhB subunits of avian SQR and *W. succinogenes* QFR as well as a typical low identity to the respective SdhC and SdhD subunits, it will not be examined extensively in this chapter.

Table 2. Structures of SQR and QFR in PDB. Only the first deposited structure for each is shown. ^a A higher resolution structure at 1.74 Å, PDB ID: 2H88, is also available. ^b The entry 1L0V supersedes the original 1FUM (Iverson *et al.*, 1999). ^c The original entry, 1QLA, was obsoleted by 2BS2 due to a better resolution (1.78 vs. 2.20 Å). Only *W. succinogenes* QFR has two haem *b* moieties with a single fused membrane anchor.

Source	PDB ID	Res. (Å)	Publication
SQR			
<i>E. coli</i>	1NEK	2.60	(Yankovskaya <i>et al.</i> , 2003)
<i>Sus scrofa</i> (pig)	1ZOY	2.40	(Sun <i>et al.</i> , 2005)
<i>Gallus gallus</i> (chicken) ^a	1YQ3	2.20	(Huang <i>et al.</i> , 2006)
QFR			
<i>E. coli</i>	1L0V ^b	3.30	(Iverson <i>et al.</i> , 2002)
<i>W. succinogenes</i>	2BS2 ^c	1.78	(Madej <i>et al.</i> , 2006)
<i>Ascaris suum</i> (nematode)	3VR8	2.81	(Shimizu <i>et al.</i> , 2012)



Fig. 4. Sequence and structural alignments of SQR, QFR and LASPO indicate evolutionary conservation of two different protein classes. (Top) Sequence alignment of *E. coli* (Ec) SQR and QFR flavoprotein subunits and LASPO together with *T. thermophilus* (Tth) SQR and LASPO. Colouring was performed at 80 % sequence identity in Jalview (Waterhouse *et al.*, 2009), which was subsequently aligned using MUSCLE (<http://www.ebi.ac.uk/Tools/msa/muscle>) (Edgar, 2004). Accession ID: *E. coli* LASPO (PDB ID: 1KNR), QFR (PDB ID: 1L0V), SQR (PDB ID: 1NEK), *T. thermophilus* LASPO (RefSeq: YP_144249.1) and SQR (RefSeq: YP_144720.1). **(Middle)** Phylogram of the proteins based on the sequence alignment, indicating the clustering of the SQR flavoproteins compared to the LASPO, was created with Phylogeny.fr using maximum likelihood (Dereeper *et al.*, 2008). **(Bottom)** The flavoprotein subunit of SQR (green; PDB ID: 1NEK) aligns well to the LASPO (coral; PDB ID: 1KNR) with a root-mean-square deviation (rmsd) of 1.42 Å, showing the fold conservation for functionally-distinct enzymes. For comparison, the *E. coli* QFR (PDB ID: 1L0V) is shown as transparent red, which has an rmsd of 1.56 Å to SQR. The alignment was generated with CCP4mg (Potterton *et al.*, 2004).

A five-type classification for SQOR based on the iron-sulphur centres, membrane anchor subunits, presence of haem moieties and the genetic organisation has been proposed (Table 3) (Lemos *et al.*, 2002); accordingly, the *T. thermophilus* SQR is of Type A with the subunit genetic loci organised as *sdhCDAB*. Together with the *E. coli* SQR, mitochondrial SQR belong to Type C. The hydrophilic subunits SdhA and SdhB compose the cytoplasmic part of the protein complex with the hydrophobic subunits SdhC and SdhD providing the anchor to the membrane. Being a redox protein, the cofactors are crucial for catalysis. The covalently-bound FAD group is located in SdhA while the iron-sulphur clusters [2Fe-2S] (centre 1), [4Fe-4S] (centre 2) and [3Fe-4S] (centre 3) are in SdhB. With a non-classical, amphipathic helices-mediated anchoring to the membrane and other features not found in the classical types, the Type E enzymes are considered different.

Probably as a result of functional importance, the SdhA and SdhB subunits are highly conserved with identical phylogeny for both; this also indicates a coevolution of these subunits (Lemos *et al.*, 2002). In contrast, the sequences of the other two anchor subunits are more divergent and, hence, may reflect differences in the lipid profile of various organisms and/or lack of functions (with the exception of interaction with haem and quinone). Consequently, enzyme complex from various sources have differential sensitivity towards quinone inhibitors. It has also been argued that simply maintaining a set of residues for the hydrophobic contact (*i.e.* any hydrophobic residues rather than a specific one) and quinone binding would be sufficient, with an associated reduced selection pressure (Lemos *et al.*, 2002).

Table 3. Sequence-based classification of SQOR superfamily. ^a The residue in this column refers to the third of the four ligands of the dinuclear centre. While most enzymes has a Cys as the third ligand, Asp and Ser may functionally replace Cys. ^b The classification of SQR or QFR are based on genomic sequence annotations. The molecular weight range of the subunits A, B, C and D are 64-79, 27-31, 13-18 and 11-16 kDa, respectively (Hägerhäll, 1997); subunits E and F are of similar lengths though their sequences are not conserved compared to the respective canonical subunits C and D (Lemos *et al.*, 2002). Table modified from (Lemos *et al.*, 2002).

SUCCINATE:QUINONE OXIDOREDUCTASE

Type	Fe-S centres					Anchor			Haem		Genetic organisation	Example organism ^b
	Centre 1 ^a			Centre 3		CD	C	EF	b _P	b _D		
	Cys	Asp	Ser	3Fe	4Fe							
A	+			+		+			+	+	<i>ABCD</i>	<i>Thermoplasma acidophilum</i> SQR
		+		+		+			+	+	<i>CDAB</i>	<i>T. thermophilus</i> SQR
											<i>CDBA</i>	<i>Natronomonas pharaonis</i> SQR
B	+			+			+		+	+	<i>CAB</i>	<i>Rhodothermus marinus</i> SQR, <i>Desulfovibrio gigas</i> QFR, <i>W. succinogenes</i> QFR
C	+			+		+			+		<i>CDAB</i>	<i>Bradyrhizobium japonicum</i> and mitochondrial SQR, <i>Ascaris suum</i> QFR
		+		+		+			+		<i>CDAB</i>	<i>E. coli</i> SQR
			+	+		+			+		<i>ABCD</i>	<i>Mycobacterium tuberculosis</i> QFR
D	+			+		+					<i>ABCD</i>	<i>E. coli</i> , <i>Proteus vulgaris</i> , <i>H. influenzae</i> QFR
E	+				+			+			<i>ABEF</i>	<i>Sulfolobus acidocaldarius</i> SQR, <i>Acidianus ambivalens</i> SQR

2.1.2 Succinate:quinone reductase

As stated above [2.1.1 Succinate:quinone oxidoreductase superfamily (classification); p.15], the SQR specifically catalyses the forward reaction (Eq. 1 and 2). The structures of *E. coli*, avian and porcine heart SQR have been published (Table 2).

2.1.2.1 SdhA – flavoprotein subunit

A large-scale analysis of 374 flavin-dependent proteins ('flavogenomics') has revealed a myriad of their functions, with 75 % of them using FAD (Fig. 5) instead of FMN and 90 % having the flavin non-covalently attached (Macheroux *et al.*, 2011). Thus, the covalently-bound flavin cofactor in SQOR is of physiological significance with regard to the necessity of having such a linkage. That the flavin is covalently attached to proteins to prevent subunit loss in a low concentration environment (Mewies *et al.*, 1998) does not seem to support the observation that mutant proteins of vanillyl-alcohol oxidase and others are active even when the flavin molecule is not covalently bound; instead, the covalent flavinylation increases the redox potential crucial for *efficient* catalysis [reviewed in Heuts *et al.* (2009)]. In addition, the covalent attachment is also postulated to confer structural stability in an evolutionarily conserved but non-essential manner (Mewies *et al.*, 1998). The covalent flavinylation and its importance to Complex II (SQR and QFR), especially in the context of redox potential, has been discussed previously (Cecchini, 2003). In a wider context, the covalent attachment of flavin moiety can be considered analogous to the different haem types whereby only cytochrome *c* is tethered through two thioether linkages to Cys residues; this forms the haem *c* binding motif –CXXCH– [see (Barker and Ferguson, 1999; Allen *et al.*, 2005; Koch and Schneider, 2007) and references therein].

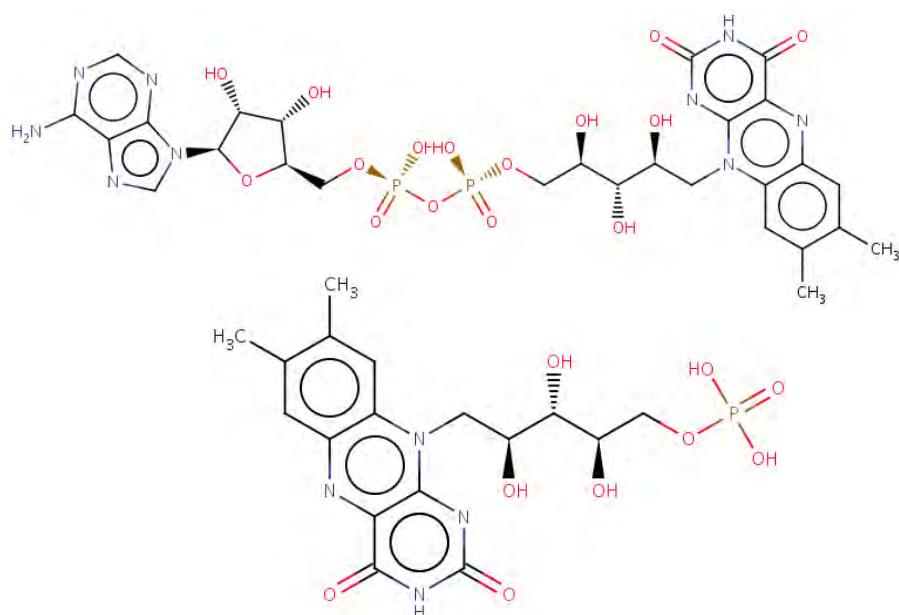


Fig. 5. Chemical structures of FAD (top) and FMN (bottom). Structures obtained from PDB (www.pdb.org) under the respective PDB ligand identifiers (Berman *et al.*, 2000).

The SdhA subunit of SQOR is a flavoprotein containing the covalently-bound catalytic flavin adenine dinucleotide (FAD) prosthetic group. Typical of other nucleotide-binding proteins, it features a Rossmann-like fold which consists of $\beta\alpha\beta\alpha\beta$ motif binding to a mononucleotide (Rossmann *et al.*, 1974). However, the folds binding NAD and NADP, and FAD are different – in the former, two of this motif are related structurally through a pseudo-two fold rotation forming a six-stranded parallel sheets straddled by the helices whereas the FAD-binding motif is a single mononucleotide-binding motif containing additionally two parallel β -strands (Bottoms *et al.*, 2002). The FAD-binding site of SQR/QFR follows the pattern R-[ST]-H-[ST]-x(2)-A-x-G-G (Prosite ID: PS00504); the *T. thermophilus* SdhA sequence motif is R-S-H-T-G-A-A-Q-G-G (Fig. 6). The His residue forms a covalent 8α -(N3)-histidyl-linkage with the FAD molecule (Walker and Singer, 1970); the linkages occurring in other systems have also been identified (Mewies *et al.*, 1998; Heuts *et al.*, 2009). While being common, the linkage is not exclusive to His residue as Cys-, Thr- and Tyr-linkages have been discovered [see (Macheroux *et al.*, 2011) and references therein]. In the case of vanillyl-alcohol

oxidase, the FAD binding promotes a change in oligomerisation states from monomers and dimers to dimers and octamers; whether such a role in the trimerisation of SQR or dimerization of QFR has yet to be investigated.

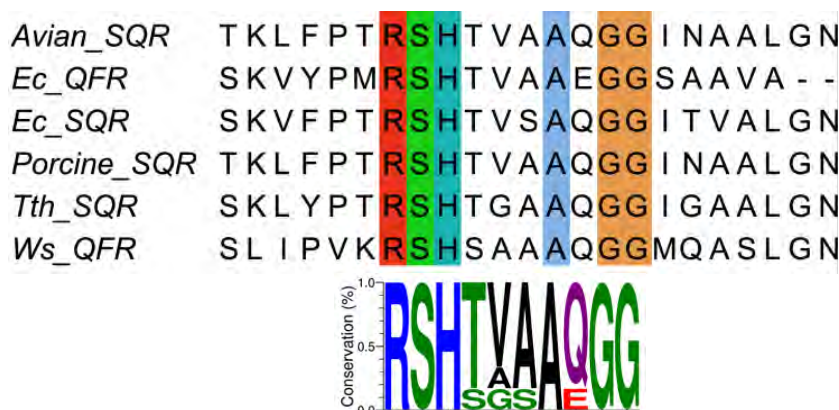


Fig. 6. Conservation of FAD-binding site in SQR and QFR flavoprotein subunit (SdhA/FrdA) from various organisms. Alignment was performed with MUSCLE (<http://www.ebi.ac.uk/Tools/msa/muscle>) (Edgar, 2004) and rendered in Jalview (Waterhouse *et al.*, 2009) with colouring at 100 % conservation. The sequence logo was generated with WebLogo 3 (<http://weblogo.threeplusone.com>) (Crooks *et al.*, 2004). With the exception of *T. thermophilus* SQR (RefSeq ID: YP_144720.1), avian SQR (PDB ID: 1YQ3), *E. coli* QFR (Ec_QFR; PDB ID: 1KF6), *E. coli* SQR (Ec_SQR; PDB ID: 1NEK), porcine SQR (PDB ID: 1ZOY) and *W. succinogenes* QFR (Ws_QFR; PDB ID: 2BS2) were from PDB.

2.1.2.2 SdhB – iron-sulphur cluster subunit

A key feature of the SdhB subunit is the presence of three Fe-S clusters comprising [2Fe-2S], [4Fe-4S] and [3Fe-4S] (PDB ligand identifiers: FES, SF4 and F3S, respectively; Centres 1-3) liganded to Cys residues. However, the Cys residues are not essential for liganding as Asp or Ser could replace it (Table 2 and Fig. 8). The biogenesis of Fe-S clusters and their different types have been described previously (Johnson *et al.*, 2005; Ayala-Castro *et al.*, 2008; Lill and Mühlenhoff, 2008). The prevalence of these clusters range from the simple [2Fe-2S] cluster to the more elaborate, polymetallic ones as found as iron-molybdenum cofactor (FeMo-co) in nitrogenase (Rubio and Ludden, 2008). The Rieske Fe-S

protein contains a unique type of [2Fe-2S] in that one of the two Fe atoms is coordinated by two His residues instead of the classical Cys, and is found as high redox potential in cytochrome bc_1 and b_6f complexes (+150 to +490 mV) and low potential in Rieske non-haem iron oxygenases (-150 to -50 mV) (Ferraro *et al.*, 2005). Together with the delocalisation of electrons over both Fe and S atoms, their structural diversity allows for widespread functions in various proteins, as shown in Fig. 7.

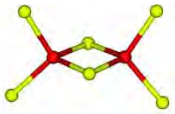
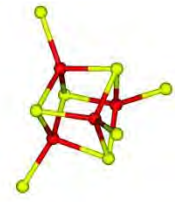
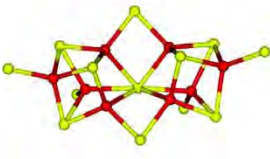
	[2Fe-2S] ²⁺	S = 0
	[2Fe-2S] ⁺	S = 1/2 or 9/2
	[3Fe-4S] ⁺	S = 1/2
	[3Fe-4S] ⁰	S = 2
	[3Fe-4S] ⁻	S = 5/2
	[3Fe-4S] ²⁻	S = ?
	[4Fe-4S] ³⁺	S = 1/2
	[4Fe-4S] ²⁺	S = 0
	[4Fe-4S] ⁺	S = 1/2 or 3/2
	[4Fe-4S] ⁰	S = 4
	[8Fe-8S] ⁵⁺	S = 7/2
	[8Fe-8S] ⁴⁺	S = 3 or 4
	[8Fe-7S] ³⁺	S = 1/2 or 5/2
	[8Fe-7S] ²⁺	S = 0
Structure	Oxidation state	Spin state

Fig. 7. Various Fe-S clusters as identified crystallographically. Fe atoms are in red and S atoms in yellow. The [3Fe-4S]⁻ cluster with the spin state of 5/2 is only observed as a fragment in heterometallic [M-3Fe-4S]⁺ clusters where M is a divalent transition metal ion (not shown here). Figure taken from (Johnson *et al.*, 2005).

The Fe-S clusters of *E. coli* SQR, for instance, are within an 11-Å distance between each other while the distance between [3Fe-4S] centre to the UQ binding site is 14 Å; the distances between redox centres are nature-designed to be less than 14 Å for an efficient electron transfer (Page *et al.*, 2003). Therefore, an electron relay passing between *all* of the Fe-S centres is crucial for its function. Interprotomer electron transfer is precluded due to an extremely long distance (~42-45 Å). In this chapter, a detailed comparison between only *E. coli* and *T. thermophilus* SQR is made due to the taxonomic nature of the two eukaryotic SQR and the functional difference between SQR and QFR. Figs. 8-11 highlight the conservation of Fe-S cluster ligands as well as their 3D representations. Further aspects of these centres, including the relationship between midpoint potential and function, are discussed below. A conversion table listing the residues acting as Fe-S cluster ligands in *T. thermophilus* SQR as well as all structurally-determined complexes are given in Table 4 based on the sequence alignment in Fig. 8 and the 3D structures; the third ligand of [2Fe-2S] cluster is not conserved in the *T. thermophilus* SQR, being replaced by an Asp instead of a Cys. Table 5 lists the reduction potentials of Fe-S clusters and haems for enzymes from various sources. That the haems have a wide ranging midpoint potential is not surprising given that their chemical environments are not similar, a fact confirmed through theoretical calculations (Mao *et al.*, 2003).

Table 4. Conversion table for the Fe-S ligands of SQR and QFR. The ligands for avian, *E. coli* QFR and SQR, porcine, *T. thermophilus* and *W. succinogenes* are based on available structure and multiple sequence alignment.

	Avian	<i>Ec</i> QFR	<i>Ec</i> SQR	Porcine	<i>Tth</i>	<i>Ws</i> QFR
[2Fe-2S]						
	C65	C57	C55	C65	C54	C57
	C70	C62	C60	C70	C59	C62
	C73	C65	D63	C73	D62	C65
	C85	C77	C75	C85	C74	D77
[4Fe-4S]						
	C158	C148	C149	C158	C144	C151
	C161	C151	C152	C161	C147	C154
	C164	C154	C155	C164	C150	C157
	C225	C214	C216	C225	C210	C218
[3Fe-4S]						
	C168	C158	C159	C168	C154	C161
	C215	C204	C206	C215	C200	C208
	C221	C210	C212	C221	C206	C214

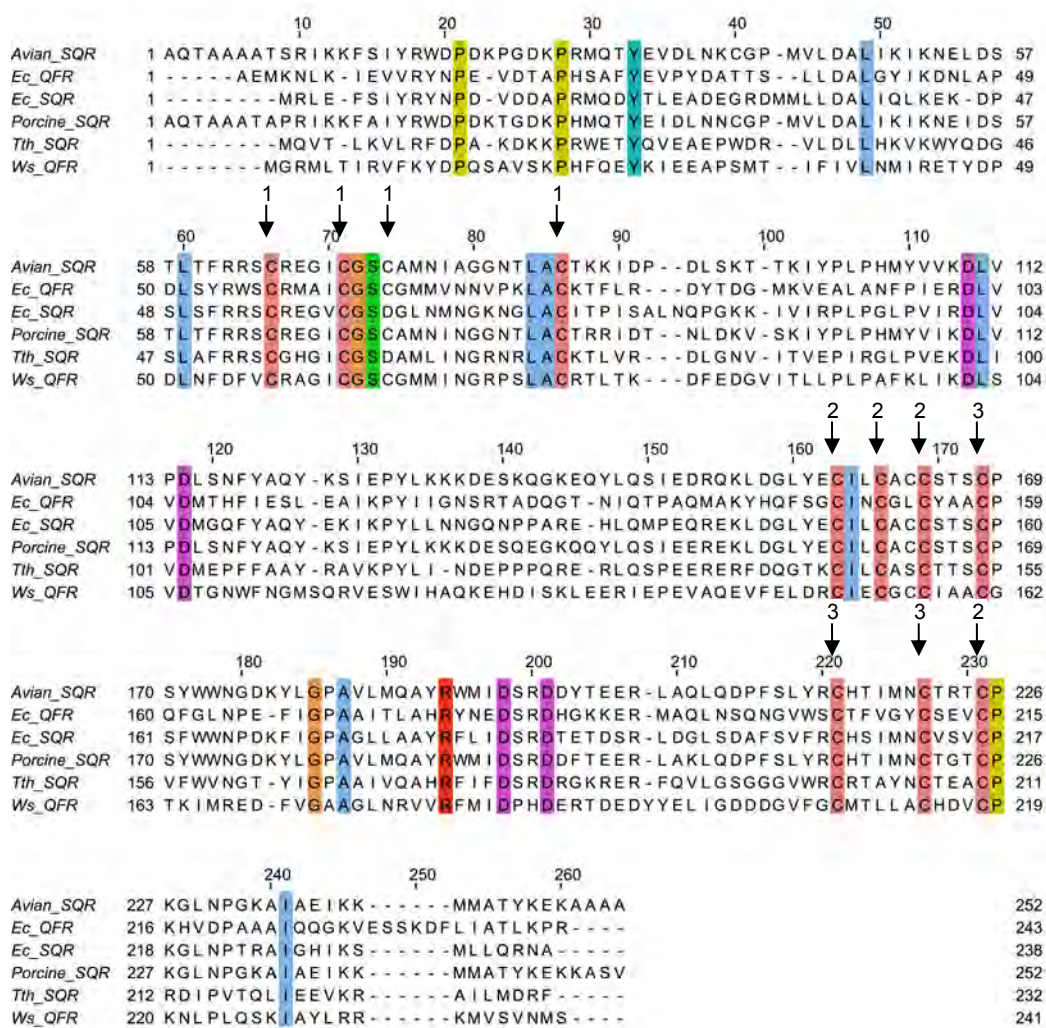


Fig. 8. Ligands of Fe-S clusters located within the SdhB/FrdB subunit. The sequences were aligned with MUSCLE (<http://www.ebi.ac.uk/Tools/msa/muscle>) (Edgar, 2004) and rendered with Jalview with colouring at 85 % identity (Waterhouse *et al.*, 2009) using the sequences from the respective crystal structures of avian SQR (PDB ID: 1YQ3), *E. coli* QFR (Ec_QFR; PDB ID: 1KF6), *E. coli* SQR (Ec_SQR; PDB ID: 1NEK), porcine SQR (PDB ID: 1ZOY) and *W. succinogenes* QFR (Ws_QFR; PDB ID: 2BS2). *T. thermophilus* SQR accession is RefSeq ID: YP_144719.1. Arrows indicate the ligands of [2Fe-2S] (1), [4Fe-4S] (2) and [3Fe-4S] (3) clusters. The third ligand of [2Fe-2S], equivalent to D63^{Ec} and D62^{Tth}, is clearly not conserved.

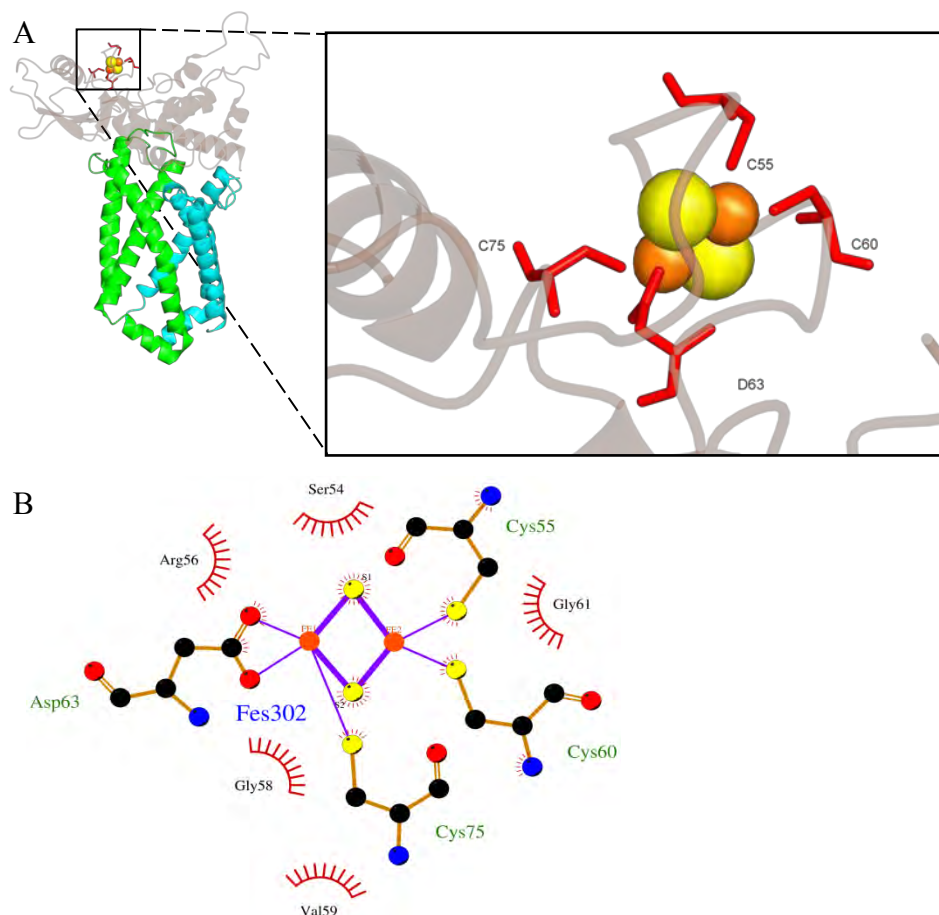


Fig. 9. [2Fe-2S] cluster of *E. coli* SQR. (A) A 3D representation of C55, C60, D63 and C75 liganding the [2Fe-2S] cluster. In spheres are the Fe atoms (orange) and sulphur (yellow). For orientation and clarity purposes, the SdhC and SdhD are in green and cyan, respectively, while SdhA is not shown and SdhB is transparent red. Image created with CCP4mg (Potterton *et al.*, 2004) with PDB ID: 1NEK **(B)** A 2D representation of (A) generated with LigPlot+ (Laskowski and Swindells, 2011). Individual atoms are coloured N (blue), O (red), C (black), S (yellow) and Fe (orange).

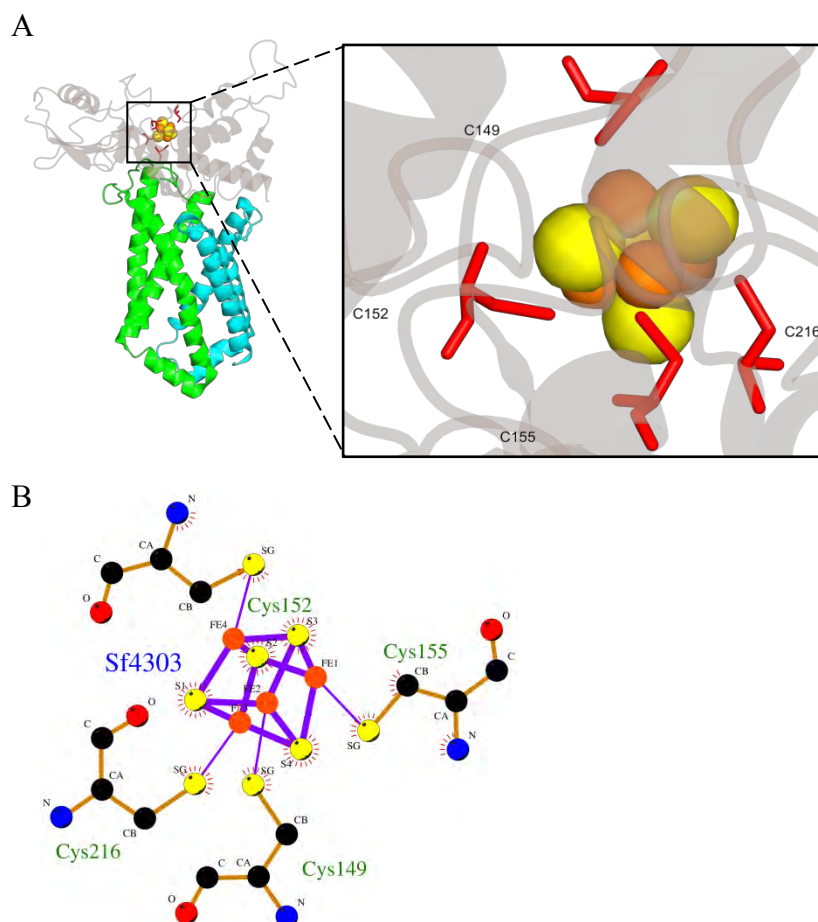


Fig. 10. [4Fe-4S] cluster of *E. coli* SQR. (A) A 3D representation of C149, C152, C155 and C216 liganding the [4Fe-4S] cluster. (B) A 2D representation of (A) generated with LigPlot+. For clarity, residues nearby the cluster are not shown. See the figure legend of Fig. 9 for details.

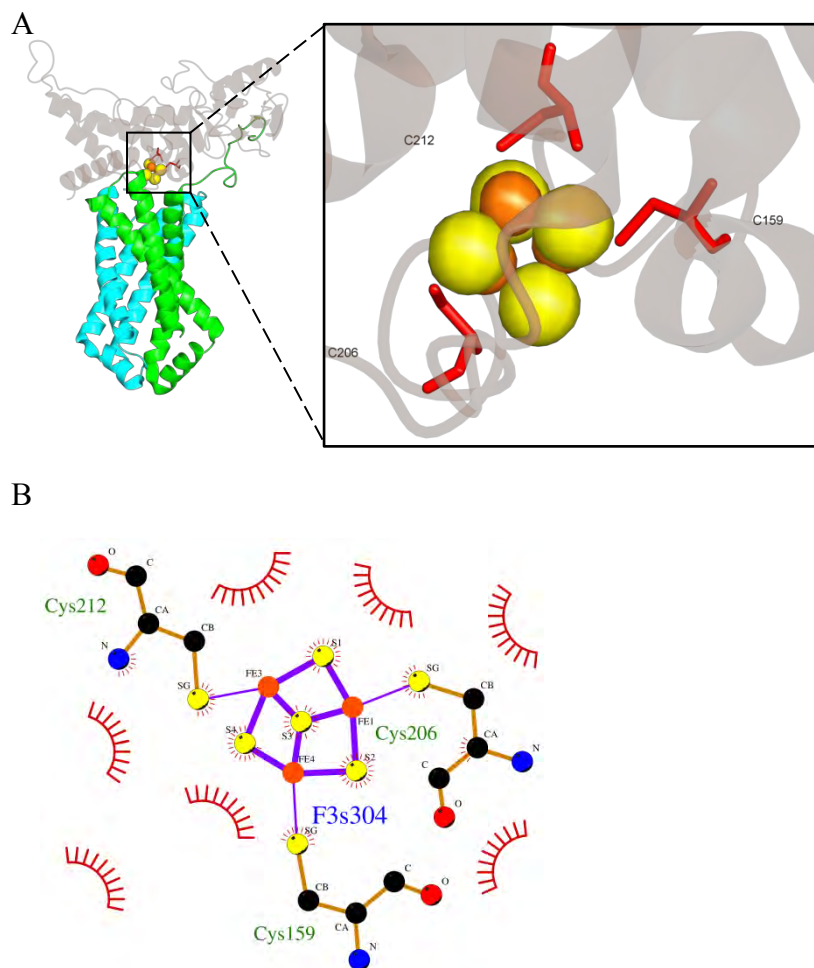


Fig. 11. [3Fe-4S] cluster of *E. coli* SQR. (A) A 3D representation of C159, C206 and C212 liganding the [3Fe-4S] cluster. (B) A 2D representation of (A) generated with LigPlot+. For clarity, residues nearby the cluster in red arcs are not labelled. See the figure legend of Fig. 9 for details.

SUCCINATE:QUINONE OXIDOREDUCTASE

Table 5. Reduction potential of reactions occurring during the SQR and QFR catalysis. The values for the Fe-containing centres refer to the reduction of Fe^{3+} to Fe^{2+} . For *T. thermophilus*, the quinone type is menaquinone (MK), mostly as MK-8, instead of ubiquinone (UQ) (Collins and Jones, 1981). (a) Bovine SQR value. Data for *E. coli* SQR and QFR were from (Yankovskaya *et al.*, 2003), *W. succinogenes* from (Lancaster, 2004), *B. subtilis* from (Christenson *et al.*, 2008) and *T. thermophilus* from native complex (Kolaj-Robin *et al.*, 2011). For comparison, the rhodoquinone (RQ)/rhodoquinol (RQH₂) pair, used by the nematode *A. suum*, has a redox potential of -63 mV. The high and low potential haems b_{H} and b_{L} , are now termed as haems b_{P} and b_{D} , respectively [(Lemos *et al.*, 2002) *cf.* (Hägerhäll and Hederstedt, 1996)].

	Redox potential (E'_0 , mV)				
	Ec SQR	Ec QFR	Ws QFR	Bs SQR	Tth
Fumarate + 2 H ⁺ + 2 e ⁻ → succinate			+30		
[FAD] + 2 H ⁺ + 2 e ⁻ → [FADH ₂]	-79 ^a	-50	-25	N/A	N/A
[2Fe-2S]	+10	-35	-60	+80	-10
[4Fe-4S]	-175	-310	< -250	-240	< -300
[3Fe-4S]	+65	-67	-30	-25	> +50
Haem $b_{\text{H}}/b_{\text{P}}$	+35		-15	+65	-20
Haem $b_{\text{L}}/b_{\text{D}}$			-150	-95	-160
UQ/UQH ₂ ; MK/MKH ₂			UQ = +110; MK = -75		

2.1.2.3 Membrane anchors – SdhC (cytochrome subunit) and SdhD (membrane anchor subunit)

To allow for the tethering of the protein complex to the inner membrane, the two subunits SdhC and SdhD form an anchor; in certain SQOR types, these may be fused (Table 2; p. 17). Consequently, Complex II has a higher proportion of soluble region to membrane-bound domain relative to the other respiratory complexes. In fact, membrane subunit-dissociated complex (SdhA and B only) still retains the succinate dehydrogenase activity but not the physiological SQOR activity (Singer *et al.*, 1973). In addition to the anchoring function as well as possessing the binding site for the lipid-soluble quinone, haem *b* moieties are also buried within these two hydrophobic subunits, similar to other metal centres, such as in cytochrome *c* oxidases (Pereira *et al.*, 2001; Noor and Soulimane, 2012) **(Paper II)**. A difference in the spatial distribution around the helical core bundle ‘wrapping’ haem moieties between *E. coli* and *W. succinogenes* with a tighter packing is observed in the former along with the presence of larger residues [FrdC-R28^{Ec} (ASA = 225 Å²), FrdC-W86^{Ec} (255 Å²) and FrdD-R81^{Ec} vs. FrdC-Q30^{Ws} (ASA = 180 Å²), FrdC-A97^{Ws} (115 Å²) and FrdC-G186^{Ws} (75 Å²)]¹; this has been attributed to the lack of any haem in *E. coli* QFR (Lancaster *et al.*, 1999; Iverson *et al.*, 1999; Cecchini, 2003). The overall sequence conservation of SdhC and SdhD subunits are illustrated in Figs. 12 and 13, respectively, while the haem *b* ligands are highlighted in Figs. 14 and 15. Relatively few residues are conserved among both anchor subunits.

¹ ASA, accessible surface areas, for amino acids were obtained from (Chothia, 1976).

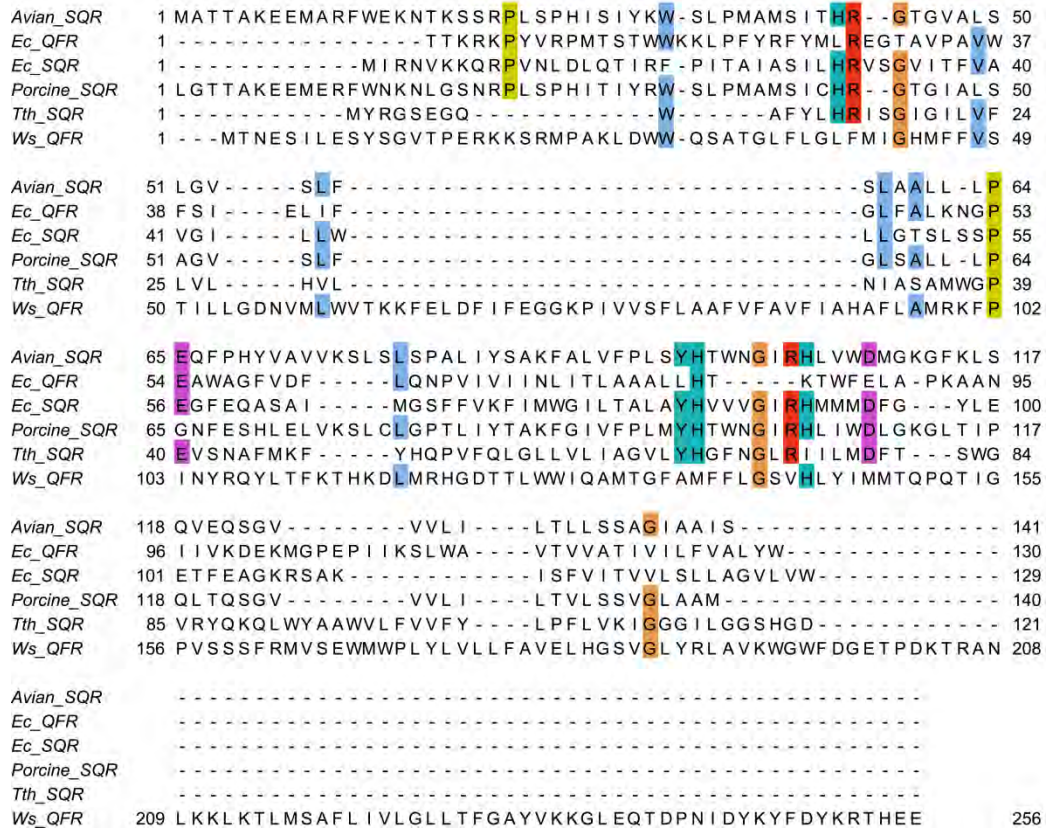


Fig. 12. Multiple sequence alignment of the membrane anchor subunit SdhC. Sequence alignment and rendering at 65 % identity, performed as for Fig. 8, clearly indicates very low sequence conservation among the anchor subunits. Sequences were from crystal structures and RefSeq (*T. thermophilus*, RefSeq ID: YP_144722.1). Notably, the FrdC subunit of *W. succinogenes* QFR is a fusion of the classical SQOR subunits C and D.

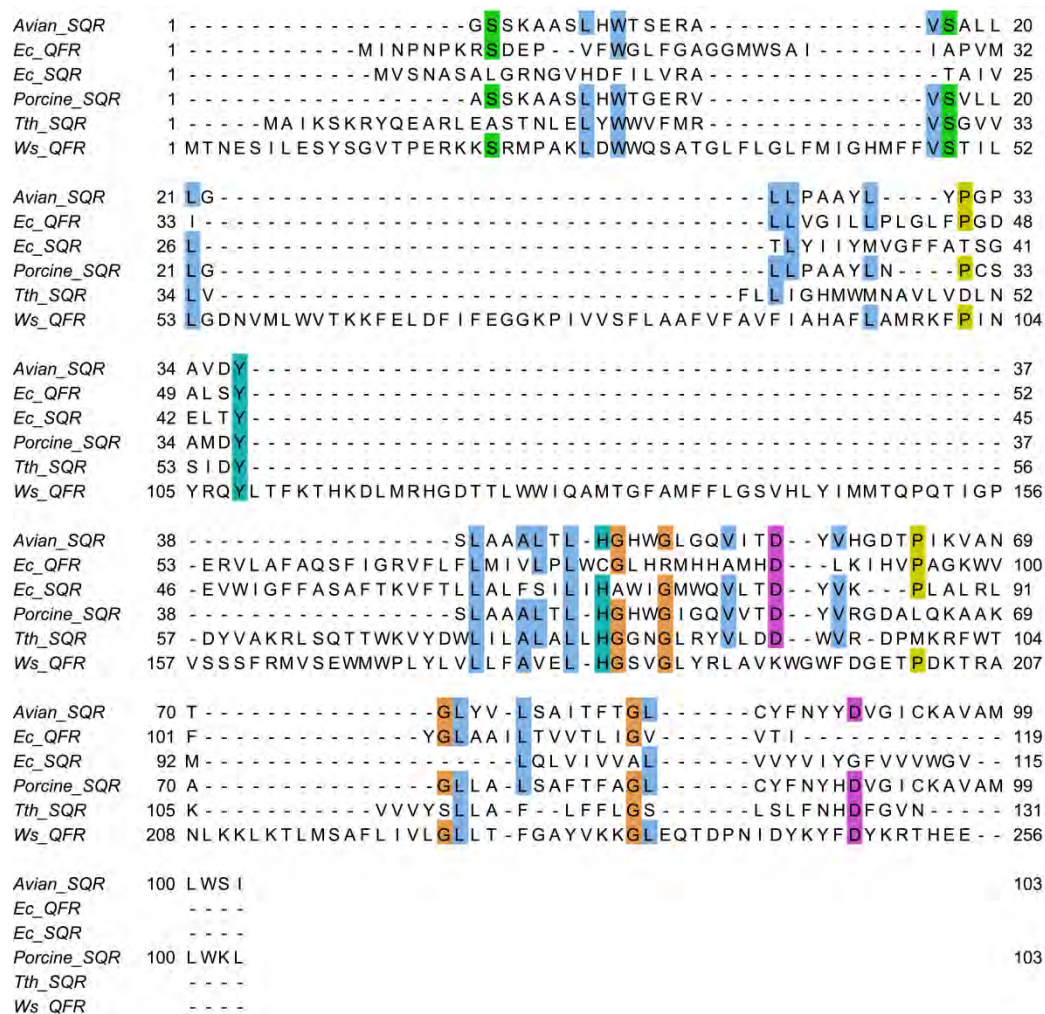


Fig. 13. Multiple sequence alignment of the membrane anchor subunit SdhD.

Sequence alignment and rendering at 65 % identity, performed as for Fig. 8, clearly indicates very low sequence conservation among both anchor subunits SdhC and SdhD. Sequences were from crystal structures and RefSeq (*T. thermophilus*, RefSeq ID: YP_144721.1). The *T. thermophilus* SQR subunits SdhC and SdhD cannot be aligned well together with the other sequences.

<i>B.subtilis_SQR_SdhC</i>	1	-----MSGNR-----EYFRRLHSLLGVIPVGI	24
<i>Tth_SQR_SdhC</i>	1	---MYRGSEGGW-----AFY---LHRISGIG-ILVF	24
<i>Ws_QFR</i>	1	MTNESILESYSGVTPERKKSRMPAKLDW-----QSATGLF-LGLF	40
<i>B.subtilis_SQR_SdhC</i>	25	LIQH-----LVVNQFAARGAEAFNSAAHFMDSLPFRYALEIFI	62
<i>Tth_SQR_SdhC</i>	25	LVLH-----VLNIASAMWGPEVSNAFMKFFYHQPVFQLGLLVL	62
<i>Ws_QFR</i>	41	MIGHMFFVSTILLGDNVMLWVTKKFELDFIFEKGGKPIVVSFLAAF	85
<i>B.subtilis_SQR_SdhC</i>	63	IFLPLIYHAV-----YGVYIAFTAKNNAGQYSYMRNWL FVL	98
<i>Tth_SQR_SdhC</i>	63	--AGVLYHGF-----NGLRIILMDFTSWGVRYQKQLWY---	93
<i>Ws_QFR</i>	86	VFAVFI AHAFLAMRKFPIN YRQYLTFKTHKDLMRHGDTTLWW--I	128
<i>B.subtilis_SQR_SdhC</i>	99	QRVTGIIITLIFVSWHWVWETRIAAQMGAEVNFDMMANILSSPAMLG	143
<i>Tth_SQR_SdhC</i>	94	-----AAWVLFVVFYLP-----	105
<i>Ws_QFR</i>	129	QAMTGFAMFFLGSVHLYIMMTQPQTI GPVSSSFR---MVSEWMP	170
<i>B.subtilis_SQR_SdhC</i>	144	FYIVGVLSTIFHFSNGLWSFAVTWGITVTPRSQRISTYVTLIIFV	188
<i>Tth_SQR_SdhC</i>	106	-FLVKIGGILGGS HGD-----	121
<i>Ws_QFR</i>	171	LYLVLLFAVELHGSVGLYRLAVKKGWFDGETPDKTRANLKKLKT	215
<i>B.subtilis_SQR_SdhC</i>	189	ALSIVGLKAI FAFV-----	202
<i>Tth_SQR_SdhC</i>			
<i>Ws_QFR</i>	216	MSAFLIVLGLLTFGAYVKKGLEQTPNIDYKYFDYKRTH	256

Fig. 14. Conserved His residues of dihaem SQOR in the SdhC subunit. Sequence colouring is at 70 % conservation, which indicates the relative conservation of the haem b_D (black triangle; SdhC-H28Th) and b_P (grey triangle; SdhC-H68Th) ligands. The second *B. subtilis* and *W. succinogenes* haem b_D ligands (red arrows) do not align with either of the *T. thermophilus* anchor proteins at all whereas the second haem b_P ligand of these two only align to the *T. thermophilus* SdhD subunit (green arrows; see Fig. 15); the *T. thermophilus* haem b_D ligands in SdhC and SdhD both align to the first haem b_D ligand of *B. subtilis* and *W. succinogenes*. Typical of Type B SQOR, the *B. subtilis* SdhC consists of fused SdhC and SdhD subunits. Alignment and rendering is as for Fig. 8 using *B. subtilis* SQR SdhC (UniProt ID: P08064) while the other sequences are as for Fig. 12.

S27^{Ec}, SdhC-I28^{Ec} and SdhD-Y83^{Ec}. These hydrophobic residues provide the necessary environment for quinone binding.

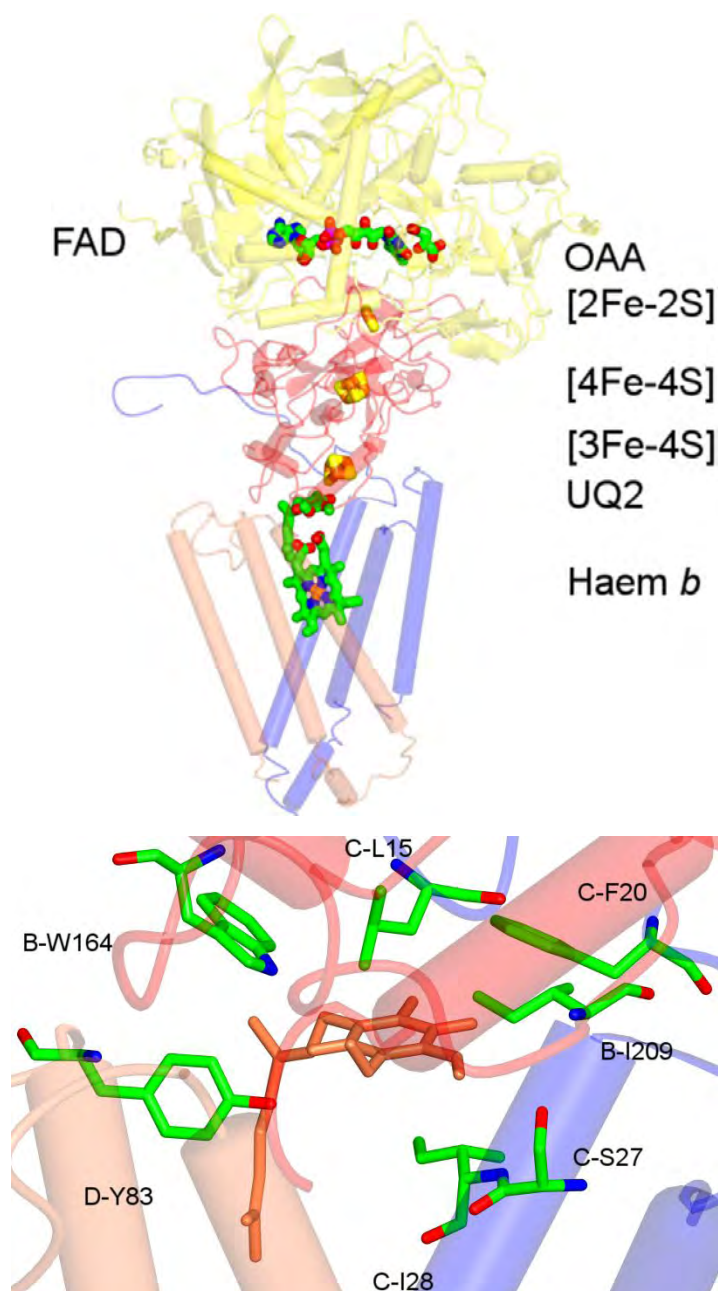


Fig. 16. Quinone binding site in the *E. coli* SQR. (Top) The peptide chains are shown as worms and tubes with SdhA (yellow), SdhB (red), SdhC (blue) and SdhD (coral) using the crystal structure (PDB ID: 1NEK). The quinone type is ubiquinone. (Bottom) Ligands of the bound ubiquinone (coral) involving the three subunits. Figures rendered with CCP4mg (Pottterton *et al.*, 2004).

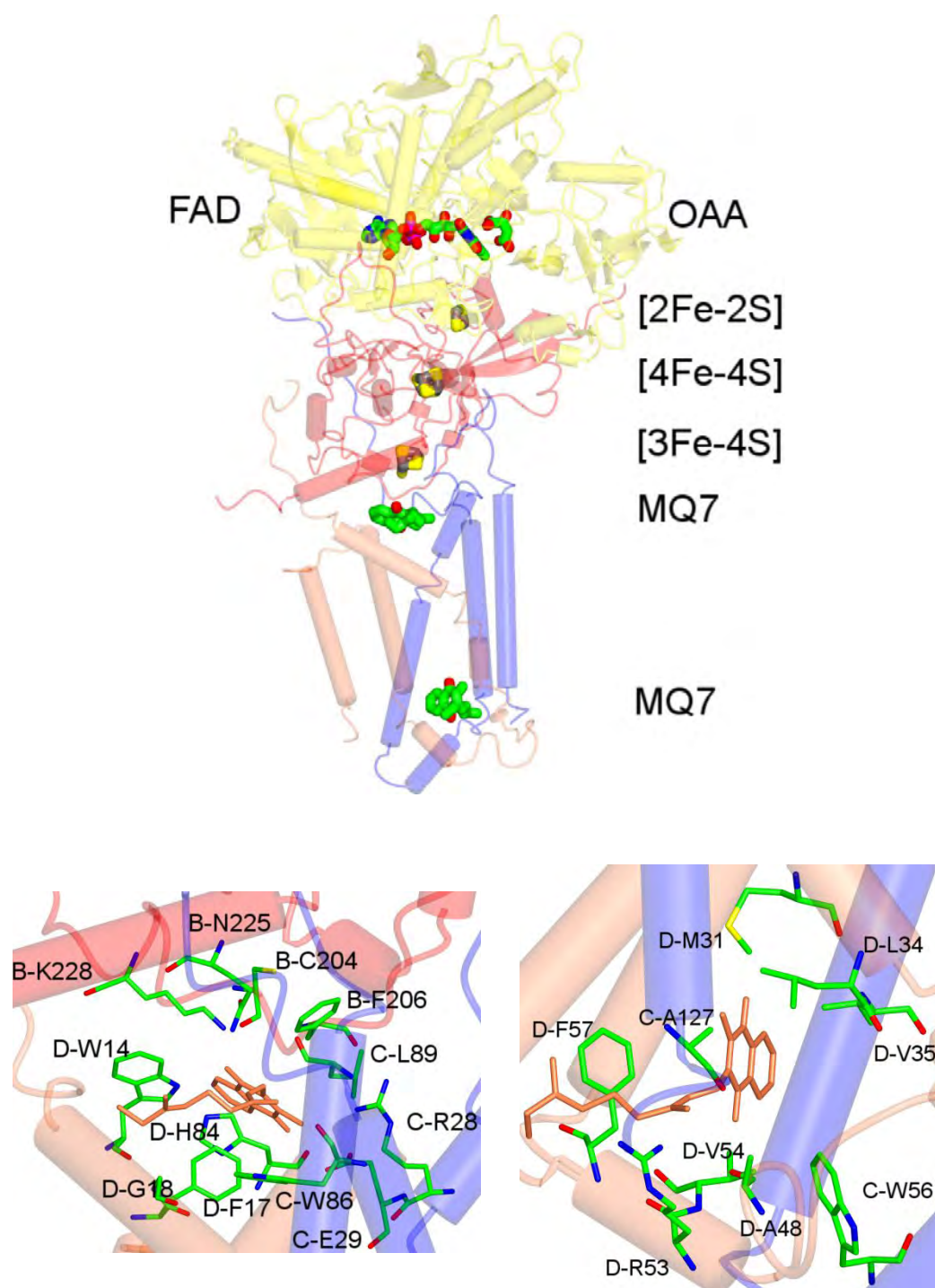
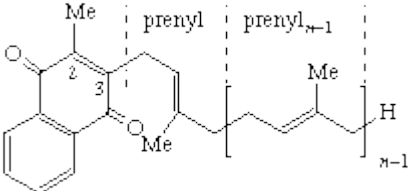
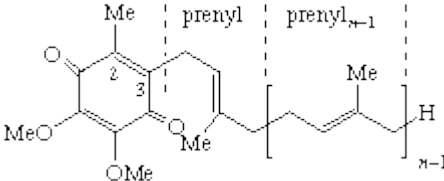


Fig. 17. Quinone binding site in the *E. coli* QFR. (Top) The peptide chains, coloured similar to Fig. 16 (PDB ID: 1L0V), show the relative positions of the two menaquinone-7 sites. **(Bottom)** The residues forming the proximal and distal binding sites are illustrated in the left and right figures, respectively. See text for details.

Table 6. Chemical structures of menaquinone and ubiquinone. The bolded names are recommended, with asterisk (*) names proposed by Committee on Nomenclature of IUNS. Modified from IUPAC-IUB Commission on Biochemical Nomenclature – Nomenclature of Quinones with Isoprenoid Side-chains (<http://www.chem.qmul.ac.uk/iupac/misc/quinone.html>).

Aromatic nucleus	Side chain	Trivial name(s)	Abbreviation(s)
1,4-Naphthoquinone 2-methyl *Menaquinone (Menadione)	3-(prenyl) _n	Menaquinone-<i>n</i> *Prenylmenaquinone-<i>n</i>	MK-<i>n</i> *MQ-<i>n</i>
			
1,4-Benzoquinone, 2,3-dimethoxy-5- methyl-	6-(prenyl) _n	Ubiquinone-<i>n</i>	Q-<i>n</i>
			

Structural alignment of the *E. coli* SdhAB (SQR) and FrdAB (QFR) subunits results in an rmsd of 1.75 Å (calculated with CCP4mg) between these two subunits. In contrast, the membrane anchor subunits have a larger rmsd with the resulting 15-Å distance between SQR quinone binding site to the QFR Q_P site (Yankovskaya *et al.*, 2003). Nearly 10 Å away (edge-to-edge distance between Fe_b and C1 of MQ-7), the haem *b* propionate of SQR occupies the Q_P site in a non-superposing manner. While it has been argued that this difference “distinguishes SQR from QFR within this family of enzymes” (Yankovskaya *et al.*, 2003), the lack of structural similarities (ideal similarity being an rmsd of peptide chain Cα close to zero) do not allow further conjectures. There is only one ubiquinone ligand bound to each of avian (PDB ID: 1YQ3) and porcine (PDB ID: 1ZOY) enzymes, although two TTFA (2-thenoyltrifluoroacetone;

inhibitor binding at quinone site) molecules were found to co-crystallise with the enzyme complex together with a single 3-nitropropanoic acid (isoelectronic to succinate). The presence of two TTFA molecules indicating two quinone binding sites seems consistent with available biochemical data. However, both the crystal structure and biochemical data are flawed by (i) the high concentration of inhibitor used in protein crystallisation resulting in non-specific binding, (ii) the absence of any redox centre connecting the two TTFA molecules about 30 Å apart with the distal TTFA being 15 Å away from haem *b* edge, and (iii) the use of membrane-bound protein complexes for the assay [see (Maklashina and Cecchini, 2010) for further discussions]. This presumably does not extend to *dihaem* SQOR as electron transfer could occur across the membrane domain, and additionally supported by the coupling activity to transmembrane electrochemical potential in dihaem complexes. Therefore, they could genuinely contain two quinone binding sites, a hypothesis that can only be confirmed by crystal structures of dihaem SQR from preferably at least two other divergent sources.

The fact that some families of SQOR (Types D and E) do not contain haem moieties at all, with others possessing only one (Table 2; p. 17), raises the question of their functional role in the electron transfer. Interestingly, succinate:UQ oxidoreductases contain a single haem while two are present in enzymes utilising MK (Matsson *et al.*, 2000). Mutations in *E. coli* SQR (SdhCD^{H71Y}AB^{Ec} and SdhC^{H84Y}DAB^{Ec}) where no haem is present show neither increased radical oxygen species (ROS) production nor significantly decreased physiological activity (Tran *et al.*, 2007). Nonetheless, both mutants are highly sensitive to detergents commonly used for the solubilisation of wild type enzyme – an unsurprising finding given that expression in a *hemaA E. coli*-deletion strain² was not successful (Nakamura *et al.*, 1996). This observation is consistent to that of *B. subtilis* mutants of heme *b_D* axial ligands that could not be detergent-purified (Matsson *et al.*, 2000). Taken together, this suggests a role for haem in the proper enzyme assembly/stability considering the haem having a close contact with the helix bundle formed by SdhCD. Notably, only a single haem moiety is

² This strain, deficient in δ -aminolevulinic acid synthase, is unable to synthesise δ -aminolevulinic acid (5-aminolevulinic acid) which is the first product in the porphyrin synthesis pathway (Frustaci *et al.*, 1991).

present in *E. coli* SQR compared to two in *T. thermophilus* SQR (Kolaj-Robin *et al.*, 2011, accepted) (**Paper I**). Furthermore, from the evolutionary perspective, it seems highly unlikely for organisms to retain the haem *and* insertion factor(s) if it is not required functionally.

Intriguingly, *aerobic* oxidation of succinate by the haem-less *E. coli* QFR generates 20-fold more reactive oxygen species than the paralogous SQR enzyme (Messner and Imlay, 2002). This finding has been used to support the argument that haem moieties act as an electron sink in the catalytic cycle, reducing/preventing contact between ubisemiquinone radical and oxidants (Yankovskaya *et al.*, 2003). However, the SdhCD^{H71Y}AB^{Ec} and SdhC^{H84Y}DAB^{Ec} mutants generate no more superoxide radicals than wild type enzymes, considering their relative succinate:ubiquinone turnover rates (Tran *et al.*, 2007).

In dihaem SQR, the haem moieties can be fully reduced by dithionite ($E'_0 = -420$ mV, pH 7) and partially reduced by succinate ($E'_0 = +30$ mV) as the two haem moieties have different midpoint potentials (Table 5; p. 33); this partial reduction is exemplified by *B. subtilis* (Matsson *et al.*, 2000) and *T. thermophilus* SQR (Kolaj-Robin *et al.*, 2011). Conversely, the single haem in bovine SQR has a very low redox potential (-185 mV) and is, therefore, not succinate reducible (Yu *et al.*, 1987). However, the haem in fully-reduced bovine SQR can be oxidised quickly by fumarate (Hatefi and Galante, 1980). As this reaction is enzymatic similar to succinate reduction (*cf.* dithionite reduction), it suggests a potential role for haem in fumarate reduction but not succinate oxidation (Cecchini, 2003). While being fully reducible by succinate (Kita *et al.*, 1989), the *E. coli* SQR haem reduction rate is slower than catalytic rate at low quinone concentrations but enhanced under saturating concentrations and anaerobic conditions (Cecchini, 2003). The fumarate reoxidation of reduced heme in *E. coli* SQR mimics that of the bovine SQR with a rate equivalent to the catalytic rate. Although these data imply a direct electron transfer from [3Fe-4S] cluster to quinone (bypassing haem) but involving haem in the reverse reaction (QFR activity), it does not provide an explanation for the existence of haem in the first place. Based on the *E. coli* SQR structure (PDB ID: 1NEK), the edge-to-edge distance between quinone and [3Fe-4S] is 7.2 Å, and between quinone and haem

is 7 Å, with a total of nearly 14 Å for a postulated pathway in the direction quinone → haem → [3Fe-4S]. In addition, the haem moiety in single haem SQR may also be in redox equilibrium with the quinone pool (Cecchini, 2003).

Perhaps a more convincing study on the role of haem is the work using pulse radiolysis whereby radiation-induced reducing equivalents are introduced into an enzyme at a time scale of picosecond to second scale coupled to a similar fast scale spectrophotometric detection, analogous to the typical flash photolysis used with cytochrome *c* oxidases [see (Wherland *et al.*, 2005; Farver and Pecht, 2008)]. The haem in *E. coli* SQR was demonstrated to truly participate in the electron transfer between [3Fe-4S] and UQ (Anderson *et al.*, 2005). Direct electron transfer from [3Fe-4S] to UQ is presumably prevented by the large ΔE of ~ 50 mV³ between [3Fe-4S] cluster and UQ compared to the smaller negative ΔE for a two-step electron transfer pathway from [3Fe-4S] cluster to haem *b* to UQ, compensating for the longer distance calculated above and notwithstanding a much higher midpoint potential of UQ pair compared to that of haem [$E_{m,8} = 60$ mV vs. -15 mV; (Tran *et al.*, 2006)]. Nonetheless, non-functional Q-site results in a much slower electron transfer from [3Fe-4S] cluster to the haem, indicating a possible gating mechanism formed by SdhB-H207^{EcSQR} that prevents direct electron tunnelling from the former to the latter; note that the distance between the two are well within the 14-Å limit (Tran *et al.*, 2006).

A possible mechanistic explanation for the haem-stimulated turnover is delocalised electrons on ubisemiquinone (USQ) decreasing the thermodynamic barrier of electron transfer from the [3Fe-4S] cluster for the second-electron reduction of USQ to UQH₂, potentially a proton-coupled electron transfer (PCET) (Tran *et al.*, 2007). Rapid electron transfer between cytochrome *c* and the homodinuclear Cu_A centre in cytochrome oxidases is also made possible by delocalized electrons [see (Noor and Soulimane, 2012) and references therein] (**Paper II**). Nonetheless, the timescale of intraprotein electron transfer and quinone reduction is μ s and ms, respectively, and might not explicate the

³ The calculation is based on the Nernst equation, which results in a large positive ΔG (Gibbs energy; non-spontaneous reaction); SQR turnover is endergonic. Detailed calculations are presented in (Anderson *et al.*, 2005).

observed magnitude of changes between the wild type and haem-less mutants⁴. Moreover, since the K_m values are quite similar while catalytic activities are not, this suggests the absence of haem has an effect only on the catalysis and not on the structure (*i.e.* the environment of Q-site binding pocket remains the same). Collectively, these two crucial studies (Anderson *et al.*, 2005; Tran *et al.*, 2007) establish a model in which haem stimulates, but is not mandatory for, activity.

2.1.4 Oligomeric states of SQR and QFR

The determination of quaternary structures of proteins, especially membrane proteins, is not a facile process. In addition to detergent micelles complicating techniques such as analytical gel filtration chromatography, there is a distinction between physiological and crystallographic oligomers. These are usually readily distinguishable, such as in the case of *T. thermophilus* *caa*₃-oxidase (PDB ID: 2YEV) where the two (crystallographic) protomers are symmetrical parallel to the membrane (one protomer stacked on top of another). Furthermore, artifactual states usually have smaller contact areas compared to biological oligomers and can be discriminated on the basis of physicochemical properties and protein surface shape (Tsuchiya *et al.*, 2008). Similar theoretical strategy has been implemented through PDB in Europe Protein Interfaces, Surfaces and Assemblies (PDBePISA, http://www.ebi.ac.uk/msd-srv/prot_int/cgi-bin/piserver). Where the axis of symmetry is a more biologically-plausibly perpendicular to membrane as is the case with bovine heart cytochrome *c* oxidase (PDB ID: 1OCC), it can be more difficult to differentiate between monomeric and dimeric assemblies.

That there is a similar discussion regarding the physiological oligomeric state of SQR and QFR is not surprising. For *E. coli* SQR, the case for a physiological trimeric assembly is evident from the tight crystal packing in both trigonal space group $R32^5$ (PDB ID: 1NEK) (Yankovskaya *et al.*, 2003) and orthorhombic

⁴ The wild type succinate:UQ turnover number is 37 s^{-1} compared to 22 and 18 s^{-1} for the mutants, with K_m for UQ of 0.20, 0.71 and 0.31 mM (Tran *et al.*, 2007).

⁵ For a trigonal unit cell with parameters $a = b \neq c$, $\alpha = \beta = 90^\circ$, $\gamma = 120^\circ$, such as for PDB ID: 1NEK, the space group is technically $R32:h$ (hexagonal), not $R32$ (rhombohedral) as described by the authors or $H32$ as defined by the PDB.

$P2_12_12_1^6$ (PDB ID: 2WDQ) (Ruprecht *et al.*, 2009) crystal forms; complementary evidence include those from *B. licheniformis* (gel filtration chromatography) (Madej *et al.*, 2007) and *Corynebacterium glutamicum* (blue native gel electrophoresis; BN-PAGE) (Kurokawa and Sakamoto, 2005). However, it has been suggested that mitochondrial SQR is a monomer of heterotetramers (Sun *et al.*, 2005) (crystal structure in $P2_12_12_1$; PDB ID: 1ZOY) similar to *Sulfolobus acidocaldarius* SQR (gel filtration chromatography) (Moll and Schäfer, 1991) whereas the *Trypanosoma cruzi* monohaem SQR is a homodimer of heterododecamer (12 subunits; high resolution clear native gel electrophoresis; hr-CNE) (Morales *et al.*, 2009). Interestingly, synthetic monomeric *T. thermophilus* SQR retains the succinate dehydrogenase activity (Kolaj-Robin *et al.*, accepted) (**Paper I**) but does not form crystals using the methods used for the trimeric variants, though the physiological SQR and the reverse QFR activities would need to be evaluated.

This differs from QFR where it forms a homodimer of heterotrimers based on the analytical ultracentrifugation study on the enzymes from *Clostridium jejuni*, *Helicobacter pylori* and *W. succinogenes* (Mileni *et al.*, 2006), confirming the crystal structure assembly of the latter. Although two molecules are present in the asymmetric unit with a symmetry axis parallel to membrane normal, the contact area between the crystallographic dimers is too small ($\sim 325 \text{ \AA}^2$) and, hence, the *E. coli* QFR is a monomer of heterotetramers (crystal structure in $P2_12_12_1$; PDB ID: 1L0V) (Iverson *et al.*, 1999).

⁶ This crystal form was obtained by exchanging the detergent on a gel filtration column from the originally used 0.05 % C₁₂E₉ (Thesit) (Yankovskaya *et al.*, 2003) to 0.2 % decylmaltoside (DM) (Ruprecht *et al.*, 2009). This newer form routinely diffracted to 3.0–3.5 Å but to 2.1–2.8 Å with the Q-site inhibitor carboxin.

2.1.5 SQOR reaction mechanism

The following describes the catalytic mechanism of succinate oxidation coupled to the quinone reduction preceding the eventual electron transfer to Complex III (bc_1 complex).

2.1.5.1 Succinate oxidation and electron transfer

The succinate oxidation forms the first step in the catalytic cycle of SQR complex. After binding to the SdhA subunit, succinate is *trans*-hydrogenated to fumarate by (i) hydride ion (H^-) transferred from the methylene group ($-CH_2$) of one succinate molecule to the N5 position of the bound FAD (Fig. 5; N5 being at the tricyclic ring isoalloxazine) and (ii) proton transfer (H^+) from the other methylene group of succinate to an Arg side chain (Fig. 18) (Lancaster, 2003). As an alternative to the step (i), two electrons could be directly tunnelled together with one proton (Lancaster *et al.*, 2001). This conserved Arg (equivalent to SdhA-R282Th) is located at the capping domain sandwiched between the FAD binding domain. The fumarate formed leaves the binding site and the FAD is reduced to FADH₂. As FAD consists of the aromatic isoalloxazine ring, it is significantly more stable, with the consequent lower energy, than FADH₂. Accordingly, electrons are then readily transferred to the [Fe-S] clusters in order to attain a more stable state. As stated earlier, electrons then pass through the haem *b* (Section 2.1.2.3 Membrane anchors) before reaching the bound quinone molecule.

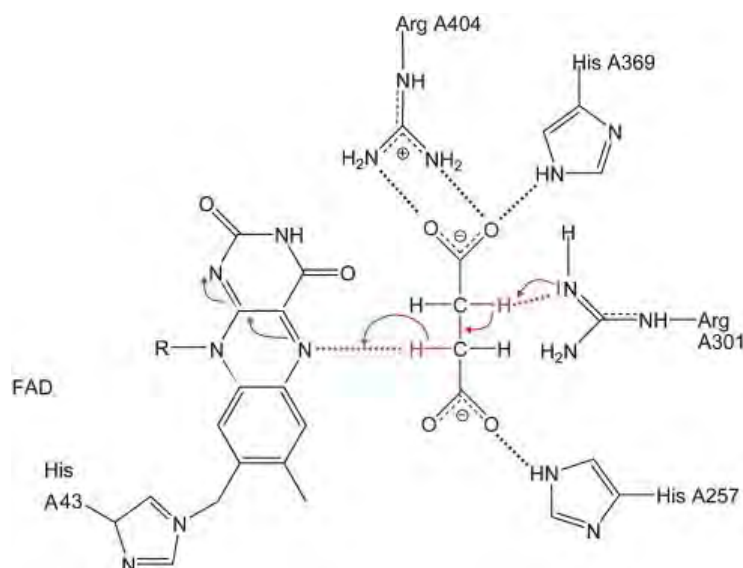


Fig. 18. Succinate oxidation. Figure taken from (Lancaster, 2003), itself modified from (Lancaster *et al.*, 2001) depicting fumarate reduction.

2.1.5.2 Quinone reduction

Quinone is reduced to quinol also as a two-electron reaction (Eq. 2; p. 15). The electrons from the [3Fe-4S] cluster or haem (see discussion above for the non-obligatory role of haem *b*) are used for this reaction. There are two conformations for the quinone binding termed the Q₁-site (located at the opening of Q-site) and a succinate oxidation-induced movement of the molecule into a second deeper site, Q₂. Much of the work resulted from the observed difference between UQ bound to *E. coli* SQR (PDB ID: 1NEK) and a Q-site inhibitor Atpenin A5 (AA5) bound to the same protein (PDB ID: 2ACZ) (Fig. 19). The rmsd of UQ in PDB ID: 1NEK and computationally-docked UQ is 2.8 Å (Horsefield *et al.*, 2006), the latter occupying a position similar to the crystallised AA5 at the Q₂-site.

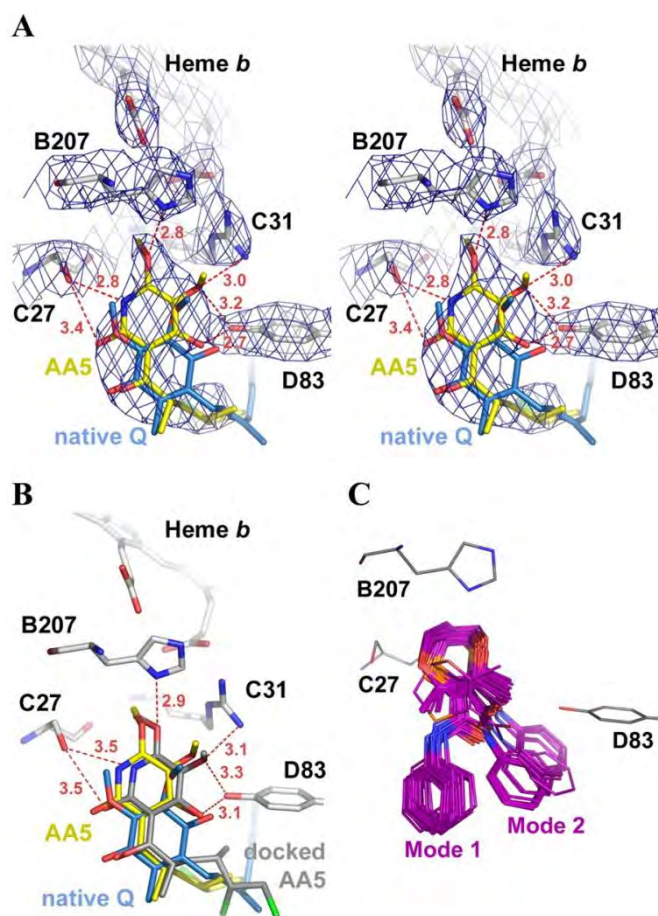


Fig. 19. Quinone binding sites in *E. coli* SQR. Both the Q₁ and Q₂ sites are shown, with a redox-induced movement of quinone initially bound at Q₁ into the Q₂ site. **(A)** Stereo view of SQR-AA5 complex (yellow; PDB ID: 2ACZ) indicating AA5 binding deeper than UQ in the native complex (blue; PDB ID: 1NEK). This is a $2F_o - F_c$ electron density map for the AA5 complex at 1.1σ . **(B)** Computational docking solution of AA5 (grey) by GOLD superimposed on native (blue) and AA5-bound (yellow) crystal structures. **(C)** Superimposed carboxin docking solutions with two alternative binding modes – 75 % in Mode 1 and 24 % in Mode 2 with one outlier. The key residues are labelled according to their positions in the respective subunits with protein-ligand interactions in red dotted lines. Figure taken from (Horsefield *et al.*, 2006).

Quinone binds readily to the enzyme complex prior to catalysis and its binding is not a rate-limiting step (Horsefield *et al.*, 2006). It is oriented at the Q₁-site through H-bonding between the O1 carbonyl of UQ and the SdhD-Y83^{EcSQR} and SdhB-W164^{EcSQR} (Fig. 20). Once electrons from succinate oxidation are present within the enzyme complex, the UQ is moved into the Q₂-site, H-bonding between the O4 carbonyl and SdhC-S27^{EcSQR}. This interaction might also be stabilised by further hydrogen bonds between the O3 methoxy group and SdhB-H207^{EcSQR}. By being at the receiving Q₂-site *prior* to electrons actually arriving there, a rate-limiting step is avoided.

After receiving the first electron, semiquinone (SQ) radical species is stabilised by the neighbouring residues. While waiting for the arrival of a second electron, the electron from SQ may also shuttle between itself and the nearby haem moiety, forming equilibrium (an electron sink). This evidently does not prevent ROS formation as both wild type and haem mutants produce the same amount of ROS (see above). The water molecule HOH39 coordinated by SdhB-H207^{EcSQR}, SdhC-R31^{EcSQR} and SdhD-D82^{EcSQR} donates two protons that subsequently disrupt H-bonding between UQ and SdhD-Y83^{EcSQR}, SdhC-S27^{EcSQR} and SdhB-H207^{EcSQR}, allowing the UQ to leave the protein complex (Horsefield *et al.*, 2006). The exact quinone redox mechanism is expected to vary not only between those utilising UQ and MK but also among the enzymes from different organisms. This is largely due to very specific, steric-imposed requirements and dissimilarities of their H-bonding to the respective Q-site (Maklashina *et al.*, 2006).

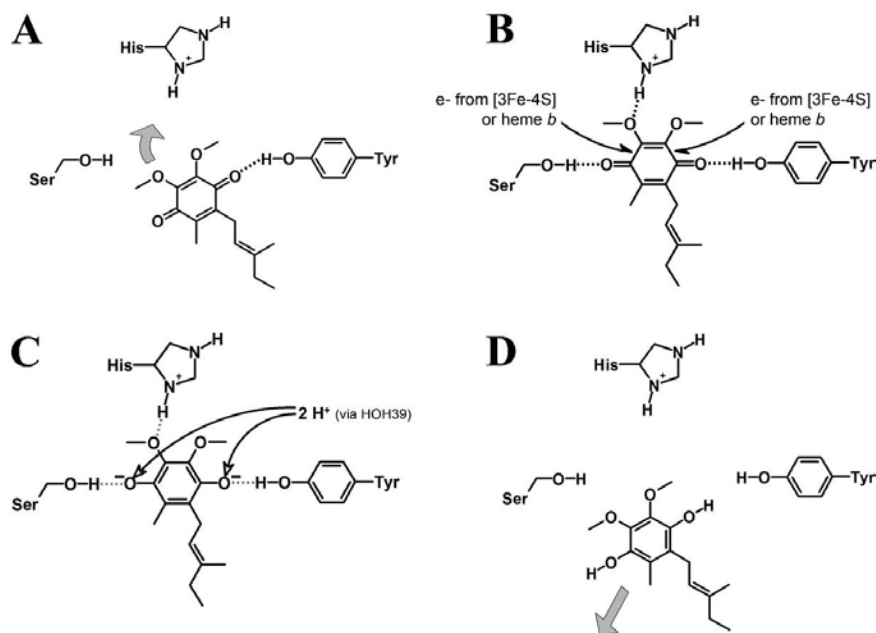


Fig. 20. Quinone reduction mechanism. (A) UQ binds at the Q_1 -site before catalysis through H-bonding (black dotted lines). (B) Redox-induced movement of UQ from Q_1 - to Q_2 -site [thick grey arrow in (A)] also stabilised by H-bonding. Two electrons are then transferred from [3Fe-4S] cluster and/or haem *b*. (C) Double protonation by water HOH39 of the phenolate dianion species formed from the two-electron reduction (B) via proton transfer pathway. (D) The protonation results in the disruption of H-bonding with SdhD-Y83^{EcSQR}, SdhC-S27^{EcSQR} and SdhB-H207^{EcSQR} (grey, dotted lines), allowing the UQH₂ to leave the Q-site (thick grey arrow). Electron and proton movements are shown by *half-black* and *full-white curly arrows*, respectively. Figure taken from (Horsefield *et al.*, 2006).

2.5.1.3 Overall proton and electron transfer

The two protons from succinate oxidation do not generally generate a transmembrane electrochemical potential Δp ⁷ as the succinate-quinone redox reaction occurs on the same side of the membrane (*i.e.* SQOR complexes are not proton pumps). This is certainly true for monohaem, Type C SQR such as the mitochondrial and *E. coli* SQR (Fig. 21a). For the haem-less *E. coli* QFR, where the reaction is reverse to that shown in Fig. 21b, protons from MKH₂ oxidation are released to the cytoplasmic space that is also the source for protons for fumarate reduction, leading to an electroneutral reaction.

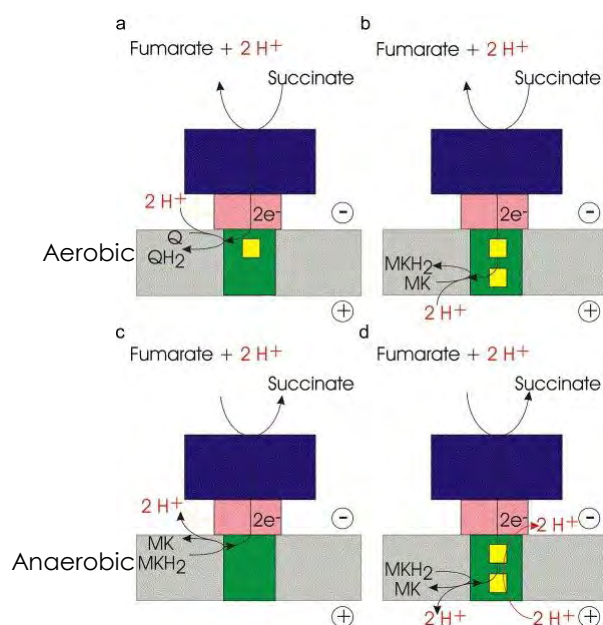


Fig. 21. Transmembrane proton transfer coupled to the electron transfer. The catalysis of Type C SQR such as mitochondrial and *E. coli* SQR (**a**) and Type D *E. coli* QFR (**b**) are electroneutral. (**c**) Types A and B enzymes utilise the transmembrane electrochemical potential Δp for catalysis. (**d**) The E-pathway for Type B QFR provides a compensatory transmembrane proton transfer. See text for details. Figure modified from (Lancaster, 2003).

⁷ $\Delta p = \Delta \Psi - Z\Delta pH$ where Δp = electrochemical proton gradient, $\Delta \Psi$ = membrane potential contributed by electrical potential difference (inside-outside), ΔpH = difference in proton concentrations and $Z = (RT \ln 10)/F$, R= molar gas constant, F= Faraday constant.

Nonetheless, two alternative scenarios are present for dihaem succinate:MK oxidoreductases and dihaem MK:fumarate oxidoreductases where the reactions are electrogenic and electroneutral, respectively. Succinate oxidation by MK is an endergonic reaction ($\Delta G > 0$; Table 5) driven by the Δp . The protons obtained from succinate oxidation are released back to the cytoplasmic space while the protons required for MK reduction comes originate from the periplasmic space; therefore, Δp is generated during the reverse reaction. That the Δp is required to support the succinate:MK oxidoreductase activity in dihaem SQR is evinced by the measurements on whole cells and isolated membrane of *B. subtilis* (Schnorpfeil *et al.*, 2001), and proteoliposome-reconstituted purified protein from *B. licheniformis* together with designed quinone analogues (Madej *et al.*, 2007). For the latter, reconstituted SQR does not exhibit MK analogue EMN (2-ethyl-3-methyl-1,4-naphthoquinone) reduction unless the protonophore CCCP (carbonyl cyanide *m*-chlorophenylhydrazone) is added (Madej *et al.*, 2007). Accordingly, the reverse reaction fumarate:MK oxidoreductase generates a Δp (Schnorpfeil *et al.*, 2001).

For dihaem MK:fumarate oxidoreductases (Fig. 21d), the reactions is electroneutral as protons consumed by fumarate reduction and released by MKH₂ oxidation into the periplasmic space are compensated by a transmembrane flow of two protons along the proton gradient together with transmembrane electron transfer. The ‘E-pathway hypothesis’ has been invoked to rationalise this observation, in which the transmembrane proton transfer pathway is only transiently open upon haem reduction (induced by the aforementioned transmembrane electron transfer) (Madej *et al.*, 2006). The transient opening prevents an uncoupling action of the fumarate reaction. Sequence alignment and the crystal structure indicate that the proton pathway consists of the ring C propionate of haem *b*_D (haem farthest from the [3Fe-4S] cluster) and FrdC-E180^{Ws}; this Glu residue is conserved in ϵ -proteobacteria dihaem QFR such as *W. succinogenes*, *C. jejuni* and *H. pylori* (Fig. 22) (Madej *et al.*, 2006). Mutation of the Glu to Gln results in an electrogenic reaction due to the impairment of the proton pathway, as shown in Fig. 23.

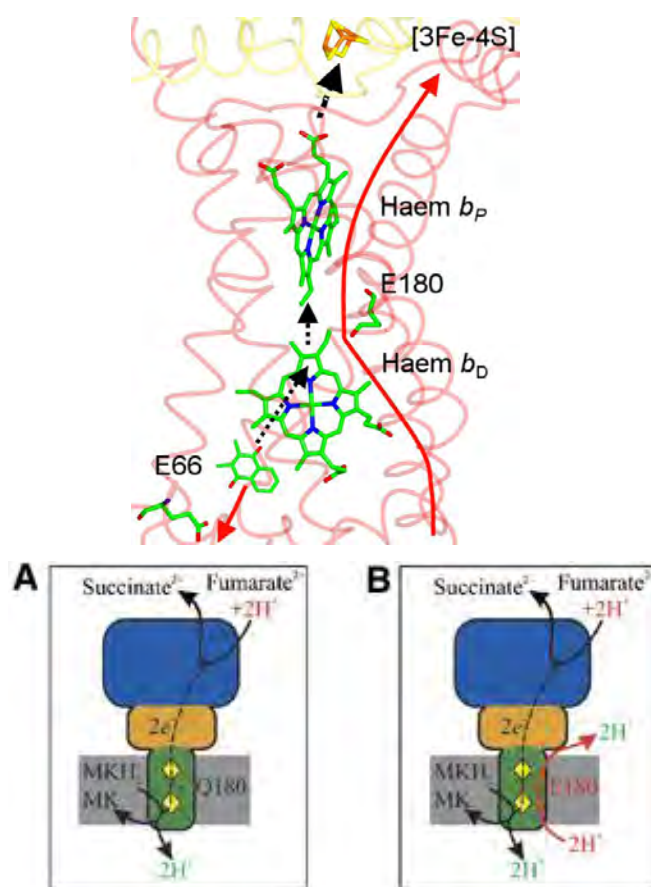


Fig. 23. Proposed E-pathway operating in the *W. succinogenes* dihaem QFR. **(Top)** Two electrons from MKH_2 oxidation travel through the haem moieties and the $[\text{3Fe-4S}]$ cluster (black dotted arrows) while two protons are released via FrdC-E66^{Ws} (red arrows). Two protons compensate the electron transfer, travelling via the ring C propionate of haem b_D and FrdC-E180^{Ws}. For clarity, MKH_2 is not labelled but is readily identifiable by the two phenol rings. Residue E180 possesses two alternate configurations, both with occupancy 0.5. Figure redrawn with CCP4mg from (Lancaster, 2002). **(Bottom)** Electrogenic and electroneutral catalysis of E180Q mutant (A) and wild type (B) enzyme. The constituent subunits A, B and C are in blue, orange and green, respectively, with haem as yellow diamonds. Protons used for fumarate reduction are in red while those released from MKH_2 oxidation are in green. These are assumed to be bulk solvent-based protons although they can be equally transported along the protein surface from the exit sites to the entry sites (Mulکیدjianian *et al.*, 2006). Figure adapted from (Madej *et al.*, 2006).

2.1.6 Crystallographic and spectroscopic investigations into Complex II to date

The crystal structures of both SQR and QFR from various organisms have been crystallised using exclusively the vapour diffusion method. Whether it is possible to use the lipidic cubic phase and/or bicelle method to crystallise membrane proteins with a huge proportion of soluble domain, such as is the case with Complex II, remains to be seen. The designed lipid for *caa*₃-oxidase crystallisation (Chapter 3) proves that a rational design is feasible and essential as an alternative to the detergent-based vapour diffusion method.

Spectroscopic studies into Complex II lags behind that of cytochrome oxidases and other haem proteins mainly due to a lack of photodissociable ligand. The haem moiety(-ies) does not bind external ligands such as CO. Nevertheless, FTIR difference spectroscopy has been used for *W. succinogenes* QFR wild type comparison against mutants (Haas *et al.*, 2005). For a more detailed mechanistic view, time-resolved FTIR and RR as well as ultrafast visible spectroscopy remain valuable but unreachable techniques.

2.1.7 Activity measurements

As mentioned above, SQR and QFR can catalyse both reactions *in vitro*. There are four types of activity assays for their catalysis – succinate dehydrogenase, fumarate reductase, succinate:quinone oxidoreductase and quinone:fumarate oxidoreductase assays; the last two are total activities and dependent on the membrane anchor subunit(s). Details of these are presented below while the redox potential of the listed compounds can be found in (Lemma *et al.*, 1990; Lancaster, 2004). Initially, it was found that the as-isolated protein complex was not fully active. Various treatments were performed as activation steps, all resulting in the removal of oxaloacetate bound tightly at the succinate binding site.

2.1.7.1 Succinate dehydrogenase

The succinate dehydrogenase activity can be monitored colourimetrically by using 5-N-methyl phenazonium sulphate (PMS), Wursters blue (the blue-coloured radical cation of the colourless *N,N,N',N'*-tetramethyl-*p*-phenylenediamine; TMPD), 2,6-dichlorophenol-indophenol (DCPIP), methylene blue or ferricyanide as the primary electron acceptors. For the *T. thermophilus* SQR, the reaction conditions have been described elsewhere (Kolaj-Robin *et al.*, 2011, accepted).

2.1.7.2 Succinate:quinone reductase

The electron acceptor for the succinate:quinone reductase are generally water-soluble quinone including 2,3-dimethyl-1,4-naphthoquinone (DMN), 2-methyl-1,4-naphthoquinone (menadione), 1,4-naphthoquinone, 2,3,5,6-tetramethyl-1,4-benzoquinone (duroquinone) or 2,3-dimethoxy-5-methyl-1,4-benzoquinone (Q₀). This assay is performed under an anaerobic condition created by the addition of glucose and commercially-available glucose oxidase-catalase mixture (Tran *et al.*, 2006), and absorbance decrease monitored at 410 nm (peak haem absorbance in oxidised state) (Tran *et al.*, 2006), 278 nm (UQ1) (Kita *et al.*, 1989) or 600 nm (UQ2 or DBH, 2,6-dichlorophenolindophenol) (Hatefi, 1978).

2.1.7.3 Fumarate reductase

This reaction is opposite to that of succinate dehydrogenase and is measured using reduced benzyl viologen (Uden and Kröger, 1986).

2.1.7.4 Quinol:fumarate reductase

The quinol:fumarate reductase activity can be determined under anoxic conditions using reduced MK-analogue DMN (DMNH₂), which can be obtained using either (i) the reducing agent sodium borohydride NaBH₄ or (ii) the coupled reaction of rat liver DT-diaphorase (EC 1.6.99.2) and NADH. The details of these reactions are well-described in the literature (Mileni *et al.*, 2006).

2.2 SUMMARY OF PUBLISHED WORK

This section summarises the work presented in (Kolaj-Robin *et al.*, accepted) (**Paper I**). Three variants of recombinant *T. thermophilus* Complex II were produced homologously to study the enzyme properties upon the addition of His-tag at different locations.

2.2.1 Materials and Methods

The recombinant proteins were overexpressed and purified according to the published methods (Kolaj-Robin *et al.*, accepted) (**Paper I**). Briefly, His-tag was added at the N- and C-termini of SdhB subunit (rCII-His₈-SdhB and rCII-SdhB-His₆) by standard PCR. For comparison with native enzyme, the entire *sdhCDAB* gene sequences were amplified and cloned into the expression plasmid vector (pDM12, containing *T. thermophilus bc* complex promoter for constitutive expression) without the addition of any tag (wt-rCII). Protein samples for recombinant His-tagged variants were performed using nickel IMAC, TMAE anion exchange and gel filtration chromatographic steps while the untagged rCII with the classical anion exchange, gel filtration and hydroxyapatite steps. Oligomerisation states were assessed with BN-PAGE and analytical gel filtration chromatography as detailed in (Kolaj-Robin *et al.*, accepted).

2.2.2 Results and Discussion

Fig. 24 below demonstrates that the C-terminal region of SdhB subunit plays a key role in the trimerisation of Complex II.

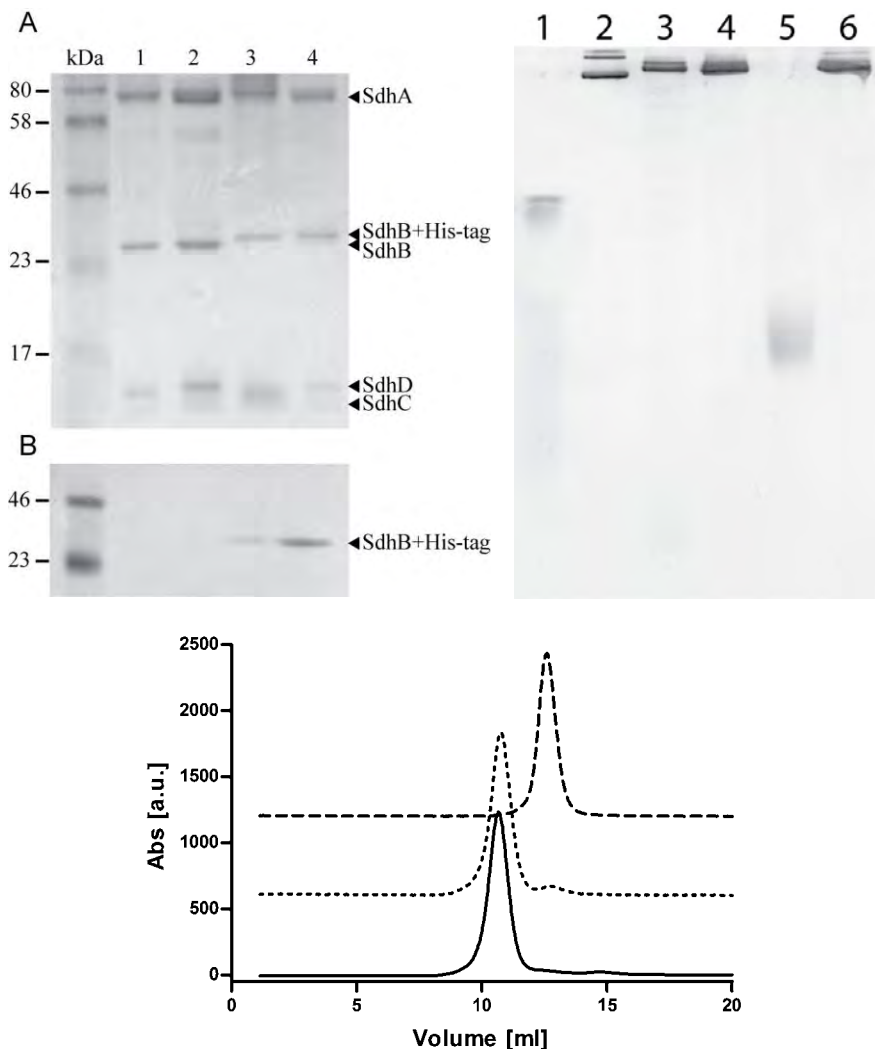


Fig. 24. Oligomerisation states of recombinant Complex II variants. (Top left) The SDS-PAGE (A) of the recombinant variants indicates high sample purity and intact His-tags (B). Lanes 1, native complex; 2, wt-rCII, 3, rCII-SdhB-His₆; 4, rCII-His₈-SdhB. The addition of C-terminal tag on the SdhB subunit abolishes trimerisation as shown by the BN-PAGE (top right) and analytical gel filtration chromatography (bottom). Lanes 1, β -amylase (200 kDa); 2, apoferritin monomer (443 kDa) and dimer (886 kDa); 3, native Complex II; 4, wt-rCII, 5, rCII-SdhB-His₆; 6, rCII-His₈-SdhB. Gel filtration chromatogram (-), wt-rCII; (- - -), rCII-SdhB-His₆; (...), rCII-His₈-SdhB. Figures taken from (Kolaj-Robin *et al.*, accepted).

For the first time, a synthetic monomeric Complex II has been generated. Moreover, it is functional based on succinate dehydrogenase activity but does not display the positive cooperativity effect seen with the native and recombinant wild type complexes. The monomer also displays a significantly reduced thermostability as characterised by circular dichroism (work performed by Olga Kolaj-Robin) and does not crystallise (see Section 2.3.2 Crystallography below). These two observations point to the stabilising property of trimeric assembly although it is not required for function.

The positive cooperativity in the succinate dehydrogenase catalysis of *T. thermophilus* Complex II has equivalent counterparts neither within the SQOR superfamily nor in other known respiratory complexes. The classical example of such an effect in haem proteins is the cooperative oxygen binding to the tetrameric haemoglobin [see (Cui and Karplus, 2008) and references therein]. It is tempting to suggest that this forms an adaptation to the stress of living at high temperatures.

2.3 UNPUBLISHED WORK

Further studies were performed on the recombinant Complex II to generate a site-directed mutagenesis system to understand the role of key residues involved in catalysis. The purified variants described in Section 2.2 Summary of Published Work, together with additional variants, were also subjected to crystallisation attempts as described below.

2.3.1 Generation of mutagenesis system

2.3.1.1 Materials and Methods

TEV protease recognition site (residues ENLYFQG) was added to the C-terminus of SdhB subunit using the PCR primer pairs as listed in Table 7. For the generation of recombinant protein rCII-TEV-His₆, primers CIIFor (Kolaj-Robin *et al.*, accepted) (**Paper I**) and SdhBTEVHisNotI were used with the wt-rCII plasmid template, and cloned into pDM12 at the NdeI/NotI restriction sites. The N-terminal His-tagged and C-terminal TEV site for rCII-His₈-SdhB-TEV10 and rCII-His₈-SdhB-TEV43 variants were generated by PCR with the primer pairs CIIFor and either SdhBTEV10NotI or SdhBTEV43NotI, respectively, on the rCII-His₈-SdhB template. The codons for the TEV site were optimised based on *T. thermophilus* codon usage obtained from <http://www.kazusa.or.jp/codon/> (Nakamura *et al.*, 2000). The cells were grown and the proteins purified using nickel IMAC and gel filtration chromatography as detailed before (Kolaj-Robin *et al.*, accepted) (**Paper I**). Two microliters of TEV protease (at a concentration of 10 mg/ml; a gift from David Russell) was added to 100 µl of protein (at 2 mg/ml) together with 1 mM DTT and 0.5 mM EDTA in the protein buffer [50 mM Tris-HCl pH 7.6, 0.025 % *n*-dodecyl-β-D-maltopyranoside (DDM)] prior to incubation at room temperature for ~ 3 h. The TEV cleavage reaction was then diluted to 250 µl prior to loading on Superdex 200 10/300 gel filtration column.

Table 7. Primer sequences for Complex II. The NotI restriction sites are **bolded**, His-tag is underlined and TEV recognition sites double underlined.

Primer name	Sequence (5' – 3')
SdhBTEVHisNotI	ATAAGAAT GCGGCCGC TTA <u>ATGATGATGATGATGATG</u> <u>CCCCTGGAAGTAGAGGTTCTC</u> CGCCCGCTTGACCTCTTCTA
SdhBTEV10NotI	GAAT GCGGCCGC TTA <u>CCCCTGGAAGTAGAGGTTCTC</u> CGCCCGCTTGACCT
SdhBTEV43NotI	GAAT GCGGCCGC TTA <u>CCCCTGGAAGTAGAGGTTCTC</u> CATGAGGATCGCCC

2.3.1.2 Results and Discussion

The different constructs made in this study are illustrated in Fig. 25. Of the five recombinant variants, only two were trimers by design. The rationale for the generation of monomeric rCII-SdhB-His₆ was to study the role of trimerisation for activity, stability and propensity to crystallise. Given that the *sdhCDAB* operon in Complex II cannot be deleted [work by Sarah O’Kane, (O’Kane, 2011)] and that purification of N-terminal tagged rCII-His₈-SdhB results in trimeric recombinant *and* native SdhB (see 2.2.2 Results and Discussion), a novel approach was taken to produce monomeric enzyme similar to rCII-SdhB-His₆ and trimerised *in vitro* after TEV protease cleavage (rCII-SdhB-TEV-His₆; Fig. 25). The first construct designed should yield a C-terminal region that is exactly the same length as native SdhB and should trimerise. However, repeated purification failed to purify the complex even though it was expressed in the cell. This could be attributed to the inherent instability of an excessively long C-terminal region in the SdhB subunit; the circular dichroism results of rCII-SdhB-His₆ already indicate that the monomeric enzyme has a significantly reduced thermostability.

Hence, two further constructs (rCII-His₈-SdhB-TEV10 and rCII-His₈-SdhB-TEV43) were made by placing a non-cleavable His-tag at the N-terminus and a TEV protease recognition site at the C-terminus. The rationale was to generate monomeric protein complexes which, upon cleavage, would yield trimeric complexes. In the former construct, the TEV site results in only one extra residue relative to native sequence and shortened to native-length upon cleavage. It was hypothesised that the addition of one residue would disrupt trimer formation. In parallel, the latter construct (rCII-His₈-SdhB-TEV43) was also made in case one extra C-terminal residue is not sufficient to disrupt trimerisation. This has four extra residues and would leave three after TEV protease cleavage.

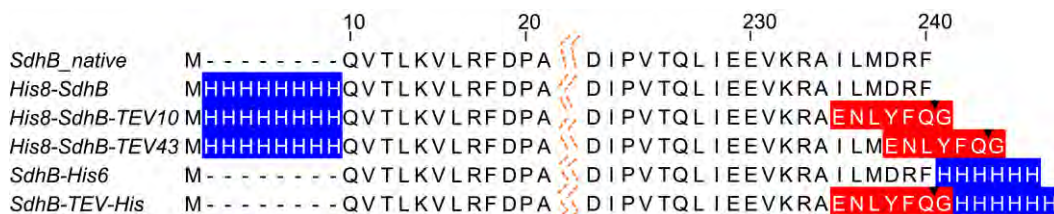


Fig. 25. Multiple sequence alignment of recombinant Complex II variants. The His-tags are shaded blue and the TEV protease recognition sites are red. The cleavage sites are indicated by black triangles. The wt-rCII variant is not shown as it has a protein sequence identical to that of native.

While both proteins could be purified as monomers (Figs. 26 and 27), the TEV cleavage reactions of purified proteins did not result in the conversion of monomers to trimers. There are two possibilities – (i) TEV protease could not access the site and, hence, no cleavage occurs, or (ii) certain assembly factor(s) is required. Both possibilities would require further investigations including C-terminal protein sequencing and cell-free protein synthesis (Uzawa *et al.*, 2002, 2003) and cleavage. Whether the latter would actually be fruitful and yield milligram amounts of protein could only be confirmed by further experiments. A possible workaround for this could be an antisense RNA-based approach (Moreno *et al.*, 2004) to silence the expression of native complex (by *in vivo* production of antisense RNA complementary to DNA sequence between the end of SdhA and beginning of SdhB). As the recombinant trimeric rCII-His₈-SdhB has residues

MHHHHHHHQVTL at the N-terminus of SdhB subunit while native has MQVTL, theoretically only the native one should be suppressed. This potentially requires two further components – (i) a single-copy plasmid replicable in *T. thermophilus* with the *Complex II* promoter, and (ii) this particular plasmid must have an origin of replication compatible with the pDM12 (*i.e.* two different origins). Although such a single-copy plasmid is yet to be described for this bacterium, the origin of replication problem could be solved by using the natural plasmids from the two recently-sequenced strains *T. thermophilus* JL18 (plasmids pTTJL1801 and pTTJL1802) and SG0.5JP17-16 (pTHTHE1601).

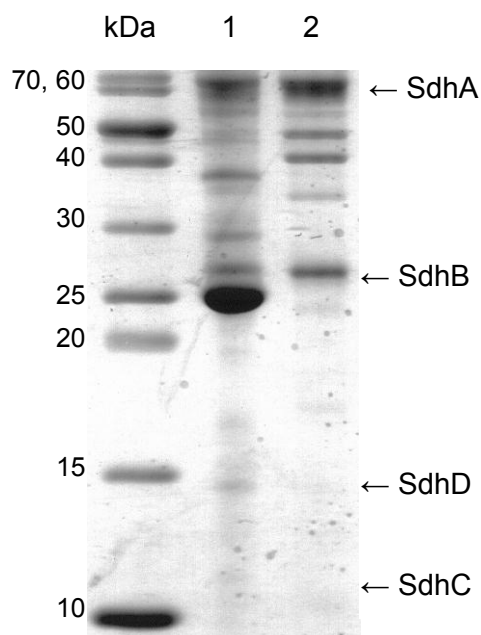


Fig. 26. SDS-PAGE of recombinant Complex II with TEV protease sites. The samples [rCII-His₈-SdhB-TEV10 (**1**) and rCII-His₈-SdhB-TEV43 (**2**)] were run on a 16 % gel.

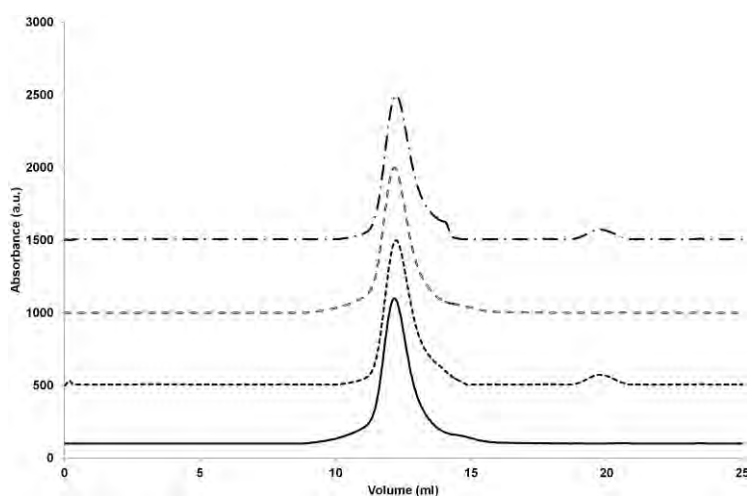


Fig. 27. Gel filtration chromatograms of recombinant Complex II with TEV sites. Absorbance was monitored at 280 nm. All forms, before and after incubation with TEV protease [rCII-His₈-SdhB-TEV10 (—); rCII-His₈-SdhB-TEV10 post-incubation (---); rCII-His₈-SdhB-TEV43 (– –); rCII-His₈-SdhB-TEV43 (– . –)], eluted at similar volumes consistent with the established volume of monomeric form rCII-SdhB-His₆ (Fig. 24). Minor peaks eluting at 19 ml represent the TEV protease present in the samples.

2.3.2 Crystallography

2.3.2.1 Materials and Methods

Protein samples of wild type untagged complex (wt-rCII) were concentrated to 10 mg/ml in 10 mM Tris-HCl pH 7.6, 0.025 % DDM. Initial optimisations were performed in CrysChem plates by mixing 0.5 μ l protein at a concentration of 4 mg/ml with 0.4 μ l of 0.1 M sodium acetate pH 4.6, 4 % PEG 4000 and 0.1 μ l of 1 M lithium sulphate; the reservoir was 300 μ l. The sodium acetate was adjusted to pH 4.6 by adding HCl to the 1 M stock at room temperature as per the method used in the preparation by the manufacturer. PEG 4000 was later changed to PEG 3350 and protein concentration to 3.5 mg/ml to reduce nucleation. PEG 3350 has a reduced polydispersity and a higher stability (lower “aging effect” in terms of pH changes) than PEG 4000 and has, therefore, been reported to typically yield better diffracting crystals (Bob Cudney, Hampton Research, personal communication).

Detergent screening was made through a mixed micelle approach with Hampton Detergent Screens 1-3. The supplied detergent solutions were diluted to twice the CMC in 10 mM Tris-HCl pH 7.6 in PCR tubes. To this, the concentrated protein at 10 mg/ml was added to a final concentration of 2.5 mg/ml. As the stock protein contains 0.025 % DDM (twice the CMC), this dilution also reduces the DDM concentration to below 1 CMC, ensuring that the protein is supported by a mixture of DDM and the second screened detergent. The entire mixture was then incubated at 4 °C with gentle rocking.

A novel approach through *in situ* diffraction was used to study the diffraction properties as membrane protein crystals are often fragile. Crystallisation drops were setup in the Crystal QuickX plate as 0.5 μ l mixture of protein, precipitant and lithium sulphate with 40- μ l reservoirs. These drop volumes are at the upper limit of the plate but were found necessary to prevent the drops from drying. Using the unique setup at the PXIII (X06DA) (Swiss Light Source, Switzerland) (Bingel-Erlenmeyer *et al.*, 2011), the plates were subjected to X-ray diffraction

(beam size of 80 μm x 45 μm , wavelength 1.0000 \AA , 100 % transmission, 1 s exposure).

For further trials and data collection, detergent exchange was performed on concentrators by first diluting the stock protein with 10 mM Tris-HCl pH 7.6 and twice the CMC of the three detergents, concentrating the protein to 2.5 mg/ml, re-diluting and re-concentrating to a total of three times. Drops were setup on CrysChem plates as both ‘concentrator-exchanged detergent’ and mixed micelle approaches prior to testing at the I24 microfocuss beamline (Diamond Light Source, UK). Cryoprotectants used were paraffin oil, PEG 600, ethylene glycol and sucrose. The cryoprotectants were added to the drop before the crystals were harvested using 0.1 mm nylon loop (Hampton) and frozen using the nitrogen cryostream. Diffraction tests were performed using 100 % transmission at 0.96860 \AA , 10 μm x 10 μm beam, 1 s exposure, 0.2 $^\circ$ oscillation with PILATUS 6M detector.

2.3.2.2 Results and Discussion

The *T. thermophilus* native Complex II crystals were initially found as a hit in Hampton Crystal Screen (0.1 M sodium acetate trihydrate pH 4.6, 8 % PEG 4000), Crystal Screen Lite (0.1 M sodium acetate trihydrate pH 4.6, 4 % PEG 4000) and MembFac (0.1 M sodium acetate trihydrate pH 4.6, 0.1 M sodium chloride, 12 % 2-propanol) at a protein concentration of 15 mg/ml in sitting-drop vapour diffusion method in CrysChem plates. Lithium sulphate was added to a final concentration of 0.1 M to produce larger and well-shaped crystals, which diffracted to an 8- \AA resolution using home source radiation. These work was performed by Sarah O’Kane (O’Kane, 2011). As this resolution was too poor, recombinant complexes were subjected to crystallisation trials as this provided a more controlled purification protocol.

The recombinant trimeric His-tagged protein (rCII-His₈-SdhB) reproducibly crystallised as microcrystals about 5-10 times smaller than the untagged variant in the same condition. This persisted even after reducing precipitant condition to 0.5 % PEG 3350 and performing a fine pH screening (3.6 to 5.6 in sodium acetate

buffer), possibly a consequence of the unavoidable microheterogeneity where a mixture of native subunits form the biological assembly together with recombinant subunits (see 2.2.2 Results and Discussion). In contrast, the monomeric protein (rCII-SdhB-His₆) crystallised neither in the native condition nor in the *de novo* screening. Furthermore, crystal sizes of both rCII-His₈-SdhB and wt-rCII could not be increased by micro- and macro-seeding or by layering the precipitant solution with a mixture of silicone and paraffin oils (Chayen, 1997). Hence, only the crystallisation of untagged variant was pursued.

Of the various conditions tested through *in situ* diffraction (a panel of 72 detergents), only a subset of three detergents [undecylmaltoside (UDM), sucrose monolaureate and Deoxy Big Chap] showed promising weak diffractions to ~ 5 Å. Detergent-dependent diffraction properties is typical for membrane proteins. Of these three, only crystals grown with UDM as the detergent and cryoprotected with 25 % PEG 600 resulted in the strong 3.8-Å diffraction when the crystals were tested at the Diamond microfocus beamline I24 (Fig. 28). Several differences can be noted between the native and recombinant crystals – (i) the size of the latter (50-100 µm x 30-50 µm) was almost half of the native, (ii) lithium sulphate converted spherulites to crystals, not making them bigger, (iii) small crystals were obtained at about 2 % PEG 3350 with larger ones at 4 % PEG 3350 at a protein concentration of 2-3 mg/ml in contrast to 15 mg/ml of native complex and, (iv) diffraction was at 3.8 Å resolution using synchrotron source. With the exception of diffraction, these differences are not easily reconcilable as both native and wt-rCII have exactly the same sequence.

Indexing of the frames with XDS (Kabsch, 2010) originally showed that the space group is *P* 1, although phenix.xtriage (Adams *et al.*, 2010) reported possible twinning. Automated twinning analysis then indicated that the space group could be either *P* 1 2 1 or *P* 1 2₁ 1 (Fig. 28). A solvent content of 60.83 % was estimated, although it should be noted that solvent content determined for membrane proteins could be misleading due to the nature of detergent molecules in that they are not in a micellar form. The relatively high solvent content also suggests possible further diffraction improvement by crystal dehydration.

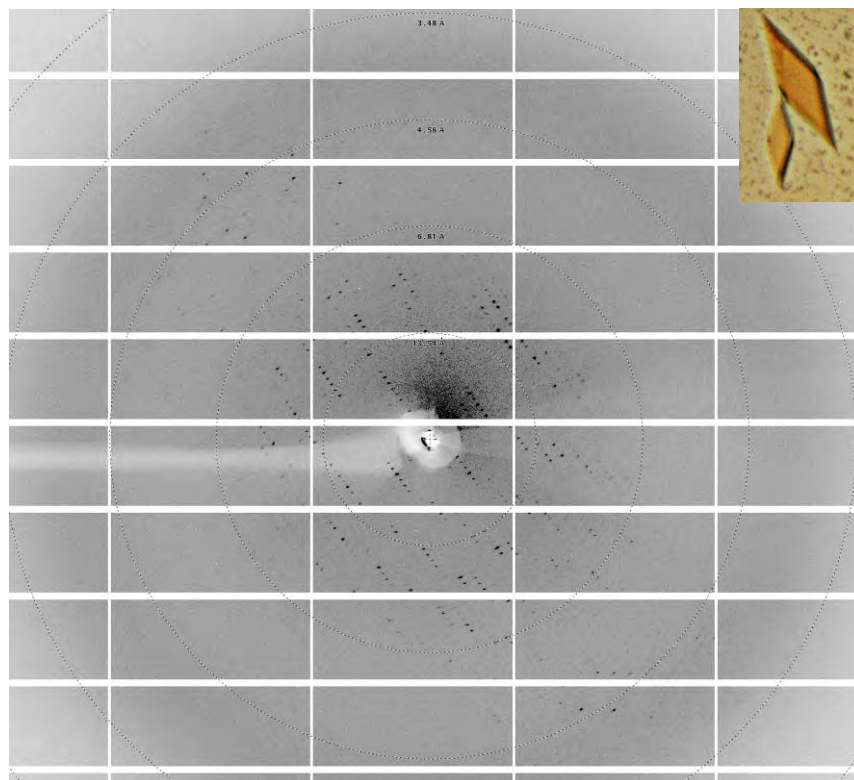


Fig. 28. Diffraction image of recombinant Complex II. The diffraction from the crystals (inset), recorded at Diamond I24, was slightly anisotropic (3.8 Å to 4.2 Å).

Table 8. Preliminary crystallographic analysis of Complex II crystals. A single molecule is considered to be a trimer of heterotetramers based on gel filtration and electrophoretic data presented above. asu, asymmetric unit.

Resolution range	50.3 - 3.8 Å
Space group	$P 1 2 1$ or $P 1 2_1 1$
Unit cell parameters	$a = 155.75 \text{ \AA}$, $b = 56.262 \text{ \AA}$, $c = 265.199 \text{ \AA}$, $\alpha = 90^\circ$, $\beta = 103.251^\circ$, $\gamma = 90^\circ$
Solvent content	60.83 %
No. of molecules in asu	1 (assuming physiological trimer as one)

2.4 CONCLUSION

The generation of synthetic monomeric enzyme has allowed the functional dissection of the role of trimer of Complex II in its thermostability as well as showing that the temperature-dependent positive cooperativity towards substrate succinate is a property exclusive to the trimeric variants. Surprisingly, the ability to generate recombinant protein complex even without including the redox cofactor biosynthesis genes indicate their supstoichiometric productions by the organism. However, the failure of recombinant Complex II to be cleaved and changed from monomer to trimer *in vitro* hampers further investigations from being undertaken with site-directed mutagenesis approach. The strategy of silencing native complex from being expressed through antisense RNA seems the only possibility given that the genetic deletion of the complex was not successful (O’Kane, 2011).

In terms of crystallography, the diffraction to 3.8 Å is interesting, although further optimisations is unquestionably required. At this point, these would be cryoprotectant screening, *in stilla* improvements such as annealing and dehydration (Kiefersauer *et al.*, 2000; Newman, 2006) and lipid-based methods. For the latter, sponge phase crystallisation is a promising avenue for better diffraction compared to the stiff cubic phase with smaller aqueous pores. In fact, *B. subtilis* Complex II (SQR) crystals have been obtained this way (Wöhri *et al.*, 2008), although no diffraction results were reported.

CHAPTER 3
CYTOCHROME C OXIDASES

3.1 INTRODUCTION

As summarised in Section 1.1.4 Complex IV – Cytochrome *c* oxidase, CcO is responsible to finally transfer the electrons to oxygen with the concomitant production of water. The three-dimensional structures of the different types of haem-copper oxidases are now available (Table 9), and shows a large structural conservation throughout evolution even when adaptations were made to accommodate the particular requirement of specific organisms. Within the same organism, the terminal oxidases of *T. thermophilus* exhibit similar subunit compositions and the presence of large oxygen cavities. An extensive discussion of both oxidases has been published previously (Noor and Soulimane, 2012) **(Paper II)**.

There are four components making up the structure and function of CcO – electron acceptance from cytochrome *c*, proton pumping, oxygen entrance and finally water exit. The classical oxidases accept electrons from soluble carriers. For charge compensation required for oxygen reduction as well as generation of transmembrane proton gradient, cytoplasmic protons are usually taken up *via* two established pathways – the D- and K-pathways, each named after the starting residues Asp and Lys, respectively. The molecular oxygen enters a dedicated channel to eventually reach the heterodinuclear centre (dnc) haem a_3 -Cu_B. The channel, being hydrophobic, naturally repels the formed water from the oxidase complex. Nonetheless, deviations from this general overview are known to occur including intact cytochrome *c* domains forming part of the complex, non-conserved proton pathways and altered oxygen channels (Fig. 29).

Table 9. Available three-dimensional structures of haem-copper oxidases. No structure is available yet for *bd*-type QOX. ¹ Unpublished result from DM-grown crystals (T. Soulimane). All A1-type structurally-known complexes are of *aa*₃-type, while A2- and B-types are from *T. thermophilus*. LCP structures of *ba*₃-oxidase was obtained with MO as the hosting lipid whereas 7.7 monoacylglycerol for the *caa*₃-oxidase. Abbreviations: DM, decylmaltoside, OG, octylglucoside; su, subunits; VD, vapour diffusion; LCP, lipidic cubic phase.

	A1		A2	B	C	QOX	
	<i>P. denitrificans</i>	<i>R. sphaeroides</i>	Bovine	<i>caa</i> ₃	<i>ba</i> ₃	<i>P. stutzeri cbb</i> ₃	<i>E. coli</i>
PDB	1AR1 (2 su) 1QLE (4 su)	1M56	1OCC	2YEV	1EHK 3S8F	3MK7	1FFT
Crystallisation condition	VD with antibody UDM (2 su), DDM (4 su)	VD in DM+DDM	DM	LCP VD ¹	VD LCP	VD in UDM+ DDM+ decanoylsucrose	VD in OG
Resolution (Å)	2.7 (2 su) 3.0 (4 su)	2.3/2.8 (anisotropic)	2.8	2.36 3.8	2.4 1.8	3.2	3.5

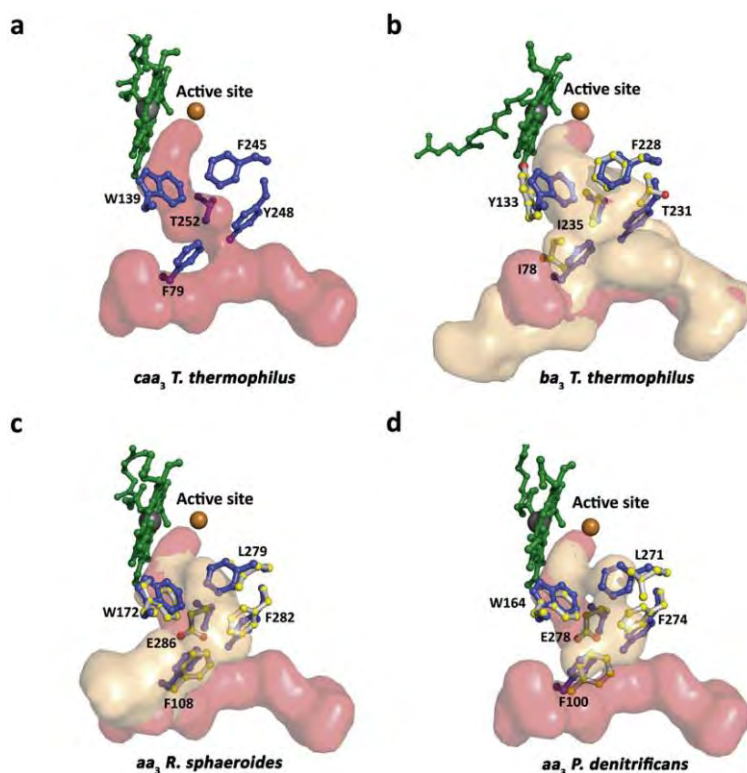


Fig. 29. Oxygen channels in Types A and B CcO. The channels were calculated using the structures of *T. thermophilus* *caa*₃- (a) and *ba*₃-oxidases (b), and *R. sphaeroides* (c) and *P. denitrificans* (d) *aa*₃-oxidases. For a clearer comparison, the *caa*₃-oxidase channel (red) was superposed in the panels b-d with those of the other oxidases (cream). Lining the cavities are hydrophobic residues depicted in ball and stick and numbered accordingly with *caa*₃-oxidase residues in blue. Figure taken from (Lyons *et al.*, 2012).

Physiologically, CcO are functional monomers although there is an ambivalence for eukaryotic oxidases; the bovine oxidase crystallises as a dimer while the shark oxidase is monomeric (Georgevich *et al.*, 1983; Suarez *et al.*, 1984; Robinson and Talbert, 1986). This stems mainly from the crystal structure of bovine enzyme where there is an axis of symmetry between two molecules perpendicular to the membrane (Fig. 30 *cf.* *caa*₃-oxidase). Whether this reflects a physiological assembly or is merely a crystallographic dimer is not entirely clear as the monomeric form retains oxygen reduction and proton pumping activities [see (Sadoski *et al.*, 2001) and references therein]. Nevertheless, the reduction rate of compound F ($\text{Fe}^{4+}=\text{O}^{2-}$; Cu_B^{2+}) from P ($\text{Fe}^{3+}-\text{O}-\text{O}^{2-}$; Cu_B^{2+}) is significantly faster in the monomeric form.

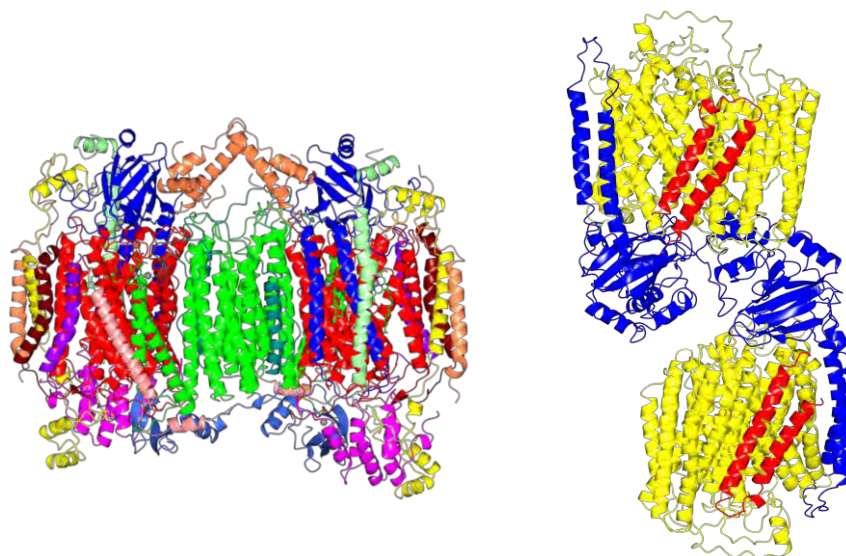


Fig. 30. Crystallographic assemblies of two Type A oxidases. The dimeric assembly of bovine oxidase (**left**) has an axis of symmetry perpendicular to the membrane clearly in contrast to that of *caa3*-oxidase with the axis being parallel to the membrane (**right**). Figures generated using PDB ID: 1OCC and 2YEV with CCP4mg (Potterton *et al.*, 2004).

3.1.1 Classification

Haem-copper oxidases are classified into three families based on sequence conservation in the proton translocation pathway - A, B and C (Pereira *et al.*, 2008). The first is split into Types A1 and A2 based on whether the key residue in the D-pathway GluI-279^{P, 8} (Fig. 31 and detailed in 3.1.2 Subunit I) is present. The Type B oxidases do not have the D-pathway with a modified K-pathway being responsible for all proton translocation. The *cbb3*-oxidases are the exclusive example of Type C with even less conservation of the K-pathway. Correspondingly, the *T. thermophilus caa3*- and *ba3*-oxidases belong to Type A2 and B, respectively. Both *T. thermophilus* oxidases display peculiar features – (i) in *caa3*-oxidase, the Glu is replaced by a Tyr-Ser pair, and (ii) in *ba3*-oxidase, no D-pathway is present with a K-analogue pathway being responsible for all proton translocation (Chang *et al.*, 2009). The modification of proton pathways relates

⁸ Unless otherwise stated, all numberings are based on the *T. thermophilus* sequences. Superscripts denote the species-specific numberings; P, *Paracoccus denitrificans*; R, *Rhodobacter sphaeroides*; B, bovine heart.

directly to their translocation efficiencies and affinity towards oxygen. Comparing the Types A and B, the efficiency of *caa*₃-oxidase is 1 H⁺ pumped/e⁻ transferred vs. 0.5 for *ba*₃-oxidase with the latter displaying a higher oxygen affinity with an enlarged and bifurcated oxygen channel (Fig. 29).

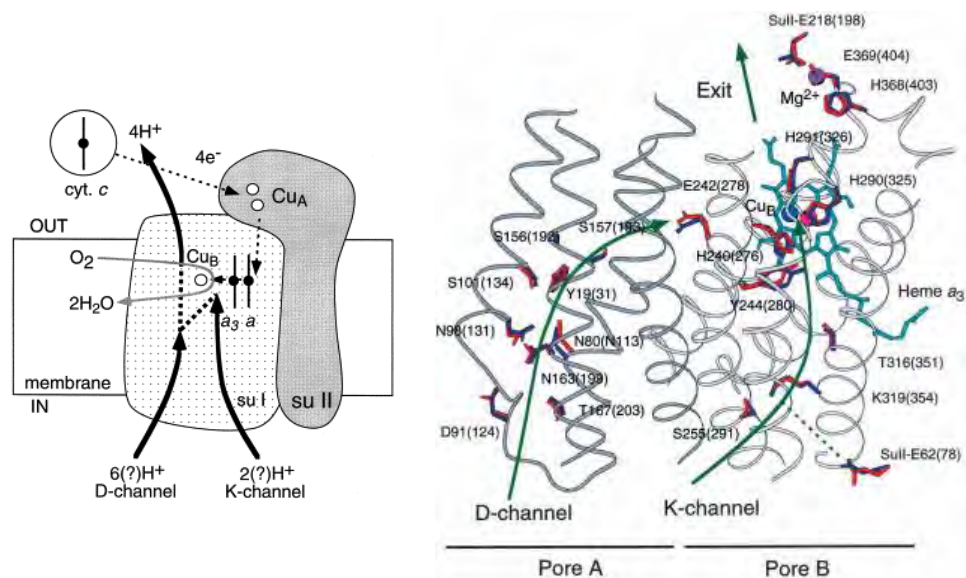


Fig. 31. Proton pumping pathways in CcO. A schematic drawing of the catalytic subunits I and II illustrates the relative positions of the redox centres (**left**) with thick arrows for the proton pumping pathways and dotted for the electron transfer pathway. The D- and K-proton pathways are detailed in **right** with numberings according to bovine oxidase residues (red) and *P. denitrificans* residues (blue, in brackets). Both figures taken from (Abramson *et al.*, 2001).

3.1.2 Subunit I

The subunit I is the catalytic centre, forming the region for proton delivery, oxygen binding and reduction as well as water formation consisting of 12 TMH in *caa*₃-oxidase and 13 in *ba*₃-oxidase. The extra TMH sets the latter apart from the canonical oxidases. This subunit contains three redox centres – low-spin haems *a/b* and a high-spin haem *a*₃-Cu_B dnc. The subunits I of both oxidases can be aligned structurally to within ~ 2 Å rmsd. Of the two proton pathways identified, there is a slight difference in the D-pathway among the Type A oxidases even when the immediate residues are well-conserved (Fig. 32). The Glu278^P (Glu242^B) is present in all Type A1 enzymes and is proposed to act as a

gating valve to prevent back leakage of protons into the cytoplasmic space (Kaila *et al.*, 2008). Mutational studies with *P. denitrificans* oxidase that replaced the Glu with the YS motif indicate that they are interchangeable in terms of proton pumping efficiencies with the caveat that activities of the mutants as a function of oxygen consumption never reach the wild type level (Backgren *et al.*, 2000).

	270	280
	
<i>P. denitrificans</i>	ILWFFGHP	EYVMLILP
<i>T. thermophilus</i>	FFWFYSH	PTVYVMLLP
<i>R. marinus</i>	FFWFYSH	PAVYIMILP
<i>A. aeolicus</i>	IFWFYSH	PVVYVQVLP
<i>Anabaena</i>	MFWFYSH	PAVYIMILP
<i>Synechocystis sp.</i>	LFWFYSH	PAVYIMILP
<i>T. vulcanus</i>	LFWFYSH	PAVYLMILP
<i>D. radiodurans</i>	FFWFYSH	PAVYVMLLP
<i>S. acidocaldarius</i>	LFWFYGH	PVVYVPPFP
<i>B. japonicum</i>	FQWWYGH	NAVGFFLTA
<i>N. pharaonis</i>	LFWYFGH	AVVYFWLMP
<i>G. stearothermophilus</i>	LFWYFGH	PLVYFWLLP

Fig. 32. Conservation of a key Glu residue in the D-pathway of different CcO. The Glu278^P can be functionally and spatially replaced by a Tyr-Ser pair (Y248-S249 for *T. thermophilus*), and sets the Type A1 oxidase from Type A2. For some, only a Tyr residue is present. The sequences are from *P. denitrificans*, *Thermus thermophilus*, *Rhodothermus marinus*, *Aquifex aeolicus*, *Anabaena sp.*, *Synechocystis sp.*, *Thermosynechococcus vulcanus*, *Deinococcus radiodurans*, *Sulfolobus acidocaldarius*, *Bradyrhizobium japonicum*, *Natronomonas pharaonis* and *Geobacillus stearothermophilus*. Figure taken from (Noor and Soulimane, 2012) (**Paper II**).

3.1.3 Subunit II

Subunit II houses the homodinuclear centre of two mixed-valence copper atoms ($\text{Cu}^{1.5+}$ - $\text{Cu}^{1.5+}$; Cu_A) in a β -barrel cupredoxin fold. The residues His-Xaa₃₅-Cys-Xaa-Glu-Xaa-Cys-Xaa₃-His-Xaa₂-Met form the binding motif for the Cu_A . Electrons from cytochrome *c* first reach Cu_A , and correspondingly the cupredoxin fold is located in the periplasmic space and anchored to the membrane by two TMH in *caa*₃-oxidase and one in *ba*₃-oxidase; the subunit IIa might be the ‘missing’ TMH for the latter. The exact electron entry site of *ba*₃-oxidase is

different from that of *aa*₃-oxidases. In the former, TrpII-121^P is responsible for accepting electrons (Zhen *et al.*, 1999; Maneg *et al.*, 2004) while AlaII-87 and PheII-88 are required in *ba*₃-oxidase (Muresanu *et al.*, 2006); the difference might lie in the nature of cytochrome *c* binding (*i.e.* electrostatic *vs.* hydrophobic interaction, respectively) (Noor and Soulimane, 2012) (**Paper II**). Based on the proposed classification, there exist family-specific loops in subunit II with functional and evolutionary implications (Fig. 33). Missing in both Type A1 and A2 *caa*₃-oxidases, it might be responsible in the interaction between soluble cytochrome *c* and the oxidase complex [see discussions in (Noor and Soulimane, 2012) (**Paper II**)].

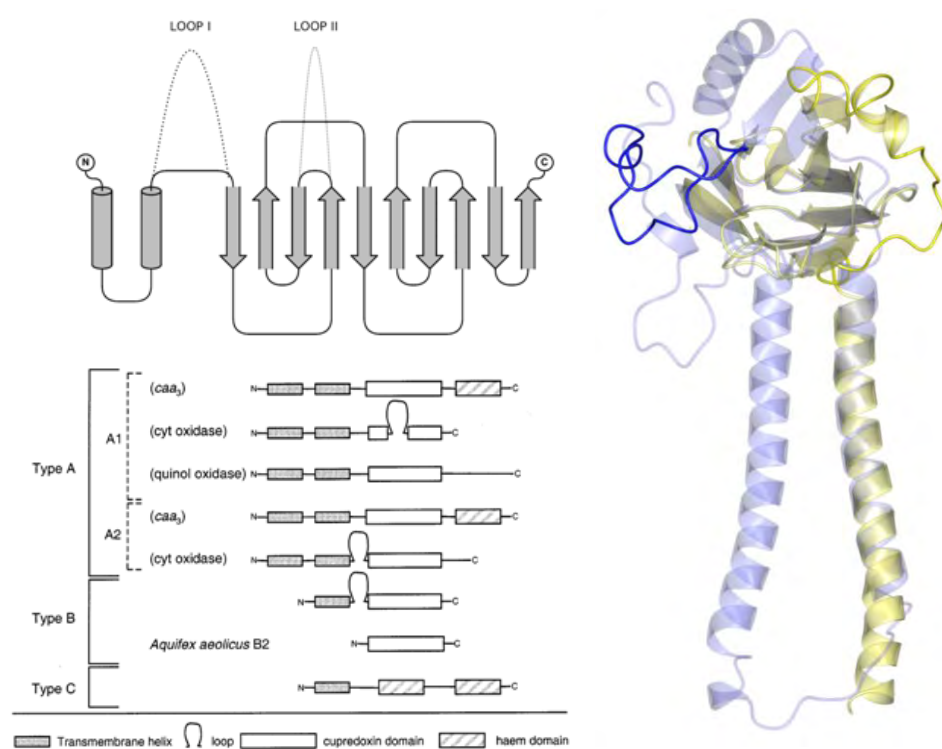


Fig. 33. Family-specific loops in subunit II of CcO. The position of loops I and II within the cupredoxin fold formed by two helices and ten β -strands (**top left**) are shown together with their distribution in different oxidase families (**bottom left**). The three-dimensional arrangement of these loops is depicted (**right**) using the subunits II of *P. denitrificans* *aa*₃-oxidase (PDB ID: 1AR1; blue) and *T. thermophilus* *ba*₃-oxidase (PDB ID: 1EHK; green). Figures taken from (Noor and Soulimane, 2012) (**Paper II**) with the redrawn top left figure originally from (Pereira *et al.*, 2001).

3.1.4 Supernumerary subunits

Whereas the subunits I and II have clear functional roles, the existence of supernumerary/accessory subunits in the structures of various oxidases implies a non-catalytic but important functions for them. For instance, *P. denitrificans* oxidase lacking the subunits III and IV retains its activity and is crystallisable (Hendler *et al.*, 1991; Pardhasaradhi *et al.*, 1991; Ostermeier *et al.*, 1997), indicating a regulatory rather than functional nature of these extra subunits. The notion of them having no role could be easily rejected as different organisms would not have retained the subunits at the expense of their transcription and translation. Such is the complexity of CcO subunit synthesis and assembly that hundreds of additional proteins are necessary to enable the import of nuclear-encoded subunits. Moreover, even when other hundreds of genes have been transferred to nuclear DNA, certain genes are still retained in the mitochondrial DNA as a consequence of the extreme protein hydrophobicity and/or its ability to regulate gene expression by coupling synthesis and assembly (Ott and Herrmann, 2010).

Limiting the discussion to bacterial oxidases, the *ba*₃-oxidase does not possess any additional subunits; interestingly, no metal ions beyond iron and copper are found in the structure (*cf.* Ca²⁺ and Mn²⁺ in *P. denitrificans* oxidase, Mg²⁺ and Zn²⁺ in bovine oxidase, Mg²⁺ in *caa*₃-oxidase, and Ca²⁺ in *cbb*₃-oxidase). A sequence and structural comparison of subunits IV also suggests that *P. denitrificans* and *R. sphaeroides* subunits are similar to each other (Fig. 34) but *T. thermophilus caa*₃-oxidase and *E. coli* QOX are not (Fig. 35). This could be explained by the shared phylogeny of the first two organisms with them being members of the *Rhodobacteraceae* family; no counterpart in any deinococci species, which is related to *Thermus*, could be identified by sequence identity. More notably, there is only one TMH in the *aa*₃-oxidase subunits IV, two in the *caa*₃-oxidase and three in the *E. coli* QOX. Remarkably, all subunits IV occupy similar spatial locations relative to each other.

Fig. 34. Sequence alignment of CcO subunits IV. (Top) Full-length sequence alignment of *P. denitrificans* *aa*₃-oxidase subunit IV. The identical sequences were obtained through BLAST (<http://www.ncbi.nlm.nih.gov/blast>), aligned with ClustalW (Larkin *et al.*, 2007) and edited with Jalview (Waterhouse *et al.*, 2009). Certain residues are highly conserved based on the coloring. RefSeq accession ID: *Caulobacter* sp. (YP001682519), *Dinoroseobacter shibae* (YP001534421), *Hirschia baltica* (YP003061314), *Hyphomonas neptunium* (YP761842), *Ketogulonicigenium vulgare* (YP003963035), *Maricaulis maris* MCS10 (YP757770), *Maritimibacter alkaliphilus* (ZP01012307), *Oceanicola batsensis* (ZP00998509), *Oceanicola granulosus* (ZP01157533), *Octadecabacter antarcticus* (ZP05050125), *Paracoccus denitrificans* (YP914242), *Phaeobacter gallaeciensis* (ZP02146294), *Rhodobacter sphaeroides* 2.4.1 (YP353819), *Rhodobacteraceae bacterium* (ZP05124183), *Rhodobacterales bacterium* (ZP05076522), *Roseobacter denitrificans* (YP683592), *Roseobacter litoralis* Och 149 (YP004691697), *Roseobacter* sp. (ZP01901752), *Roseovarius nubinhibens* (ZP00961167), *Roseovarius* sp. (ZP01034571), *Ruegeria pomeroyi* (YP165566), *Ruegeria* sp. (ZP05090278), *Sagittula stellata* (ZP01744118), *Silicibacter lacuscaerulensis* (ZP05785555), *Silicibacter* sp. TrichCH4B (ZP05739143), *Sulfitobacter* sp. (ZP00948401) and *Thalassiosibium* sp. (ZP05343554). **(Bottom)** Full-length sequence alignment of *T. thermophilus* *caa*₃-oxidase subunit IV. The *T. thermophilus* HB27 sequence is identical to the HB8 and was, therefore, not included in the alignment. The coloring scheme is based on sequence conservation. RefSeq accession ID: *Marinithermus hydrothermalis* (YP004367070), *Meiothermus ruber* (YP003507538), *Meiothermus silvanus* (YP003684273), *Oceanithermus profundus* (YP004056929), *Thermus aquaticus* (ZP03496982), *Thermus scotoductus* (YP004203506), *Thermus thermophilus* HB8 (YP145129) and *Thermus thermophilus* SG0.5JP17-16 (AEG34269).

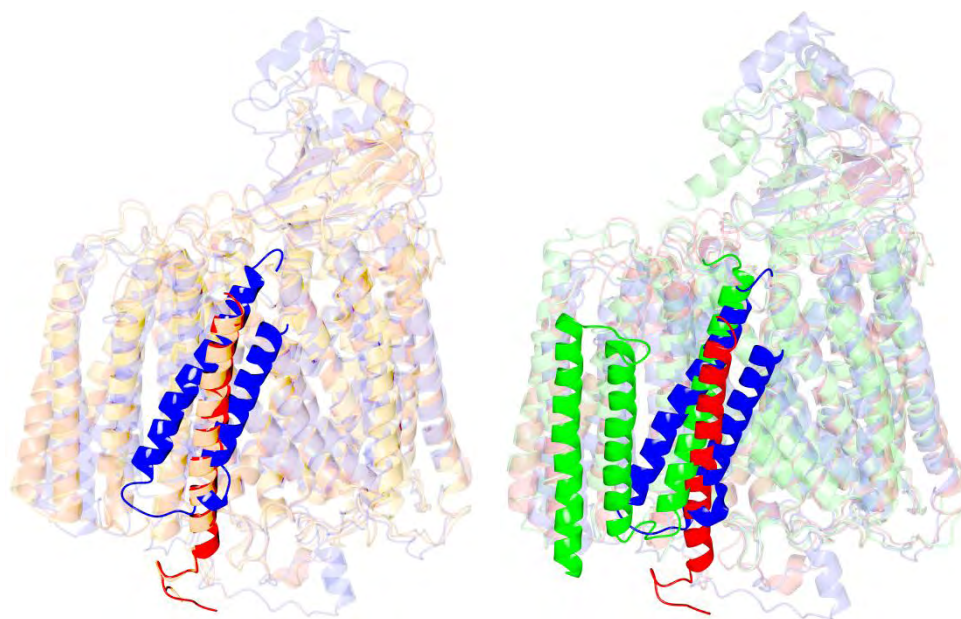


Fig. 35. Structural alignment of subunit IV. (Left) The subunit IV from *Paracoccus denitrificans* (PDB ID: 1QLE; red) and *Rhodobacter sphaeroides* (PDB ID: 1M56; coral) aa_3 -oxidase and *Thermus thermophilus* caa_3 -oxidase (PDB ID: 2YEV; blue) are shown with the superposition of subunits I, II and III in the corresponding transparent and lighter colors. Note that the periplasmic domain of *T. thermophilus* polypeptide containing subunit II is more extensive due to the presence of fused cytochrome *c* and the subunit IV uniquely consists of two helices. (Right) Structural alignment of subunits IV of *Escherichia coli* QOX (PDB ID: 1FFT; green), and *T. thermophilus* (blue) and *P. denitrificans* oxidases (red). The other subunits are in the corresponding transparent and lighter colors. The *R. sphaeroides* oxidase is not shown for clarity. Figures created using CCP4mg (Potterton *et al.*, 2004).

3.1.5 Catalytic cycle

The precise catalytic cycle of CcO involves multiple stages, most of which can be followed spectroscopically by the (dis)appearance of certain peaks in the UV/Vis range. As summarised in Fig. 36, the enzyme is taken to initially exist in oxidised state (**O**). Two electrons reduce the complex to **R**², following which oxygen enters resulting in the formation of ferric-superoxo state (**S**). Taking up two protons located at the dnc end of the K-pathway successively, the **S** goes through **P** and **P**₀. A second water molecule is then formed from the two initial protons and two electrons (**F**_I). This compound also has a feature at 607 nm and was termed as **P**_M in the old literature. **F**_{II} is the state with peak absorbance at 580 nm after another electron enters the system. The enzyme is then reoxidized with the acceptance of fourth electron and proton pumped.

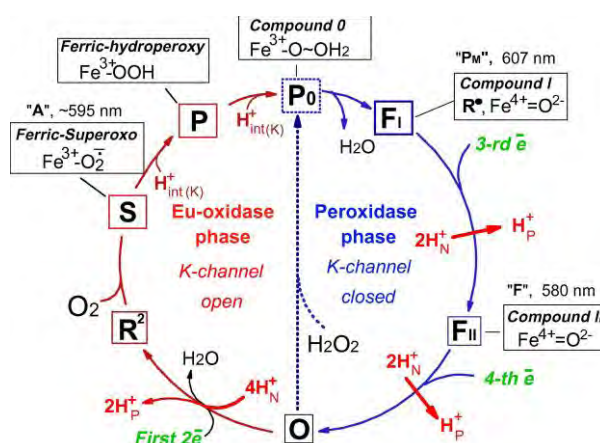


Fig. 36. Various states during CcO catalysis. The **P** (ferric-hydroperoxy) and **P**₀ (ferric-dihydroperoxy) intermediate states have not been observed experimentally but are similar to the cytochrome P450 and peroxidase intermediates. The **P** state analogue has been trapped using synthetic CcO model at a low temperature. Not shown in this figure are the singly-reduced **R**¹ and the unprotonated ferric-peroxo ($\text{Fe}^{3+}\text{-O-O}^-$) states between **S** and **P**. The protons marked as $\text{H}^+_{\text{int(K)}}$ refers to those originating from the end of K-pathway near the dnc and are distinct from that of cytoplasmic bulk phase (H^+_N). Figure taken from (Konstantinov, 2012).

3.1.6 Cytochrome *c*

The monoheme cytochrome c_{552} is the electron carrier between Complex III and CcO and discussed here for completeness in relation to the results presented later. The CXXCH motif defines the unique covalent bond between the vinyl group ($-\text{CH}=\text{CH}_2$) of haem *c* and the Cys residues leading to two thioether linkages (Fig. 37). The imidazole of His and a Met residue about 40 residues downstream form the ligands to the Fe atom. Within the cytochrome *c* domain of cytochrome c_{552} , subunit II/*c* of *caa*₃-oxidase and cytochrome *c* subunit of Complex III, relatively only a few residues is highly conserved apart from the CXXCH motif (Fig. 38).

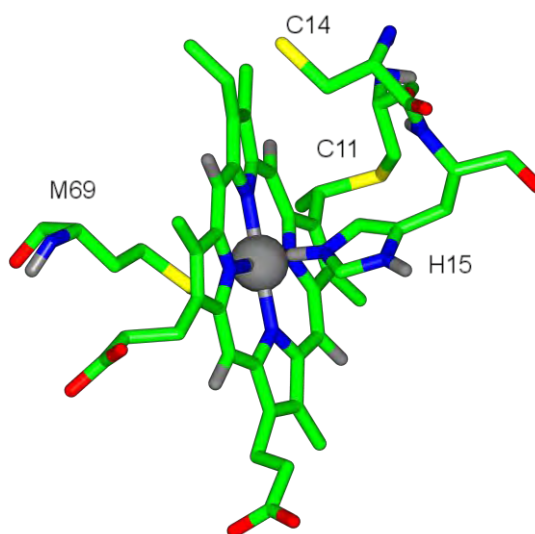


Fig. 37. Covalent attachment of haem *c* to protein residues. Atoms are coloured according to their types: C, green; O, red; N, blue; S, yellow; H, grey and Fe, grey sphere. Figure created from PDB ID: 1C52 with CCP4mg (Potterton *et al.*, 2004).

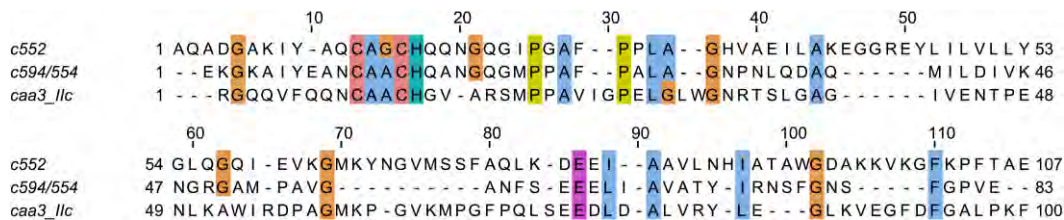


Fig. 38. Sequence alignment of *T. thermophilus* cytochromes *c*. The sequences of cytochrome *c*₅₅₂ (*c*₅₅₂), cytochrome *c* subunit of Complex III (*c*_{549/554}) and cytochrome *c* domain of *caa*₃-oxidase (*caa*_{3_IIC}) were truncated to highlight only regions with high conservation among each other and edited manually. The alignment was rendered at 100 % conservation with Jalview (Waterhouse *et al.*, 2009). Accession ID: cytochrome *c*₅₅₂ (YP144689), *c*_{549/554} (YP145199) and subunit II/c (YP143577).

3.2 MATERIALS AND METHODS

3.2.1 Recombinant protein production

The *caa*₃-oxidase overexpression plasmid was constructed by PCR amplification of the entire putative operon consisting of CtaA/B, subunits I/III and II/c using the primer pairs CtaAB_F_NdeI and Caa₃_R_NotI (Table 10) and blunt-end cloned into the *Sma*I site of pK19 (p3C1.1⁹). Using the *Nde*I/*Not*I restriction enzymes, the operon fragment was gel-purified from p3C1.1 and cloned into the corresponding restriction sites of pDM12 resulting in p3C1.2. A His₆-tag at the C-terminus of I/III was already added in the PCR primer.

The plasmids were transformed according to the established method (Kolaj-Robin *et al.*, 2012) into *T. thermophilus* HB27:: Δ *caa*₃¹⁰ strain constructed in a previous study (O’Kane, 2011). The *T. thermophilus* HB27:: Δ *caa*₃ culture was then used to inoculate 10 L of medium for protein purification. Fe²⁺ and Cu²⁺ were added to the large-scale medium at concentrations of 100 μ M and 10 μ M, respectively (Studier, 2005) in the form of chloride salts; a 2 M FeCl₂ solution was made in acidified water by adding concentrated HCl (32 %; ~ 10 M) to the water at a ratio of 1:9 to prevent Fe³⁺ (rust) formation. Cell membrane was solubilised with 5 % Triton X-100 in 50 mM Tris-HCl, 200 mM NaCl. Prior to loading on Ni Sepharose Fast Flow (GE Healthcare), imidazole from a 5 M stock solution (pH 7.6) was added to a final concentration of 10 mM. All other steps were identical to the purification of recombinant tagged Complex II (rCII-SdhB-His₆) (Kolaj-Robin *et al.*, accepted) (**Paper I**). Protein concentration was determined based on the dithionite reduced-*minus*-oxidised absorbance using a molar extinction coefficient of 12 000 M⁻¹ cm⁻¹ (van Gelder, 1966).

⁹ Nomenclature for *caa*₃-oxidase cloning is as follows. The 3C indicates that three polypeptides (CtaA/B, subunit II/c and subunit I/III, in that order) are present. The number immediately following identifies the mutation, 1 being wild type and 2 for Y249F. As the cloning involved two separate plasmids, the last number distinguishes them apart with 1 for pK19 derivatives and 2 for pDM12.

¹⁰ The genes encoding for subunits I/III and II/c have been deleted and replaced by a bleomycin resistance gene.

The Y248F (TAC → TTC) mutant was made with QuikChange Site-Directed Mutagenesis Kit (Agilent Technologies, Ireland) with the mutagenic primers Pr3C2F and Pr3C2R using p3C1.1 as the template and the mutant DNA clone (p3C2.1) was sequenced throughout the insert to ensure no secondary mutations before being subcloned into a fresh pDM12 at the same restriction sites (p3C2.2).

Table 10. Primers for *caa3*-oxidase expression. The restriction sites are **bolded**, His-tag is underlined and the mutagenic region is *italicised*.

Primer	Sequence (5' – 3')
CtaAB_F_NdeI	ATATA CATATG AAGACCCCTGCTTGGTCCAGACTCG
Caa3_R_NotI	ATAT GCGGCCGC TTA <u>ATGATGATGATGATGATGATGATG</u> CCAGACGTAGAAGATGGTGACGATCACCAGCCAGA CGGCGTC
Pr3C2F	GTTCTTCTGGTTC <i>TTC</i> TCCCACCCACGGTC
Pr3C2R	GACCGTGGGGTGGGA <i>GAA</i> GAACCAGAAGAAC

3.2.2 Circular dichroism

The secondary structure of wild type *caa3*-oxidase was assessed with a Chirascan CD spectrometer (Applied Photophysics). Data were acquired and processed using Pro-Data Chirascan and Viewer, respectively, as detailed in (Kolaj-Robin *et al.*, accepted) (**Paper I**). Full spectra were obtained in the far UV range of 190 to 280 nm with quartz suprasil cuvettes (10 mm pathlength; Hellma GmbH). Protein samples were diluted to 10 µg/ml in buffer (5 mM Tris-HCl pH 7.6, 0.025 % DDM; total volume of 3.5 ml). The urea-induced denaturation of wild type oxidase was measured in the range of 190-260 nm due to the extreme interference at lower wavelengths (Greenfield, 2007). Samples were incubated at 20 °C for 12 h prior to measurements in duplicates. Secondary structure content was estimated with CDNN (Böhm *et al.*, 1992).

3.2.3 Ultrafast spectroscopy

The kinetics of *caa*₃-oxidase was investigated using ultrafast spectroscopy in collaboration with Marten Vos (Laboratory for Optical Biosciences, École Polytechnique, Paris). Samples of recombinant wild type *caa*₃-oxidase was prepared at a concentration of 100 μM (Soret absorbance of 0.7) in a quartz cuvette (1 mm pathlength, 200 μl samples) and degassed with argon. Dithionite and ascorbate solutions were made by dissolving sodium dithionite and sodium ascorbate, respectively, to final concentrations of 1 M in protein buffer (50 mM Tris-HCl, 0.025 % DDM) and degassed with argon. Protein samples were reduced with dithionite anaerobically prior to binding with CO and 1 % NO. Mixed-valence *caa*₃-oxidase (Fe_c^{3+} , $\text{Cu}_A^{1.5+}$ - $\text{Cu}_A^{1.5+}$, Fe_a^{3+} , Fe_{a3}^{2+} , Cu_B^+) was attempted by binding CO directly with oxidised protein as well as by pre-reducing the protein with substoichiometric dithionite and ascorbate (Koutsoupakis *et al.*, 2012). The experimental setup for ultrafast spectroscopy has been described previously (Martin and Vos, 1994).

3.2.4 Computational analyses of CcO

Electron transfer kinetics between Complex III and IV as mediated by cytochrome *c*₅₅₂ were investigated using stopped-flow absorption spectroscopy in collaboration with Alessandro Giuffrè (CNR Institute of Molecular Biology and Pathology, Rome, Italy). Docking and anisotropic modelling were performed as described in (Soulimane *et al.*, submitted) (**Paper III**).

3.3 RESULTS AND DISCUSSION

3.3.1 Protein purification

Given the successful overexpression of Complex II (see Chapter 2) using the Complex III promoter, a similar strategy was chosen for *caa*₃-oxidase. An examination of its crystal structure shows that all the C-termini of the constituent polypeptides are located in the periplasmic space. Therefore, a His-tag was added to the C-terminus of subunit I/III as it would be easier for future modifications compared to subunit II/c which is located between CtaA/B and subunit I/III in the genome. Following nickel IMAC and gel filtration chromatographic steps, it was found that the purification yield was ~ 1 mg/L culture. With an estimated wet cell mass of 10 g/L, this amount is similar to the native protein (Lyons *et al.*, 2012). While a five-fold increase was observed for Complex II corresponding to the ~ 6-8 copies of pDM12 per cell (~37 mg recombinant *cf.* 8 mg native per 100 g) (Kolaj-Robin *et al.*, accepted), such a level was not observed for *caa*₃-oxidase. That the expression system does yield recombinant protein is an indication of its functionality, although this would require further optimisations as outlined in Chapter 4. Interestingly, the subunit IV was found to be associated with the recombinant *caa*₃-oxidase even when it was not included in the expression plasmid (Fig. 39). Analytical gel filtration also shows that the protein is in a homogeneous state, suitable for crystallisation and other biochemical/biophysical studies (Fig. 39).

As a proof of concept that the mutagenesis system is functional, a single site-directed mutant (Y248F) was designed and confirmed to contain the intended mutation at the DNA level (Fig. 40 *cf.* Fig. 41). Based on codon analysis [<http://www.kazusa.or.jp/codon/>] (Nakamura *et al.*, 2000), the TTC codon was chosen instead of TTT. Targeting the YS pair in the D-pathway (Fig. 32), this mutant is expressed at a much lower amount than the wild type (~ 0.3 mg/L mutant *cf.* 1 mg/L wild type), possibly as a consequence of its non-functionality and/or destabilising property. Investigations using CD spectroscopy on its stability were hampered by the lower yield and no further analysis was performed.

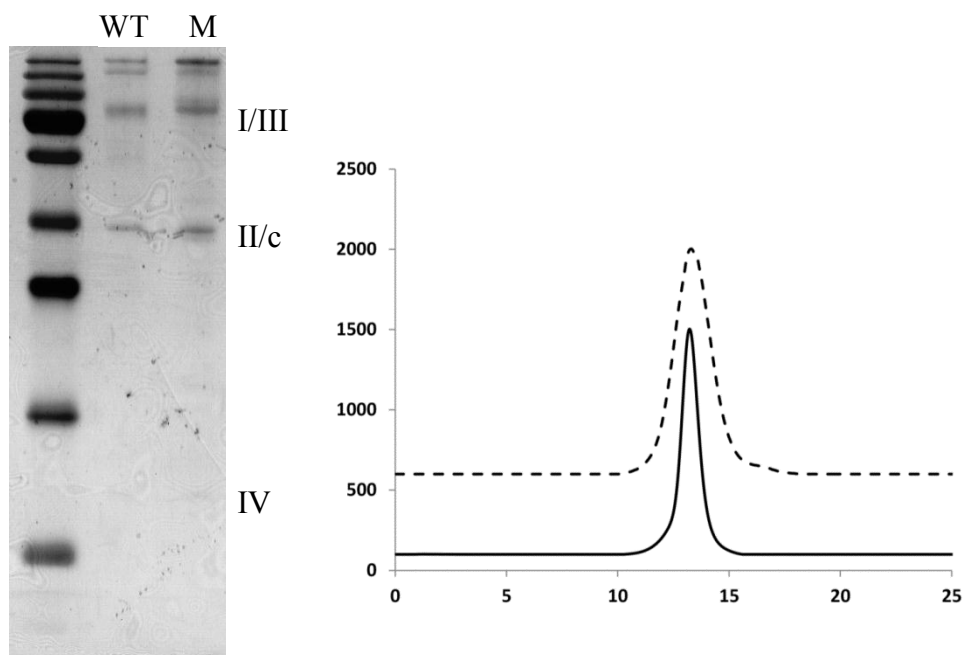


Fig. 39. Purity and homogeneity of recombinant wild type and Y248F mutant *caa*₃-oxidases. The SDS-PAGE (left) shows the presence of all constituent subunits in wild type (WT) and mutant (M). The theoretical and apparent molecular weights of the subunits I/III, II/c and IV are 89.2/60, 37.3/32 and 7.3/8 kDa, respectively. Both wild type and Y248F mutant can be purified homogeneously in DDM.

For redox proteins, their cofactor sensitivity to their immediate chemical environment means any perturbation would affect their spectral features. One of the best examples is the series of investigations into *T. thermophilus* cytochrome *c*₅₅₂ (Fee *et al.*, 2004). This effect could easily be used to ensure that the cofactors have been inserted in stoichiometric amounts in recombinantly overexpressed oxidases. The oxidised, dithionite reduced and CO-reduced spectra of wild type (Fig. 42) and mutant (Fig. 43) oxidase display the properties as observed for the native enzyme.

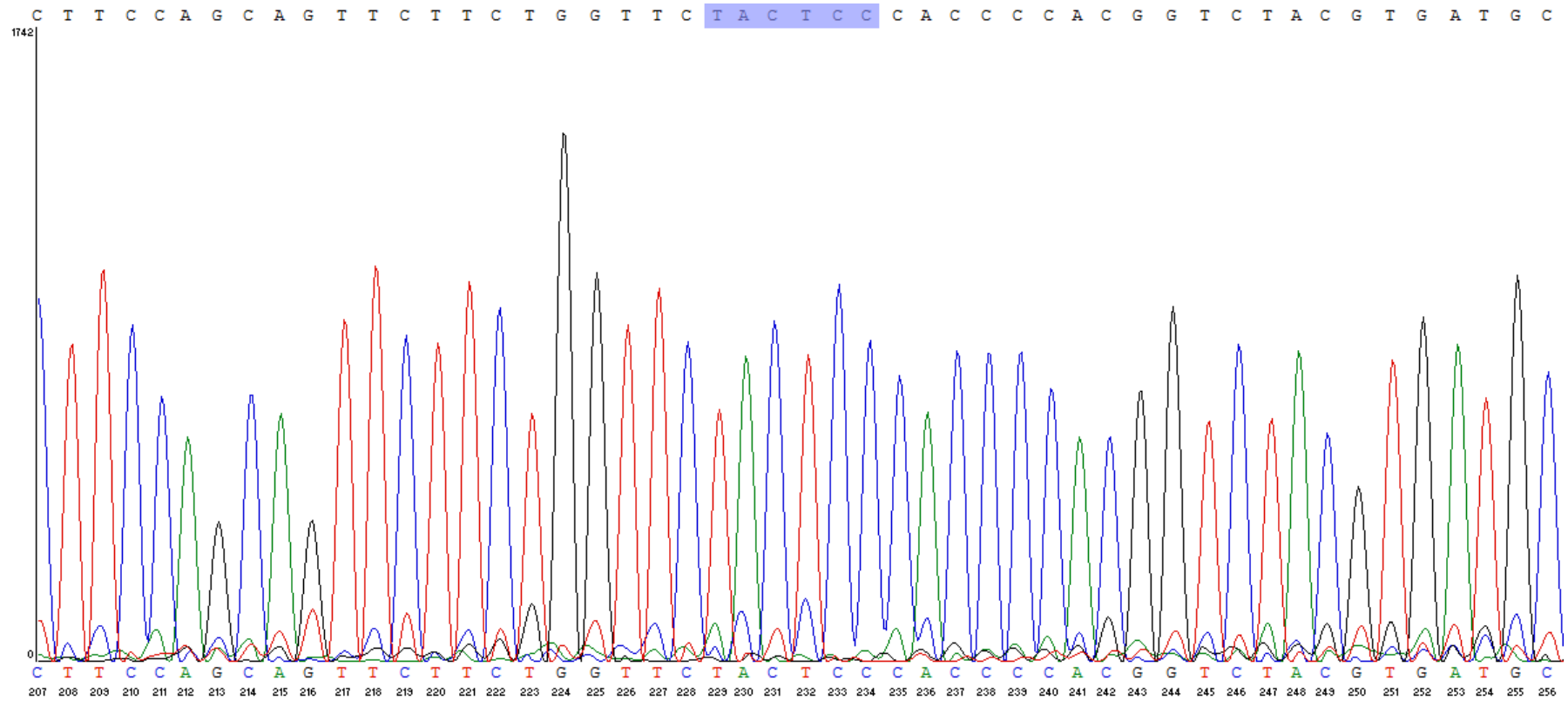


Fig. 40. Chromatogram of recombinant wild type *caa*₃-oxidase plasmid. The region for YS pair (TAC and TCC, respectively) is highlighted.

CYTOCHROME C OXIDASES

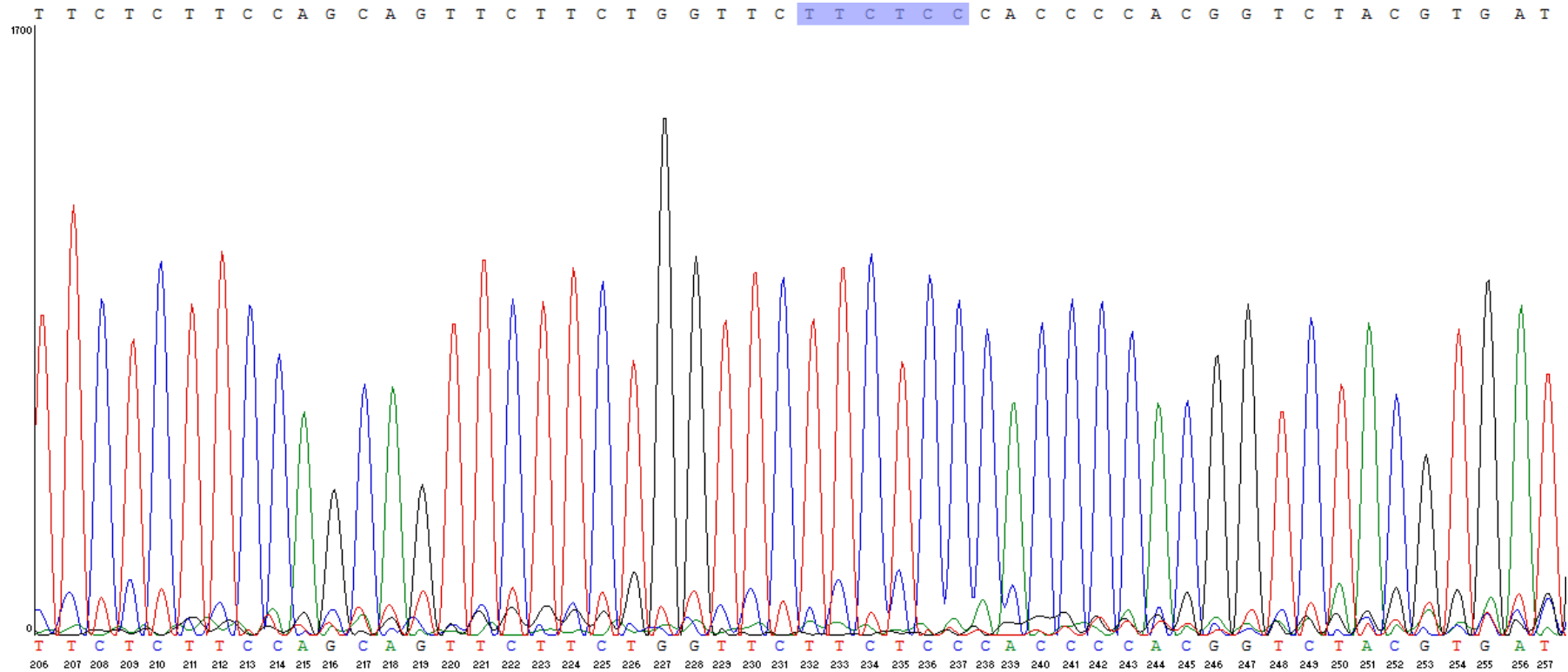


Fig. 41. Chromatogram of recombinant Y249F mutant *caa3*-oxidase. The highlighted region is FS pair (TTC and TCC, respectively). Note that the heavy ratio of GC bases at the wobble position, which also guided the codon choice.

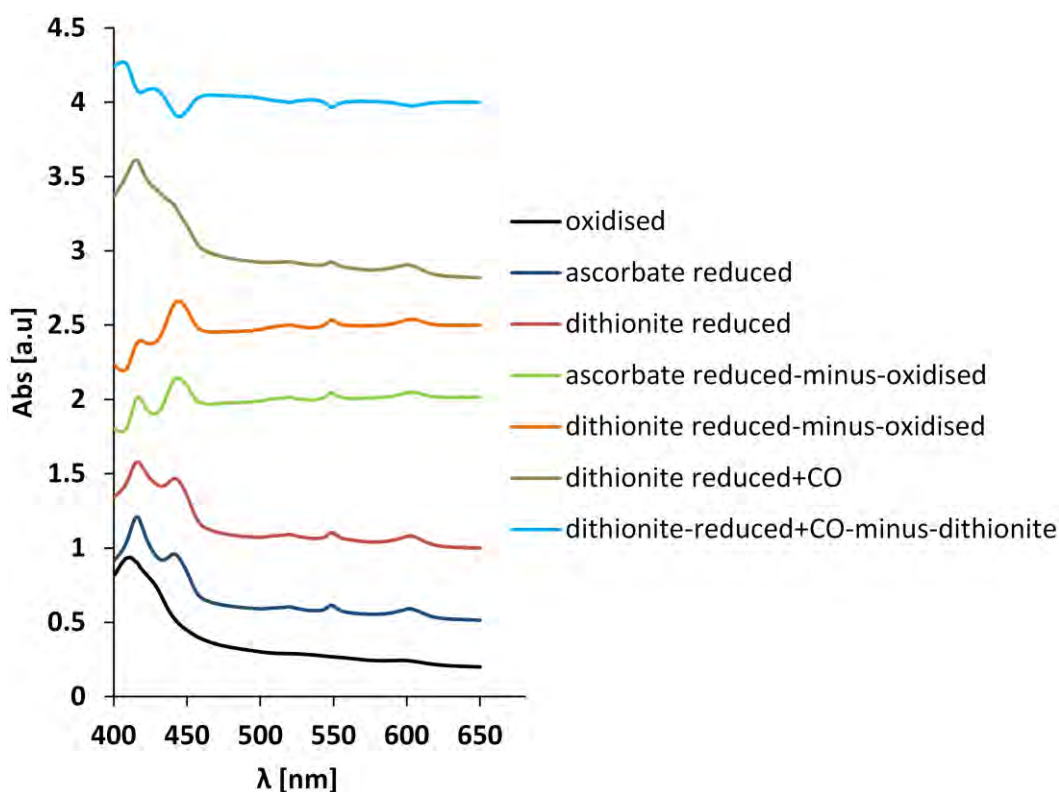


Fig. 42. Absorption spectra of recombinant wild type *caa3*-oxidase. The ascorbate and dithionite reduced-*minus*-oxidised spectra unambiguously indicate the presence of haem *c* and *a* at a ratio of 1:2, as observed for native protein, based on their peaks at 418/549 nm and 445/604 nm. All spectra were recorded after degassing the protein and dithionite solution with argon.

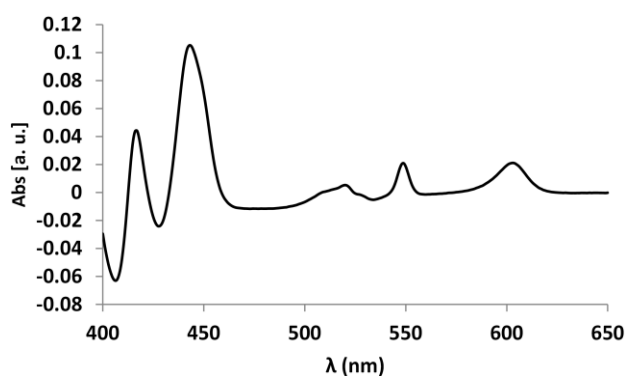


Fig. 43. Dithionite reduced-*minus*-oxidised absorption spectrum of Y248F mutant *caa3*-oxidase. The spectrum was obtained by adding dithionite without prior degassing and is identical to that of wild type oxidase.

3.3.2 Folding of recombinant protein

The characteristic CD features of a mainly alpha-helical protein – twin negative peaks at 210 nm and 220 nm and a positive peak at 195 nm – indicate that the recombinant oxidase does not suffer from folding problems (Fig. 44). The deconvoluted spectrum reveals ~ 20 % helix and ~ 40 % random coil¹¹, inconsistent with the crystal structure [PDB ID: 2YEV; (Lyons *et al.*, 2012)] which consists of ~ 60 % helix. The difference could be related to the deconvolution algorithm and/or neural network training datasets comprising soluble proteins in addition to the indeterminate nature of detergent and lipid molecules.

Attempts to measure the thermal stability of *caa3*-oxidase were not successful due to the immediate protein precipitation at about 50 - 55 °C. As an alternative, its stability was ascertained as a function of denaturant urea concentrations (Fig. 45). In contrast to the relatively good signal-to-noise ratio of only the protein over 180 – 260 nm range, urea addition increased the noise at wavelengths lower than 200 nm¹². Nevertheless, two main observations could be made – (i) the positive peak at 195 nm shifts to 200 nm after the addition of urea and (ii) the negative peaks become featureless (*i.e.* no twin peaks could be seen) only when denatured at between 8 and 9 M urea. The exact secondary structure content was not determined due to the aforementioned poor signal quality below 200 nm coupled with the incorrect CD spectrum deconvolution relative to wild type undenatured oxidase.

Circular dichroism (CD) spectroscopy is a method of determining overall secondary and tertiary structures of proteins. While it lacks the wealth of information given by nuclear magnetic resonance (NMR), it requires only low amounts of sample and the dichroic activity can be investigated over a range of temperatures. It is also an emerging technique to determine suitability of

¹¹ The spectrum was deconvoluted based on a proteinaceous molecular weight of 133.886 kDa from the corresponding subunit entries in UniProt (1194 residues). Average helical content of the PDB entry was obtained from the DSSP secondary structure assignment.

¹² The photomultiplier tube (PMT) registered saturated high tension voltages between 180 and 200 nm.

membrane protein samples prior to more extensive crystallisation trials (Tulumello and Deber, 2012). In this study, CD spectroscopy was used to assess the folding of recombinant *caa₃*-oxidase to ensure that overexpression does not result in incorrectly folded protein – a common problem in heterologous membrane protein overexpression. Both folding and stability analyses of the recombinant oxidase together with analytical gel filtration chromatography illustrate that the recombinant production results in homogeneous and correctly folded *caa₃*-oxidase.

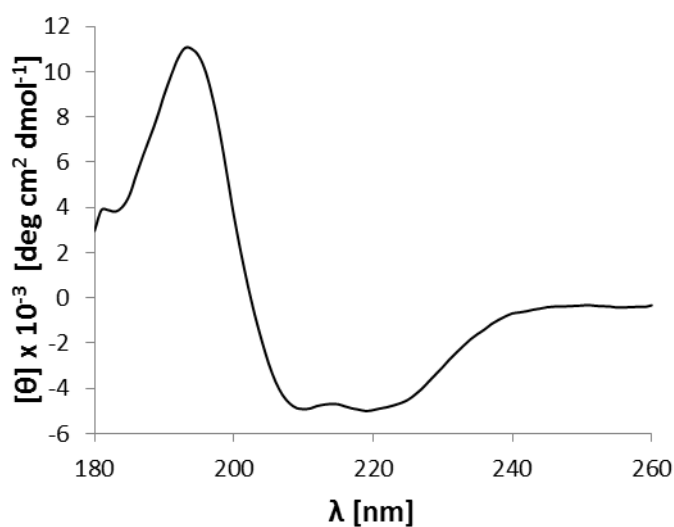


Fig. 44. CD spectrum of wild type *caa*₃-oxidase. Circular dichroic activity was measured from 180 nm to 260 nm with a protein concentration of 10 μg/ml in 5 mM Tris-HCl 7.6, 0.025 % DDM.

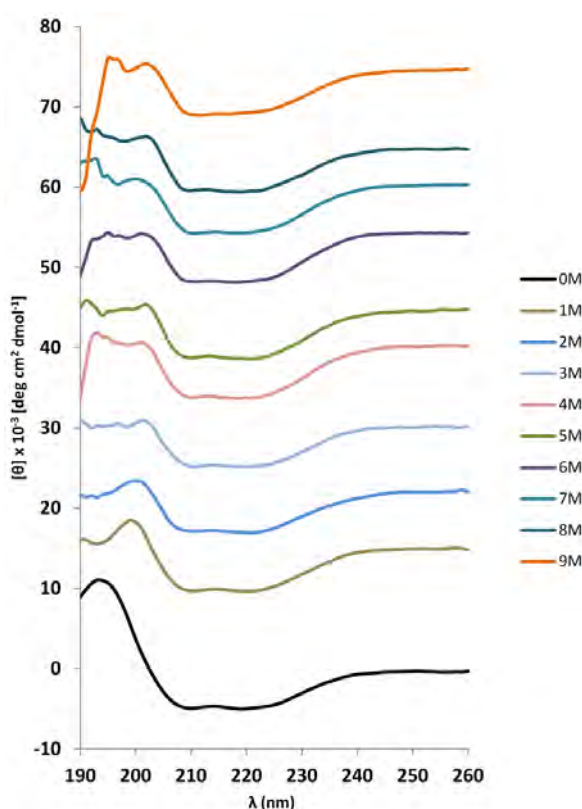


Fig. 45. Urea-induced denaturation of wild type *caa*₃-oxidase. The positive peak at 195 nm shifts to 200 nm upon urea addition together with less intense negative peaks at 210 and 220 nm with increasing denaturant concentrations.

3.3.3 Ultrafast spectroscopy

The two haem *a* moieties of fully reduced and CO- and NO-reduced oxidases were selectively excited by a 590 nm pulse; excitation at the α -band avoids coherent response associated with excitation at the Soret band and reduces the excess energy after photodissociation (Liebl *et al.*, 1999). However, due to the spectral distribution, this does not result in an exclusive excitation. For the fully reduced oxidase, within the time scale of < 30 ps, the haem *a* absorbance is clearly visible and dominant (Fig. 46, top). Similar to other haem proteins (Iben *et al.*, 1991; Liebl *et al.*, 2002), the 1.4 ps component is attributable to an excited state with a recombination of His ligand dissociated from haem *a* at 6.7 ps (Fig. 46, bottom). The remaining constant phase could correspond to a slower phase in the His ligand rebinding. Whether this slower phase is artifactual due to the difference between the enzyme optimum and experimental temperatures could not be investigated as the protein precipitated at ~ 50 °C.

Further experiments were then performed with the CO-reduced complex. The signal bleaching, occurring within 10 ps (Fig. 47, top), is larger compared to the fully reduced complex as both haem *a* and a_3 -CO are excited with a blue-shift for the latter. For up to 4 ns, which is the maximum timescale that can be probed with the ultrafast setup, the signals are constant and might reflect the CO transfer to Cu_B . As in other CcO, the CO molecule is likely bound to the copper for a further few microseconds prior to equilibrating with the bulk solution (Dyer *et al.*, 1989; Woodruff *et al.*, 1991; Einarsdóttir *et al.*, 1993; Heitbrink *et al.*, 2002).

The decay-associated spectra (DAS), surprisingly, reveal a species with spectral properties at 280 ps distinct from the earlier phases (Fig. 47, bottom). This might represent a recombination of CO from haem a_3 in a subpopulation where Cu_B is inaccessible with the consequent spectral difference (*i.e.* heterogeneous sample population). Alternatively, structural relaxation of the dissociated haem could occur resulting in a blue shift. Spectroscopic studies in the infrared region using FTIR as well as resonance Raman indicate that *caa*₃-oxidase can adopt two conformations in the dnc (Pavlou *et al.*, 2011). Unfortunately, the current crystal structure of the oxidase was only resolved to

2.4 Å, a resolution too low to identify the structural nature of spectroscopic heterogeneity. In *ba*₃-oxidase, only 80-85 % of CO photolysed from haem *a*₃ bind to Cu_B whereas the rest travels to nearby the ring A propionate of haem and then rebinds to haem (Koutsoupakis *et al.*, 2003). However, the differences in ligand binding ascertained from FTIR data (Pavlou *et al.*, 2011) preclude any extension of *ba*₃-oxidase photolysis yield to *caa*₃-oxidase. It has also been postulated that the Cu_B of *caa*₃-oxidase only has a weak effect in the formation of the α-form due to a different steric forces to the Fe-C-O bond, in contrast to those in *ba*₃- and *aa*₃-oxidases (Pavlou *et al.*, 2011).

Attempts were also made to prepare a mixed valence CO-bound complex (Fe_c^{3+} , $\text{Cu}_A^{1.5+}$ - $\text{Cu}_A^{1.5+}$, Fe_a^{3+} , Fe_{a3}^{2+} , Cu_B^+) according to (Koutsoupakis *et al.*, 2012). As the enzyme concentration used in the previous study (1 mM for FTIR measurements) was too high for absorption spectroscopy, it was reduced to 200 μM so as to maintain a Soret region absorbance of 0.6-1. The addition of substoichiometric dithionite and ascorbate [\sim 25-50 μM in keeping with the ratio in (Koutsoupakis *et al.*, 2012)] also did not allow mixed valence complex formation.

To study the ligand binding of NO to *caa*₃-oxidase, the haem *a*₃-NO complex was made by adding 1 % NO to ascorbate-reduced oxidase; 10 % NO caused protein precipitation. As illustrated in Fig. 48 (top), the predominant initial signal is from haem *a*. The small shoulder around 430 nm is attributable to the *a*₃-NO complex and remains beyond 40 ps. At the maximum accessible time scale of 4 ns, an almost-complete signal decay is observed. Two exponentials were fitted to the decay at 140 ps and 930 ps, together with a relatively small constant (Fig. 48, bottom). Both figures also show changes in the spectral shape during NO recombination and blue shift of the induced absorption lobe. The multiexponential NO rebinding kinetics is at variance with the previous study (Pilet *et al.*, 2004). For *P. denitrificans aa*₃-oxidase, and probably by extension other *aa*₃-oxidases, a 200-ps single exponential recombination exists with NO:oxidase stoichiometry-dependent amplitude (Pilet *et al.*, 2004) because at high NO concentrations, two NO molecules are present in the dnc in the form of *a*₃-NO and Cu_B-NO complexes prior to dissociation (Vos *et al.*, 2001). No

recombination was observed at subnanosecond scale for *ba*₃-oxidase regardless of the NO:oxidase ratio. The latter, together with *caa*₃-oxidase, exhibits NO reductase activity ($2\text{NO} + 2\text{e}^- + 2\text{H}^+ \rightarrow \text{N}_2\text{O} + \text{H}_2\text{O}$) (Giuffrè *et al.*, 1999), resulting in an immediate reduction (and hence no recombination) of NO as soon as two molecules are present. Therefore, the NO recombination seen here with *caa*₃-oxidase could be caused by (i) absence of NO reductase activity in the experimental condition used, or (ii) total non-binding or only transient binding of Cu_B to NO. The results obtained herein also reveal a rather peculiar behavior of NO – multiexponential NO rebinding kinetics have only been demonstrated so far in haem proteins, such as NO synthase (Négrerie *et al.*, 1999) and myoglobin (Négrerie *et al.*, 2006), but not CcO. Both the multiexponential kinetics and spectral changes imply a heterogeneous population of docking sites that cannot interconvert. Again, protein precipitation prevented a more physiological-like investigation at higher temperatures.

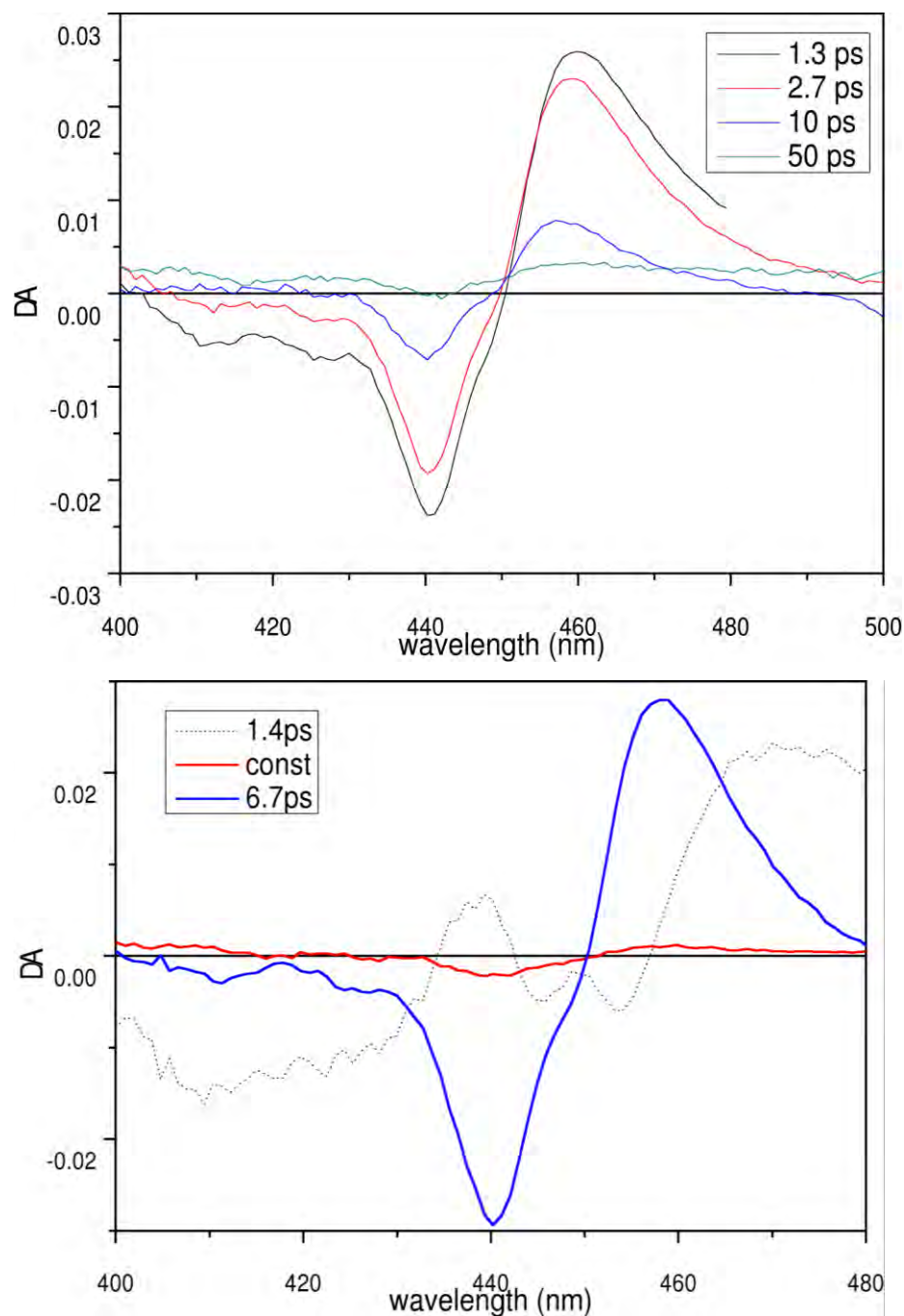


Fig. 46. Spectra of fully-reduced wild type *caa3*-oxidase excited with 590-nm laser pulse. The global analysis in terms of decay-associated spectra is shown below in which the 1.4 ps component is the excited state and 6.7 ps is a recombinant of His ligand dissociated from haem *a*.

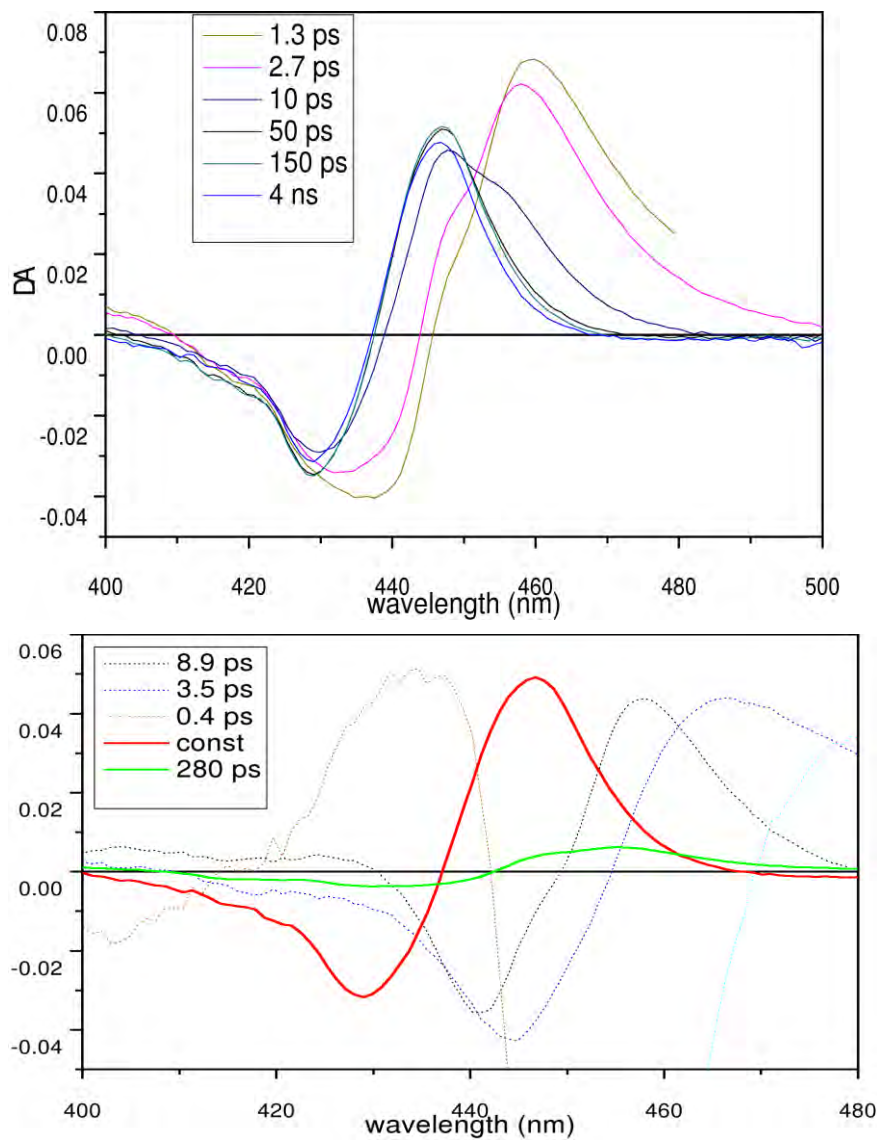


Fig. 47. Excitation of CO-reduced *caa*₃-oxidase. (Top) Visible spectra at different time points. **(Bottom)** Decay-associated spectra from a global analysis, indicating a species at 280 ps different from the earlier phases.

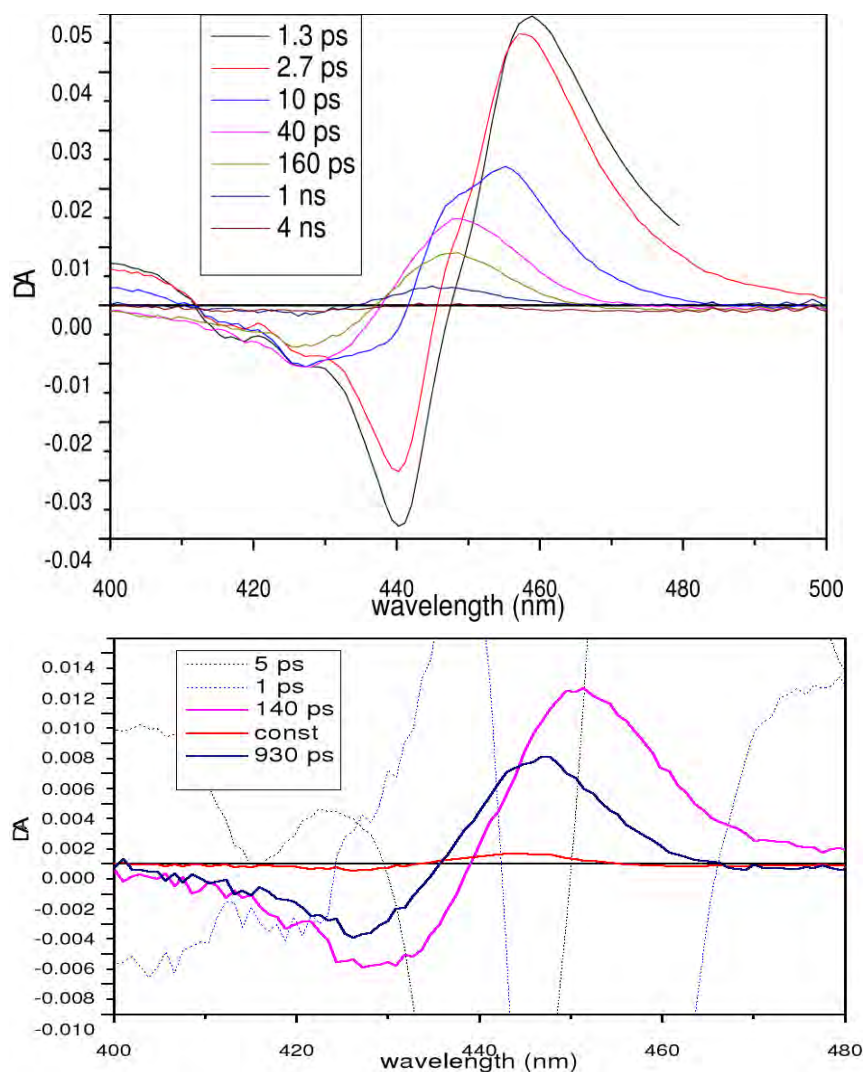


Fig. 48. Excitation of NO-bound *caa*₃-oxidase. **(Top)** Visible spectra in the Soret region at different time points. **(Bottom)** Two exponential values are clearly visible in the decay-associated spectra, indicating multiexponential NO rebinding kinetics.

3.3.4 Computational analyses

A detailed discussion on the electron transfer between Complex III (*bc* complex) and whole complexes of *ba*₃- and *caa*₃-oxidases are presented in (Soulimane *et al.*, submitted) (**Paper III**), of which key points are highlighted here. Using stopped-flow kinetics, the electron transfer between Complexes III and IV were studied at the millisecond scale. In contrast to the previous study that only used water soluble domains (Janzon *et al.*, 2007), cytochrome *c*₅₅₂ is shown to mediate the electron transfer between the two respiratory complexes and negating the proposed branched pathway (Complex III → *caa*₃-oxidase directly, Complex III → cytochrome *c*₅₅₂ → *caa*₃-oxidase, Complex III → cytochrome *c*₅₅₂ → *ba*₃-oxidase). Furthermore, the interaction between the cytochrome *c* subunit (*c_{bc}*) and cytochrome *c*₅₅₂ is dependent on the ionic strength at variance with the mode between cytochrome *c*₅₅₂ and *ba*₃-oxidase.

A computational approach was then taken to understand the docking of cytochrome *c*₅₅₂ to both oxidases, given that the crystal structures of all the protein, with the exception of Complex III, are available. Two simulations were performed – (i) molecular docking of cytochrome *c*₅₅₂ to each of the CcO, and (ii) structural dynamics of CcO. The cytochrome *c*₅₅₂-*caa*₃-oxidase docking suggests an edge-to-edge distance of ~ 16 Å between haem *c* of cytochrome *c*₅₅₂ and either haem *c* or Cu_A of *caa*₃-oxidase, nearly at the 14-Å limit for direct electron transfer (Page *et al.*, 2003). Direct electron transfer from cytochrome *c*₅₅₂ to Cu_A bypassing cytochrome *c* of *caa*₃-oxidase cannot be discounted with the available data. Additionally, anisotropic network modelling of the *caa*₃-oxidase shows large structural movements that could potentially ‘hold’ the cytochrome *c*₅₅₂ and release it only upon changes in the redox state(s) of the metal centre(s). Both findings imply a rather stabilizing nature of the *caa*₃-oxidase cytochrome *c* domain during the electron transfer, although the reason is open to discussion considering the absence of such a ‘feature’ in *aa*₃- or *ba*₃-oxidases. Also not apparent is the evolutionary pressure to retain the haem *c* moiety if the cytochrome *c* domain is merely for a stabilisation purpose.

3.4 CONCLUSION

Presented here is a recombinant homologous protein expression system for *caa₃*-oxidase to allow for more detailed studies of its mechanism of action through site-directed mutagenesis. The functionality of the system is indicated by the protein homogeneity and stability analyses by analytical gel filtration chromatography and circular dichroism spectroscopy as well as femtosecond absorption spectroscopy. Nonetheless, further challenges remain in increasing the expression level of mutants to at least the wild type level, including by the addition of subunit IV and change in the promoter. The preliminary ultrafast spectroscopic results demonstrate non-homogeneous CO rebinding based on a subpopulation with distinct spectral properties, similar to FTIR measurements. So far, the structural nature of this dual conformation in the active site remains mysterious; structures with sub-angstrom resolution allowing for the detailed visualisation of dnc remains difficult compared to that achievable for soluble proteins. Whether the multiexponential NO recombination corresponds to the physiological events can only be answered by kinetics studied as a function of temperature and NO concentration.

CHAPTER 4
OVERALL CONCLUSION
AND OUTLOOK

4. OVERALL CONCLUSION AND OUTLOOK

The results presented in Chapters 2 and 3 are only the starting points for further investigations into the respective enzyme complexes. Crucially, a mutagenesis system is required for the Complex II to allow a deeper understanding of its electron transfer pathways, including the removal of either of the two haem moieties. There are various possible options of generating such a system, either by silencing the native complex or by *in vitro* conversion of monomers to trimers. Nonetheless, the ability to create a synthetic functional monomer shows for the first time that electron transfer from succinate to quinone occurs within a protomer, not between them. The crystallographic work at the current 3.8 Å would also require further optimisations, mainly by a more detailed screening for cryoprotectants and *in stilla* modifications, to obtain a higher diffraction (~ 2.0-2.5 Å). However, any structural model built must also consider the redox states of the metal centres to ensure that it represents the as-crystallised state. Fortunately, this can be facilitated by the recent advances in online UV/Vis and Raman spectrometer at synchrotron beamlines.

Similar to Complex II, the protein overexpression system for *caa3*-oxidase also yields homogeneous, well-folded protein. Indicating that the homogeneous systems do not suffer from folding and redox cofactor insertion problems common with heterologous membrane protein expression, the yield might be boosted to that of Complex II with the addition of subunit IV to the expression plasmid. High-throughput expression screening to investigate the maximum yield under different growth media, temperature and oxygen level in a factorial fashion could be made by fusion of the superfolder green fluorescent protein (sGFP) (Cava *et al.*, 2008) to the C-terminus of subunit I/III as has been performed for *E. coli*-based membrane protein overexpression (Drew *et al.*, 2006), although it should be noted that the C-terminus of all *caa3*-oxidase subunits are located in the periplasmic space. Attempts to measure protein stability and kinetics at high temperatures have been frustrated by the protein precipitation. In this regard, a factorial approach based on differential scanning fluorimetry (“ThermoFluor”) (Niesen *et al.*, 2007) might be required to find the most stabilising condition, although the crystallisation condition (in decylmaltoside) appears attractive.

Finally, as the crystallisation condition for native *caa*₃-oxidase is known, the recombinant wild type and mutant oxidases should also be crystallised to obtain a structural understanding of spectroscopic studies.

In summary, the following would represent future work:

Complex II:

- i. Generation of mutagenesis system
- ii. Optimisation and manipulation of crystal diffraction to 2.0 – 2.5 Å
- iii. Characterisation of SQR and QFR activities

Cytochrome *c* oxidase:

- i. Improvement of protein production yield
- ii. Proton pumping and oxygen consumption (activity) assays
- iii. Crystallisation of wild type and selected mutants
- iv. Stabilisation of recombinant protein at high temperatures

REFERENCES

- Abramson, J., Svensson-Ek, M., Byrne, B., Iwata, S., 2001. Structure of cytochrome *c* oxidase: a comparison of the bacterial and mitochondrial enzymes. *Biochim. Biophys. Acta - Protein Structure and Molecular Enzymology* 1544, 1–9.
- Adams, P.D., Afonine, P.V., Bunkóczi, G., Chen, V.B., Davis, I.W., Echols, N., Headd, J.J., Hung, L.-W., Kapral, G.J., Grosse-Kunstleve, R.W., McCoy, A.J., Moriarty, N.W., Oeffner, R., Read, R.J., Richardson, D.C., Richardson, J.S., Terwilliger, T.C., Zwart, P.H., 2010. PHENIX: a comprehensive Python-based system for macromolecular structure solution. *Acta Crystallogr. D* 66, 213–221.
- Allen, J.W.A., Barker, P.D., Daltrop, O., Stevens, J.M., Tomlinson, E.J., Sinha, N., Sambongi, Y., Ferguson, S.J., 2005. Why isn't "standard" heme good enough for *c*-type and *d*₁-type cytochromes? *Dalton Trans.* 3410–3418.
- Anderson, R.F., Hille, R., Shinde, S.S., Cecchini, G., 2005. Electron transfer within Complex II - succinate:ubiquinone oxidoreductase of *Escherichia coli*. *J. Biol. Chem.* 280, 33331–33337.
- Arias-Cartin, R., Grimaldi, S., Pommier, J., Lanciano, P., Schaefer, C., Arnoux, P., Giordano, G., Guigliarelli, B., Magalon, A., 2011. Cardiolipin-based respiratory complex activation in bacteria. *Proc. Natl. Acad. Sci. USA* 108, 7781–7786.
- Ayala-Castro, C., Saini, A., Outten, F.W., 2008. Fe-S Cluster Assembly Pathways in Bacteria. *Microbiol. Mol. Biol. Rev.* 72, 110–125.
- Backgren, C., Hummer, G., Wikström, M., Puustinen, A., 2000. Proton translocation by cytochrome *c* oxidase can take place without the conserved glutamic acid in subunit I. *Biochemistry* 39, 7863–7867.
- Barker, P.D., Ferguson, S.J., 1999. Still a puzzle: why is haem covalently attached in *c*-type cytochromes? *Structure* 7, R281–R290.
- Bauchop, T., Elsdén, S.R., 1960. The growth of micro-organisms in relation to their energy supply. *J. Gen. Microbiol.* 23, 457–469.
- Bekker, M., de Vries, S., Ter Beek, A., Hellingwerf, K.J., de Mattos, M.J.T., 2009. Respiration of *Escherichia coli* can be fully uncoupled via the nonelectrogenic terminal cytochrome *bd*-II oxidase. *J. Bacteriol.* 191, 5510–5517.

- Belevich, I., Bloch, D.A., Belevich, N., Wikström, M., Verkhovsky, M.I., 2007. Exploring the proton pump mechanism of cytochrome *c* oxidase in real time. *Proc. Natl. Acad. Sci. USA* 104, 2685–2690.
- Berman, H.M., Westbrook, J., Feng, Z., Gilliland, G., Bhat, T.N., Weissig, H., Shindyalov, I.N., Bourne, P.E., 2000. The Protein Data Bank. *Nucl. Acids Res.* 28, 235–242.
- Berry, S., 2003. Endosymbiosis and the design of eukaryotic electron transport. *Biochim. Biophys. Acta - Bioenergetics* 1606, 57–72.
- Bingel-Erlenmeyer, R., Olieric, V., Grimshaw, J.P.A., Gabadinho, J., Wang, X., Ebner, S.G., Isenegger, A., Schneider, R., Schneider, J., Glettig, W., Pradervand, C., Panepucci, E.H., Tomizaki, T., Wang, M., Schulze-Briese, C., 2011. SLS crystallization platform at beamline X06DA - a fully automated pipeline enabling in situ X-ray diffraction screening. *Cryst. Growth Des.* 11, 916–923.
- Böhm, G., Muhr, R., Jaenicke, R., 1992. Quantitative analysis of protein far UV circular dichroism spectra by neural networks. *Protein Eng.* 5, 191–195.
- Bottoms, C.A., Smith, P.E., Tanner, J.J., 2002. A structurally conserved water molecule in Rossmann dinucleotide-binding domains. *Protein Sci.* 11, 2125–2137.
- Calhoun, M.W., Oden, K.L., Gennis, R.B., de Mattos, M.J., Neijssel, O.M., 1993. Energetic efficiency of *Escherichia coli*: effects of mutations in components of the aerobic respiratory chain. *J. Bacteriol.* 175, 3020–3025.
- Cape, J.L., Bowman, M.K., Kramer, D.M., 2006. Understanding the cytochrome *bc* complexes by what they don't do. The Q-cycle at 30. *Trends Plant Sci.* 11, 46–55.
- Cape, J.L., Bowman, M.K., Kramer, D.M., 2007. A semiquinone intermediate generated at the Q_o site of the cytochrome *bc*₁ complex: Importance for the Q-cycle and superoxide production. *Proc. Natl. Acad. Sci. USA* 104, 7887–7892.
- Castresana, J., Saraste, M., 1995. Evolution of energetic metabolism: the respiration-early hypothesis. *Trends Biochem. Sci.* 20, 443–448.
- Cava, F., Pedro, D., Angel, M., Blas-Galindo, E., Waldo, G.S., Westblade, L.F., Berenguer, J., 2008. Expression and use of superfolder green fluorescent

- protein at high temperatures in vivo: a tool to study extreme thermophile biology. *Environ. Microbiol.* 10, 605–613.
- Cecchini, G., 2003. Function and structure of Complex II of the respiratory chain. *Annu. Rev. Biochem.* 72, 77–109.
- Chang, H.-Y., Hemp, J., Chen, Y., Fee, J.A., Gennis, R.B., 2009. The cytochrome *ba*₃ oxygen reductase from *Thermus thermophilus* uses a single input channel for proton delivery to the active site and for proton pumping. *Proc. Natl. Acad. Sci. USA* 106, 16169–16173.
- Chayen, N.E., 1997. A novel technique to control the rate of vapour diffusion, giving larger protein crystals. *J. Appl. Cryst.* 30, 198–202.
- Chothia, C., 1976. The nature of the accessible and buried surfaces in proteins. *J. Mol. Biol.* 105, 1–12.
- Christenson, A., Gustavsson, T., Gorton, L., Hägerhäll, C., 2008. Direct and mediated electron transfer between intact succinate:quinone oxidoreductase from *Bacillus subtilis* and a surface modified gold electrode reveals redox state-dependent conformational changes. *Biochim. Biophys. Acta - Bioenergetics* 1777, 1203–1210.
- Collins, M.D., Jones, D., 1981. Distribution of isoprenoid quinone structural types in bacteria and their taxonomic implication. *Microbiol. Rev.* 45, 316–354.
- Crofts, A.R., Lhee, S., Crofts, S.B., Cheng, J., Rose, S., 2006. Proton pumping in the *bc*₁ complex: A new gating mechanism that prevents short circuits. *Biochim. Biophys. Acta - Bioenergetics* 1757, 1019–1034.
- Crooks, G.E., Hon, G., Chandonia, J.-M., Brenner, S.E., 2004. WebLogo: a sequence logo generator. *Genome Res.* 14, 1188–1190.
- Cui, Q., Karplus, M., 2008. Allostery and cooperativity revisited. *Protein Sci.* 17, 1295–1307.
- Darrouzet, E., Moser, C.C., Dutton, P.L., Daldal, F., 2001. Large scale domain movement in cytochrome *bc*₁: a new device for electron transfer in proteins. *Trends Biochem. Sci.* 26, 445–451.
- Dereeper, A., Guignon, V., Blanc, G., Audic, S., Buffet, S., Chevenet, F., Dufayard, J.-F., Guindon, S., Lefort, V., Lescot, M., Claverie, J.-M., Gascuel, O., 2008. Phylogeny.fr: robust phylogenetic analysis for the non-specialist. *Nucleic Acids Res.* 36, W465–469.

- Dimroth, P., von Ballmoos, C., Meier, T., 2006. Catalytic and mechanical cycles in F-ATP synthases. *EMBO Rep.* 7, 276–282.
- Drew, D., Lerch, M., Kunji, E., Slotboom, D.-J., de Gier, J.-W., 2006. Optimization of membrane protein overexpression and purification using GFP fusions. *Nat. Meth.* 3, 303–313.
- Dyer, R.B., Einarsdottir, O., Killough, P.M., Lopez-Garriga, J.J., Woodruff, W.H., 1989. Transient binding of photodissociated carbon monoxide to Cu_B^+ of eukaryotic cytochrome oxidase at ambient temperature. Direct evidence from time-resolved infrared spectroscopy. *J. Am. Chem. Soc.* 111, 7657–7659.
- Edgar, R.C., 2004. MUSCLE: Multiple sequence alignment with high accuracy and high throughput. *Nucl. Acids Res.* 32, 1792–1797.
- Efremov, R.G., Sazanov, L.A., 2011. Respiratory complex I: “steam engine” of the cell? *Curr. Opin. Struc. Biol.* 21, 532–540.
- Einarsdóttir, O., Dyer, R.B., Lemon, D.D., Killough, P.M., Hubig, S.M., Atherton, S.J., López-Garriga, J.J., Palmer, G., Woodruff, W.H., 1993. Photodissociation and recombination of carbonmonoxy cytochrome oxidase: dynamics from picoseconds to kiloseconds. *Biochemistry* 32, 12013–12024.
- Farver, O., Pecht, I., 2008. Elucidation of electron transfer pathways in copper and iron proteins by pulse radiolysis experiments, in: Karlin, K.D. (Ed.), *Progress in Inorganic Chemistry*. John Wiley & Sons, Inc., pp. 1–78.
- Fee, J.A., Todaro, T.R., Luna, E., Sanders, D., Hunsicker-Wang, L.M., Patel, K.M., Bren, K.L., Gomez-Moran, E., Hill, M.G., Ai, J., Loehr, T.M., Oertling, W.A., Williams, P.A., Stout, C.D., McRee, D., Pastuszyn, A., 2004. Cytochrome rC552, formed during expression of the truncated, *Thermus thermophilus* cytochrome *c*₅₅₂ gene in the cytoplasm of *Escherichia coli*, reacts spontaneously to form protein-bound 2-formyl-4-vinyl (spirographis) heme. *Biochemistry* 43, 12162–12176.
- Ferraro, D.J., Gakhar, L., Ramaswamy, S., 2005. Rieske business: structure–function of Rieske non-heme oxygenases. *Biochem. Biophys. Res. Commun.* 338, 175–190.

- Frustaci, J.M., Sangwan, I., O'Brian, M.R., 1991. Aerobic growth and respiration of a δ -aminolevulinic acid synthase (*hemA*) mutant of *Bradyrhizobium japonicum*. J. Bacteriol. 173, 1145–1150.
- Gao, Y., Meyer, B., Sokolova, L., Zwicker, K., Karas, M., Brutschy, B., Peng, G., Michel, H., 2012. Heme-copper terminal oxidase using both cytochrome *c* and ubiquinol as electron donors. Proc. Natl. Acad. Sci. USA 109, 3275–3280.
- Garcia-Horsman, J.A., Barquera, B., Rumbley, J., Ma, J., Gennis, R.B., 1994. The superfamily of heme-copper respiratory oxidases. J. Bacteriol. 176, 5587–5600.
- Georgevich, G., Darley-Usmar, V.M., Malatesta, F., Capaldi, R.A., 1983. Electron transfer in monomeric forms of beef and shark heart cytochrome *c* oxidase. Biochemistry 22, 1317–1322.
- Giuffrè, A., Stubauer, G., Sarti, P., Brunori, M., Zumft, W.G., Buse, G., Soulimane, T., 1999. The heme-copper oxidases of *Thermus thermophilus* catalyze the reduction of nitric oxide: Evolutionary implications. Proc. Natl. Acad. Sci. USA 96, 14718–14723.
- Greenfield, N.J., 2007. Determination of the folding of proteins as a function of denaturants, osmolytes or ligands using circular dichroism. Nat. Protoc. 1, 2733–2741.
- Gribaldo, S., Talla, E., Brochier-Armanet, C., 2009. Evolution of the haem copper oxidases superfamily: a rooting tale. Trends Biochem. Sci. 34, 375–381.
- Griffith, G.R., Chandler, J.L., Gholson, R.K., 1975. Studies on the *de novo* biosynthesis of nicotinamide adenine dinucleotide in *Escherichia coli*: the separation of the *nadB* gene product and its purification. Eur. J. Biochem. 54, 239–245.
- Haas, A.H., Sauer, U.S., Gross, R., Simon, J., Mäntele, W., Lancaster, C.R.D., 2005. FTIR difference spectra of *Wolinella succinogenes* quinol:fumarate reductase support a key role of Glu C180 within the “E-Pathway Hypothesis” of coupled transmembrane electron and proton transfer. Biochemistry 44, 13949–13961.
- Hägerhäll, C., 1997. Succinate: quinone oxidoreductases: Variations on a conserved theme. Biochim. Biophys. Acta - Bioenergetics 1320, 107–141.

- Hägerhäll, C., Hederstedt, L., 1996. A structural model for the membrane-integral domain of succinate:quinone oxidoreductases. *FEBS Lett.* 389, 25–31.
- Hatefi, Y., 1978. Introduction - preparation and properties of the enzymes and enzymes complexes of the mitochondrial oxidative phosphorylation system. *Meth. Enzymol.* 53, 3–4.
- Hatefi, Y., Galante, Y.M., 1980. Isolation of cytochrome b_{560} from complex II (succinate:ubiquinone oxidoreductase) and its reconstitution with succinate dehydrogenase. *J. Biol. Chem.* 255, 5530–5537.
- Hederstedt, L., 2003. Complex II is complex too. *Science* 299, 671–672.
- Heitbrink, D., Sigurdson, H., Bolwien, C., Brzezinski, P., Heberle, J., 2002. Transient binding of CO to Cu(B) in cytochrome *c* oxidase is dynamically linked to structural changes around a carboxyl group: a time-resolved step-scan Fourier transform infrared investigation. *Biophys. J.* 82, 1–10.
- Helling, R.B., 2002. Speed versus efficiency in microbial growth and the role of parallel pathways. *J. Bacteriol.* 184, 1041–1045.
- Hendler, R.W., Pardhasaradhi, K., Reynafarje, B., Ludwig, B., 1991. Comparison of energy-transducing capabilities of the two- and three-subunit cytochromes aa_3 from *Paracoccus denitrificans* and the 13-subunit beef heart enzyme. *Biophys. J.* 60, 415–423.
- Heuts, D.P.H.M., Scrutton, N.S., McIntire, W.S., Fraaije, M.W., 2009. What's in a covalent bond? *FEBS J.* 276, 3405–3427.
- Hong, S., Pedersen, P.L., 2004. Mitochondrial ATP synthase: A bioinformatic approach reveals new insights about the roles of supernumerary subunits g and A6L. *J. Bioenerg. Biomembr.* 36, 515–523.
- Horsefield, R., Yankovskaya, V., Sexton, G., Whittingham, W., Shiomi, K., Ōmura, S., Byrne, B., Cecchini, G., Iwata, S., 2006. Structural and computational analysis of the quinone-binding site of Complex II (succinate-ubiquinone oxidoreductase) - A mechanism of electron transfer and proton conduction during ubiquinone reduction. *J. Biol. Chem.* 281, 7309–7316.
- Huang, L., Sun, G., Cobessi, D., Wang, A.C., Shen, J.T., Tung, E.Y., Anderson, V.E., Berry, E.A., 2006. 3-nitropropionic acid is a suicide inhibitor of mitochondrial respiration that, upon oxidation by Complex II, forms a

- covalent adduct with a catalytic base arginine in the active site of the enzyme. *J. Biol. Chem.* 281, 5965–5972.
- Hunte, C., Zickermann, V., Brandt, U., 2010. Functional modules and structural basis of conformational coupling mitochondrial Complex I. *Science* 329, 448–451.
- Iben, I.E., Cowen, B.R., Sanches, R., Friedman, J.M., 1991. Carboxy Mb at pH 3. Time-resolved resonance Raman study at cryogenic temperatures. *Biophys. J.* 59, 908–919.
- Iverson, T.M., Luna-Chavez, C., Cecchini, G., Rees, D.C., 1999. Structure of the *Escherichia coli* fumarate reductase respiratory complex. *Science* 284, 1961–1966.
- Iverson, T.M., Luna-Chavez, C., Croal, L.R., Cecchini, G., Rees, D.C., 2002. Crystallographic studies of the *Escherichia coli* quinol-fumarate reductase with inhibitors bound to the quinol-binding site. *J. Biol. Chem.* 277, 16124–16130.
- Jacobs, N.J., Jacobs, J.M., 1975. Fumarate as alternate electron acceptor for the late steps of anaerobic heme synthesis in *Escherichia coli*. *Biochem. Biophys. Res. Commun.* 65, 435–441.
- Janzon, J., Ludwig, B., Malatesta, F., 2007. Electron transfer kinetics of soluble fragments indicate a direct interaction between complex III and the *caa₃* oxidase in *Thermus thermophilus*. *IUBMB Life* 59, 563–569.
- Johnson, D.C., Dean, D.R., Smith, A.D., Johnson, M.K., 2005. Structure, function, and formation of biological iron-sulfur clusters. *Annu. Rev. Biochem.* 74, 247–281.
- Jonckheere, A.I., Smeitink, J.A.M., Rodenburg, R.J.T., 2012. Mitochondrial ATP synthase: architecture, function and pathology. *J. Inherit. Metab. Dis.* 35, 211–225.
- Jormakka, M., Byrne, B., Iwata, S., 2003. Protonmotive force generation by a redox loop mechanism. *FEBS Lett.* 545, 25–30.
- Kabsch, W., 2010. XDS. *Acta Crystallogr. D* 66, 125–132.
- Kaila, V.R.I., Verkhovsky, M.I., Hummer, G., Wikström, M., 2008. Glutamic acid 242 is a valve in the proton pump of cytochrome *c* oxidase. *Proc. Natl. Acad. Sci. USA* 105, 6255–6259.

- Kiefersauer, R., Than, M.E., Dobbek, H., Gremer, L., Melero, M., Strobl, S., Dias, J.M., Soulimane, T., Huber, R., 2000. A novel free-mounting system for protein crystals: transformation and improvement of diffraction power by accurately controlled humidity changes. *J. Appl. Cryst.* 33, 1223–1230.
- Kita, K., Vibat, C.R., Meinhardt, S., Guest, J.R., Gennis, R.B., 1989. One-step purification from *Escherichia coli* of complex II (succinate: ubiquinone oxidoreductase) associated with succinate-reducible cytochrome *b*₅₅₆. *J. Biol. Chem.* 264, 2672–2677.
- Koch, H.-G., Schneider, D., 2007. Folding, assembly, and stability of transmembrane cytochromes. *Curr. Chem. Biol.* 1, 59–74.
- Kolaj-Robin, O., Noor, M.R., O’Kane, S.R., Baymann, F., Soulimane, T., Atypical features of *Thermus thermophilus* succinate:quinone reductase. *PLoS One* (accepted).
- Kolaj-Robin, O., O’Kane, S.R., Nitschke, W., Léger, C., Baymann, F., Soulimane, T., 2011. Biochemical and biophysical characterization of succinate: quinone reductase from *Thermus thermophilus*. *Biochim. Biophys. Acta - Bioenergetics* 1807, 68–79.
- Konstantinov, A.A., 2012. Cytochrome *c* oxidase: Intermediates of the catalytic cycle and their energy-coupled interconversion. *FEBS Lett.* 586, 630–639.
- Koutsoupakis, C., Soulimane, T., Varotsis, C., 2003. Docking site dynamics of *ba*₃-cytochrome *c* oxidase from *Thermus thermophilus*. *J. Biol. Chem.* 278, 36806–36809.
- Koutsoupakis, C., Soulimane, T., Varotsis, C., 2012. Spectroscopic and kinetic investigation of the fully reduced and mixed valence states of *ba*₃-cytochrome *c* oxidase from *Thermus thermophilus*: a Fourier transform infrared (FTIR) and time-resolved step-scan FTIR study. *J. Biol. Chem.* 287, 37495–37507.
- Krulwich, T.A., Sachs, G., Padan, E., 2011. Molecular aspects of bacterial pH sensing and homeostasis. *Nat. Rev. Microbiol.* 9, 330–343.
- Kurokawa, T., Sakamoto, J., 2005. Purification and characterization of succinate:menaquinone oxidoreductase from *Corynebacterium glutamicum*. *Arch. Microbiol.* 183, 317–324.
- Lancaster, C.R.D., 2002. *Wolinella succinogenes* quinol:fumarate reductase - 2.2-Å resolution crystal structure and the E-pathway hypothesis of coupled

- transmembrane proton and electron transfer. *Biochim. Biophys. Acta - Biomembranes* 1565, 215–231.
- Lancaster, C.R.D., 2003. *Wolinella succinogenes* quinol:fumarate reductase and its comparison to *E. coli* succinate:quinone reductase. *FEBS Lett.* 555, 21–28.
- Lancaster, C.R.D., 2004. Structure and function of succinate:quinone oxidoreductases and the role of quinol:fumarate reductases in fumarate respiration, in: Zannoni, D. (Ed.), *Respiration in Archaea and Bacteria*, Vol. 1: Diversity of Prokaryotic Electron Transport Carriers. Kluwer, Dordrecht, NL., pp. 57–85.
- Lancaster, C.R.D., Groß, R., Simon, J., 2001. A third crystal form of *Wolinella succinogenes* quinol:fumarate reductase reveals domain closure at the site of fumarate reduction. *Eur. J. Biochem.* 268, 1820–1827.
- Lancaster, C.R.D., Kröger, A., Auer, M., Michel, H., 1999. Structure of fumarate reductase from *Wolinella succinogenes* at 2.2 Å resolution. *Nature* 402, 377–385.
- Larkin, M.A., Blackshields, G., Brown, N.P., Chenna, R., McGettigan, P.A., McWilliam, H., Valentin, F., Wallace, I.M., Wilm, A., Lopez, R., Thompson, J.D., Gibson, T.J., Higgins, D.G., 2007. Clustal W and Clustal X version 2.0. *Bioinformatics* 23, 2947–2948.
- Laskowski, R.A., Swindells, M.B., 2011. LigPlot+: multiple ligand–protein interaction diagrams for drug discovery. *J. Chem. Inf. Model.* 51, 2778–2786.
- Lemma, E., Uden, G., Kröger, A., 1990. Menaquinone is an obligatory component of the chain catalyzing succinate respiration in *Bacillus subtilis*. *Arch. Microbiol.* 155, 62–67.
- Lemos, R.S., Fernandes, A.S., Pereira, M.M., Gomes, C.M., Teixeira, M., 2002. Quinol:fumarate oxidoreductases and succinate:quinone oxidoreductases: phylogenetic relationships, metal centres and membrane attachment. *Biochim. Biophys. Acta - Bioenergetics* 1553, 158–170.
- Liebl, U., Bouzhir-Sima, L., Négrerie, M., Martin, J.-L., Vos, M.H., 2002. Ultrafast ligand rebinding in the heme domain of the oxygen sensors FixL and Dos: General regulatory implications for heme-based sensors. *Proc. Natl. Acad. Sci. USA* 99, 12771–12776.

- Liebl, U., Lipowski, G., Négrerie, M., Lambry, J.-C., Martin, J.-L., Vos, M.H., 1999. Coherent reaction dynamics in a bacterial cytochrome *c* oxidase. *Nature* 401, 181–184.
- Lill, R., Mühlhoff, U., 2008. Maturation of iron-sulfur proteins in eukaryotes: mechanisms, connected processes, and diseases. *Annu. Rev. Biochem.* 77, 669–700.
- Lyons, J.A., Aragão, D., Slattery, O., Soulimane, T., Caffrey, M., 2012. Structural insights into electron transfer in *caa3*-type cytochrome oxidase. *Nature* 487, 514–518.
- Macheroux, P., Kappes, B., Ealick, S.E., 2011. Flavogenomics – a genomic and structural view of flavin-dependent proteins. *FEBS J.* 278, 2625–2634.
- Madej, M.G., Nasiri, H.R., Hilgendorff, N.S., Schwalbe, H., Lancaster, C.R.D., 2006. Evidence for transmembrane proton transfer in a dihaem-containing membrane protein complex. *EMBO J.* 25, 4963–4970.
- Madej, M.G., Nasiri, H.R., Hilgendorff, N.S., Schwalbe, H., Unden, G., Lancaster, C.R.D., 2007. Experimental evidence for proton motive force-dependent catalysis by the diheme-containing succinate:menaquinone oxidoreductase from the Gram-positive bacterium *Bacillus licheniformis*. *Biochemistry* 45, 15049–15055.
- Maklashina, E., Cecchini, G., 2010. The quinone-binding and catalytic site of complex II. *Biochim. Biophys. Acta - Bioenergetics* 1797, 1877–1882.
- Maklashina, E., Hellwig, P., Rothery, R.A., Kotlyar, V., Sher, Y., Weiner, J.H., Cecchini, G., 2006. Differences in protonation of ubiquinone and menaquinone in fumarate reductase from *Escherichia coli*. *J. Biol. Chem.* 281, 26655–26664.
- Maneg, O., Malatesta, F., Ludwig, B., Drosou, V., 2004. Interaction of cytochrome *c* with cytochrome oxidase: two different docking scenarios. *Biochim. Biophys. Acta - Bioenergetics* 1655, 274–281.
- Mao, J., Hauser, K., Gunner, M.R., 2003. How cytochromes with different folds control heme redox potentials. *Biochemistry* 42, 9829–9840.
- Martin, J.-L., Vos, M.H., 1994. Femtosecond measurements of geminate recombination in heme proteins, in: Everse, J., Vandegriff, K.D., Winslow, R. (Eds.), *Hemoglobins Part C: Biophysical Methods*. Academic Press, pp. 416–430.

- Matsson, M., Tolstoy, D., Aasa, R., Hederstedt, L., 2000. The distal heme center in *Bacillus subtilis* succinate:quinone reductase is crucial for electron transfer to menaquinone. *Biochemistry* 39, 8617–8624.
- Mattevi, A., Tedeschi, G., Bacchella, L., Coda, A., Negri, A., Ronchi, S., 1999. Structure of L-aspartate oxidase: implications for the succinate dehydrogenase/fumarate reductase oxidoreductase family. *Structure* 7, 745–756.
- Messner, K.R., Imlay, J.A., 2002. Mechanism of superoxide and hydrogen peroxide formation by fumarate reductase, succinate dehydrogenase, and aspartate oxidase. *J. Biol. Chem.* 277, 42563–42571.
- Mewies, M., McIntire, W.S., Scrutton, N.S., 1998. Covalent attachment of flavin adenine dinucleotide (FAD) and flavin mononucleotide (FMN) to enzymes: The current state of affairs. *Protein Sci.* 7, 7–20.
- Mileni, M., MacMillan, F., Tziatzios, C., Zwicker, K., Haas, A.H., Mäntele, W., Simon, J., Lancaster, C.R.D., 2006. Heterologous production in *Wolinella succinogenes* and characterization of the quinol:fumarate reductase enzymes from *Helicobacter pylori* and *Campylobacter jejuni*. *Biochem. J.* 395, 191.
- Miller, M.J., Gennis, R.B., 1983. The purification and characterization of the cytochrome *d* terminal oxidase complex of the *Escherichia coli* aerobic respiratory chain. *J. Biol. Chem.* 258, 9159–9165.
- Mimaki, M., Wang, X., McKenzie, M., Thorburn, D.R., Ryan, M.T., 2012. Understanding mitochondrial complex I assembly in health and disease. *Biochim. Biophys. Acta - Bioenergetics* 1817, 851–862.
- Mitchell, P., 1966. Chemiosmotic coupling in oxidative and photosynthetic phosphorylation. Glynn Research.
- Mitchell, P., 2011. Chemiosmotic coupling in oxidative and photosynthetic phosphorylation. *Biochim. Biophys. Acta - Bioenergetics* 1807, 1507–1538.
- Möbius, K., Arias-Cartin, R., Breckau, D., Hännig, A.-L., Riedmann, K., Biedendieck, R., Schröder, S., Becher, D., Magalon, A., Moser, J., Jahn, M., Jahn, D., 2010. Heme biosynthesis is coupled to electron transport chains for energy generation. *Proc. Natl. Acad. Sci. USA* 107, 10436–10441.

- Moll, R., Schäfer, G., 1991. Purification and characterisation of an archaeobacterial succinate dehydrogenase complex from the plasma membrane of the thermoacidophile *Sulfolobus acidocaldarius*. Eur. J. Biochem. 201, 593–600.
- Morales, J., Mogi, T., Mineki, S., Takashima, E., Mineki, R., Hirawake, H., Sakamoto, K., Ōmura, S., Kita, K., 2009. Novel mitochondrial Complex II isolated from *Trypanosoma cruzi* is composed of 12 peptides including a heterodimeric Ip subunit. J. Biol. Chem. 284, 7255–7263.
- Moreno, R., Hidalgo, A., Cava, F., Fernández-Lafuente, R., Guisán, J.M., Berenguer, J., 2004. Use of an antisense RNA strategy to investigate the functional significance of Mn-catalase in the extreme thermophile *Thermus thermophilus*. J. Bacteriol. 186, 7804–7806.
- Mortarino, M., Negri, A., Tedeschi, G., Simonic, T., Duga, S., Gassen, H.G., Ronchi, S., 1996. L-aspartate oxidase from *Escherichia coli* -I. Characterization of coenzyme binding and product inhibition. Eur. J. Biochem. 239, 418–426.
- Muench, S.P., Trinick, J., Harrison, M.A., 2011. Structural divergence of the rotary ATPases. Q. Rev. Biophys. 44, 311–356.
- Mulkiđjanian, A.Y., Heberle, J., Cherepanov, D.A., 2006. Protons @ interfaces: Implications for biological energy conversion. Biochim. Biophys. Acta - Bioenergetics 1757, 913–930.
- Muresanu, L., Pristovsek, P., Löhr, F., Maneg, O., Mukrasch, M.D., Rüterjans, H., Ludwig, B., Lücke, C., 2006. The electron transfer complex between cytochrome *c*₅₅₂ and the Cu_A domain of the *Thermus thermophilus* *ba*₃ oxidase. J. Biol. Chem. 281, 14503–14513.
- Nakamura, K., Yamaki, M., Sarada, M., Nakayama, S., Vibat, C.R.T., Gennis, R.B., Nakayashiki, T., Inokuchi, H., Kojima, S., Kita, K., 1996. Two hydrophobic subunits are essential for the heme *b* ligation and functional assembly of Complex II (succinate-ubiquinone oxidoreductase) from *Escherichia coli*. J. Biol. Chem. 271, 521–527.
- Nakamura, Y., Gojobori, T., Ikemura, T., 2000. Codon usage tabulated from international DNA sequence databases: status for the year 2000. Nucl. Acids Res. 28, 292–292.

- Nasu, S., Wicks, F.D., Gholson, R.K., 1982. L-aspartate oxidase, a newly discovered enzyme of *Escherichia coli*, is the B protein of quinolinate synthetase. *J. Biol. Chem.* 257, 626–632.
- Négrerie, M., Berka, V., Vos, M.H., Liebl, U., Lambry, J.-C., Tsai, A.-L., Martin, J.-L., 1999. Geminate recombination of nitric oxide to endothelial nitric-oxide synthase and mechanistic implications. *J. Biol. Chem.* 274, 24694–24702.
- Négrerie, M., Kruglik, S.G., Lambry, J.-C., Vos, M.H., Martin, J.-L., Franzen, S., 2006. Role of heme iron coordination and protein structure in the dynamics and geminate rebinding of nitric oxide to the H93G myoglobin mutant: Implications for nitric oxide sensors. *J. Biol. Chem.* 281, 10389–10398.
- Newman, J., 2006. A review of techniques for maximizing diffraction from a protein crystal *in stilla*. *Acta Cryst.* D62, 27–31.
- Niesen, F.H., Berglund, H., Vedadi, M., 2007. The use of differential scanning fluorimetry to detect ligand interactions that promote protein stability. *Nat. Protoc.* 2, 2212–2221.
- Noji, H., Yoshida, M., 2001. The rotary machine in the cell, ATP synthase. *J. Biol. Chem.* 276, 1665–1668.
- Noor, M.R., Soulimane, T., 2012. Bioenergetics at extreme temperature: *Thermus thermophilus* *ba*₃- and *caa*₃-type cytochrome *c* oxidases. *Biochim. Biophys. Acta - Bioenergetics* 1817, 638–649.
- O’Kane, S.R., 2011. Respiratory complexes from *Thermus thermophilus*: Native and recombinant production of both complex II and *caa*₃-type cytochrome *c* oxidase for structural studies. PhD thesis, University of Limerick.
- Ostermeier, C., Harrenga, A., Ermler, U., Michel, H., 1997. Structure at 2.7 Å resolution of the *Paracoccus denitrificans* two-subunit cytochrome *c* oxidase complexed with an antibody FV fragment. *Proc. Natl. Acad. Sci. USA* 94, 10547–10553.
- Osyczka, A., Moser, C.C., Daldal, F., Dutton, P.L., 2004. Reversible redox energy coupling in electron transfer chains. *Nature* 427, 607–612.
- Ott, M., Herrmann, J.M., 2010. Co-translational membrane insertion of mitochondrially encoded proteins. *Biochim. Biophys. Acta - Molecular Cell Research* 1803, 767–775.

- Page, C.C., Moser, C.C., Dutton, P.L., 2003. Mechanism for electron transfer within and between proteins. *Curr. Opin. Chem. Biol.* 7, 551–556.
- Pardhasaradhi, K., Ludwig, B., Hendler, R.W., 1991. Potentiometric and spectral studies with the two-subunit cytochrome *aa*₃ from *Paracoccus denitrificans*. Comparison with the 13-subunit beef heart enzyme. *Biophys. J.* 60, 408–414.
- Pavlou, A., Soulimane, T., Pinakoulaki, E., 2011. Evidence for the presence of two conformations of the heme *a*₃-Cu_B pocket of cytochrome *caa*₃ from *Thermus thermophilus*. *J. Phys. Chem. B* 115, 11455–11461.
- Pereira, M.M., Bandejas, T.M., Fernandes, A.S., Lemos, R.S., Melo, A.M.P., Teixeira, M., 2004. Respiratory chains from aerobic thermophilic prokaryotes. *J. Bioenerg. Biomembr.* 36, 93–105.
- Pereira, M.M., Santana, M., Teixeira, M., 2001. A novel scenario for the evolution of haem-copper oxygen reductases. *Biochim. Biophys. Acta - Bioenergetics* 1505, 185–208.
- Pereira, M.M., Sousa, F.L., Veríssimo, A.F., Teixeira, M., 2008. Looking for the minimum common denominator in haem-copper oxygen reductases: Towards a unified catalytic mechanism. *Biochim. Biophys. Acta - Bioenergetics* 1777, 929–934.
- Pilet, E., Nitschke, W., Rappaport, F., Soulimane, T., Lambry, J.-C., Liebl, U., Vos, M.H., 2004. NO binding and dynamics in reduced heme-copper oxidases *aa*₃ from *Paracoccus denitrificans* and *ba*₃ from *Thermus thermophilus*. *Biochemistry* 43, 14118–14127.
- Potterton, L., McNicholas, S., Krissinel, E., Gruber, J., Cowtan, K., Emsley, P., Murshudov, G.N., Cohen, S., Perrakis, A., Noble, M., 2004. Developments in the CCP4 molecular-graphics project. *Acta Cryst. D* 60, 2288–2294.
- Robinson, N.C., Talbert, L., 1986. Triton-X-100 induced dissociation of beef heart cytochrome c oxidase into monomers. *Biochemistry* 25, 2328–2335.
- Rossmann, M.G., Moras, D., Olsen, K.W., 1974. Chemical and biological evolution of nucleotide-binding protein. *Nature* 250, 194–199.
- Rubio, L.M., Ludden, P.W., 2008. Biosynthesis of the iron-molybdenum cofactor of nitrogenase. *Annu. Rev. Microbiol.* 62, 93–111.

- Ruprecht, J., Yankovskaya, V., Maklashina, E., Iwata, S., Cecchini, G., 2009. Structure of *Escherichia coli* succinate:quinone oxidoreductase with an occupied and empty quinone-binding site. *J. Biol. Chem.* 284, 29836–29846.
- Rutherford, A.W., Osyczka, A., Rappaport, F., 2012. Back-reactions, short-circuits, leaks and other energy wasteful reactions in biological electron transfer: Redox tuning to survive life in O₂. *FEBS Lett.* 586, 603–616.
- Sadoski, R.C., Zaslavsky, D., Gennis, R.B., Durham, B., Millett, F., 2001. Exposure of bovine cytochrome c oxidase to high Triton X-100 or to alkaline conditions causes a dramatic change in the rate of reduction of compound F. *J. Biol. Chem.* 276, 33616–33620.
- Schnorpfeil, M., Janausch, I.G., Biel, S., Kröger, A., Unden, G., 2001. Generation of a proton potential by succinate dehydrogenase of *Bacillus subtilis* functioning as a fumarate reductase. *Eur. J. Biochem.* 268, 3069–3074.
- Shimizu, H., Osanai, A., Sakamoto, K., Inaoka, D.K., Shiba, T., Harada, S., Kita, K., 2012. Crystal structure of mitochondrial quinol–fumarate reductase from the parasitic nematode *Ascaris suum*. *J. Biochem.* 151, 589–592.
- Singer, T.P., Kearney, E.B., Kenney, W.C., 1973. Succinate dehydrogenase, in: Meister, A. (Ed.), *Adv Enzymol Relat Areas Mol Biol*. John Wiley & Sons, Inc., pp. 189–272.
- Smith, P.M., Fox, J.L., Winge, D.R., 2012. Biogenesis of the cytochrome *bc*₁ complex and role of assembly factors. *Biochim. Biophys. Acta - Bioenergetics* 1817, 276–286.
- Soto, I.C., Fontanesi, F., Liu, J., Barrientos, A., 2012. Biogenesis and assembly of eukaryotic cytochrome c oxidase catalytic core. *Biochim. Biophys. Acta - Bioenergetics* 1817, 883–897.
- Soulimane, T., Noor, M.R., Arese, M., Forte, E., McCarthy, M., Sarti, P., Giuffrè, A., Cytochrome *c*₅₅₂ mediates electron transfer between Complexes III and IV of *Thermus thermophilus*. (submitted)
- Studier, F.W., 2005. Protein production by auto-induction in high-density shaking cultures. *Prot. Expr. Purif.* 41, 207–234.
- Suarez, M.D., Revzin, A., Narlock, R., Kempner, E.S., Thompson, D.A., Ferguson-Miller, S., 1984. The functional and physical form of mammalian cytochrome c oxidase determined by gel filtration, radiation

- inactivation, and sedimentation equilibrium analysis. *J. Biol. Chem.* 259, 13791–13799.
- Sun, F., Huo, X., Zhai, Y., Wang, A., Xu, J., Su, D., Bartlam, M., Rao, Z., 2005. Crystal structure of mitochondrial respiratory membrane protein Complex II. *Cell* 121, 1043–1057.
- Tedeschi, G., Negri, A., Mortarino, M., Ceciliani, F., Simonic, T., Faotto, L., Ronchi, S., 1996. L-aspartate oxidase from *Escherichia coli* -II. Interaction with C₄ dicarboxylic acids and identification of a novel L-aspartate:fumarate oxidoreductase activity. *Eur. J. Biochem.* 239, 427–433.
- Tedeschi, G., Zetta, L., Negri, A., Mortarino, M., Ceciliani, F., Ronchi, S., 1997. Redox potentials and quinone reductase activity of L-aspartate oxidase from *Escherichia coli*. *Biochemistry* 36, 16221–16230.
- Tran, Q.M., Rothery, R.A., Maklashina, E., Cecchini, G., Weiner, J.H., 2006. The quinone binding site in *Escherichia coli* succinate dehydrogenase is required for electron transfer to the heme *b*. *J. Biol. Chem.* 281, 32310–32317.
- Tran, Q.M., Rothery, R.A., Maklashina, E., Cecchini, G., Weiner, J.H., 2007. *Escherichia coli* succinate dehydrogenase variant lacking the heme *b*. *Proc. Natl. Acad. Sci. USA* 104, 18007–18012.
- Tsuchiya, Y., Nakamura, H., Kinoshita, K., 2008. Discrimination between biological interfaces and crystal-packing contacts. *Adv. Appl. Bioinform Chem.* 1, 99–113.
- Tulumello, D.V., Deber, C.M., 2012. Efficiency of detergents at maintaining membrane protein structures in their biologically relevant forms. *Biochim. Biophys. Acta - Biomembranes* 1818, 1351–1358.
- Uden, G., Kröger, A., 1986. Reconstitution of a functional electron-transfer chain from purified formate dehydrogenase and fumarate reductase complexes. *Meth. Enzymol.* 126, 387–399.
- Uzawa, T., Yamagishi, A., Oshima, T., 2002. Polypeptide synthesis directed by DNA as a messenger in cell-free polypeptide synthesis by extreme thermophiles, *Thermus thermophilus* HB27 and *Sulfolobus tokodaii* strain 7. *J Biochem* 131, 849–853.

- Uzawa, T., Yamagishi, A., Oshima, T., 2003. Continuous cell-free protein synthesis directed by messenger DNA and catalyzed by extract of *Thermus thermophilus* HB27. *Biosci. Biotechnol. Biochem.* 67, 639–642.
- van Gelder, B.F., 1966. On cytochrome c oxidase I. The extinction coefficients of cytochrome *a* and cytochrome *a*₃. *Biochim. Biophys. Acta - Enzymology* 118, 36–46.
- Vos, M.H., Lipowski, G., Lambry, J.-C., Martin, J.-L., Liebl, U., 2001. Dynamics of nitric oxide in the active site of reduced cytochrome *c* oxidase *aa*₃. *Biochemistry* 40, 7806–7811.
- Walker, W.H., Singer, T.P., 1970. Identification of the covalently bound flavin of succinate dehydrogenase as 8 α -(histidyl) flavin adenine dinucleotide. *J. Biol. Chem.* 245, 4224–4225.
- Waterhouse, A.M., Procter, J.B., Martin, D.M.A., Clamp, M., Barton, G.J., 2009. Jalview Version 2-a multiple sequence alignment editor and analysis workbench. *Bioinformatics* 25, 1189–1191.
- Wherland, S., Farver, O., Pecht, I., 2005. Intramolecular electron transfer in nitrite reductases. *ChemPhysChem* 6, 805–812.
- Wikström, M., Hummer, G., 2012. Stoichiometry of proton translocation by respiratory complex I and its mechanistic implications. *Proc. Natl. Acad. Sci. USA* 109, 4431–4436.
- Wöhri, A.B., Johansson, L.C., Wadsten-Hindrichsen, P., Wahlgren, W.Y., Fischer, G., Horsefield, R., Katona, G., Nyblom, M., Öberg, F., Young, G., Cogdell, R.J., Fraser, N.J., Engström, S., Neutze, R., 2008. A lipidic-sponge phase screen for membrane protein crystallization. *Structure* 16, 1003–1009.
- Woodruff, W.H., Einarsdóttir, O., Dyer, R.B., Bagley, K.A., Palmer, G., Atherton, S.J., Goldbeck, R.A., Dawes, T.D., Kliger, D.S., 1991. Nature and functional implications of the cytochrome *a*₃ transients after photodissociation of CO-cytochrome oxidase. *Proc. Natl. Acad. Sci. USA* 88, 2588–2592.
- Yankovskaya, V., Horsefield, R., Törnroth, S., Luna-Chavez, C., Miyoshi, H., Léger, C., Byrne, B., Cecchini, G., Iwata, S., 2003. Architecture of succinate dehydrogenase and reactive oxygen species generation. *Science* 299, 700–704.

REFERENCES

- Yu, L., Xu, J.X., Haley, P.E., Yu, C.A., 1987. Properties of bovine heart mitochondrial cytochrome b_{560} . *J. Biol. Chem.* 262, 1137–1143.
- Zhen, Y., Hoganson, C.W., Babcock, G.T., Ferguson-Miller, S., 1999. Definition of the interaction domain for cytochrome c on cytochrome c oxidase. *J. Biol. Chem.* 274, 38032–38041.

APPENDIX

Atypical features of *Thermus thermophilus* succinate:quinone reductase

Olga Kolaj-Robin*, Mohamed R. Noor*, Sarah R. O’Kane*, Frauke Baymann †¹ and Tewfik Soulimane*¹

* Chemical and Environmental Sciences Department and Materials & Surface Science Institute, University of Limerick, Limerick, Ireland

† Laboratoire de Bioénergétique et Ingénierie des Protéines, BIP/CNRS, UMR7281, AMU, 31, chemin Joseph Aiguier, 13402 Marseille cedex 20, France

¹ Corresponding authors: F. Baymann: email: baymann@imm.cnrs.fr; tel: +33491164672 and T. Soulimane: email: tewfik.soulimane@ul.ie; tel: +35361234133; fax: +35361202568

Synopsis

The *Thermus thermophilus* succinate:quinone reductase (SQR), serving as the respiratory complex II, has been homologously produced under the control of a constitutive promoter and subsequently purified. The detailed biochemical characterization of the resulting wild type (wt-rcII) and His-tagged (rcII-His₈-SdhB and rcII-SdhB-His₆) complex II variants showed the same properties as the native enzyme with respect to the subunit composition, redox cofactor content and sensitivity to the inhibitors malonate, oxaloacetate, 3-nitropropionic acid and nonyl-4-hydroxyquinoline-N-oxide (NQNO). The position of the His-tag determined whether the enzyme retained its native conformation or its trimerization was disrupted with the consequent monomeric form. Only the former showed positive cooperativity at high temperatures. The EPR signal of the [2Fe-2S] cluster showed increased rhombicity in the presence of substrate succinate in the native and in all recombinant forms of the enzyme. A detailed analysis of the shape of this signal as a function of pH, substrate concentration and in the presence of various inhibitors and quinones was carried out. This led to the proposition of a model for the molecular mechanism that underlies the influence of substrate succinate on the rhombicity of the EPR signal of the proximal iron-sulfur cluster.

Keywords: Complex II; succinate:quinone oxidoreductase; EPR; cooperativity; iron-sulfur cluster; *Thermus thermophilus*.

Abbreviations

1,4-NQ, 1,4-naphthoquinone; 3-NP, 3-Nitropropionic acid; BN-PAGE, Blue Native PAGE; BV, benzylviologen, DCPIP, 2,6-dichlorophenolindophenol; DDM, dodecyl- β -D-maltoside; DQ, duroquinone; MK, menaquinone; NQNO, nonyl-4-hydroxyquinoline-N-oxide; *p*-BQ, *p*-benzoquinone; PMS, phenazine methosulfate; QFR, quinol:fumarate reductases; SHE, standard hydrogen electrode; SQOR, succinate:quinone oxidoreductases; SQR, succinate:quinone reductase.

INTRODUCTION

The succinate:quinone oxidoreductases (SQOR) superfamily (EC 1.3.5.1) comprises enzymes serving as the respiratory complex II and are classified depending on the direction of the reaction catalyzed *in vivo*. While the succinate:quinone reductases (SQRs) mediate the oxidation of succinate to fumarate coupled with the reduction of quinone to quinol, the quinol:fumarate reductases (QFRs) catalyze the reverse reaction [1]. SQR and QFR are homologous proteins that evolved from a common evolutionary ancestor and can catalyze both reactions *in vitro* and in the cell under the appropriate conditions [2, 3]. SQRs are involved in the aerobic metabolism and, as well as being a part of the respiratory chain, constitute the only membrane-bound enzyme of the tricarboxylic acid cycle [4]. In contrast, QFRs participate in the anaerobic respiration with fumarate as the terminal electron acceptor [5, 6]. SQORs typically consist of three to four subunits: the hydrophilic subunits A (SdhA) and B (SdhB) containing a covalently-bound flavin cofactor and [2Fe-2S], [4Fe-4S], and [3Fe-4S] iron-sulfur clusters, respectively, and one large or two small membrane-bound subunits (C or C and D). The dicarboxylate oxidation/reduction and quinone reduction/oxidation sites are located in the subunit A and in the membrane anchor subunit(s), respectively. While the hydrophilic subunits are highly conserved among members of all domains of life, the sequence similarities between the membrane domains of complex II are significantly lower. SQORs are classified into five types (A-E) based on the number of membrane-bound domains and differences in the heme *b* composition. Enzymes with only one membrane subunit are grouped into type B as opposed to the all other types containing two hydrophobic domains. The heme content varies between zero (type D and E), one (type C) and two (types A and B). With the advent of the crystal structure of type D QFR from *Escherichia coli* more than a decade ago [7] followed by the structures of two prokaryotic and three mitochondrial SQORs [8-12], novel results have constantly emerged such as evidence for transmembrane proton transfer in di-heme QFR from *Wolinella succinogenes* [13]. Nonetheless, many questions are yet to be answered.

Previously, we have purified SQR from the extremely thermophilic bacterium *Thermus thermophilus* [14] and characterized it as a trimeric, di-heme, menaquinone (MK)-utilizing enzyme. The redox midpoint potential of its [3Fe-4S] center was determined to be at least 60 mV higher than that of its [2Fe-2S] center. This is in contrast to the hypothesis that MK-reducing SQRs are characterized by a higher midpoint potential for the [2Fe-2S] center with respect to the [3Fe-4S] center [1]. In addition, NQNO, a semiquinone analog and inhibitor of quinone reactions in complex II, showed no influence on the redox behavior of the heme *b* moieties at variance with the equivalent *Bacillus subtilis* enzyme, where it was reported to induce a downshift of the midpoint potential of heme *b_L* [15] and a hysteresis in the titration behavior of both *b*-hemes [16]. Furthermore, characterization of *T. thermophilus* SQR revealed several novel features. These include the interprotomer temperature-dependent positive cooperativity in the trimeric complex as well as the modification of the EPR signal of the [2Fe-2S] iron-sulfur cluster, an immediate electron acceptor from the active site flavin, in the presence of the substrate succinate [14].

Most of the analyses on SQRs performed to date have involved the purification of native enzymes with the exception of organisms for which genetic manipulation techniques are well established, such as *E. coli* [9], *B. subtilis* [17, 18] or *Paracoccus denitrificans* [19]. Here we

present a system for the recombinant expression of the *T. thermophilus* SQR and detailed characterizations of recombinant enzyme variants. Due to a modified purification procedure, expression of the recombinant form of the enzyme resulted in a higher quality complex II in larger quantities. This consequently allowed a more detailed biophysical characterization of the protein. The results presented herein represent a significant step towards the elucidation of a three-dimensional structure of type A SQOR, not available to date. Moreover, a detailed analysis of succinate influence in the active site on the shape of the EPR signal of the [2Fe-2S] cluster was also performed. Possible molecular bases of this phenomenon that may be of experimental use to monitor the occupancy of the active site of the enzyme by its substrate are discussed in this paper.

EXPERIMENTAL

Recombinant production of complex II from *T. thermophilus* HB8

Generation of vectors for recombinant production of wild type enzyme (wt-rcII) and complex II with His-tag on the C- or N-terminus of the SdhB subunit (rcII-SdhB-His₆ and rcII-His₈-SdhB, respectively) is described in Supplementary Material.

For homologous expression, *T. thermophilus* HB8 was transformed with the generated expression vectors by electroporation and 50 mL liquid cultures were prepared from several colonies selected on 50 µg/mL kanamycin at 70 °C in a water-saturated atmosphere. After an overnight growth in LB medium at 70 °C, cell membranes were isolated and the expression clone was selected based on the most prominent signal judged by Western blot (His-tagged constructs) and on the absorbance at 558 nm in the dithionite reduced-*minus*-oxidized spectrum (wt-rcII).

The large-scale productions of all forms of the enzyme were performed in 5 L of LB supplemented with kanamycin at a final concentration of 50 µg/mL, at 70 °C and 250 rpm for 24 h, yielding ~ 30 - 40 g wet biomass that was stored at – 80 °C until use.

Isolation of membranes

T. thermophilus cells were resuspended in 0.25 M Tris-HCl (pH 7.6) buffer containing 0.2 M KCl (Buffer A) in the ratio of 5 mL buffer to each gram of cell pellet and subsequently homogenized. Lysozyme was later added to a final concentration of 0.6 µM and the suspension was stirred for 3 h at room temperature. After centrifugation at 53936 x *g* for 45 min at 4 °C, the supernatant containing *T. thermophilus* soluble proteins was removed. The pelleted membranes were then resuspended in a small volume of Buffer A and protein concentration was analyzed using BCA Protein Assay Kit (Thermo Scientific Pierce) standardized against bovine serum albumin. Approximately 60 µg of membrane proteins was used in the subsequent SDS-PAGE and Western blotting analyses. For protein purification the membrane extract was diluted to a protein concentration of 10 mg/mL with the appropriate buffer and membrane proteins were solubilized by incubation for 3 h at 4 °C in the presence of 5 % Triton X-100 (Sigma Aldrich). Non-solubilized proteins were removed by centrifugation at 53936 x *g* for 1 h at 4 °C, yielding a clear membrane suspension.

Purification of recombinant complex II from *T. thermophilus* HB8

Purification of wt-rcII was performed essentially as described for the native enzyme [14] with the omission of the first anion exchange purification step on DEAE-Biogel agarose (Biorad). All chromatographic steps were performed using the Äkta Prime or Äkta Explorer systems (GE Healthcare). The isolated membranes were solubilized in 0.01 M Tris-HCl, pH 7.6, 0.1 % Triton X-100 and applied directly onto an XK 26/20 column, packed with 30 mL of Fractogel EMD TMAE (Merck) previously equilibrated with the same buffer. All further purification steps were performed as previously described [14].

Both His-tagged versions of the enzyme, rcII-SdhB-His₆ and rcII-His₈-SdhB, were purified according to the same protocol. Isolated membranes were solubilized in 0.05 mM Tris-HCl, pH 7.6, 300 mM NaCl, 10 mM imidazole and membrane proteins were solubilized with Triton X-100 as described above. The prepared extract was applied onto an XK 26/20 column, packed with 30 mL of Nickel Sepharose 6 Fast Flow resin (GE-Healthcare) pre-equilibrated with the same buffer. After sample binding to the resin, a detergent exchange step was performed by washing the column extensively with 0.05 M Tris-HCl, pH 7.6, 300 mM NaCl, 10 mM imidazole and 0.05 % dodecyl- β -D-maltoside (DDM) (Anatrace) until Triton X-100 has been removed from the sample, as determined from the 280 nm absorbance contributed by Triton X-100. Elution was performed with a linear gradient of 0 to 0.4 M imidazole, for 1 h at a flow rate of 1 mL/min. Complex II-rich fractions were pooled and diluted with 0.01 M Tris-HCl (pH 7.6), 0.05 % DDM to reduce the conductivity to < 2 mS/cm and subsequently applied onto an XK 26/20 column, packed with 30 mL of Fractogel EMD TMAE (Merck) previously equilibrated with 0.01 M Tris-HCl (pH 7.6), 0.05 % DDM. Proteins were eluted with a linear gradient of 0 to 0.5 M NaCl, for 1 h at a flow rate of 2 mL/min. The fractions containing complex II were pooled and concentrated to 2 mL using a centrifugal filter (Vivaspin 20 MWCO 100 kDa, Sartorius) and applied onto a HiLoad XK 16/60 Superdex 200 gel filtration column (GE-Healthcare) previously equilibrated with 0.05 M Tris-HCl (pH 7.6), 0.05 % DDM. The purified His-tagged complex II was concentrated to 10-15 mg/mL (Vivaspin 2 MWCO 100 kDa, Sartorius), aliquoted and snap frozen at - 80°C.

Analytical SEC analyses of complex II were performed by applying 250 μ g of purified protein onto a Superdex 200 10/300 GL gel filtration column (GE-Healthcare) previously equilibrated with 0.05 M Tris-HCl (pH 7.6), 0.05 % DDM. The chromatography was carried out at the flow rate of 0.5 ml/min.

Protein analysis

Determination of protein concentrations, Blue Native PAGE analysis, redox titration and activity measurements were performed as described previously [14]. In addition, the enzyme activity was assayed at 30 °C in the presence of DCPIP, 0.05 mM nonyl-4-hydroxyquinoline-N-oxide (NQNO) and Vit. K₃, DQ, 1,4-NQ or *p*-BQ at concentrations of 0 - 1 mM.

Circular dichroism (CD) analysis was performed using a Chirascan CD spectrometer (Applied Photophysics) and Chirascan Pro-Data acquisition software. For the CD analysis in the far UV range (180 to 280 nm), quartz suprasil (QS) cuvettes of 0.1 mm path length (Hellma

GmbH) were used. The baseline spectra and spectra for each protein sample were collected in triplicate with 4 s time points and 1 nm bandwidth. Baselines and protein spectra were separately averaged, and the averaged baselines were subtracted from the relevant averaged protein spectra and smoothed with the Savitsky-Golay algorithm. For thermal stability analyses, changes in the observed ellipticity at a single wavelength of 222 nm were analyzed in triplicates at increasing and subsequently decreasing temperatures in the 20 – 90 °C range with 1 °C ramp using quartz suprasil (QS) cuvettes of 10 mm path length (Hellma GmbH); the cuvette was covered with a lid to overcome the problem of rapid evaporation. Complex II was analyzed in 50 mM Tris-HCl (pH 7.6), 0.02 % DDM at a concentration of 1 mg/mL (total volume 30 µL) for scans in the 180-280 nm range and 0.01 mg/mL (total volume 3.5 mL) for thermal analyses at 222 nm.

EPR spectra were recorded on a Bruker ElexSys X-band spectrometer fitted with an Oxford Instrument He-cryostat and temperature control system. Buffers used were either 50 mM MOPS at pH 7 or a mixture of 100 mM MOPS and 100mM piperazine for the pH experiments. Samples were reduced by addition of 5 mM ascorbate, succinate (from a 1 M stock solution in water) or dithionite (from a 200 mM stock solution in 1 M MOPS buffer, pH 7). Additions of reducing agents were performed at room temperature followed by vortexing and freezing of the sample in liquid nitrogen within 5 min after addition. The addition of NQH₂ and succinate in the presence of dithionite was done under argon. Protein concentration was 5 - 10 µM as indicated in the figure legends.

RESULTS AND DISCUSSION

Generation of recombinant complex II

In order to provide valuable insights into the mechanism of action of a thermophilic SQR, we have developed a homologous expression system for SQR from the extremely thermophilic bacterium *T. thermophilus* forming a continuity of the characterizations of the native protein performed previously [14]. In addition to the enabling of future site-directed mutagenesis studies of this enzyme, this approach was expected to facilitate crystallogensis and biophysical characterization of the protein by providing larger amounts of high quality enzyme through a simpler, reproducible method.

Three recombinant variants of the enzyme were generated, all produced constitutively under the control of *bc* complex promoter from a *E. coli/T. thermophilus* shuttle vector [20] in the latter host. Expression clone for the production of the wild type complex II (wt-rcII) was selected based on the highest absorbance at 558 nm in the reduced-*minus*-oxidized spectrum of isolated membranes. The generated wt-rcII was purified to ~ 95 % homogeneity as described previously for the native enzyme [14] the with omission of the initial DEAE anion exchange chromatography. This purification procedure resulted in almost five-fold higher amounts of the protein in comparison to the native purification [14], corresponding to ~ 6-8 copies of vector per cell, and yielded ~ 37 mg of pure complex II from 100 g of *T. thermophilus* biomass. The existence of four subunits (SdhA, B, C and D) within the purified protein was confirmed by SDS-PAGE analysis (Fig. 1A, lane 1), while a single peak of Gaussian distribution after the final size exclusion chromatography demonstrates the sample homogeneity (Fig. 2). The heme *b*

content in the purified sample was 16.43 nmol/mg of protein (Table S1), a value close to the theoretical content of 16.6 nmol/mg of protein considering the molecular weight of the complex as 119.78 kDa and the existence of two heme moieties per protein monomer.

The oligomerization state of the enzyme was evaluated by BN-PAGE as described previously [14]. The wt-rcII sample shows a single band migrating in accordance to the native enzyme and indicates the trimeric nature of the protein, corresponding to ~ 500 kDa considering 360 kDa from protein and an unknown contribution of detergent and lipid [14] (Fig. 3). Analysed by visible redox spectroscopy, the protein exhibited the same features as the native enzyme with absorption peaks at 425 and 559 nm and a shoulder around 412 nm upon reduction with succinate, indicating a partial reduction of heme *b*, and peaks at 425, 525 and 558 nm upon the addition of dithionite. The existence of two heme *b* cofactors within wt-rcII was confirmed by optical Vis redox titration. From the two titration waves, the data points were fitted to a sum of two one-electron Nernst curves with equal amplitudes and midpoint potentials of + 5 mV and - 150 mV relative to the standard hydrogen electrode (SHE); these were attributed to hemes b_H and b_L , respectively. The midpoint potential values are in agreement with those determined for hemes b_H and b_L of the native enzyme (- 20 mV and - 160 mV, respectively [14]). The presence of all redox cofactors of complex II, *i.e.* [2Fe-2S], [3Fe-4S] and [4Fe-4S] clusters, heme *b* and flavin was confirmed by EPR spectroscopy. Similar to the native enzyme [14], the rhombicity of the signal of the [2Fe-2S] center was higher in the presence of succinate than after reduction with ascorbate or dithionite (see below).

Through steady-state kinetic measurements, the native complex II was found to display classical Michaelis-Menten kinetics at 30 °C, but exhibits positive cooperativity at a higher temperature (70 °C) [14]. This behavior was not noted to date in other complexes II and, therefore, to further confirm that the observed cooperativity is a genuine phenomenon, an artificial monomeric version of the enzyme was generated. Since the cooperativity is strictly related to multiple binding sites within a protein, and, hence, in the case of complex II, to its trimeric nature, it is expected that it will be abolished in the artificial monomeric version of the enzyme. Based on the generated homology model of *T. thermophilus* complex II, we have identified the C-terminus of the iron-sulfur subunit (SdhB) as the ideal location for protein engineering to disrupt the oligomerization (Fig. S1). In addition, to combine the generation of a monomeric complex II with the simplification of protein purification, we have decided to introduce a hexahistidine affinity tag on the aforementioned C-terminus of the iron-sulfur subunit.

A derivative of *E. coli/T. thermophilus* shuttle vector [20] encoding the His-tagged version of complex II (rcII-SdhB-His₆) was prepared and the clone exhibiting the highest expression levels was selected based on the signal of the SdhB-His₆ subunit detected by Western blotting in isolated membranes. The enzyme was purified sequentially through nickel immobilized metal affinity chromatography, TMAE anion exchange and size exclusion chromatography steps and yielded ~ 35 mg of the ~ 98 % pure rcII-SdhB-His₆ from 100 g of *T. thermophilus* biomass with the content of heme *b* in the purified sample of 16.6 nmol/mg of protein, (Fig. 1, lane 3; Table S1). The rcII-SdhB-His₆ reproducibly eluted later in the gel filtration chromatography compared to the native and wt-rcII complexes (Fig. 2). While this fact was an early indication of the successful creation of a monomeric recombinant complex II, the purified rcII-SdhB-His₆ was subjected to BN-PAGE to further evaluate whether the positioning of a His-tag on the C-

terminus of SdhB subunit affected the oligomeric state of the protein. The band corresponding to rcII-SdhB-His₆ (Fig. 3) migrates significantly faster than the trimeric native and wt-rcII as well as β -amylase (200 kDa). Therefore, we concluded that trimerization was disrupted in rcII-SdhB-His₆ due to the insertion of a hexahistidine tag on the C-terminus of SdhB subunit and the resulting protein complex could only form a monomer.

To further facilitate purification process, the subsequent crystallization trials and future site-directed mutagenesis studies, the decision to generate another His-tagged version of the enzyme was made. The major challenge was to choose an ideal location for the placement of the affinity tag that retains native complex oligomeric state. Furthermore, the length of His residues was increased from six to eight to increase the probability of a sufficient exposure of the tag in the folded complex and ensure a tight binding of the latter to the Ni-Sepharose resin. This approach has been employed successfully for a number of proteins including membrane-bound receptors [21, 22]. A careful place for tag insertion is crucial as it may not only abolish the native oligomeric state of the protein but may also promote a non-native oligomerization [23]. An insertion within the linear protein sequence was judged to be less preferable than an insertion at a terminal location of each subunit. Therefore, we identified the N-terminus of SdhB subunit as an appropriate site for the affinity tag. A derivative of *E. coli/T. thermophilus* shuttle vector [20] encoding the rcII-His₈-SdhB was prepared and the enzyme was generated and purified as described above for the rcII-SdhB-His₆. This yielded ~ 35 mg of the ~ 98 % pure rcII-His₈-SdhB from 100 g of *T. thermophilus* biomass with the heme *b* content in the purified sample of 16.6 nmol/mg of protein (Table S1). Placing the affinity tag on the N-terminus of the SdhB subunit did not affect the native trimeric state demonstrated on the BN-PAGE gel (Fig. 3).

On SDS-PAGE all four subunits of the rcII-His₈-SdhB complex were detected, with a doublet for the band corresponding to SdhB (Fig. 1A, lane 4). While the upper band of this doublet represents the His-tagged SdhB subunit (Fig. 1B), the lower band migrates identically to the SdhB subunits of the native and wt-rcII complex II and therefore most likely corresponds to a native, non-tagged SdhB subunit. The addition of fumarate, the end product of the reaction catalyzed by SQR, at a concentration up to 50 mM [24] did not inhibit the expression of the native complex II as obtained total yields of the rcII-His₈-SdhB as well as the ratio between the untagged and His-tagged SdhB subunit remained unchanged. Therefore, due to the trimeric nature of the protein, the formation of the complexes containing mixed, His-tagged and untagged SdhB species is not surprising. As expected, due to enhanced expression of the His-tagged complex and the affinity method of purification, the His₈-SdhB comprises a significant majority of the observed species in SdhB hybrid. An obvious way to overcome this problem and to enable mutagenesis studies would be the overexpression of the enzyme in the *T. thermophilus* strain where background expression of any enzymes capable of succinate oxidase activity is eliminated. Although complex II deletion strains of *E. coli* [25] and *B. subtilis* [17] exist, despite our best efforts, the trials to generate *sdhCDAB* deletion strain of *T. thermophilus* have been unsuccessful so far. This difficulty may well be explained by the essential nature of the protein complex for *T. thermophilus* energy conservation as it does not encode a QFR, unlike *E. coli*. The ability to generate the monomeric version of the enzyme, further tag cleavage and *in vitro* trimerization of the complex II may seem to be a solution for generation of mutants. We believe, however, that the residues on the C-terminus of SdhB subunit residual post cleavage would still impede trimer formation due to the sensitive location of the affinity tag (Figure S1).

Both rcII-SdhB-His₆ and rcII-His₈-SdhB exhibited the same features as the native and wt-rcII enzymes as determined by visible redox spectroscopy. The presence of all redox cofactors of complex II was confirmed by EPR spectroscopy and the higher rhombicity of the signal of the [2Fe-2S] center in the presence of succinate was also observed. Optical redox titration confirmed the existence of two heme *b* cofactors with the midpoint potentials of b_H and b_L evaluated to be -10 mV and -170 mV for rcII-SdhB-His₆ and +10 mV and -215 mV for rcII-His₈-SdhB, respectively, relative to SHE, in agreement with both native and wt-rcII.

Similar to the native protein [14], the recombinant untagged variant has also been crystallized with the maximum crystal size being only about half. Given the increased purity of recombinant protein, this is a perplexing observation. A preliminary screening of the crystals resulted in an anisotropic diffraction to 3.8 Å in the best direction using synchrotron radiation in contrast to the maximum of 8 Å with native protein crystals [14] using home source. Presumably, the smaller recombinant crystals froze better than the larger crystals of native complex. As this resolution is judged to be too low for biological interpretation, even without considering the possible data truncation due to the anisotropy, we are currently attempting further optimizations.

Stability analysis of recombinant complex II

The thermal stability and protein fold of all the three forms of recombinant complex II were investigated using CD spectroscopy, a technique that is becoming increasingly important in the structural investigations of membrane proteins [26]. The spectra recorded at 20 °C exhibit bands characteristic for both predominantly-helical soluble and membrane proteins with twin negative bands at ~222 and ~210 nm and a positive band at ~192 nm [27]; this is identical to the native complex II [14]. It is not possible to observe a typical thermal unfolding curve with clearly defined folded and unfolded states separated by a steep unfolding transition for highly thermostable enzymes due to hardware limitation that can only operate at a maximum temperature of 90 °C. However, several conclusions can be drawn from the plot of the observed ellipticity at 222 nm to temperature profiles obtained for all recombinant versions of complex II (Fig. 4). Since the temperature profiles at 222 nm were identical for wt-rcII and rcII-His₈-SdhB, only the results for rcII-His₈-SdhB and rcII-SdhB-His₆ are presented for clarity. The recombinant trimeric versions of complex II, wt-rcII and rcII-His₈-SdhB exhibit a rather constant ellipticity at 222 nm throughout the temperature range tested, with only a slight difference observed between 20 and ~90 °C. Moreover, this change was almost completely reversible in the presented setup (Fig. 4). Compared to the native enzyme [14], the wt-rcII and rcII-His₈-SdhB show a significantly higher thermostability. This may possibly be attributed to the much shorter purification procedure and a more limited contact with the relatively harsh detergent Triton X-100 – a consequence of higher protein expression level that could prevent protein delipidation. In contrast, monomeric rcII-SdhB-His₆ exhibited a significantly lowered, almost completely irreversible thermostability profile (Fig. 4). Although adopting higher oligomerization states is one of the evolutionary strategies to attain a higher thermostability [28], we cannot consider it as the case for complex II as many of the homologous enzymes from mesophilic prokaryotes also exist as trimers [9, 29]. Undoubtedly, however, the disruption of the trimeric nature of the protein negatively affects its stability, as one would expect.

Kinetic analysis of recombinant complex II from *T. thermophilus* HB8

The succinate dehydrogenase activity of the recombinant versions of complex II was measured using solution assays with PMS as the intermediate and DCPIP as the terminal electron acceptor. The results summarizing the steady-state kinetic analysis of the complex II are presented in Table 1 and they show that all forms of the enzyme exhibit classical Michaelis-Menten kinetics at 30 °C with the K_M values for the recombinant complex II in the range of 0.33 - 0.39 mM, reasonably in agreement with the native enzyme (0.21 mM). The turnover numbers (k_{cat}) for the recombinant forms of the enzyme are up to two fold higher in comparison to the native complex II (Table 1). This higher specific activity is rather less likely to be related to the enzyme purity which is very comparable between the generated variants of complex II; instead, it is an effect of enzyme stability in the recombinant samples. Indeed, the specific activity expressed by the turnover number is lower for the native enzyme and the monomeric rcII-SdhB-His₆, which is reflected in their limited stability in comparison to the trimeric recombinant forms of the complex (see above). At a higher temperature (70 °C), both trimeric wt-rcII and rcII-His₈-SdhB exhibit positive cooperativity as observed previously for the native complex II with k' ranging between 0.25 and 0.28 mM (native enzyme $k' = 0.39$ mM). The calculated Hill coefficients h for these enzymes are remarkably similar (Table 1) and indicate a minimum, and most likely the actual number of three substrate binding sites on the oligomeric enzyme with one site per protomer. As mentioned before, it was anticipated that the positive cooperativity observed for the native complex II at high temperatures will not be observed in the artificially produced monomeric rcII-SdhB-His₆ version of the enzyme due to the lack of multiple active sites within the protein. Indeed, rcII-SdhB-His₆ shows a standard Michaelis-Menten kinetics at 70 °C with an unchanged affinity for the substrate in comparison to 30 °C ($K_{M, 70^\circ C} = 0.29$ mM vs. $K_{M, 30^\circ C} = 0.33$ mM) and more than a three-fold increase in turnover number, typical at higher temperatures. The generation of the monomeric complex II and the obtained steady-state kinetic measurements undoubtedly confirm the existence of cooperatively interacting active sites within the trimeric complex II at higher temperatures and establish the *T. thermophilus* complex II as the first SQOR with such a kinetic behavior. It is difficult to predict how the disruption of the native oligomeric state of the enzyme will affect its activity as in some cases the existence of one particular oligomeric state is absolutely essential to retain activity of an enzyme [30-32] while generation of non-native oligomeric forms showing enhanced activity has also been reported [33]. For the complex II, our results clearly show that trimerization is not a prerequisite factor for the activity of the enzyme. Although based on edge-to-edge distances between the redox centers it has been suggested that electron transfer in SQR from *E. coli* likely occurs within each protomer rather than between adjacent ones [9], to the best of our knowledge, this report is the first one that confirms this theory.

As previously investigated with the native enzyme, the influence of standard inhibitors targeting the active site (malonate, oxaloacetate and 3-NP) on the succinate dehydrogenase activity of the wt-rcII, rcII-SdhB-His₆ and rcII-His₈-SdhB was tested using the PMS/DCPIP assay at 30 °C (Table 1). Although the obtained K_i values, in particular for oxaloacetate, suggest a slightly altered sensitivity of some recombinant versions of the enzyme when compared to the native one, they remained within the same order of magnitude and therefore can be considered as similar. Moreover, the addition of 1,4-naphthoquinone (1,4-NQ) as a direct electron acceptor

increased the succinate dehydrogenase activity by a factor of two in comparison to when DCPIP was used as the only electron acceptor for all forms of the protein.

NQNO, a semiquinone analog, has a negligible effect on the DCPIP/PMS activity as expected based on the previous reports [1, 14, 29, 34]. It inhibited the DCPIP/1,4NQ and the DCPIP only activity to 40 % and 70 %, respectively, in a non-competitive mode with a K_i in the range of 70 – 88 μM throughout all the generated variants of the complex II (Table 1). This is further discussed in the EPR section below.

Other tested quinone analogs (DQ and Vit. K_3) did not influence the DCPIP-only activity while increasing amounts of *p*-BQ delayed the onset and the reduction of DCPIP. The reduction of DCPIP was followed in the presence of *p*-BQ for a prolonged period of time. The reaction was found to be delayed for the amount of time that is directly proportional to the concentration of *p*-BQ added (up to ~ 30 min in the analyzed set up in the presence of 1 mM *p*-BQ). As published previously [14], we suggest that the electrons of succinate oxidation accumulate in the *p*-BQ pool due to the high redox midpoint potential of the latter. Only once the *p*-BQ pool is mainly reduced can the electrons proceed to DCPIP.

EPR signature of the [2Fe-2S] cluster

In the preceding paper [14], we reported that the rhombicity of the EPR signal of the [2Fe-2S] cluster from the native complex II from *T. thermophilus* was dependent on the reductant used in the assay. The signal appeared axial with a g_x at 2.02 and a $g_{y/z}$ at 1.926 if the sample has been reduced by ascorbate but rhombic with a g_x at 2.027, a g_y at 1.927 and a g_z at 1.912 if succinate was the electron donor. The same phenomenon has been observed with all three constructs of recombinant complex II and therefore its detailed characterization has been performed in this work.

To the best of our knowledge, the change in the rhombicity of the EPR signal of the [2Fe-2S] cluster under different experimental conditions was reported only by Beinert and coworkers on mitochondrial complex II [35]. They observed increasing rhombicity of the EPR signal in the course of a dithionite titration. In the case of *T. thermophilus* complex II, a similar but less pronounced increase in the rhombicity (g_x at 2.022 and a $g_{y/z}$ at 1.926) was observed when 100-fold excess of dithionite was added to the enzyme (Figure S2). In both cases, the resulting signal is of a much smaller rhombicity than the signal that has been observed for the enzyme in the presence of succinate.

To further investigate the succinate effect, we probed EPR spectra of the [2Fe-2S] center at different pH values (Fig. 6A-B), in the presence of different amounts of succinate (Fig. 6C-D), and in the presence of the inhibitors malate, 3-NP and NQNO and various quinones and mediators (Fig. 5). The amount of succinate necessary to induce the transition from the axial to the rhombic EPR signal of the [2Fe-2S] signal was in the hundreds of micromolar, close to the K_M of succinate determined by activity assays (Table 1; the K_M value determined by activity measurements reflects the presence of succinate in the active site if the electron transfer from succinate to DCPIP is slower than the dissociation of product fumarate from the active site). In the presence of 40 mM succinate, a pK value of 5.8 was determined for the transition from the axial to the rhombic EPR signal of the [2Fe-2S] cluster (Fig. 6B). The suicide inhibitor 3-NP that covalently binds to the active side [10] prevented the transition to the rhombic signal when

succinate was added, whereas malate could induce the rhombic signal in the absence of succinate (Fig. 5). NQNO, a semiquinone analog that inhibits complex II activity [1] had no significant influence on the [2Fe-2S] signal. If the flavin in the active site was pre-reduced by addition of an excess of dithionite, three times the concentration of succinate were necessary to induce the rhombic signal, in agreement with literature values on the influence of the redox state of the active site on the K_M of succinate [36, 37]. Taken together, these results suggest that succinate or the chemically similar malate, localized in or close to the active site, have an influence on the rhombicity of the [2Fe-2S] EPR signal.

Changes in the rhombicity of the EPR signal of [2Fe-2S] clusters have been attributed to a change in the angle between the iron/iron plane of the cluster and the plane between the sulfur ligand and its adjacent carbon atom [38], therefore implying a structural rearrangement of the cluster environment. Some of the several available 3D structures of complexes II resolve the position of water molecules and show several of them at the interface between subunits A and B close to the flavin and the [2Fe-2S] cluster, connecting the two cofactors *via* a hydrogen bond network. Fig. 7A shows the structure of SQR from *Gallus gallus* with 3-NP bound. The glutamic acid residue at position 67 of the iron-sulfur subunit (SdhB-E67^{Gg}) which is a part of the CxExxCGxC motif ligating the [2Fe-2S] cluster, has been replaced by a histidine that occupies the equivalent position in *T. thermophilus* (SdhB-H56Th) according to multiple sequence alignments (Fig. S3). If an interaction between the substrate in the active site and the [2Fe-2S] cluster indeed occurs *via* the H-bond network, the presence of a His residue in this network may result in the pK of 5.8 that we observed for the appearance of the succinate-induced rhombic EPR signal. In Fig. 7B, the entrance channel to the active site of *Gallus gallus* SQR can be seen to be situated at the interface between the flavin and the Fe-S cluster subunits. The His residue that replaces Glu67 from *G. gallus* surfaces in the entrance channel. In the *W. succinogenes* structure (not shown), access to the active site is slightly different and the corresponding residue, an alanine, surfaces in a side lobe of the entrance channel.

The expected structural changes that induce the change in the rhombicity of the [2Fe-2S] cluster EPR signal are too small to be detected by X-ray crystallographic analysis, unless at an ultra-high resolution (better than 1 Å) and may not have any influence on the complex function. They are, however, a precious experimental probe to assess the occupancy of the active site. As an example, different quinones, generally used as mediators in redox titrations, prevented transition from the axial to the rhombic EPR signal when succinate was added (Fig. 5). Adding these quinones to a succinate-reduced sample induced transition of the signal back to its axial form. Small concentrations at 20 μM *p*-BQ and 10 μM 1,4-NQ were sufficient to obtain the axial signal in the presence of 20 mM succinate from a 6 μM rcII sample. The 1,4-NQH₂ had the same effect as 1,4-NQ. Antraquinones, however, induced an increased rhombicity of the [2Fe-2S] signal in a succinate-reduced sample. We do not know at present why these quinone act differently on the [2Fe-2S] EPR signal but we postulate that the fact that they disturb the effect of succinate on the [2Fe-2S] signal indicates that they reach a position in or close to the enzyme active site. Kinetic experiments with NQNO support this interpretation. Available data (reviewed in [1]) have been interpreted as NQNO blocking a quinone binding site on the membrane anchor subunit(s) of complex II. In the activity assays of *T. thermophilus* complex II, the addition of NQNO partially inhibits enzyme activity in a non-competitive manner, indicating that mediators

can accept electrons from one of the cofactors of the enzyme outside the quinone binding site. PMS/DCPIP activity assays are inhibited to only 5% by NQNO, whereas DCPIP-only activity is inhibited to 70%, translating the capacity of the small PMS molecule to more efficiently access complex II cofactors. DCPIP/1,4-NQ activity is inhibited to 40% by NQNO, showing that 1,4-NQ, just as PMS, can accept electrons from complex II elsewhere than from the quinone binding site blocked by NQNO. Since we discovered that 1,4-NQ perturbs the succinate-induced rhombicity of the [2Fe-2S] signal, it may interact with the active site and not with the membrane anchor subunit as proposed in our previous report [14]. This result is certainly of no physiological relevance since the quinones present in the membrane of organisms should not reach the active site. It signifies, however, that caution has to be taken when studying the interaction of exogenous quinones with complex II under the assumption that they interact exclusively with the quinone binding site of the complex.

Concluding remarks

The homologous production of the complex II from *T. thermophilus* under the control of the *bc* complex promoter presented herein made possible an efficient preparation method of the enzyme for structural and functional studies. By placing an affinity tag on different positions of the SdhB subunit, as guided by the examination of crystal structures of the enzyme from other organisms, trimeric as well as monomeric forms of the enzyme were successfully created. Only the trimeric forms exhibited cooperativity at high temperatures. This provided the experimental evidence that this novel feature of SQORs reported previously for the native *T. thermophilus* complex II is a genuine phenomenon of the trimeric enzyme and that each protomer is indeed involved in succinate oxidation.

All recombinant forms of the enzyme exhibits an EPR signal of the [2Fe-2S] cluster, the rhombicity of which depends on the presence of succinate or its analog malate in or close to the active site. Mediators, such as quinones, interfered with this effect, indicating that these molecules have access to the active site and not (only) to the quinone binding sites as thought previously. This finding has consequences on the interpretation of activity assays on complex II. Rhombicity of the [2Fe-2S] signal of *T. thermophilus* complex II provides a specific probe for occupancy of the active site and may, therefore, be of experimental use to address the molecular mechanism of succinate binding and primary electron transfer events in this enzyme. We propose a model for the molecular basis of the succinate influence on the geometry of the proximal iron-sulfur cluster ligand environment based on the available SQOR crystal structures and on sequence information.

Acknowledgments

The authors would like to thank Prof. Bernd Ludwig at Goethe Universität, Frankfurt, Germany where the attempts to generate an *sdhCDAB* deficient strain of *T. thermophilus* took place and for supplying us with the pDM12 plasmid. Wolfgang Nitschke is acknowledged for discussions and critical reading of the manuscript.

Funding

This work was supported by the Science Foundation Ireland [BICF685], by the Irish Research Council for Science, Engineering and Technology EMBARK Ulysses Research Visit to France 2009 grants (TS) and PhD Scholarship (MRN) and by the French National Center for Scientific Research (CNRS).

References:

- 1 Hägerhäll, C. (1997) Succinate: quinone oxidoreductases. Variations on a conserved theme. *Biochim. Biophys. Acta.* **1320**, 107-141
- 2 Guest, J. R. (1981) Partial replacement of succinate dehydrogenase function by phage- and plasmid-specified fumarate reductase in *Escherichia coli*. *J. Gen. Microbiol.* **122**, 171-179
- 3 Maklashina, E., Berthold, D. A. and Cecchini, G. (1998) Anaerobic expression of *Escherichia coli* succinate dehydrogenase: functional replacement of fumarate reductase in the respiratory chain during anaerobic growth. *J. Bacteriol.* **180**, 5989-5996
- 4 Saraste, M. (1999) Oxidative phosphorylation at the fin de siecle. *Science.* **283**, 1488-1493
- 5 Kröger, A., Geisler, V., Lemma, E., Theis, F. and Lenger, R. (1992) Bacterial fumarate respiration. *Arch. Microbiol.* **158**, 311-314
- 6 Kröger, A. (1978) Fumarate as terminal acceptor of phosphorylative electron transport. *Biochim. Biophys. Acta.* **505**, 129-145
- 7 Iverson, T. M., Luna-Chavez, C., Cecchini, G. and Rees, D. C. (1999) Structure of the *Escherichia coli* fumarate reductase respiratory complex. *Science.* **284**, 1961-1966
- 8 Lancaster, C. R., Kröger, A., Auer, M. and Michel, H. (1999) Structure of fumarate reductase from *Wolinella succinogenes* at 2.2 Å resolution. *Nature.* **402**, 377-385
- 9 Yankovskaya, V., Horsefield, R., Tornroth, S., Luna-Chavez, C., Miyoshi, H., Léger, C., Byrne, B., Cecchini, G. and Iwata, S. (2003) Architecture of succinate dehydrogenase and reactive oxygen species generation. *Science.* **299**, 700-704
- 10 Huang, L. S., Sun, G., Cobessi, D., Wang, A. C., Shen, J. T., Tung, E. Y., Anderson, V. E. and Berry, E. A. (2006) 3-nitropropionic acid is a suicide inhibitor of mitochondrial respiration that, upon oxidation by complex II, forms a covalent adduct with a catalytic base arginine in the active site of the enzyme. *J. Biol. Chem.* **281**, 5965-5972
- 11 Sun, F., Huo, X., Zhai, Y., Wang, A., Xu, J., Su, D., Bartlam, M. and Rao, Z. (2005) Crystal structure of mitochondrial respiratory membrane protein complex II. *Cell.* **121**, 1043-1057
- 12 Shimizu, H., Osanai, A., Sakamoto, K., Inaoka, D. K., Shiba, T., Harada, S. and Kita, K. (2012) Crystal structure of mitochondrial quinol-fumarate reductase from the parasitic nematode *Ascaris suum*. *J Biochem.* **151**, 589-592
- 13 Madej, M. G., Nasiri, H. R., Hilgendorff, N. S., Schwalbe, H. and Lancaster, C. R. (2006) Evidence for transmembrane proton transfer in a dihaem-containing membrane protein complex. *EMBO J.* **25**, 4963-4970
- 14 Kolaj-Robin, O., O'Kane, S. R., Nitschke, W., Léger, C., Baymann, F. and Soulimane, T. (2011) Biochemical and biophysical characterization of succinate: quinone reductase from *Thermus thermophilus*. *Biochim. Biophys. Acta.* **1807**, 68-79

- 15 Smirnova, I. A., Hägerhäll, C., Konstantinov, A. A. and Hederstedt, L. (1995) HOQNO interaction with cytochrome *b* in succinate:menaquinone oxidoreductase from *Bacillus subtilis*. *FEBS Lett.* **359**, 23-26
- 16 Christenson, A., Gustavsson, T., Gorton, L. and Hägerhäll, C. (2008) Direct and mediated electron transfer between intact succinate:quinone oxidoreductase from *Bacillus subtilis* and a surface modified gold electrode reveals redox state-dependent conformational changes. *Biochim. Biophys. Acta.* **1777**, 1203-1210
- 17 Matsson, M., Tolstoy, D., Aasa, R. and Hederstedt, L. (2000) The distal heme center in *Bacillus subtilis* succinate:quinone reductase is crucial for electron transfer to menaquinone. *Biochemistry.* **39**, 8617-8624
- 18 Azarkina, N. and Konstantinov, A. A. (2002) Stimulation of menaquinone-dependent electron transfer in the respiratory chain of *Bacillus subtilis* by membrane energization. *J. Bacteriol.* **184**, 5339-5347
- 19 Hederstedt, L. (2002) Succinate:quinone oxidoreductase in the bacteria *Paracoccus denitrificans* and *Bacillus subtilis*. *Biochim. Biophys. Acta.* **1553**, 74-83
- 20 Mooser, D., Maneg, O., Corvey, C., Steiner, T., Malatesta, F., Karas, M., Soulimane, T. and Ludwig, B. (2005) A four-subunit cytochrome *bc*(1) complex complements the respiratory chain of *Thermus thermophilus*. *Biochim. Biophys. Acta.* **1708**, 262-274
- 21 Grishammer, R., White, J. F., Trinh, L. B. and Shiloach, J. (2005) Large-scale expression and purification of a G-protein-coupled receptor for structure determination - an overview. *J. Struct. Funct. Genomics.* **6**, 159-163
- 22 Yeliseev, A. A., Wong, K. K., Soubias, O. and Gawrisch, K. (2005) Expression of human peripheral cannabinoid receptor for structural studies. *Protein Sci.* **14**, 2638-2653
- 23 Mohanty, A. K. and Wiener, M. C. (2004) Membrane protein expression and production: effects of polyhistidine tag length and position. *Protein Expr. Purif.* **33**, 311-325
- 24 Unden, G., Hackenberg, H. and Kroger, A. (1980) Isolation and functional aspects of the fumarate reductase involved in the phosphorylative electron transport of *Vibrio succinogenes*. *Biochim. Biophys. Acta.* **591**, 275-288
- 25 Westenberg, D. J., Gunsalus, R. P., Ackrell, B. A., Sices, H. and Cecchini, G. (1993) *Escherichia coli* fumarate reductase frdC and frdD mutants. Identification of amino acid residues involved in catalytic activity with quinones. *J. Biol. Chem.* **268**, 815-822
- 26 Wallace, B. A. and Janes, R. W. (2001) Synchrotron radiation circular dichroism spectroscopy of proteins: secondary structure, fold recognition and structural genomics. *Curr. Opin. Chem. Biol.* **5**, 567-571
- 27 Wallace, B. A., Lees, J. G., Orry, A. J., Loble, A. and Janes, R. W. (2003) Analyses of circular dichroism spectra of membrane proteins. *Protein Sci.* **12**, 875-884
- 28 Luke, K. A., Higgins, C. L. and Wittung-Stafshede, P. (2007) Thermodynamic stability and folding of proteins from hyperthermophilic organisms. *FEBS J.* **274**, 4023-4033
- 29 Kurokawa, T. and Sakamoto, J. (2005) Purification and characterization of succinate:menaquinone oxidoreductase from *Corynebacterium glutamicum*. *Arch. Microbiol.* **183**, 317-324
- 30 Peterson, J., Fujimoto, W. Y. and Brunzell, J. D. (1992) Human lipoprotein lipase: relationship of activity, heparin affinity, and conformation as studied with monoclonal antibodies. *J. Lipid Res.* **33**, 1165-1170

- 31 Darke, P. L., Cole, J. L., Waxman, L., Hall, D. L., Sardana, M. K. and Kuo, L. C. (1996) Active human cytomegalovirus protease is a dimer. *J. Biol. Chem.* **271**, 7445-7449
- 32 Lazazzera, B. A., Bates, D. M. and Kiley, P. J. (1993) The activity of the *Escherichia coli* transcription factor FNR is regulated by a change in oligomeric state. *Genes Dev.* **7**, 1993-2005
- 33 Sytkowski, A. J., Lunn, E. D., Davis, K. L., Feldman, L. and Siekman, S. (1998) Human erythropoietin dimers with markedly enhanced *in vivo* activity. *Proc. Natl. Acad. Sci. U S A.* **95**, 1184-1188
- 34 Hägerhäll, C., Friden, H., Aasa, R. and Hederstedt, L. (1995) Transmembrane topology and axial ligands to hemes in the cytochrome *b* subunit of *Bacillus subtilis* succinate:menaquinone reductase. *Biochemistry.* **34**, 11080-11089
- 35 Beinert, H., Ackrell, B. A., Kearney, E. B. and Singer, T. P. (1975) Iron-sulfur components of succinate dehydrogenase: stoichiometry and kinetic behavior in activated preparations. *Eur. J. Biochem.* **54**, 185-194
- 36 Ackrell, B. A., Cochran, B. and Cecchini, G. (1989) Interactions of oxaloacetate with *Escherichia coli* fumarate reductase. *Arch. Biochem. Biophys.* **268**, 26-34
- 37 Kotlyar, A. B. and Vinogradov, A. D. (1984) Interaction of the membrane-bound succinate dehydrogenase with substrate and competitive inhibitors. *Biochim. Biophys. Acta.* **784**, 24-34
- 38 Gambarelli, S. and Mouesca, J. M. (2004) Correlation between the magnetic g tensors and the local cysteine geometries for a series of reduced [2Fe-2S*] protein clusters. A quantum chemical density functional theory and structural analysis. *Inorg. Chem.* **43**, 1441-1451

FIGURE CAPTIONS:

Fig. 1. SDS-PAGE (A) and Western blot (B) analysis of purified complex II from *T. thermophilus*.

Lanes: 1 – native cII, 2 – wt-rcII, 3 – rcII-SdhB-His₆, 4 – rcII-His₈-SdhB.

Fig. 2. Stacked SEC elution profiles of wt-rcII (-), rcII-SdhB-His₆ (- - -) and rcII-His₈-SdhB (...).

Fig. 3. BN-PAGE analysis of purified complex II from *T. thermophilus*.

Lanes: 1 – β -amylase (200 kDa), 2 – apoferritin monomer (443 kDa) and dimer (886 kDa), 3 – native complex II from *T. thermophilus*, 4 – wt-rcII, 5 – rcII-SdhB-His₆, 6 – rcII-His₈-SdhB.

Fig. 4. Circular dichroism stability analysis of recombinant complex II from *T. thermophilus*.

The dichroic activity at 222 nm of rcII-His₆-SdhB (triangles) and rcII-SdhB-His₈ (circles) recorded at increasing (\blacktriangle , \bullet) and subsequently decreasing (Δ , \circ) temperature.

Fig. 5. Influence of redox mediators, buffer and inhibitors on the EPR spectra of the succinate-reduced recombinant complex II from *T. thermophilus*.

The rcII (5 μ M) was reduced by the addition of 20 mM succinate followed by the addition of *p*-BQ, 1,4-NQ, NQH₂, AQ (100 μ M each), as well as 3-NP (30 μ M) and NQNO (700 μ M). The spectrum labeled ‘asc’ was obtained on a sample reduced by 5 mM ascorbate, ‘malate’ by addition of 20mM malate, ‘dith’ by addition of 1 mM dithionite. Vertical lines indicate the position of the g_x -signal. Spectra were recorded at a temperature of 50 K, microwave power of 64 mW and a modulation amplitude of 1 mT.

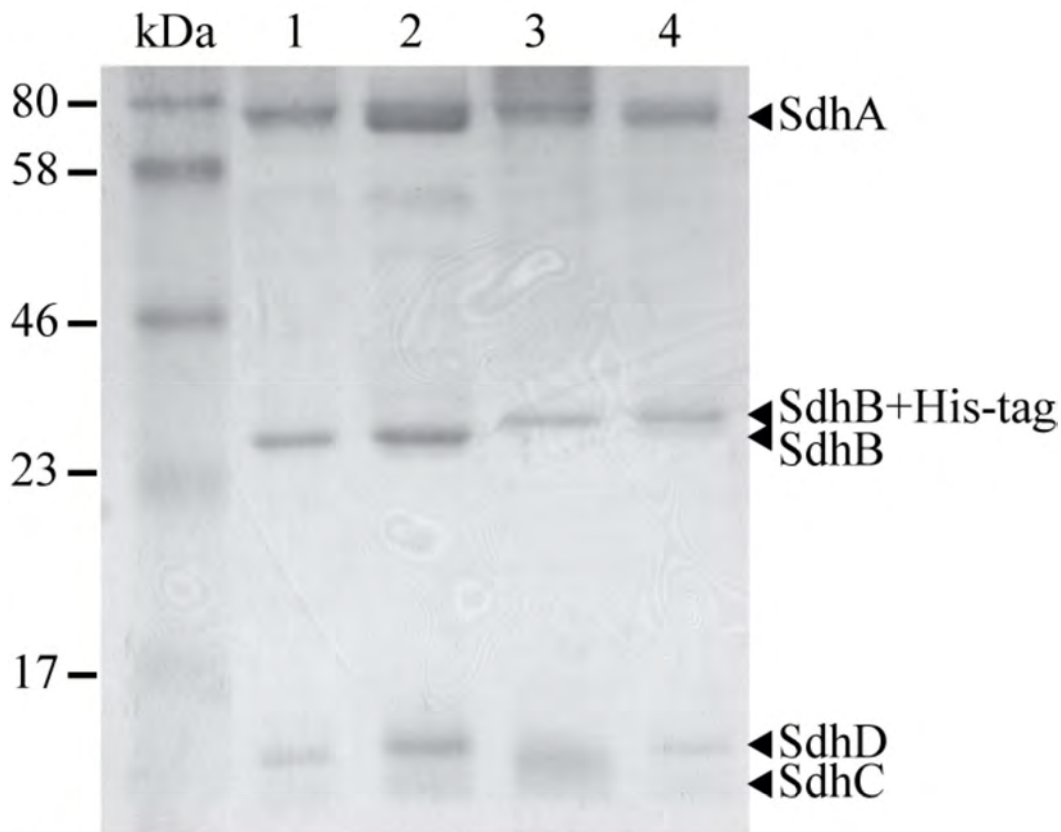
Fig. 6. Influence of pH and increasing amounts of succinate on the EPR spectrum of the [2Fe-2S] cluster of *T. thermophilus* recombinant complex II.

A – EPR spectra of recombinant complex II (6 μ M protein) in the presence of 40 mM succinate at the pH-values indicated (MOPS/Piperazine buffer 100mM each); **B** – half width of the $g_{y/z}$ signal of the [2Fe-2S] cluster of succinate- (\bullet) and ascorbate-reduced (\circ) recombinant complex II. **C** – EPR spectra of the [2Fe-2S] cluster in the presence of 0 mM (black) 0.03 mM (red), 0.06 mM (green), 0.3 mM (blue), 3 mM (cyan), 30 mM (magenta) and 60 mM (orange) succinate. The dashed line represents the spectrum recorded after passing the sample with 60 mM succinate over a desalting column to remove succinate; **D** – The increase in half width of the $g_{y/z}$ signal as a function of the succinate concentration with respect to the signal of the ascorbate-reduced sample (\blacksquare) was fitted with a K_M of 0.22 mM. Pre-reduction of the sample by an excess of dithionite (\square) resulted in a K_M of 1.7 mM. Protein concentration was 10 μ M. Spectra were recorded at a temperature of 50 K, microwave power of 64 mW and a modulation amplitude of 1 mT.

Fig. 7. H-bond network between the flavin and the [2Fe-2S] cluster in complex II.

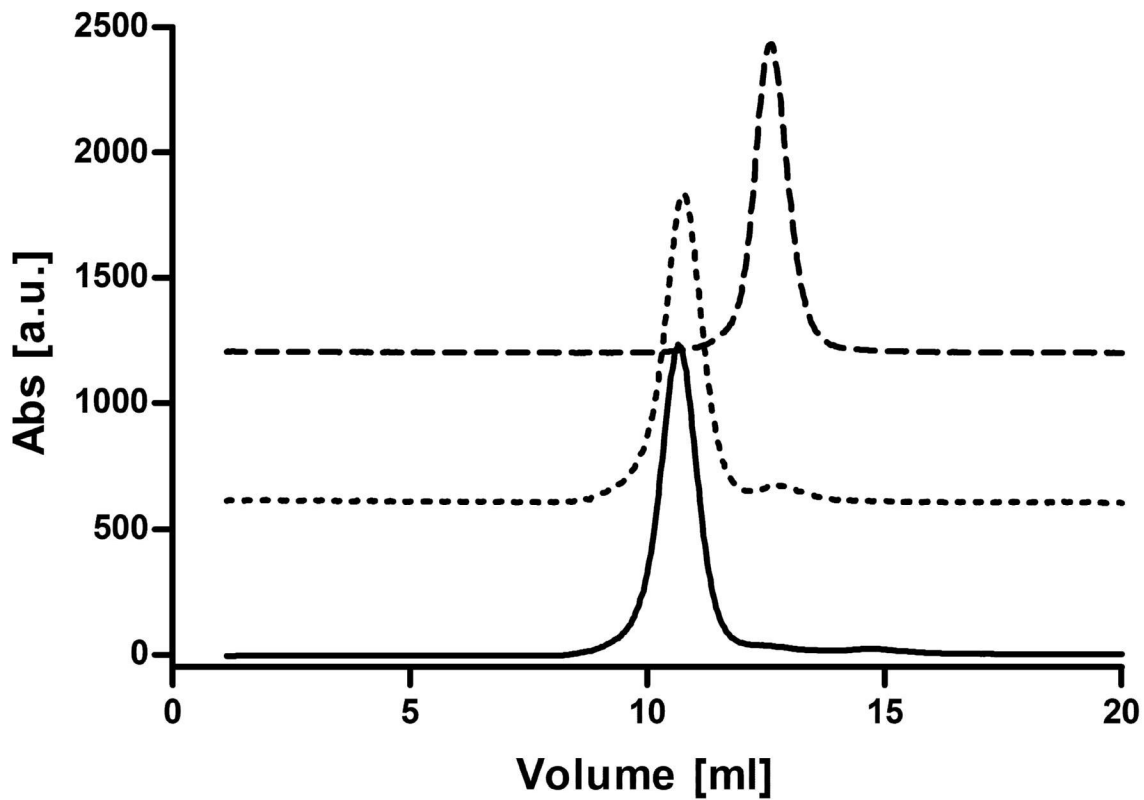
A – The active site of the succinate reductase from *Gallus gallus* with 3-NP bound (PDB ID: 1YQ4) where Glu 67 from the iron-sulfur subunit was replaced by His. An H-bond network connects one of the Cys ligand to the [2Fe-2S] cluster to the histidine that covalently links the flavin via two water molecules and a His residue. The arrow indicates the entrance channel to the active site; **B** – surface representation of the surroundings of the entrance channel to the active site. Iron-sulfur subunit and flavin subunit are presented in blue and yellow, respectively. The His residue in the place of Glu 67 is shown in green; van der Waals ratios of O, N and C were set to 60, 65 and 70 respectively. The stick model represents the flavin cofactor.

A



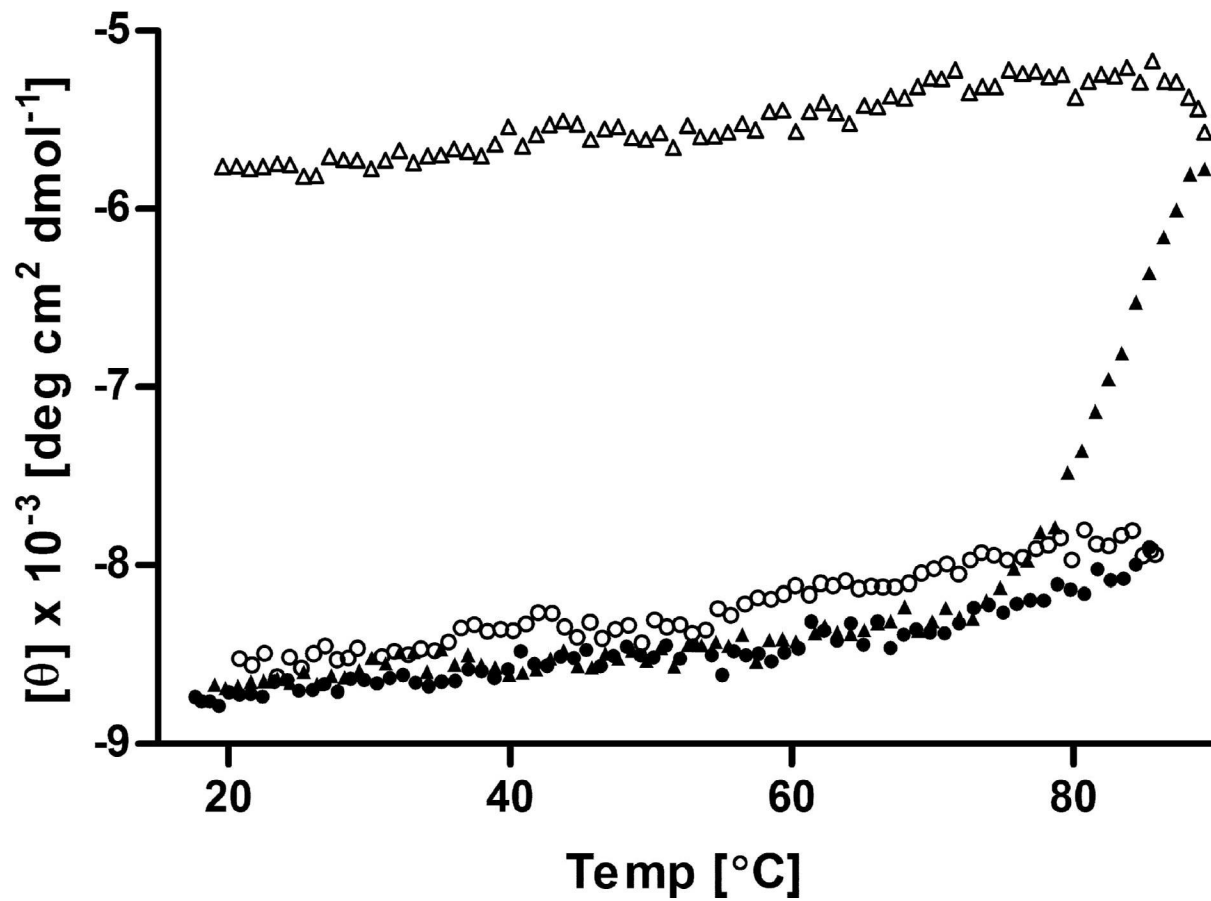
B

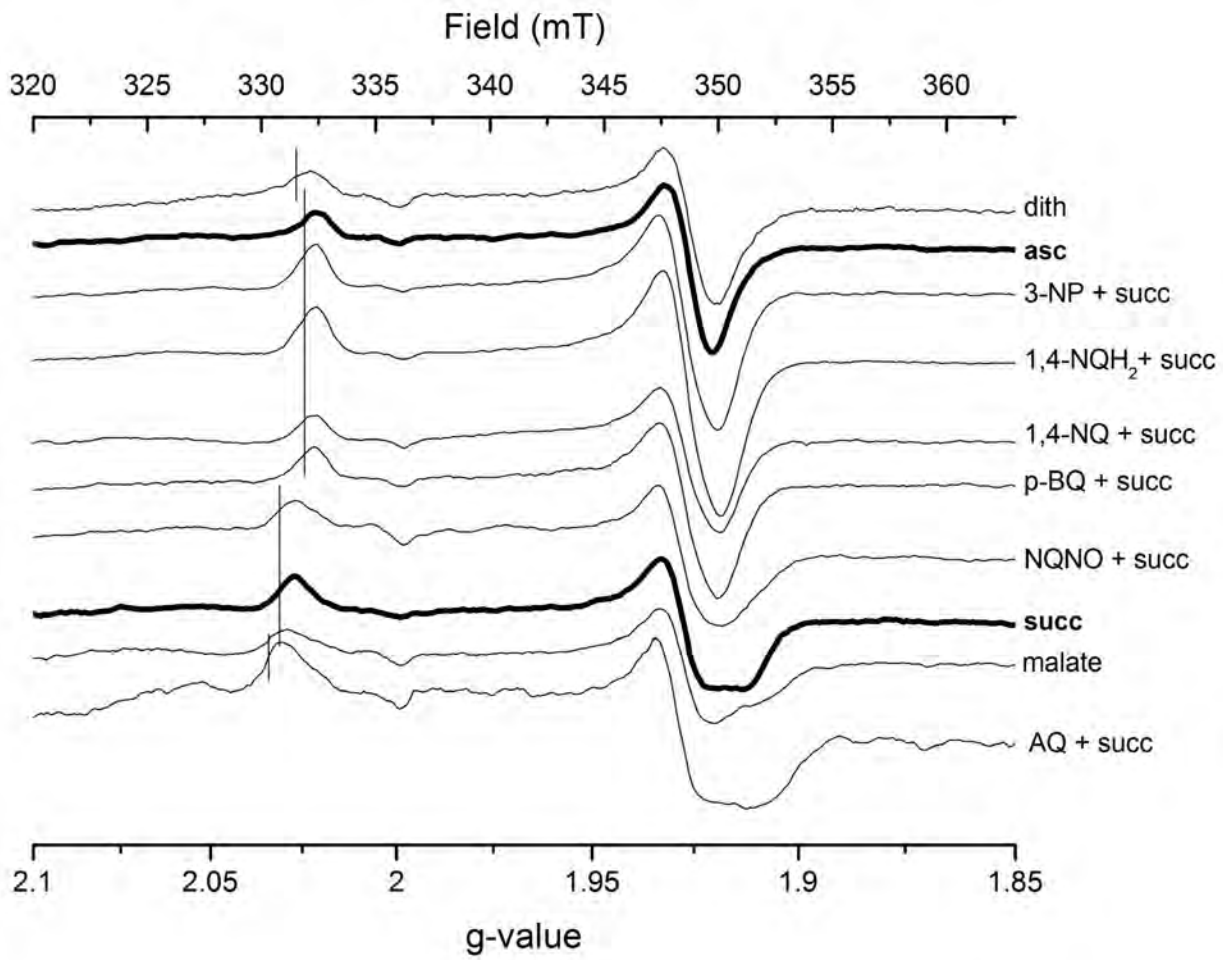


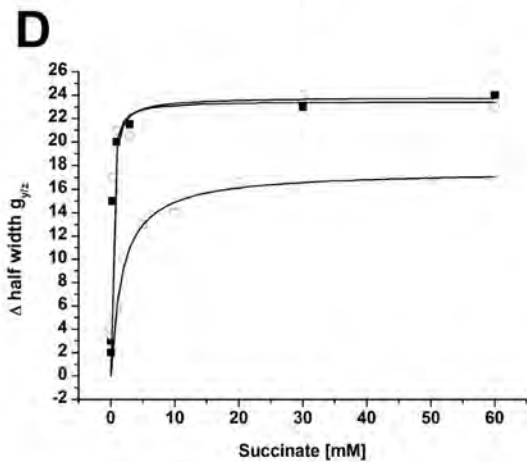
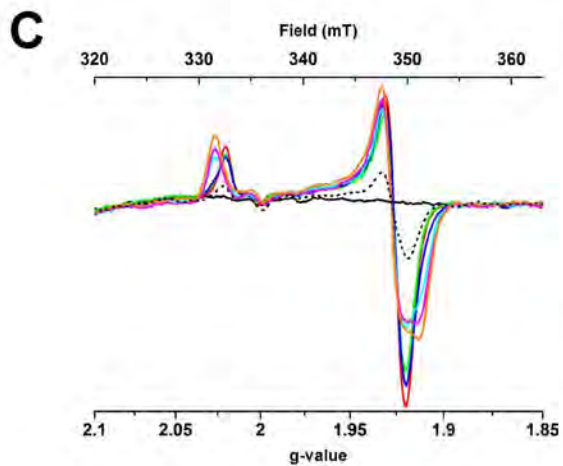
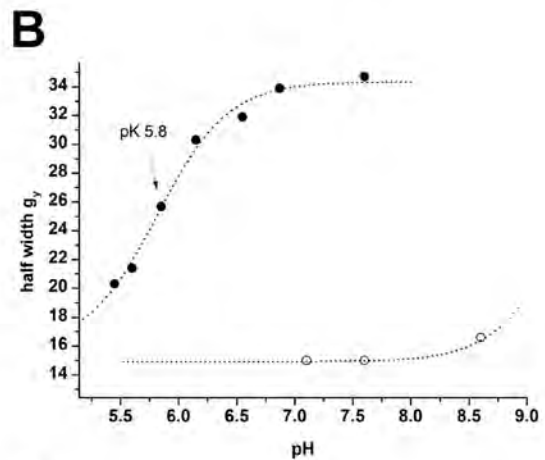
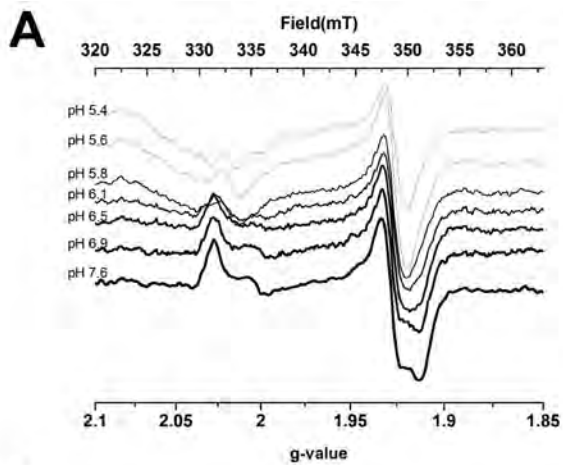


1 2 3 4 5 6









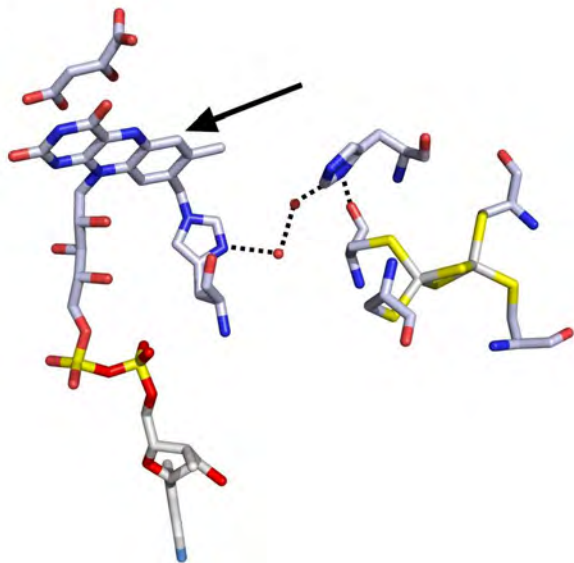
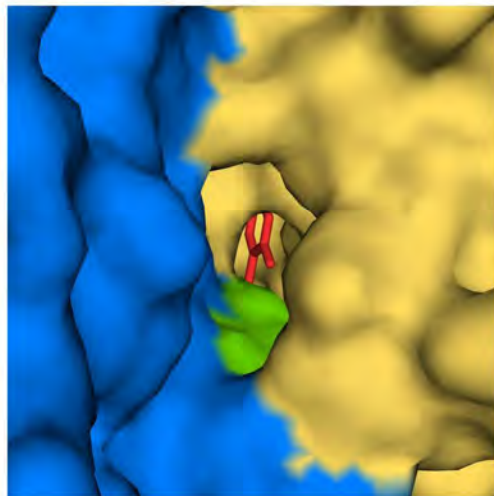
A**B**

Table 1. Summary of succinate dehydrogenase activity of complex II from *T. thermophilus*.

	Native complex II	wt-rcll	rcll-SdhB-His₆	rcll-His₈-SdhB
Kinetics at 30°C	$K_M = 0.21 \pm 0.01$ mM $k_{cat} = 500 \pm 10$ min ⁻¹	$K_M = 0.36 \pm 0.01$ mM $k_{cat} = 1020 \pm 4$ min ⁻¹	$K_M = 0.33 \pm 0.01$ mM $k_{cat} = 760 \pm 6$ min ⁻¹	$K_M = 0.39 \pm 0.03$ mM $k_{cat} = 890 \pm 16$ min ⁻¹
Kinetics at 70°C	$k' = 0.39 \pm 0.08$ mM $h = 2.105 \pm 0.183$	$k' = 0.25 \pm 0.03$ mM $h = 2.285 \pm 0.128$	$K_M = 0.29 \pm 0.02$ mM $k_{cat} = 2500 \pm 31$ min ⁻¹	$k' = 0.28 \pm 0.04$ mM $h = 2.698 \pm 0.204$
Malonate inhibition	^c $K_i = 40 \pm 4$ μM	^c $K_i = 65 \pm 8$ μM	^c $K_i = 58 \pm 4$ μM	^c $K_i = 55 \pm 5$ μM
Oxaloacetate inhibition	^c $K_i = 17 \pm 2$ μM	^c $K_i = 51 \pm 3$ μM	^c $K_i = 21 \pm 2$ μM	^c $K_i = 85 \pm 12$ μM
3-NP inhibition	ⁱ $K_{iapp} = 0.23 \pm 0.06$ mM	ⁱ $K_{iapp} = 0.2 \pm 0.02$ mM	ⁱ $K_{iapp} = 0.29 \pm 0.06$ mM	ⁱ $K_{iapp} = 0.27 \pm 0.07$ mM
NQNO inhibition*	ⁿ $K_i = 70 \pm 5$ μM	ⁿ $K_i = 88 \pm 6$ μM	ⁿ $K_i = 80 \pm 8$ μM	ⁿ $K_i = 77 \pm 8$ μM

^c – competitive inhibition

ⁱ – irreversible inhibition

ⁿ – non-competitive inhibition

* – measured in the DCPIP/1,4-NQ set up; all other measurements performed in the PMS/DCPIP set up



Invited review

Bioenergetics at extreme temperature: *Thermus thermophilus* *ba*₃- and *caa*₃-type cytochrome *c* oxidases[☆]

Mohamed Radzi Noor, Tewfik Soulimane^{*}

Department of Chemical and Environmental Sciences and Materials & Surface Science Institute (MSSI), University of Limerick, Limerick, Ireland

ARTICLE INFO

Article history:

Received 31 May 2011

Received in revised form 11 August 2011

Accepted 12 August 2011

Keywords:

*ba*₃-oxidase*caa*₃-oxidase

Respiratory complex

Thermus thermophilus

ABSTRACT

Seven years into the completion of the genome sequencing projects of the thermophilic bacterium *Thermus thermophilus* strains HB8 and HB27, many questions remain on its bioenergetic mechanisms. A key fact that is occasionally overlooked is that oxygen has a very limited solubility in water at high temperatures. The HB8 strain is a facultative anaerobe whereas its relative HB27 is strictly aerobic. This has been attributed to the absence of nitrate respiration genes from the HB27 genome that are carried on a mobilizable but highly-unstable plasmid. In *T. thermophilus*, the nitrate respiration complements the primary aerobic respiration. It is widely known that many organisms encode multiple biochemically-redundant components of the respiratory complexes. In this minireview, the presence of the two cytochrome *c* oxidases (CcO) in *T. thermophilus*, the *ba*₃- and *caa*₃-types, is outlined along with functional considerations. We argue for the distinct evolutionary histories of these two CcO including their respective genetic and molecular organizations, with the *caa*₃-oxidase subunits having been initially 'fused'. Coupled with sequence analysis, the *ba*₃-oxidase crystal structure has provided evolutionary and functional information; for example, its subunit I is more closely related to archaeal sequences than bacterial and the substrate–enzyme interaction is hydrophobic as the elevated growth temperature weakens the electrostatic interactions common in mesophiles. Discussion on the role of cofactors in intra- and intermolecular electron transfer and proton pumping mechanism is also included. This article is part of a Special Issue entitled: Respiratory Oxidases.

© 2011 Elsevier B.V. All rights reserved.

1. Introduction

Thermus thermophilus is a Gram-negative and an extremely-thermophilic bacterium. The genomes of two very closely-related strains, HB8 and HB27, have been sequenced (NCBI GPID: 13202 and 10617) [1]. HB8 is a facultative anaerobe, with a nitrate reductase gene cluster (GenBank ID: Y10124) being responsible for growth on nitrate under anaerobic conditions [2]. In the sequenced genome, the genes were not detected and it has been suggested that the conjugative plasmid carrying the genes is not stable [3]. The strictly-aerobic HB27 strain can be engineered to grow on nitrate anaerobically by the gene transfer through conjugation [4]. This has been exploited to develop the *T. thermophilus* HB27::*nar* strain for anoxia-inducible protein expression system [5].

However, sequence analysis alone is insufficient to provide an explanation of its overall bioenergetic mechanisms, including the existence

of two terminal oxidases. At 70 °C, the solubility of O₂ in water is only ~60% compared to at 25 °C [6]. *T. thermophilus* has been revealed to encode two cytochrome *c* oxidases (CcO). The low O₂-affinity *caa*₃-oxidase is constitutively expressed whereas the *ba*₃-oxidase possesses high affinity and is coexpressed with the *caa*₃-oxidase under low oxygen tension.

The intriguing facts surrounding the CcO of *T. thermophilus* are not limited to their structure–function relationships. Apart from being able to reduce nitric oxide (NO) [7], their general features including the hydrophobic substrate–enzyme interaction and subunit compositions do not conform to the canonical features of bacterial and mitochondrial complexes. Within three decades, old data have been revised and new data are being constantly obtained. The *ba*₃-oxidase originally described as comprising only one subunit [8] was later found to contain three subunits [9], the *c*₁-cytochrome of *caa*₃-oxidase [10–12] is actually a covalently-bound cytochrome *c* [13,14] and the two-polypeptide, three-subunit *caa*₃-oxidase [15] is now known as a three-polypeptide, four-subunit complex (T. Soulimane, unpublished data).

2. Terminal oxidases of *T. thermophilus*

The transfer of electrons to the terminal acceptor O₂ is catalyzed by a group of proteins in the heme-copper oxidases (HCO) superfamily.

Abbreviations: HEF, hydroxyethylfarnesyl; HEGG, hydroxyethylgeranylgeranyl; SD, Shine–Dalgarno sequence; TMH, transmembrane helices

[☆] This article is part of a Special Issue entitled: Respiratory Oxidases.

^{*} Corresponding author at: L2-009 Lonsdale Building, Chemical and Environmental Sciences, University of Limerick, Limerick, Ireland. Tel.: +353 61 234133; fax: +353 61 202568.

E-mail address: tewfik.soulimane@ul.ie (T. Soulimane).

This superfamily does not encompass all terminal oxidases, as evidenced by the *bd*-type quinol oxidases with no copper redox center [16,17]. It is divided into two distinct families – the CcO and quinol oxidase, with the latter lacking the mixed-valence homodinuclear copper center Cu_A [18]. The sequence motif of the Cu_A binding region (His-Xaa₃₅-Cys-Xaa-Glu-Xaa-Cys-Xaa₃-His-Xaa₂-Met) allows for the classification of an oxidase as either a CcO or quinol oxidase [19]. Surprisingly, the distribution of these HCO does not correlate with growth conditions [20] and the heme type is not related to the phylogeny of the organism, the electron donor or sequence similarities between the enzymes [18]. Thus, HCO are best classified according to their proton pumping-related sequence conservation where three types (A, B and C) have been proposed [21]. The A-type is split into the A1 and A2 subfamilies; both are similar in that the oxidases have the D- and K-pathways for proton pumping except for sequence conservation. For instance, the *T. thermophilus* *caa*₃-oxidase is of the A2-type because the Glu1-278^P, ¹ residue at the hydrophilic end of the D-pathway, which is otherwise highly conserved in members of the A1, is absent. The Glu1-278^P residue may be functionally replaced by the conserved Tyr-Ser residues in the *caa*₃-oxidase (YS motif; Section 2.2.1) [20]. Accordingly, the *ba*₃-type oxidase belongs to the B-type HCO as it does not have the classical D- and K-pathways for proton pumping but instead has a pathway analogous to the K-pathway (K-analogue) [22]. Finally, the C-type consists of *ccb*₃-oxidases which do not show significant sequence similarities among themselves or to the other types. A classification tool and database for HCO (<http://www.evocell.org/hco>) has been developed recently [23]. This tool does not include the splitting of the B-type oxidases into several other HCO types as proposed by Hemp and Gennis [24]. These new types are designated D, E, F, G and H, of which the D–F types are found exclusively within the *Sulfolobales* class of the *Crenarchaeota* phylum. While the number of prokaryotic genome sequences is increasing, detailed biochemical and biophysical studies into these unique HCO lags far behind those from the ‘model’ organisms.

2.1. *ba*₃-type CcO

Unlike the *caa*₃-oxidase subunits, the *ba*₃-type CcO subunits of both *T. thermophilus* strains are identical (Table 1). They are encoded by the loci TTHA1133–1135 on the chromosome of HB8 and TTC0768–0770 in HB27. This contiguous locus encodes all the three subunits – I, II and IIa.

2.1.1. Subunit I

The subunit I contains 13 transmembrane helices (TMH) and shows only a distant similarity to the other members of the HCO superfamily, indicating a possible early gene duplication event prior to the divergence of *Archaea* and *Bacteria*. Although Pereira *et al.* [18] suggested that the terminal oxidases in *Archaea* were acquired from *Bacteria*, more recent analyses indicate that B-type oxygen reductases originated from *Crenarchaeota* [25]. The presence of 13 TMH differentiates the *T. thermophilus* CcO from most of the members of HCO, as the canonical number of TMH is 12. The shortened loops, which are found connecting the TMH, have been generally postulated to play a role in enhancing the thermostability of proteins by decreasing the entropy of unfolding [26,27]. The crystal structure shows that the first nine residues (MAVRASEIS) predicted from the gene sequence are absent from the subunit I sequence (UniProt ID: Q5SJ79) [9]. Although it is likely the protein undergoes cleavage, prediction of cleavage sites using PeptideCutter (<http://www.expasy.ch/tools/peptidecutter>) in-

Table 1

Genetic loci encoding cytochrome *c* oxidases in the two sequenced *Thermus thermophilus* strains. The *caa*₃-oxidase subunits of HB8 and HB27 strains differ to an extent while *ba*₃-oxidase subunits are completely identical.

Subunits	Genetic loci		Differing residues between HB8 and HB27
	HB8	HB27	
<i>caa</i> ₃ -oxidase			
I/III	TTHA0312	TTC1671	V175I
IIc	TTHA0311	TTC1672	F96L, M117L, A170S, A226Q, W269L, V318A
<i>ba</i> ₃ -oxidase			
I	TTHA1135	TTC0770	–
II	TTHA1134	TTC0769	–
IIa	TTHA1133	TTC0768	–

icates that there is no recognition site for a protease at the C-terminus of the last serine residue. Further, N-terminal sequencing of the crystallized protein shows that the residues are not retained. However, the recombinant *ba*₃-oxidase retains the residues SEIS at the N-terminus of subunit I (PDB ID: 1XME) [28,29]. As the only difference between the native and recombinant *ba*₃-oxidase is the presence of a hexahistidine tag between the Met and the first Ala, this could be the reason for the retention of the SEIS residues. Interestingly, the structures of recombinant *ba*₃-oxidase at 1.8 Å resolution (PDB ID: 3S8F and PDB ID: 3S8G) shows the retention of only the last Ser of the MAVRASEIS-like sequence [31].

Three of the four redox centers – low-spin heme *b*, high-spin heme *a*₃ and a single Cu ion (Cu_B) – are located within the subunit I; the iron in heme *a*₃ together with Cu_B form a heterodinuclear center [9]. Based on the crystal structure, His72 and His386 act as the axial ligands of heme *b* whereas His233, His282, His283, His384 and Tyr237 form the coordination sphere of the heterodinuclear center. The metal centers are buried within the protein to avoid the release of reactive oxygen species during catalysis [18].

A formyl group at C8 and a hydrophobic hydroxyethylgeranylgeranyl (HEGG) moiety are present on the heme *a*₃. This is in contrast with the typical heme *a* structure where hydroxyethylfarnesyl (HEF) is present on C2, as exemplified by the *Paracoccus denitrificans* *aa*₃-type CcO. HEGG is straight and reaches the cytoplasmic side without interfering with the proton pathways, and the increased hydrophobicity of HEGG compared to HEF might stabilize the heme at high growth temperatures [32,33]. This hypothesis fits with the shared phylogeny between the *T. thermophilus* *ba*₃-oxidase and the investigated archaeal CcO. Nevertheless, there are studies indicating otherwise – the *b(o/a)*₃-type² CcO of the thermophilic *Geobacillus stearothermophilus* (basonym *Bacillus stearothermophilus*) is related to archaea (B-family) but no heme *A*_s could be detected [34]; the CcO of the mesophilic *Corynebacterium glutamicum* is of *aa*₃-type with mass spectrometry analysis indicating presence of heme *A*_s [35]. Studies utilizing the *aa*₃ CcO-related *Escherichia coli* *bo*₃-type quinol oxidase has also shown that the long hydrocarbon side chain is crucial for the function of the high-spin heme iron center, but not for the low-spin one [36,37]. The structural analysis of the *Pseudomonas stutzeri* *ccb*₃-oxidase shows the absence of HEF in the native enzyme [38], raising questions about the requirements for the side chain in distant but related CcO types. Notably, the electron transfer mechanism in *ccb*₃-oxidase occurs without a Cu_A site but instead through a series of heme moieties before reaching the dinuclear center.

2.1.2. Subunit II

Cytochrome *c*₅₅₂, which acts as the electron donor, interacts with the subunit II that forms a single TMH as well as being the only subunit with a polar (periplasmic) domain of β-barrels. The primary

¹ Unless otherwise stated, all numberings are based on the *T. thermophilus* sequences. Superscripts denote the species-specific numberings; P, *Paracoccus denitrificans*; R, *Rhodobacter sphaeroides*; B, bovine heart.

² The high-spin heme is mainly heme O and partly heme A.

site of electron entry into the whole complex is through the homodinuclear copper redox center, Cu_A. The first Cu atom (CU1) is coordinated by the Cys149, Cys153, His157 and Gln151 while the Cys149, Cys153, His114 and Met160 coordinate the second atom (CU2). Theoretical calculations postulated that the presence of two Cu atoms in cytochrome oxidases instead of one promotes the electron transfer from cytochrome *c* to the Cu_A due to a highly-delocalised electron hole and significantly-reduced electron transfer reorganization energy so as to ensure rapid electron transfer [39–43]. The bridging ligands between the Cu atoms are the two thiolate groups of the cysteines. In *P. denitrificans*, TrpII-121^P is the only entry point for electrons from the electron donor cytochrome *c* to redox center Cu_A and the interaction between the substrate and the binding site on the complex is electrostatic [44,45]; the Trp residue is most likely strictly-required due to steric reasons [46]. It has also been shown that two conserved arginine residues Arg481^R and Arg482^R play a key role in the intermolecular electron transfer in the *Rhodobacter sphaeroides* CcO [47]; substrate binding is also electrostatic [44]. Contrarily, the electron transfer is mediated by the Ala87 and Phe88 in *T. thermophilus* *ba*₃-oxidase [48], with a hydrophobic substrate–enzyme interaction [49]. This could be another adaptation by the thermophilic bacterium for growth as electrostatic interactions are weakened at elevated temperatures.

Pereira *et al.* noted that the subunit II of the HCO superfamily displays a family-specific loop of probable functional and, hence, evolutionary importance [18]. The loops of representative members are grouped into ‘loop I’ and ‘loop II’ types based on their actual position within the subunit II (Fig. 1). Found exclusively within the type A1 *aa*₃-oxidases and not in the other subtypes (*viz.* A1 *caa*₃- and quinol oxidases) are the loop II located between the two conserved

aromatic residues (TrpII-121^P and 123^P) and the first Cu_A ligand HisII-181^P; neither of the *T. thermophilus* oxidases has such a loop, though they both have the conserved aromatic residues (PheII-88 and TyrII-90 in the *ba*₃-oxidase, and PheII-109 and TrpII-111 in the *caa*₃-oxidase). In the cyanobacterial A2 oxidases and type B oxidases, loop I is present directly between the transmembrane helix and the cupredoxin-like domain. The comparative structural positions of both loops are indicated in Fig. 1. However, the loop in the *ba*₃-oxidase is shorter than that in the cyanobacterial enzyme, perhaps as an adaptation to its elevated growth temperature. The loops connecting the subunit I TMH are also characteristically shortened. The absence of loop II in the other CcO and quinol oxidases has been argued to be a consequence of the lack of interaction between a soluble cytochrome *c* and the enzymes [18]. It may at least be due to the absence of electrostatic interactions (our interpretation). The authors’ reasoning does not fully explain the absence of loop II in A2 *aa*₃ and B-type CcO, unless the loop I in these families is a structural and/or functional replacement of loop II. This might also be linked to the nature of substrate–enzyme interaction. The interaction between the *T. thermophilus* cytochrome *c*₅₅₂ and *ba*₃-oxidase is not ionic strength-dependent but largely hydrophobic whereas the cyanobacterial cytochrome *c*_{6-aa}₃ oxidase interaction is greatly dependent on the ionic strength. However, there are conflicting reports on the actual effect of increased ionic strength in cyanobacterial substrate–enzyme interactions, and it has been suggested to be due to inherent differences between unicellular and filamentous species [50,51].

2.1.3. Subunit IIa

Prior to the determination of *T. thermophilus* *ba*₃-oxidase crystal structure, it was first described as a single-subunit enzyme [8] and

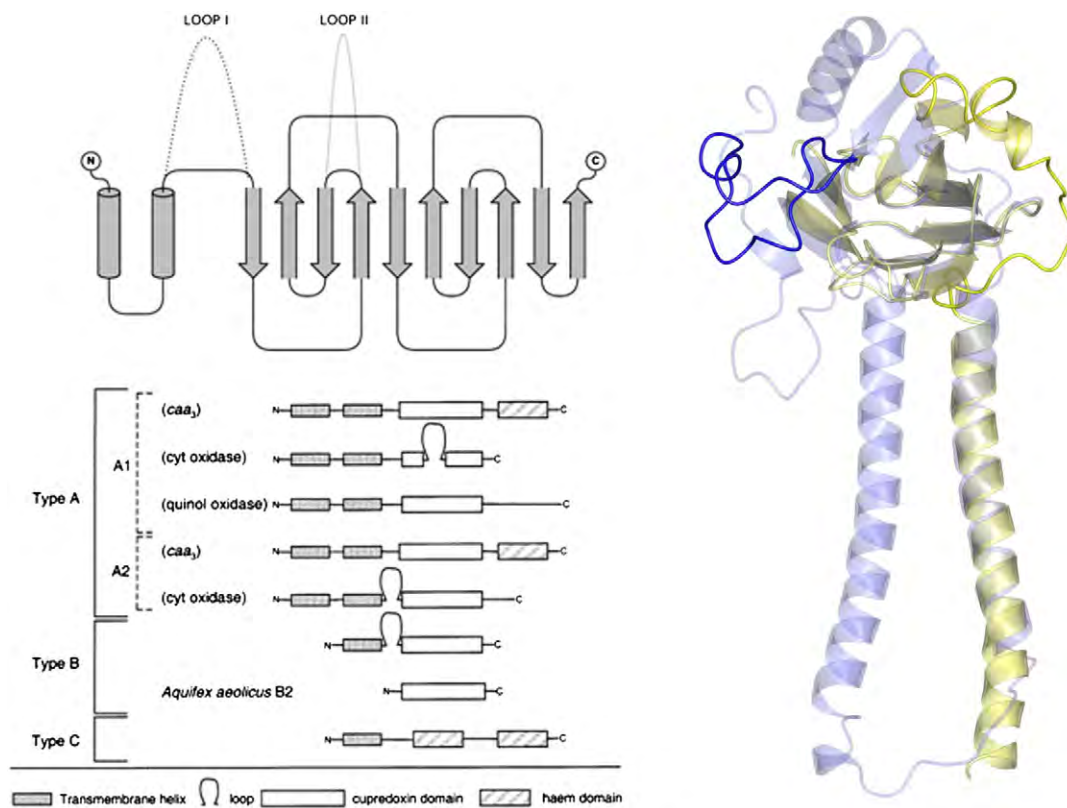


Fig. 1. Representation of loops within the subunit II of *Paracoccus denitrificans* *aa*₃- (PDB ID: 1AR1) and *Thermus thermophilus* *ba*₃-oxidases (PDB ID: 1EHK). Top left: The subunit consists of two helices and ten β -strands forming the cupredoxin fold, where the position of loops I and II is indicated. Redrawn from [18] using TopDraw [128] implemented within the CCP4 suite. Bottom: Presence of loops in the different oxidase families. The *T. thermophilus* *caa*₃- and *ba*₃-oxidases are of the A2 and B families, respectively, while the *Aquifex aeolicus* subunit II putatively consists of only the cupredoxin domain [129]. Adapted from [18]. Right: Superposition of subunit II of *ba*₃-oxidase (green) onto the *aa*₃-oxidase (blue). The loop positions are shown in the darker colors while the main chains are transparent. Figure created with CCP4mg [130].

subsequently shown to comprise two subunits [52]. The third subunit (IIa) was only identified later [9]. It is a short polypeptide of 34 residues and forms a TMH [53]. By searching for homologous sequences using Basic Local Alignment Search Tool (BLAST), the subunit IIa *per se* seems to exist only in *T. thermophilus*, *Thermus aquaticus* and *Meiothermus silvanus*, with all of them predicted to be with the same polarity across the membrane (Fig. 2); it is also 35% identical to the subunit IV of *Natronomonas pharaonis* ba_3 -oxidase CcO [53].

Furthermore, the helical region of subunit IIa superimposes with the first TMH of subunit II of all the structurally-known CcO (bovine, *R. sphaeroides* and *P. denitrificans*) but with an opposite polarity (Fig. 3). The canonical number of TMH of the subunit II is two. Hence, it could be the ‘missing’ helix of *Thermus* subunit II and functionally/structurally complement the latter. Indeed, cloning experiments of the ba_3 -oxidase in which only the subunits I and II were cloned and expressed did not provide overexpression. Only after the addition of subunit IIa to the overexpression vector could the recombinant ba_3 -oxidase be obtained, signifying its subunit II-stabilizing function [28]. The peculiarities of ba_3 -oxidase are not only limited to the hydrophobic interaction with its electron donor, the lower proton pumping efficiency and the presence of HEGG; there are also no other metal ions such as Mg^{2+} or Ca^{2+} in both the native [based on the inductively-coupled plasma-atomic emission spectroscopy (ICP-AES) and electron density map] [54] and recombinant ba_3 -oxidase structures, in contrast to the bovine heart, *R. sphaeroides*, *P. denitrificans* CcO and *P. stutzeri* cbb_3 -oxidase.

Soulimane *et al.* have previously questioned the role of a region within the gene encoding subunit IIa that lies between the promoter and the coding Met residue of the protein as this region also has a codon for a Met (Fig. 4) [53]. Given that the distance between the promoter and the Shine–Dalgarno (SD) sequence is ~50 nucleotides (the optimal distance being 5–20 nucleotides) and between SD and the initiation codon of the coding Met is ~7 nucleotides (optimal is 4–9 nucleotides), we now believe that the SD is within this region. An SD sequence between two initiation codons promotes the gene expression from the codon downstream the SD as long as it is the better initiation site. For this, the distance between the downstream codon and SD should be optimal and strong enough to bind to the ribosome, though an exact complementarity between the mRNA and the 16S rRNA is not a prerequisite for translation [55]. Moreover, the presence of SD itself has been shown not to be required for translation as not all gene sequences contain SD [56,57].

2.2. caa_3 -type CcO

The four-subunit caa_3 -type CcO is unusual in that the subunits are encoded as fused polypeptides — the subunit I with III (I/III) and the subunit II with the soluble electron donor, cytochrome c_{549} (II/c) [14,15] (Section 2.2.1). The genes are organized as part of a classical operon by the loci TTHA0311–0312 and TTC1671–1672 in HB8 and HB27, respectively (Table 1). Recently, an additional, third polypeptide (subunit IV) was found to co-purify and co-crystallize with caa_3 (T. Soulimane; unpublished results). As determined by SDS-PAGE, N-terminal sequencing and mass spectrometry, this 2-TMH, 7-kDa subunit is present in the purified caa_3 -oxidase and single crystals

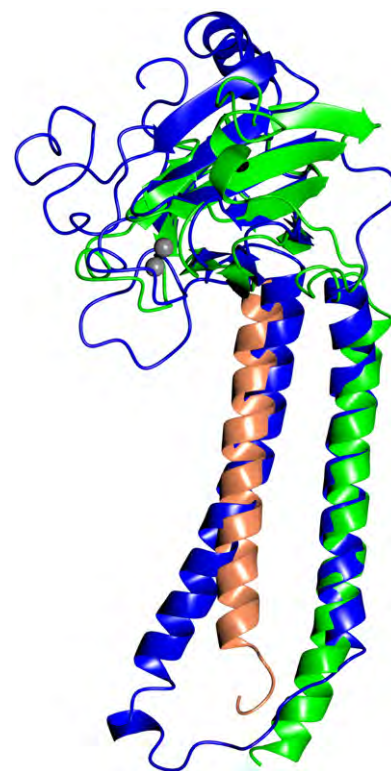


Fig. 3. Ribbon representations of *Thermus thermophilus* ba_3 -oxidase subunits II (green) and IIa (coral) superposed with the *Paracoccus denitrificans* aa_3 -oxidase subunit II (blue). The accession IDs are PDB ID: 1EHK and PDB ID: 1AR1, respectively. The *Thermus* subunit IIa structurally and functionally complements the single TMH of the subunit II. The two copper atoms in the homodinuclear Cu_A center are shown as gray spheres. Figure created with CCP4mg [130].

grown in sitting drops; it shows a significant similarity exclusively to proteins encoded by members of the *Deinococcus–Thermus* phylum as discussed later (Section 2.2.2). Protein sequence analyses show that the subunits differ between the HB8 and HB27 strains; the Val175 of the subunit I/III in HB27 has been replaced with Ile (with respect to HB8) while the subunit II/c exhibit a six-residue difference (Table 1). To our best knowledge, no study has been performed to investigate the effects of these differences on the enzyme properties.

2.2.1. Subunits I/III and II/c

The subunit I/III contains the redox center heme *a* (low spin) and heme a_3 (high spin) and the Cu_B ; O_2 reduction occurs at the a_3 - Cu_B dinuclear center. The homodinuclear Cu center Cu_A is located within the subunit II/c, which also contains the covalently-linked heme *c* electron donor. No exact function has been assigned to the region encoding the subunit III. Topologically, there are 19 predicted TMH, of which 12 are based on the subunit I-like sequence [15]. The subunit II/c has two TMH and both the N- and C-termini are located on the periplasmic side, as expected [14]. As with the ba_3 -oxidase, the *a*-type hemes of the caa_3 -oxidase contain the HEGG side chain [33].



Fig. 2. Sequence alignment of *Thermus thermophilus* HB8 (HB8) ba_3 -oxidase subunit IIa with other similar sequences in *T. thermophilus* HB27 (HB27), *T. aquaticus* (Taq) and *Meiothermus silvanus* (MS) using ClustalW. The topology of the subunit is indicated above the HB8 sequence based on the crystal structure of ba_3 -oxidase. NCBI RefSeq ID: YP144399, YP004741, ZP03497340 and ZP04034717, respectively. Alignment created using ClustalX 2 [131] and modified with GeneDoc and GIMP.

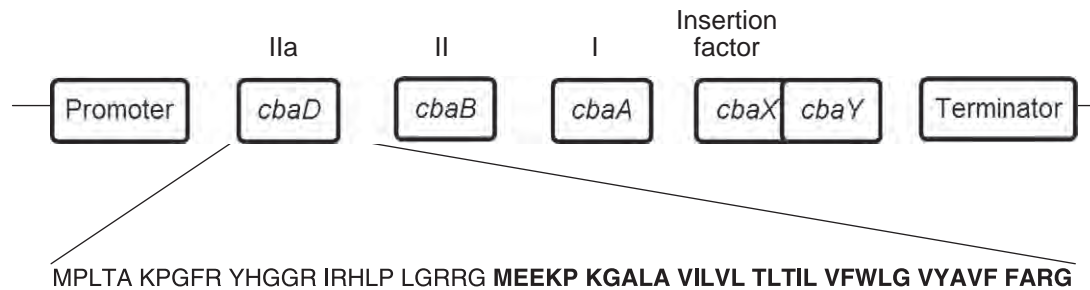


Fig. 4. Organization of the ba_3 -oxidase operon. The sequence of *cbaD* is shown as enlarged with two possible Met residues, of which only the second one is translated into the subunit IIa (bold). The products of the other genes are indicated above the genes. The ORF of *cbaY* overlaps with *cbaX*. The figure is not drawn to scale with respect to the gene size and intergenic space.

The identity of the electron donor to the caa_3 -oxidase has been a subject of controversy [58,59]. Recently, however, using a recombinant soluble cytochrome *c* domain of caa_3 -oxidase, it has been determined that electrons can be received directly from the hydrophilic cytochrome *c* of *bc* (c_{bc} , or $c_{549/554}$, named after its spectroscopically-split α band). This is a largely non-ionic strength dependent process involving hydrophobic interactions [60], and is similar to the cytochrome c_{552} - ba_3 -oxidase interaction (see Section 2.1). However, preliminary data from our laboratory shows the absence of an efficient direct interaction between the c_{bc} and the whole-complex caa_3 -oxidase (T. Soulimane and A. Giuffrè, unpublished results); in addition, the caa_3 -oxidase can also receive electrons from the cytochrome c_{552} [60]. While physiological studies are technically more challenging and sometimes unfeasible, it is doubtful that these *in vitro* studies reflect the actual electron transfer dynamics at low oxygen tension. For instance, fast and efficient electron transfer between the c_{bc} complex and caa_3 -oxidase would exclude a necessity for the cytochrome c_{552} involvement. A complex interplay of rates, equilibrium constants, O_2 affinities, and protein expression dynamics exists that will then determine the proportion of electrons transferred directly to the caa_3 -oxidase and through the cytochrome c_{552} to both the ba_3 - and caa_3 -oxidases.

In the A2-type *T. thermophilus* caa_3 -oxidase, the Glu278^P is replaced by a highly-conserved Tyr-Ser pair, residues 248 and 249 (Fig. 5). This pair of residues probably act in a physicochemically similar way to the Glu-278^P, which is conserved in the A1-type. The thermohalophilic *Rhodothermus marinus* caa_3 -oxidase belongs to

		310	320
A1 aa3	<i>P. denitrificans</i>	ILWFFGHEEIVYMLILP	
A2 caa3	<i>T. thermophilus</i>	FFWFYSHPTVYVMLLP	
A2 caa3	<i>R. marinus</i>	FFWFYSHPAVYIMILP	
B2	<i>A. aeolicus</i>	IFWFYSHPVVYVQLP	
A2 aa3	<i>Anabaena</i>	MFWFYSHPAVYIMILP	
A2 aa3	<i>Synechocystis</i> sp.	LFWFYSHPAVYIMILP	
A2 aa3	<i>T. vulcanus</i>	LFWFYSHPAVYIMILP	
A2 caa3	<i>D. radiodurans</i>	FFWFYSHPAVYVMLLP	
A2 aa3	<i>S. acidocaldarius</i>	LFWFYSHPVVYVPPFP	
C cbb3	<i>B. japonicum</i>	FQWYFGHNAVGFLLTA	
B ba3	<i>N. pharaonis</i>	LFWFYFGHAVVYFWLMP	
B b(o/a)3	<i>G. stearothermophilus</i>	LFWFYFGHPLVYFWLLP	

Fig. 5. Multiple sequence alignment of oxidases with the YS-motif and Y-only sequence. The *Paracoccus denitrificans* sequence shows the conservation of the Glu278^P involved in D-pathway whereas it is replaced by either Tyr and Ser or Tyr only in the other sequences. Accession numbers: *P. denitrificans* (UniProt ID: P08305), *Thermus thermophilus* (UniProt ID: P98005), *Rhodothermus marinus* (UniProt ID: CAC08532), *Aquifex aeolicus* (UniProt ID: O67935), *Anabaena* sp. (UniProt ID: CAB10935), *Synechocystis* sp. (UniProt ID: Q06473), *Thermosynechococcus vulcanus* (UniProt ID: P50676), *Deinococcus radiodurans* (UniProt ID: Q9RR77), *Sulfolobus acidocaldarius* (UniProt ID: P98004), *Bradyrhizobium japonicum* (UniProt ID: Q03073), *Natronomonas pharaonis* (UniProt ID: CAA71525), and *Geobacillus stearothermophilus* (UniProt ID: O82837). Alignment created using ClustalX 2 [131] and modified with GeneDoc.

the A2 group whereas the *Bacillus subtilis* caa_3 -oxidase is of A1 type. As the YS motif is found in the evolutionarily deepest-branching organisms (based on 16S rRNA phylogeny) whereas the Glu-278^P-containing oxidases can only be found within purple bacteria, Gram-positive bacteria and mitochondria, the former oxidases may be ancestral to the latter [61].

2.2.2. Subunit IV

Evidently, the subunit IV of the aa_3 - and caa_3 -oxidases are not only located outside the main oxidase coding region but are also not required for their functionality [62,63]; for quinol oxidases, the subunit IV plays an indispensable role in the complex biosynthesis/activity [64–67]. The subunit IV of *P. denitrificans* (RefSeq ID: YP914242) is found on the chromosome 1 while the subunits I (RefSeq ID: YP915727), II (RefSeq ID: YP918081) and III (RefSeq ID: YP918077) are on the chromosomes 1, 2 and 2 respectively; these locations are in contrast to the results published ten years prior to the genome sequencing [68]. Similarly, in *R. sphaeroides*, the subunits I (RefSeq ID: YP351928), II (RefSeq ID: YP351875), III (RefSeq ID: YP351879) and IV (RefSeq ID: YP353819) are all on the chromosome 1 but not contiguously.³

Perhaps due to such a relaxed necessity, the subunit IV from the structurally-known oxidases does not display any sequence similarity to distantly-related organisms. For example, the *T. thermophilus* caa_3 -oxidase subunit IV shows similarity only to sequences within the *Thermaceae* family; no sequence motifs have been identified (T. Soulimane, unpublished results). Since the subunit IV is not required for functional reasons, the question of why it is retained in diverse organisms arises; the *Deinococcus-Thermus* phylum is phylogenetically ancient whereas *Alphaproteobacteria*, of which *P. denitrificans* and *R. sphaeroides* are members, is as recent as to be the closest extant relative of mitochondria [69]. Interestingly, there are two TMH predicted in the *T. thermophilus* subunit IV while there is only one each in the bacterial oxidases; one of the helices could have been deleted over the course of the oxidase evolution. The presence of subunit IV instead of its complete loss could also be possibly related to the fact that their bovine counterpart has 13 subunits, of which 9 are supernumerary, and that these may be needed to reduce reactive oxygen species production and for expression regulation [70,71].

2.2.3. Heme a insertion factor

The uniqueness of the sequence similarities of the ba_3 -oxidase subunit IIa and the caa_3 -oxidase subunit IV (Sections 2.1.3 and 2.2.2) further extends to the heme *a* insertion factors for both oxidases. Sequence analyses of the genes within the putative caa_3 -oxidase operon indicate the presence of fused polypeptides encoding the heme *a* insertion factor and the constituent subunits of the oxidase. The

³ The *R. sphaeroides* structure was obtained from the strain JS100 but its genome sequence is not available, so the sequences from the type strain 2.4.1 are used here instead while Ref. [62] was based on strain 1222.

insertion of the two heme *a* moieties into the *caa*₃-oxidase apoprotein requires the action of an insertion factor, encoded by TTHA0310 (CtaA/B) in *T. thermophilus* HB8. The residues 12–294 of CtaA/B form the heme A synthase domain (CtaA) while the residues 340–598 form the heme O synthase (CtaB) domain. Heme A is synthesized through a three-step process; the *B. subtilis* CtaB is responsible for the farnesylation of heme B to heme O which is then acted upon by the monooxygenase/dehydrogenase CtaA in a two-step reaction [72,73].

A PSI-BLAST search for sequences homologous to the fused *T. thermophilus* CtaA/B limited to a length similar to that of the CtaA/B revealed the presence of such a sequence mostly only in the phylogenetically-ancient lineages of *Deinococcus-Thermus* and *Chloroflexi* (Table 2). Interestingly, *Bacteriovorax marinus* is a Gram-negative predatory bacterium that preys on other Gram-negative bacteria [74] and, consequently, the fused CtaA/B gene could have been horizontally transferred.

A similar situation exists for the subunit I/III, where the CcO subunit can only be found in the *Deinococcus-Thermus* and *Crenarchaeota* phyla (Table 3). Compared to the relatively more widespread presence of ‘fused’ CtaA/B, the ‘fused’ subunit I/III is only limited to the *Deinococcus-Thermus* phylum. Unexpectedly, the CcO of *Aeropyrum pernix* is of *aa*₃-type [75]. Possibly due to the architecture of the A1 and A2 *caa*₃-oxidases themselves, the subunits II and cytochrome *c* are encoded as fused polypeptides in a wide-range of organisms. It is found in both as phylogenetically-ancient lineages as the *Deinococcus-Thermus* and as phylogenetically-recent lineages as the *Proteobacteria*.

We, therefore, propose that at the beginning of aerobic respiration, the *caa*₃-oxidase subunits and the insertion factor were encoded as ‘fused’ polypeptides and were split more recently. The reason for the split is more likely to be due to an absence of any selection pressure to maintain them as fused polypeptides rather than because of evolutionary pressure to split them. Theoretically, a protein complex encoded by a single gene would be more efficient in terms of transcription, translation, complex assembly and function compared to two separately-encoded genes.

Furthermore, neither the structural subunits of the *caa*₃-oxidase nor the CtaA/B has significant sequence similarities to the *ba*₃-oxidase subunits and its heme *a* insertion factor CbaX [76], suggesting divergent evolutionary histories of the two oxidases. The CbaX, which only exists in the *Thermaceae* family, does not have any identifiable conserved domain (<http://www.ncbi.nlm.nih.gov/Structure/cdd/wrpsb.cgi>) with no significant matches against *B. subtilis* in contrast to the CtaA/B. It is also considerably smaller than the CtaA/B (17 kDa vs. 66 kDa), raising questions on the differences between the synthesis and insertion of heme *a* moieties into the *ba*₃- and *caa*₃-oxidases, including the presence of two heme *a* moieties in the latter. The details of CcO biogenesis have been recently reviewed [77].

2.2.4. Loops

Transmembrane helices are connected to each other by loops. For thermophilic proteins, the loops tend to be shorter than their

Table 2

Distribution of the fused CtaA/B. With the exception of *Proteobacteria*, all phyla are ancient. The hit of HB27 against the *T. thermophilus* HB8 is not included. Some of the protein sequences do not display complete conserved CtaA domain based on CD search but are instead truncated at the N-termini (a) or C-termini (b).

Phylum	Species name (RefSeq ID)	Identity (%)
<i>Deinococcus-Thermus</i>	<i>T. aquaticus</i> (ZP03496720)	86
	<i>T. scotoductus</i> (YP004201293)	88
<i>Chloroflexi</i>	<i>Roseiflexus castenholzii</i> (YP001434348) ^a	36
	<i>Sphaerobacter thermophilus</i> (YP003321390) ^a	36
	<i>Thermomicrobium roseum</i> (YP002523677)	37
	<i>Bacteriovorax marinus</i> (CBW25150)	22
<i>Proteobacteria</i>		
<i>Euryarchaeota</i>	<i>Halalkalicoccus jeotgali</i> (YP003737487) ^b	33
	<i>Natrialba magadii</i> (YP003480427) ^b	30

Table 3

Distribution of the fused subunit I/III. The subunit is only found fused in the *Deinococcus-Thermus* phylum, and the *Aeropyrum pernix* of which the CcO is *aa*₃-type.

Phylum	Species name (RefSeq ID)	Identity (%)
<i>Deinococcus-Thermus</i>	<i>Deinococcus deserti</i> (YP002786574)	58
	<i>Deinococcus geothermalis</i> (YP603878)	58
	<i>Deinococcus radiodurans</i> (NP296339)	58
	<i>Meiothermus ruber</i> (YP003506497)	56
	<i>Meiothermus silvanus</i> (YP003684057)	66
	<i>T. aquaticus</i> (ZP03496722)	95
	<i>T. scotoductus</i> (ADW20746)	93
	<i>Oceanithermus profundus</i> (YP004057123)	73
<i>Crenarchaeota</i>	<i>Aeropyrum pernix</i> (NP147500)	34

mesophilic counterparts (Section 2.1.1). However, the loop connecting the subunit I to the subunit III of the *caa*₃-oxidase is predicted to be of 72 residues and located on the cytoplasmic part (residues 483–555 as predicted by the TMHMM server <http://www.cbs.dtu.dk/services/TMHMM-2.0/>). This is longer than the average loop length of 20 residues predicted for the rest of the protein sequence and the structurally-determined length for the *ba*₃-oxidase subunits I and II; the loops predicted for the CtaA/B are also about 20 residues with the loop directly between CtaA and CtaB domains consisting of 37 residues. Moreover, this 72-residue loop also exists in the *A. pernix* CcO subunit I/III (Table 3) with a predicted 154 residues and in *Deinococcus radiodurans* with 75 residues.

Whether such a long loop is required to maintain a certain spatial distance between the subunits I and III or is involved in protein-protein interactions would require extensive mutagenesis including deletion of certain parts of the loop. It appears that this might be a feature common to all CcO where the subunits I/III are fused. That the *Thermus* loop is a thermophile feature can be excluded based on its presence in the closely-related *Deinococcus* species, though the thermophilic *A. pernix* (optimum growth temperature of 90–95 °C [78]) has a longer loop.

3. Mechanistic analysis (electron transfer and proton pumping)

3.1. Overview of *ba*₃-oxidase functional mechanism

Three processes central to the *ba*₃-oxidase catalysis are the electron transfer from the *bc* complex via the soluble cytochrome *c*₅₅₂, proton pumping across the membrane to generate the gradient required for ATP generation and the reduction of molecular oxygen to water.

3.2. Intermolecular electron transfer (from substrate to enzyme complex)

Residues important for CcO function, such as the heme and Cu ligands as well as those involved in the electron transfer described above, are highly conserved among all the structurally-determined CcO sequences. The electron transfer pathway between the cytochrome *c*₅₅₂ and the Cu_A has been elucidated by nuclear magnetic resonance (NMR), where it is proposed that the electron from the porphyrin ring in the cytochrome *c*₅₅₂ is sequentially transferred via the residues Ala87, Phe88 and His114 before reaching the CU2 atom of Cu_A [48]. The edge-to-edge distance between the heme and the imidazole of His114 is 10.9 Å. An analysis of structures in PDB shows that the majority of edge-to-edge distances between redox cofactors are less than 14 Å, thereby minimizing mutational or thermal fluctuation effects [79]. Alternatively, longer electron jumps through space could occur directly to Phe88, His114 and the Cu atoms; it is also possible to bypass the His residue. With a total distance of 13.5 Å, the rate would be very low.

3.3. Intramolecular electron transfer (from Cu_A to Cu_B)

The electrons from Cu_A are transferred to Cu_B, probably via heme *b* and possibly via heme *a*₃. His114, Arg449 and Arg450 together with the propionates of heme *b* provide a pathway for electron transfer between Cu_A and heme *b*; either Phe385 or His384 and His386 (heme *a*₃ and *b* ligands, respectively) can further transfer the electrons to the high-spin heme. These residues are all conserved in the *Thermus* *ba*₃-oxidase compared to the other CcO. Alternatively, electron tunneling may allow for the transfer from Cu_A through Gln151 to Tyr136, Trp229 (a through-space jump using hydrogen bond) and His283 (Cu_B ligand) before reaching the Cu_B itself. With the exception of *ccb*₃-oxidase that has no Cu_A center, the distance between Cu_A and Cu_B is ~22 Å in all the structurally-determined CcO, even greater than the Cu_A to Fe_{a/b} distance of 19 Å. Direct electron transfer from the two Cu centers will be very slow compared to the indirect pathways.

3.4. Coupling of electron transfer to proton pumping

For more than a billion years, since oxygen appeared in the atmosphere, respiratory complexes have evolved to sustain energetically-efficient mechanisms. High-energy intermediates in these complexes can be avoided through the proton-coupled electron transfer (PCET) and pathways in which electron transfer is followed by proton transfer [80]. The proton gradient required for the ATP generation by the ATP synthase complex is generated by the pumping of protons across the membrane into the periplasmic/intermembrane space by a series of oxidoreductases. The leakage of protons back into the cytoplasm/mitochondrial matrix is thermodynamically favored. Molecular dynamics simulation (MDS) has identified the putative valve-like residue Glu1-242^B (Glu1-278^P) as being responsible to prevent this intraprotein back leakage [81].

In the A-type (mitochondrial-like) CcO, two proton pathways, the D- and K-pathways have been identified. The D-pathway leads from the Asp1-124^P to the Glu1-278^P through which six or seven protons are transferred per catalytic cycle (four of which are pumped across the membrane). The K-pathway leads from a Lys1-354^P to the cross-linked His1-276^P/Tyr1-280^P in the active site and transfers one or two protons to Cu_B center for O₂ reduction (reviewed in [21]). Both pathways are functional prerequisites for full enzyme function. In addition, a possible H-pathway, composed of a network of hydrogen bonds and waters, was identified by an examination of the crystal structure of bovine heart CcO [82]. Its existence in *P. denitrificans* [83,84] and *R. sphaeroides* [85] is controversial, but it is argued by Shimokata *et al.* [86] that the presently available mutagenesis studies do not disprove the existence of such H-pathways.

Soulimane *et al.* have previously identified three potential proton pumping pathways based on the *ba*₃-oxidase crystal structure [9]. Two are spatially analogous to the D- and K-pathways and the third (the Q-pathway) leads from a Gln254 to the heme *a*₃ axial His ligands [9]. Of all the B-type CcO sequences analyzed, only the residues forming the K-pathway analogue [22] are conserved. This contrasts with the high conservation of similar K-pathway residues within the A-type and implies that only a K-analogue is functional in the B family. A series of mutagenesis studies has identified the residues important for catalysis and electron transfer/proton pumping coupling. These have been mapped onto the *ba*₃-oxidase structure to identify those with the potential to form a K-analogue pathway. It leads from the Glu1-15 to the subunit I residues Thr315, Tyr248, Thr312, Ser309, Tyr244 and Tyr237. When mutated to non-polar, non-H-bonding residues, the capability to reduce O₂ is abolished. Similar mutations on the possible D- or Q-pathway residues in the *ba*₃-oxidase generally affect neither catalysis nor proton pumping. The presence of an unknown proton pathway can be excluded as mutants with a blocked K-analogue pathway show retarded reduction and oxidation rates for the hemes *b* and *a*₃. The *Thermus* *ba*₃-oxidase has a reduced

proton-pumping efficiency, as only 0.4–0.5 protons are pumped per electron transferred compared to the standard 1 H⁺/e⁻ in classical heme-copper oxidases. A single H⁺/e⁻ is necessarily used for water formation [87].

3.5. Water pool in *ba*₃-oxidase

Water molecules accumulate above the heme propionates in the oxidase structure (PDB ID: 1EHK) to create a water 'pool' as in the CcO from *P. denitrificans*, *R. sphaeroides* and bovine heart mitochondria; the surrounding residues are also conserved [82,88,89]. Unfortunately, the low reported resolutions of the *ccb*₃-oxidase (PDB ID: 3MK7) [38] and *bo*₃ quinol oxidase (PDB ID: 1FFT) [67] at 3.2 and 3.5 Å, respectively, do not allow water pool comparisons with the other oxidases. By being connected to the bulk solvent in the periplasmic space, a fast equilibrium between the water pool and the bulk solvent could occur, thereby facilitating proton exit and rapid acceptance of both pumped protons and water molecules formed at the active site [90]. In the *E. coli* *bo*₃ quinol oxidase, the stabilization of the Δ-propionate of high-spin heme *o*₃ is a consequence of the electrostatic interactions by (i) the conserved Arg481^{E. coli} and Arg482^{E. coli} (equivalent to Arg438^B and Arg439^B), (ii) H bonding of Arg481^{E. coli} (Arg438^B) and Trp126^B, and (iii) a water molecule residing between the propionate and His291^B that coordinates as axial Cu_B ligand [90]. Proton pumping capability is removed by mutating both Arg residues, implicating the Δ-propionate in proton pumping. The three proposed pathways for proton acceptance by the Δ-propionate are (i) directly from Glu242^B [91], (ii) from the Glu242^B via the bound water molecules [92] and (iii) from the Glu242^B via the water molecules and the Cu_B ligand His291^B [93].

Similarly in the *P. denitrificans* *aa*₃-type CcO, water-filled cavities are present in both the D- and K-pathways. The non-conserved (compared to the D-pathway in bovine CcO [82]), nonpolar Ala and Gly residues line the D-pathway in *P. denitrificans*, and, as such, water molecules might behave as polar 'side chains' to facilitate the proton translocation [88]. In contrast, MDS results imply that the idea of water-assisted proton transfer might be misguided; it seems energetically expensive to use water molecules to transfer protons between acidic residues [94]. In our opinion, proteins, especially those as large as respiratory complexes, could have regions of energetically-unfavorable interactions but still maintain net favorable interactions when considered wholly.

3.6. O₂ reduction through O₂ input pathway

Hydrophobic cavities within protein structures can be identified using Xe and Kr, and have been employed for more than forty years [95,96]. As O₂ is more soluble in organic solvents [96], it enters and diffuses within the lipid bilayer [97,98]. The input pathway of O₂ into the dinuclear center is the Xe1 site. Although CO is transferred to the high-spin heme from the Cu_B [96], and by extension the physico-chemically-similar O₂, [99], two residues (Trp229 and His283) block direct access from the Xe1 site to the Cu_B [30]. Mostly hydrophobic residues line the O₂ access pathway that is favorable to O₂ but not to the produced water molecules. The authors suggested that water molecules are repelled by these residues and attracted by the hydrophilic 'vent' leading to the water pool [30]. In addition, the other structurally-determined CcO display features obstructing O₂ access – there is a constriction point in *R. sphaeroides* (pathway diameter is reduced to ~1.7 Å), with conservation of the same residues in *P. denitrificans* and bovine heart mitochondria (Fig. 6); it is very likely that they require structural rearrangements for O₂ access. As mentioned previously, the *ba*₃-oxidase is a high-affinity CcO and the lack of such constricting features along with a large cavity volume (390 Å³, compared to 140, 409 and 87 Å³ in the *P. denitrificans*, *R. sphaeroides* and bovine heart enzymes) and a

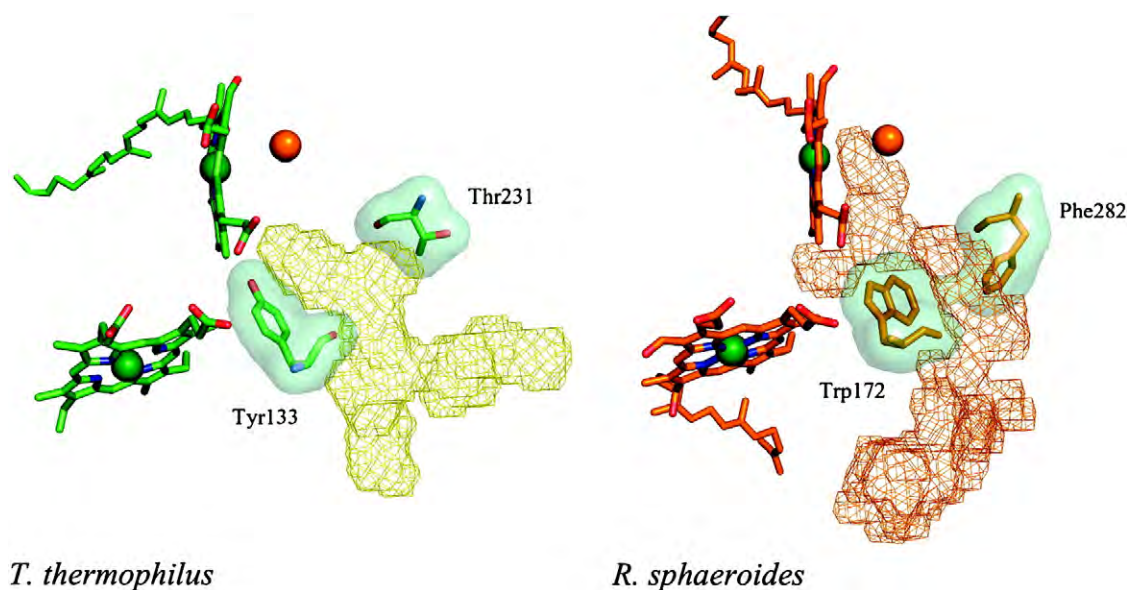


Fig. 6. Spatial accessibility of molecular oxygen to the active site of CcO of *Thermus thermophilus* and *Rhodobacter sphaeroides*. In the latter, a constriction point prevents direct access to the active site without structural rearrangement, a feature not present in the former. Reprinted with permission from [30]. Copyright 2008 American Chemical Society.

bifurcated oxygen entrance pathway [30] may partly explain its properties. Furthermore, the hydrophilic Glu278^P in *P. denitrificans* is substituted by the hydrophobic Ile235 in *T. thermophilus*; the residue replacement is also similar where the hydrophobic Val is present in the thermoacidophilic archaeon *Sulfolobus acidocaldarius* *caa*₃-quinol oxidase and the moderately-thermophilic haloalkaliphilic archaeon *N. pharaonis* *ba*₃-cytochrome oxidase [9,100].

3.7. Overall O₂ chemistry and reaction mechanism of *ba*₃-oxidase

Density functional theory (DFT) is a computational method that allows the modeling of the electronic structures, energetics and properties of atoms and molecules in a complex system. Initially used in solid state physics, it is now used in computational chemistry, and can be applied to biological systems (see Refs. [101–107] for the theory of DFT and its applications in biological contexts). Although experimental evidence for the exact *ba*₃-oxidase reaction mechanism is still scarce, a 14-step catalytic mechanism has been proposed using DFT in combination with experimental data [108]. It should be noted that the spectral properties of heme moieties do not allow for the investigation of Cu_B states. The *ba*₃-oxidase is known to pump H⁺ with an experimental stoichiometry of only 0.5 H⁺ per electron transferred, and the proposed mechanism does not conform to this stoichiometry. This inconsistency could be attributed to the enzyme preparations themselves that undergo a harsh purification process as well as the non-optimal experimental temperatures used. It is well-known that many thermophilic proteins display temperature-dependent activity.

3.8. Mechanistic analysis of *caa*₃-oxidase

Without the availability of its 3D structure, detailed mechanistic analysis of *caa*₃-oxidase is impossible. *In surfo* and *in meso* crystals have been generated [109]; the diffraction quality and radiation sensitivity problems were solved and the structure is forthcoming (J. A. Lyons, D. Aragão, T. Soulimane, M. Caffrey, PDB ID:2YEV). However, a few biophysical methods have been used to probe its active site and electrochemical properties. Resonance Raman spectroscopy indicates that this enzyme is fundamentally similar to the *aa*₃-oxidases of bovine heart and *P. denitrificans* [110]. As such, their mechanisms would also very likely be similar. Interestingly, the side chain of heme

a moieties in the bacterial *R. marinus* is HEGG and, therefore, of A₃ type [111]. The investigation into its proton pumping activity has shown that the *Thermus caa*₃-oxidase has a stoichiometry of 1 H⁺/e⁻ [112,113].

Homology modeling of *R. marinus caa*₃-oxidase suggests that the hydroxyl of the highly-conserved Tyr (YS motif) spatially replaces the carboxyl of Glu278^P residue and that the Ser could play a role in the proton transfer [114]; the Glu278^P-like residue is also missing in *T. thermophilus caa*₃-oxidase. In an elegant experiment, when the Glu-278^P in *P. denitrificans* was mutated to Ala, proton pumping and activity were both abolished as was the G275S mutation; none of the mutations resulted in a wild type-like activity although proton pumping was restored as long as the mutation in Glu-278^P was complemented by F274Y with or without G275S [115]. This shows that while the Glu can be replaced by a Tyr, the Ser is not required. The pK_a of Tyr side chain is ~10.5; at physiological pH (~7.2), the side chain would be mostly protonated and unable to further transfer protons. There are two possible explanations regarding the high pK_a of Tyr in solution and its protonation – (i) since pK_a values of residues are dependent on their exact environment, the Tyr pK_a within the protein could well differ from the in-solution value [116], or (ii) the Tyr is not functionally replacing Glu278 but might orient chains of water molecules [114]. Notwithstanding these observations regarding the *R. marinus caa*₃-oxidase, Fourier-transform infrared (FTIR) technique revealed the protonation of a Tyr upon reduction of the *Thermus* enzyme [117].

It should also be noted that though the bound cytochrome *c* is recognized as a substrate for the *Rhodothermus* enzyme, it displays a ten-fold higher activity with a *high*-potential iron-sulfur protein (HiPIP) as the electron donor [118]. As an implication, drawing any similarity of electron transfer mechanism between the two enzymes should be treated cautiously.

4. Overall functional and evolutionary significance

4.1. Possible additional functions

While the existence of multiple aerobic respiratory enzymes has been known for some time [119], there is no conclusive evidence to explain such redundancy; there is even no study suggesting an explanation for *T. thermophilus*. This is a critical issue since thermophiles

have comparatively much smaller genomes (<http://www.ncbi.nlm.nih.gov/genomes/lproks.cgi>). In the mesophilic *E. coli* (genome size of non-pathogenic strains of ~4.6 Mbp) and *Pseudomonas putida* (~6 Mbp), three (cytochrome *bd-I*, *bd-II* and *bo*; see [120] and references therein) and five terminal oxidases [121] have been identified, respectively. Hence, we speculate that the existence of two terminal oxidases in this extreme thermophile extends beyond their affinities toward oxygen. It is very likely that the O₂ affinity anticorrelates to the proton pumping stoichiometry for structural and/or functional reasons. As noted previously [21], a comparison of the exact physiological stoichiometries is hampered by the large deviance of the experimental procedures from the physiological conditions, such as the different lipidic environments, pH values and the ionic strengths. In addition, the additional functions of the terminal oxidases, including the scavenging of reactive oxygen species similar to *E. coli* [122], should be investigated.

4.2. Functional relationship with other CcO

For both the *ba*₃- and *caa*₃-oxidases, a significant divergence of their actual mechanisms is not expected since the heterodinuclear redox centers are Fe_{a3}-Cu_B, and are likely to be similar to what is already known. In fact, substitution of the high-spin heme at the heterodinuclear center generally inactivates the enzyme [36] but replacing the low-spin heme has no functional effect [123]; an exception does exist [124]. In contrast, the *cbb*₃-type oxidase has a heme *b*₃ as the heme at the O₂-reducing center; it is highly divergent from the other two types of CcO [18,125]. Of the four predicted *cbb*₃-oxidase subunits, only three could be purified as the canonical '*cbb*₃-oxidase' complex [125]. Nevertheless, only some of the residues that act as K-analogue pathway in the *ba*₃-oxidase are conserved in the *cbb*₃-oxidase [18], while the crystal structure shows a blocked D-pathway [38]. Other features indicative of its different evolutionary lineage from the other types of CcO include the absence of Cu_A (which is characteristic of quinol oxidases) and the presence of multiple heme moieties functioning as redox centers. Among the striking structural elements of the *cbb*₃-oxidase is a novel periplasmic cavity, very likely acting as a water exit pathway, and a membrane cavity connecting O₂ entry to the high-spin heme *b*₃. These, and the unique conformation of redox-linked moieties, exemplify nature's engineering to create a high O₂-affinity enzyme. The 'best' model organism to study all the three types in a thermophilic physiology would be *R. marinus* as it possesses the A2- [126], B- [127] and C-type enzymes [111], and is genetically tractable. As stated above, the substrate-enzyme (electron donor-CcO) interactions are hydrophobic at higher growth temperatures.

5. Conclusion

An important point that must be recognized is that the determination of a crystal structure of any protein is merely a starting point to rationalize pre-determination experimental data. While having a structure could answer many questions, it could give rise to equally more questions. It has been about ten years since the publication of the *ba*₃-oxidase structure by Soulimane *et al.* [9], yet our understanding of the enzyme is still incomplete. Reasonable progress in this area is illustrated by the wealth of available data, both experimental and computational. We now know that the *ba*₃-oxidase interacts hydrophobically with the cytochrome *c*₅₅₂ and the identities of the residues involved in the electron transfer from the substrate to the dinuclear center. Further adding to its 'aberrant' nature is the use of a single proton pathway for catalysis. For the *caa*₃-oxidase, very limited data are available. Under low oxygen tension, it is coexpressed with the *ba*₃-oxidase, therefore making available multiple pathways for electron transfer between the *bc* complex and the CcO.

Among the other questions are (i) whether the true *ba*₃-oxidase proton pumping efficiency reaches 1 H⁺/e⁻ with assays performed at the *T. thermophilus* optimal growth temperature of 70 °C instead of at 'mesophilic' temperatures and the delipidation following the extensive purification, (ii) possible dynamic regulation of both CcO expressions as an adaptation by the bacterium under differential O₂ tension and (iii) the structure-function relationship of the *caa*₃-oxidase.

The sequence and structure analyses of the *ba*₃- and *caa*₃-oxidases indicate various interesting aspects from the protein thermostability and thermophilic bioenergetics perspectives. It would be extremely difficult to define the precise borders between these two adaptations. Nonetheless, a summary is provided here based on the comparison with their mesophilic counterparts; (i) the *Thermus ba*₃-oxidase has a higher O₂ affinity provided by the larger O₂ cavity as an adaptation to the reduced O₂ solubility at high temperatures, (ii) the *ba*₃- and *caa*₃-oxidases have shortened loops as a thermostability adaptation although there is an extended fusion linker connecting the *caa*₃-oxidase subunits I/III, (iii) the substrate-enzyme interaction between the cytochrome *c*₅₅₂ and *ba*₃-oxidase is of hydrophobic nature. Beyond the investigation into the *T. thermophilus* oxidases, more detailed characterization studies involving other thermophilic oxidases should be undertaken to increase our understanding of thermophile-specific features and the actual diversity of this important family of enzymes. Obviously, these will eventually be directly linked to their physiology.

Note added in the proof

Recently, Han *et al.* (doi:10.1073/pnas.1018958108) demonstrated that the *caa*₃- and *ba*₃-oxidases have proton pumping stoichiometries of 1 and 0.5 H⁺/e⁻ at room temperature. Therefore, the stoichiometry is not temperature-dependent and the latter does indeed pump protons with a lower efficiency.

Acknowledgements

Research in the authors' laboratory is funded by the Government of Ireland through the Science Foundation Ireland (BICF685) to TS and the Irish Research Council for Science, Engineering and Technology (EMBARK Initiative) to MRMN.

References

- [1] A. Henne, H. Brüggemann, C. Raasch, A. Wiezer, T. Hartsch, H. Liesegang, A. Johann, T. Lienard, O. Gohl, R. Martinez-Arias, C. Jacobi, V. Starkuviene, S. Schlenczeck, S. Dencker, R. Huber, H.P. Klenk, W. Kramer, R. Merkl, G. Gottschalk, H.J. Fritz, The genome sequence of the extreme thermophile *Thermus thermophilus*, *Nat. Biotechnol.* 22 (2004) 547–553.
- [2] S. Ramírez-Arcos, L.A. Fernández-Herrero, J. Berenguer, A thermophilic nitrate reductase is responsible for the strain specific anaerobic growth of *Thermus thermophilus* HB8, *Biochim. Biophys. Acta Gene Struct. Expr.* 1396 (1998) 215–227.
- [3] H. Brüggemann, C. Chen, Comparative genomics of *Thermus thermophilus*: plasticity of the megaplasmid and its contribution to a thermophilic lifestyle, *J. Biotechnol.* 124 (2006) 654–661.
- [4] S. Ramírez-Arcos, L.A. Fernández-Herrero, I. Marin, J. Berenguer, Anaerobic growth, a property horizontally transferred by an Hfr-like mechanism among extreme thermophiles, *J. Bacteriol.* 180 (1998) 3137–3143.
- [5] R. Moreno, O. Zafra, F. Cava, J. Berenguer, Development of a gene expression vector for *Thermus thermophilus* based on the promoter of the respiratory nitrate reductase, *Plasmid* 49 (2003) 2–8.
- [6] E. Wilhelm, R. Battino, R.J. Wilcock, Low-pressure solubility of gases in liquid water, *Chem. Rev.* 77 (1977) 219–262.
- [7] A. Giuffrè, G. Stubauer, P. Sarti, M. Brunori, W.G. Zumft, G. Buse, T. Soulimane, The heme-copper oxidases of *Thermus thermophilus* catalyze the reduction of nitric oxide: evolutionary implications, *Proc. Natl. Acad. Sci. U. S. A.* 96 (1999) 14718–14723.
- [8] B.H. Zimmermann, C.I. Nitsche, J.A. Fee, F. Rusnak, E. Münck, Properties of a copper-containing cytochrome *ba*₃: a second terminal oxidase from the extreme thermophile *Thermus thermophilus*, *Proc. Natl. Acad. Sci. U. S. A.* 85 (1988) 5779–5783.

- [9] T. Soulimane, G. Buse, G.P. Bourenkov, H.D. Bartunik, R. Huber, M.E. Than, Structure and mechanism of the aberrant *ba*₃-cytochrome *c* oxidase from *Thermus thermophilus*, *EMBO J.* 19 (2000) 1766–1776.
- [10] J.A. Fee, M.G. Choc, K.L. Findling, R. Lorence, T. Yoshida, Properties of a copper-containing cytochrome *c*₁*aa*₃ complex: a terminal oxidase of the extreme thermophile *Thermus thermophilus* HB8, *Proc. Natl. Acad. Sci. U. S. A.* 77 (1980) 147–151.
- [11] K. Hon-nami, T. Oshima, Cytochrome oxidase from an extreme thermophile, HB 8, *Biochem. Biophys. Res. Commun.* 92 (1980) 1023–1029.
- [12] J.A. Fee, M.W. Mather, P. Springer, S. Hensel, G. Buse, Isolation and partial sequence of the A-protein gene of *Thermus thermophilus* cytochrome *c*₁*aa*₃, *Ann. N. Y. Acad. Sci.* 550 (1988) 33–38.
- [13] G. Buse, S. Hensel, J.A. Fee, Evidence for cytochrome oxidase subunit I and a cytochrome *c*-subunit II fused protein in the cytochrome “*c*₁*aa*₃” of *Thermus thermophilus*, *Eur. J. Biochem.* 181 (1989) 261–268.
- [14] M.W. Mather, P. Springer, J.A. Fee, Cytochrome oxidase genes from *Thermus thermophilus*. Nucleotide sequence and analysis of the deduced primary structure of subunit IIc of cytochrome *caa*₃, *J. Biol. Chem.* 266 (1991) 5025–5035.
- [15] M.W. Mather, P. Springer, S. Hensel, G. Buse, J.A. Fee, Cytochrome oxidase genes from *Thermus thermophilus*. Nucleotide sequence of the fused gene and analysis of the deduced primary structures for subunits I and III of cytochrome *caa*₃, *J. Biol. Chem.* 268 (1993) 5395–5408.
- [16] M.J. Miller, R.B. Gennis, The purification and characterization of the cytochrome *d* terminal oxidase complex of the *Escherichia coli* aerobic respiratory chain, *J. Biol. Chem.* 258 (1983) 9159–9165.
- [17] J.A. Garcia-Horsman, B. Barquera, J. Rumbley, J. Ma, R.B. Gennis, The superfamily of heme-copper respiratory oxidases, *J. Bacteriol.* 176 (1994) 5587–5600.
- [18] M.M. Pereira, M. Santana, M. Teixeira, A novel scenario for the evolution of haem-copper oxygen reductases, *Biochim. Biophys. Acta Bioenerg.* 1505 (2001) 185–208.
- [19] H. Michel, J. Behr, A. Harrenga, A. Kannt, Cytochrome *c* oxidase: structure and spectroscopy, *Annu. Rev. Biophys. Biomol. Struct.* 27 (1998) 329–356.
- [20] M.M. Pereira, M. Teixeira, Proton pathways, ligand binding and dynamics of the catalytic site in haem-copper oxygen reductases: a comparison between the three families, *Biochim. Biophys. Acta Bioenerg.* 1655 (2004) 340–346.
- [21] M.M. Pereira, F.L. Sousa, A.F. Verissimo, M. Teixeira, Looking for the minimum common denominator in haem-copper oxygen reductases: towards a unified catalytic mechanism, *Biochim. Biophys. Acta Bioenerg.* 1777 (2008) 929–934.
- [22] H.-Y. Chang, J. Hemp, Y. Chen, J.A. Fee, R.B. Gennis, The cytochrome *ba*₃ oxygen reductase from *Thermus thermophilus* uses a single input channel for proton delivery to the active site and for proton pumping, *Proc. Natl. Acad. Sci. U. S. A.* 106 (2009) 16169–16173.
- [23] F.L. Sousa, R.J. Alves, J.B. Pereira-Leal, M. Teixeira, M.M. Pereira, A bioinformatics classifier and database for heme-copper oxygen reductases, *PLoS One* 6 (2011) e19117.
- [24] J. Hemp, R.B. Gennis, Diversity of the heme-copper superfamily in Archaea: insights from genomics and structural modeling, in: G. Schäfer, H.S. Penefsky (Eds.), *Bioenergetics*, Springer Berlin Heidelberg, Berlin, Heidelberg, 2008, pp. 1–31.
- [25] C. Brochier-Armanet, E. Talla, S. Gribaldo, The multiple evolutionary histories of dioxygen reductases: implications for the origin and evolution of aerobic respiration, *Mol. Biol. Evol.* 26 (2009) 285–297.
- [26] M.J. Thompson, D. Eisenberg, Transproteomic evidence of a loop-deletion mechanism for enhancing protein thermostability, *J. Mol. Biol.* 290 (1999) 595–604.
- [27] A. Razvi, J.M. Scholtz, Lessons in stability from thermophilic proteins, *Protein Sci.* 15 (2006) 1569–1578.
- [28] Y. Chen, L. Hunsicker-Wang, R.L. Pacoma, E. Luna, J.A. Fee, A homologous expression system for obtaining engineered cytochrome *ba*₃ from *Thermus thermophilus* HB8, *Protein Expr. Purif.* 40 (2005) 299–318.
- [29] L.M. Hunsicker-Wang, R.L. Pacoma, Y. Chen, J.A. Fee, C.D. Stout, A novel cryoprotection scheme for enhancing the diffraction of crystals of recombinant cytochrome *ba*₃ oxidase from *Thermus thermophilus*, *Acta Crystallogr. D* 61 (2005) 340–343.
- [30] V.M. Luna, Y. Chen, J.A. Fee, C.D. Stout, Crystallographic studies of Xe and Kr binding within the large internal cavity of cytochrome *ba*₃ from *Thermus thermophilus*: structural analysis and role of oxygen transport channels in the heme-Cu oxidases, *Biochemistry* 47 (2008) 4657–4665.
- [31] T. Tiefenbrunn, W. Liu, Y. Chen, V. Katritch, C.D. Stout, J.A. Fee, V. Cherezov, High resolution structure of the *ba*₃ cytochrome *c* oxidase from *Thermus thermophilus* in a lipidic environment, *PLoS One* 6 (2011) e22348.
- [32] G. Schafer, M. Engelhard, V. Muller, Bioenergetics of the Archaea, *Microbiol. Mol. Biol. Rev.* 63 (1999) 570–620.
- [33] M. Lübben, K. Morand, Novel prenylated hemes as cofactors of cytochrome oxidases. Archaea have modified hemes A and O, *J. Biol. Chem.* 269 (1994) 21473–21479.
- [34] J. Sakamoto, Y. Handa, N. Sone, A novel cytochrome *b(o/aa)*₃-type oxidase from *Bacillus stearothermophilus* catalyzes cytochrome *c*-551 oxidation, *J. Biochem.* 122 (1997) 764–771.
- [35] J. Sakamoto, T. Shibata, T. Mine, R. Miyahara, T. Torigoe, S. Noguchi, K. Matsushita, N. Sone, Cytochrome *c* oxidase contains an extra charged amino acid cluster in a new type of respiratory chain in the amino-acid-producing Gram-positive bacterium *Corynebacterium glutamicum*, *Microbiology* 147 (2001) 2865–2871.
- [36] J. Hill, V.C. Goswitt, M. Calhoun, J.A. Garcia-Horsman, L. Lemieux, J.O. Alben, R.B. Gennis, Demonstration by FTIR that the *bo*-type ubiquinol oxidase of *Escherichia coli* contains a heme-copper binuclear center similar to that in cytochrome oxidase and that proper assembly of the binuclear center requires the *cyoE* gene product, *Biochemistry* 31 (1992) 11435–11440.
- [37] K. Saiki, T. Mogi, Y. Anraku, Heme O biosynthesis in *Escherichia coli*: the *cyoE* gene in the cytochrome BO operon encodes a protoheme IX farnesyltransferase, *Biochem. Biophys. Res. Commun.* 189 (1992) 1491–1497.
- [38] S. Buschmann, E. Warkentin, H. Xie, J.D. Langer, U. Ermiler, H. Michel, The structure of *cbb*₃ cytochrome oxidase provides insights into proton pumping, *Science* 329 (2010) 327–330.
- [39] S. Larsson, B. Källbring, P. Wittung, B.G. Malmström, The Cu_A center of cytochrome-*c* oxidase: electronic structure and spectra of models compared to the properties of Cu_A domains, *Proc. Natl. Acad. Sci. U. S. A.* 92 (1995) 7167–7171.
- [40] O. Farver, Y. Lu, M.C. Ang, I. Pecht, Enhanced rate of intramolecular electron transfer in an engineered purple Cu_A azurin, *Proc. Natl. Acad. Sci. U. S. A.* 96 (1999) 899–902.
- [41] S. DeBeer George, M. Metz, R.K. Szilagy, H. Wang, S.P. Cramer, Y. Lu, W.B. Tolman, B. Hedman, K.O. Hodgson, E.I. Solomon, A quantitative description of the ground-state wave function of Cu_A by X-ray absorption spectroscopy: comparison to plastocyanin and relevance to electron transfer, *J. Am. Chem. Soc.* 123 (2001) 5757–5767.
- [42] M.H.M. Olsson, U. Ryde, Geometry, reduction potential, and reorganization energy of the binuclear Cu_A site, studied by density functional theory, *J. Am. Chem. Soc.* 123 (2001) 7866–7876.
- [43] M.G. Savelieff, Y. Lu, Cu_A centers and their biosynthetic models in azurin, *J. Biol. Inorg. Chem.* 15 (2010) 461–483.
- [44] Y. Zhen, C.W. Hoganson, G.T. Babcock, S. Ferguson-Miller, Definition of the interaction domain for cytochrome *c* on cytochrome *c* oxidase, *J. Biol. Chem.* 274 (1999) 38032–38041.
- [45] O. Maneg, F. Malatesta, B. Ludwig, V. Drosou, Interaction of cytochrome *c* with cytochrome oxidase: two different docking scenarios, *Biochim. Biophys. Acta Bioenerg.* 1655 (2004) 274–281.
- [46] V. Drosou, F. Malatesta, B. Ludwig, Mutations in the docking site for cytochrome on the *Paracoccus* heme *aa*₃ oxidase, *Eur. J. Biochem.* 269 (2002) 2980–2988.
- [47] J. Qian, D.A. Mills, L. Geren, K. Wang, C.W. Hoganson, B. Schmidt, C. Hiser, G.T. Babcock, B. Durham, F. Millet, S. Ferguson-Miller, Role of the conserved arginine pair in proton and electron transfer in cytochrome *c* oxidase, *Biochemistry* 43 (2004) 5748–5756.
- [48] L. Muresanu, P. Pristovsek, F. Löhr, O. Maneg, M.D. Mukrasch, H. Rüterjans, B. Ludwig, C. Lücke, The electron transfer complex between cytochrome *c*₅₅₂ and the Cu_A domain of the *Thermus thermophilus* *ba*₃ oxidase, *J. Biol. Chem.* 281 (2006) 14503–14513.
- [49] O. Maneg, B. Ludwig, F. Malatesta, Different interaction modes of two cytochrome-*c* oxidase soluble Cu_A fragments with their substrates, *J. Biol. Chem.* 278 (2003) 46734–46740.
- [50] P. Nicholls, C. Obinger, H. Niederhauser, G. Peschek, Cytochrome oxidase in *Anacystis nidulans*: stoichiometries and possible functions in the cytoplasmic and thylakoid membranes, *Biochim. Biophys. Acta Bioenerg.* 1098 (1992) 184–190.
- [51] M. Bernroither, M. Zamocky, M. Pairer, P.G. Furtmüller, G.A. Peschek, C. Obinger, Heme-copper oxidases and their electron donors in cyanobacterial respiratory electron transport, *Chem. Biodivers.* 5 (2008) 1927–1961.
- [52] J.A. Keightley, B.H. Zimmermann, M.W. Mather, P. Springer, A. Pastuszyn, D.M. Lawrence, J.A. Fee, Molecular genetic and protein chemical characterization of the cytochrome *ba* from *Thermus thermophilus* HB8, *J. Biol. Chem.* 270 (1995) 20345–20358.
- [53] T. Soulimane, G. Buse, M. Dewor, M.E. Than, R. Huber, Primary structure of a novel subunit in *ba*₃-cytochrome oxidase from *Thermus thermophilus*, *Protein Sci.* 9 (2000) 2068–2073.
- [54] M.E. Than, T. Soulimane, *ba*₃-Cytochrome *c* oxidase from *Thermus thermophilus*, in: A. Messerschmidt, R. Huber, T. Poulas, K. Wieghardt (Eds.), *Handbook of Metalloproteins*, John Wiley & Sons, Ltd., Chichester, 2006.
- [55] H. Jin, Q. Zhao, E.I. Gonzalez de Valdivia, D.H. Ardell, M. Stenstrom, L.A. Isaksson, Influences on gene expression *in vivo* by a Shine–Dalgarno sequence, *Mol. Microbiol.* 60 (2006) 480–492.
- [56] N. Jacques, M. Dreyfus, Translation initiation in *Escherichia coli*: old and new questions, *Mol. Microbiol.* 4 (1990) 1063–1067.
- [57] J. Ma, A. Campbell, S. Karlin, Correlations between Shine–Dalgarno sequences and gene features such as predicted expression levels and operon structures, *J. Bacteriol.* 184 (2002) 5733–5745.
- [58] K. Honnami, T. Oshima, Purification and characterization of cytochrome *c* oxidase from *Thermus thermophilus* HB8, *Biochemistry* 23 (1984) 454–460.
- [59] T. Soulimane, M. von Walter, P. Hof, M.E. Than, R. Huber, G. Buse, Cytochrome-*c*₅₅₂ from *Thermus thermophilus*: a functional and crystallographic investigation, *Biochem. Biophys. Res. Commun.* 237 (1997) 572–576.
- [60] J. Janzon, B. Ludwig, F. Malatesta, Electron transfer kinetics of soluble fragments indicate a direct interaction between complex III and the *caa*₃ oxidase in *Thermus thermophilus*, *IUBMB Life* 59 (2007) 563–569.
- [61] M. Santana, M.M. Pereira, N.P. Elias, C.M. Soares, M. Teixeira, Gene cluster of *Rhodothermus marinus* high-potential iron–sulfur protein: oxygen oxidoreductase, a *caa*₃-type oxidase belonging to the superfamily of heme-copper oxidases, *J. Bacteriol.* 183 (2001) 687–699.
- [62] H. Witt, B. Ludwig, Isolation, analysis, and deletion of the gene coding for subunit IV of cytochrome *c* oxidase in *Paracoccus denitrificans*, *J. Biol. Chem.* 272 (1997) 5514–5517.
- [63] Y. Zhen, J. Qian, K. Follmann, T. Hayward, T. Nilsson, M. Dahn, Y. Hilmi, A.G. Hamerl, J.P. Hosler, S. Ferguson-Miller, Overexpression and purification of

- cytochrome *c* oxidase from *Rhodobacter sphaeroides*, Protein Expr. Purif. 13 (1998) 326–336.
- [64] G. Villani, M. Tattoli, N. Capitanio, P. Glaser, S. Papa, A. Danchin, Functional analysis of subunits III and IV of *Bacillus subtilis* *aa*₃-600 quinol oxidase by *in vitro* mutagenesis and gene replacement, Biochim Biophys Acta Bioenerg. 1232 (1995) 67–74.
- [65] K. Saiki, H. Nakamura, T. Mogi, Y. Anraku, Probing a role of subunit IV of the *Escherichia coli* *bo*-type ubiquinol oxidase by deletion and cross-linking analyses, J. Biol. Chem. 271 (1996) 15336–15340.
- [66] H. Nakamura, K. Saiki, T. Mogi, Y. Anraku, Assignment and functional roles of the *cyoABCDE* gene products required for the *Escherichia coli* *bo*-type quinol oxidase, J. Biochem. 122 (1997) 415–421.
- [67] J. Abramson, S. Riistama, G. Larsson, A. Jasaitis, M. Svensson-Ek, L. Laakkonen, A. Puustinen, S. Iwata, M. Wikström, The structure of the ubiquinol oxidase from *Escherichia coli* and its ubiquinone binding site, Nat. Struct. Mol. Biol. 7 (2000) 910–917.
- [68] C. Winterstein, B. Ludwig, Genes coding for respiratory complexes map on all three chromosomes of the *Paracoccus denitrificans* genome, Arch. Microbiol. 169 (1998) 275–281.
- [69] M.W. Gray, G. Burger, B.F. Lang, The origin and early evolution of mitochondria, Genome Biol. 2 (2001) (reviews1018.1–reviews1018.5).
- [70] Y. Planques, N. Capitanio, G. Capitanio, E. De Nitto, G. Villani, S. Papa, Role of supernumerary subunits in mitochondrial cytochrome *c* oxidase, FEBS Lett. 258 (1989) 285–288.
- [71] J. Das, S.T. Miller, D.L. Stern, Comparison of diverse protein sequences of the nuclear-encoded subunits of cytochrome *c* oxidase suggests conservation of structure underlies evolving functional sites, Mol. Biol. Evol. 21 (2004) 1572–1582.
- [72] T. Mogi, K. Saiki, Y. Anraku, Biosynthesis and functional role of haem O and haem A, Mol. Microbiol. 14 (1994) 391–398.
- [73] T. Mogi, Over-expression and characterization of *Bacillus subtilis* heme O synthase, J. Biochem. 145 (2009) 669–675.
- [74] M.L. Baer, J. Ravel, S.A. Pineiro, D. Guether-Borg, H.N. Williams, Reclassification of salt-water *Bdellovibrio* sp. as *Bacteriovorax marinus* sp. nov. and *Bacteriovorax litoralis* sp. nov. Int. J. Syst. Evol. Microbiol. 54 (2004) 1011–1016.
- [75] R. Ishikawa, Y. Ishido, A. Tachikawa, H. Kawasaki, H. Matsuzawa, T. Wakagi, *Aeropyrum pernix* K1, a strictly aerobic and hyperthermophilic archaeon, has two terminal oxidases, cytochrome *ba*₃ and cytochrome *aa*₃, Arch. Microbiol. 179 (2002) 42–49.
- [76] C. Werner, O.-M.H. Richter, B. Ludwig, A novel heme *a* insertion factor gene cotranscribes with the *Thermus thermophilus* cytochrome *ba*₃ oxidase locus, J. Bacteriol. 192 (2010) 4712–4719.
- [77] A. Hannappel, F.A. Bundschuh, P. Greiner, M. Alles, C. Werner, O.M. Richter, B. Ludwig, Bacterial model systems for cytochrome *c* oxidase biogenesis, Indian J. Chem. A 50A (2011) 374–382.
- [78] Y. Sako, N. Nomura, A. Uchida, Y. Ishida, H. Morii, Y. Koga, T. Hoaki, T. Maruyama, *Aeropyrum pernix* gen. nov., sp. nov., a novel aerobic hyperthermophilic archaeon growing at temperatures up to 100 °C, Int. J. Syst. Bacteriol. 46 (1996) 1070–1077.
- [79] C.C. Page, C.C. Moser, P.L. Dutton, Mechanism for electron transfer within and between proteins, Curr. Opin. Chem. Biol. 7 (2003) 551–556.
- [80] M.H.V. Huynh, T.J. Meyer, Proton-coupled electron transfer, Chem. Rev. 107 (2007) 5004–5064.
- [81] V.R.I. Kaila, M.I. Verkhovskiy, G. Hummer, M. Wikström, Glutamic acid 242 is a valve in the proton pump of cytochrome *c* oxidase, Proc. Natl. Acad. Sci. U. S. A. 105 (2008) 6255–6259.
- [82] T. Tsukihara, H. Aoyama, E. Yamashita, T. Tomizaki, H. Yamaguchi, K. Shinzawa-Itoh, R. Nakashima, R. Yaono, S. Yoshikawa, The whole structure of the 13-subunit oxidized cytochrome *c* oxidase at 2.8 Å, Science 272 (1996) 1136–1144.
- [83] U. Pfützner, A. Odenwald, T. Ostermann, L. Weingard, B. Ludwig, O.-M.H. Richter, Cytochrome *c* oxidase (heme *aa*₃) from *Paracoccus denitrificans*: analysis of mutations in putative proton channels of subunit I, J. Bioenerg. Biomembr. 30 (1998) 89–97.
- [84] J. Salje, B. Ludwig, O.-M.H. Richter, Is a third proton-conducting pathway operative in bacterial cytochrome *c* oxidase? Biochem. Soc. Trans. 33 (2005) 829–831.
- [85] H.-mo Lee, T.K. Das, D.L. Rousseau, D. Mills, S. Ferguson-Miller, R.B. Gennis, Mutations in the putative H-channel in the cytochrome *c* oxidase from *Rhodobacter sphaeroides* show that this channel is not important for proton conduction but reveal modulation of the properties of heme *a*, Biochemistry 39 (2000) 2989–2996.
- [86] K. Shimokata, Y. Katayama, H. Murayama, M. Suematsu, T. Tsukihara, K. Muramoto, H. Aoyama, S. Yoshikawa, H. Shimada, The proton pumping pathway of bovine heart cytochrome *c* oxidase, Proc. Natl. Acad. Sci. U. S. A. 104 (2007) 4200–4205.
- [87] A. Kannt, T. Soulimane, G. Buse, A. Becker, E. Bamberg, H. Michel, Electrical current generation and proton pumping catalyzed by the *ba*₃-type cytochrome *c* oxidase from *Thermus thermophilus*, FEBS Lett. 434 (1998) 17–22.
- [88] C. Ostermeier, A. Harrenga, U. Emler, H. Michel, Structure at 2.7 Å resolution of the *Paracoccus denitrificans* two-subunit cytochrome *c* oxidase complexed with an antibody FV fragment, Proc. Natl. Acad. Sci. U. S. A. 94 (1997) 10547–10553.
- [89] M. Svensson-Ek, J. Abramson, G. Larsson, S. Törnroth, P. Brzezinski, S. Iwata, The X-ray crystal structures of wild-type and EQ(I-286) mutant cytochrome *c* oxidases from *Rhodobacter sphaeroides*, J. Mol. Biol. 321 (2002) 329–339.
- [90] A. Puustinen, M. Wikström, Proton exit from the heme-copper oxidase of *Escherichia coli*, Proc. Natl. Acad. Sci. U. S. A. 96 (1999) 35–37.
- [91] S. Iwata, C. Ostermeier, B. Ludwig, H. Michel, Structure at 2.8 Å resolution of cytochrome *c* oxidase from *Paracoccus denitrificans*, Nature 376 (1995) 660–669.
- [92] I. Hofacker, K. Schulten, Oxygen and proton pathways in cytochrome *c* oxidase, Proteins 30 (1998) 100–107.
- [93] J.E. Morgan, M.I. Verkhovskiy, M. Wikström, The histidine cycle: a new model for proton translocation in the respiratory heme-copper oxidases, J. Bioenerg. Biomembr. 26 (1994) 599–608.
- [94] A.V. Pislakov, P.K. Sharma, Z.T. Chu, M. Haranczyk, A. Warshel, Electrostatic basis for the unidirectionality of the primary proton transfer in cytochrome *c* oxidase, Proc. Natl. Acad. Sci. U. S. A. 105 (2008) 7726–7731.
- [95] B.P. Schoenborn, Binding of xenon to horse haemoglobin, Nature 208 (1965) 706–762.
- [96] T. Prangé, M. Schiltz, L. Pernot, N. Colloc'h, S. Longhi, W. Bourguet, R. Fourme, Exploring hydrophobic sites in proteins with xenon or krypton, Proteins 30 (1998) 61–73.
- [97] S. Fischkoff, J. Vanderkooi, Oxygen diffusion in biological and artificial membranes determined by the fluorochrome pyrene, J. Gen. Physiol. 65 (1975) 663–676.
- [98] D.F. Wilson, W.L. Rumsey, T.J. Green, J.M. Vanderkooi, The oxygen dependence of mitochondrial oxidative phosphorylation measured by a new optical method for measuring oxygen concentration, J. Biol. Chem. 263 (1988) 2712–2718.
- [99] D.D. Lemon, M.W. Calhoun, R.B. Gennis, W.H. Woodruff, The gateway to the active site of heme-copper oxidases, Biochemistry 32 (1993) 11953–11956.
- [100] J.L. Robinson, B. Pyzyra, R.G. Atrasz, C.A. Henderson, K.L. Morrill, A.M. Burd, E. DeSoucy, R.E. Fogleman, J.B. Naylor, S.M. Steele, D.R. Elliott, K.J. Leyva, R.F. Shand, Growth kinetics of extremely halophilic Archaea (Family Halobacteriaceae) as revealed by Arrhenius plots, J. Bacteriol. 187 (2005) 923–929.
- [101] W. Kohn, A.D. Becke, R.G. Parr, Density functional theory of electronic structure, J. Phys. Chem. 100 (1996) 12974–12980.
- [102] M.D. Segall, Applications of *ab initio* atomistic simulations to biology, J. Phys. Condens. Matter. 14 (2002) 2957–2973.
- [103] L.J.D. Frink, A.G. Salinger, M.P. Sears, J.D. Weinhold, A.L. Frischknecht, Numerical challenges in the application of density functional theory to biology and nanotechnology, J. Phys. Condens. Matter. 14 (2002) 12167–12187.
- [104] P. Geerlings, F. De Proft, W. Langenaeker, Conceptual density functional theory, Chem. Rev. 103 (2003) 1793–1874.
- [105] A. Fernández-Ramos, J.A. Miller, S.J. Klippenstein, D.G. Truhlar, Modeling the kinetics of bimolecular reactions, Chem. Rev. 106 (2006) 4518–4584.
- [106] Y. Zhao, D.G. Truhlar, Density functionals with broad applicability in chemistry, Acc. Chem. Res. 41 (2008) 157–167.
- [107] A.J. Cohen, P. Mori-Sanchez, W. Yang, Insights into current limitations of density functional theory, Science 321 (2008) 792–794.
- [108] J.A. Fee, D.A. Case, L. Noodleman, Toward a chemical mechanism of proton pumping by the B-type cytochrome *c* oxidases: application of density functional theory to cytochrome *ba*₃ of *Thermus thermophilus*, J. Am. Chem. Soc. 130 (2008) 15002–15021.
- [109] O. Slattery, M. Caffrey, T. Soulimane, S11.36 Crystallisation and preliminary X-ray diffraction analysis of *caa*₃-cytochrome *c* oxidase from *Thermus thermophilus*, Biochim. Biophys. Acta Bioenerg. 1777 (2008) S74.
- [110] S. Gerscher, P. Hildebrandt, T. Soulimane, G. Buse, Resonance Raman spectroscopic study of the *caa*₃ oxidase from *Thermus thermophilus*, Biospectroscopy 4 (1998) 365–377.
- [111] M.M. Pereira, J.N. Carita, R. Anglin, M. Saraste, M. Teixeira, Heme centers of *Rhodothermus marinus* respiratory chain. Characterization of its *ccb*₃ oxidase, J. Bioenerg. Biomembr. 32 (2000) 143–152.
- [112] J.A. Fee, T. Yoshida, K.K. Surerus, M.W. Mather, Cytochrome *caa*₃ from the thermophilic bacterium *Thermus thermophilus*: a member of the heme-copper oxidase superfamily, J. Bioenerg. Biomembr. 25 (1993) 103–114.
- [113] T. Yoshida, J.A. Fee, Studies on cytochrome *c* oxidase activity of the cytochrome *c*₁*aa*₃ complex from *Thermus thermophilus*, J. Biol. Chem. 259 (1984) 1031–1036.
- [114] C.M. Soares, A.M. Baptista, M.M. Pereira, M. Teixeira, Investigation of protonatable residues in *Rhodothermus marinus* *caa*₃ haem-copper oxygen reductase: comparison with *Paracoccus denitrificans* *aa*₃ haem-copper oxygen reductase, J. Biol. Inorg. Chem. 9 (2004) 124–134.
- [115] C. Backgren, G. Hummer, M. Wikström, A. Puustinen, Proton translocation by cytochrome *c* oxidase can take place without the conserved glutamic acid in subunit I, Biochemistry 39 (2000) 7863–7867.
- [116] M.M. Pereira, M. Santana, C.M. Soares, J. Mendes, J.N. Carita, A.S. Fernandes, M. Saraste, M.A. Carrondo, M. Teixeira, The *caa*₃ terminal oxidase of the thermohalophilic bacterium *Rhodothermus marinus*: a HiPIP: oxygen oxidoreductase lacking the key glutamate of the D-channel, Biochim. Biophys. Acta Bioenerg. 1413 (1999) 1–13.
- [117] P. Hellwig, T. Soulimane, W. Mantele, Electrochemical, FT-IR and UV/VIS spectroscopic properties of the *caa*₃ oxidase from *T. thermophilus*, Eur. J. Biochem. 269 (2002) 4830–4838.
- [118] M.M. Pereira, J.N. Carita, M. Teixeira, Membrane-bound electron transfer chain of the thermohalophilic bacterium *Rhodothermus marinus*: characterization of the iron-sulfur centers from the dehydrogenases and investigation of the high-potential iron-sulfur protein function by *in vitro* reconstitution of the respiratory chain, Biochemistry 38 (1999) 1276–1283.
- [119] R.K. Poole, G.M. Cook, Redundancy of aerobic respiratory chains in bacteria? Routes, reasons and regulation, Adv. Microb. Physiol. 43 (2000) 165–224.
- [120] M. Bekker, S. de Vries, A. Ter Beek, K.J. Hellingwerf, M.J.T. de Mattos, Respiration of *Escherichia coli* can be fully uncoupled via the nonelectrogenic terminal cytochrome *bd-II* oxidase, J. Bacteriol. 191 (2009) 5510–5517.

- [121] A. Ugidos, G. Morales, E. Rial, H.D. Williams, F. Rojo, The coordinate regulation of multiple terminal oxidases by the *Pseudomonas putida* ANR global regulator, *Environ. Microbiol.* 10 (2008) 1690–1702.
- [122] A. Lindqvist, J. Membrillo-Hernández, R.K. Poole, G.M. Cook, Roles of respiratory oxidases in protecting *Escherichia coli* K12 from oxidative stress, *Antonie Van Leeuwenhoek* 78 (2000) 23–31.
- [123] A. Puustinen, J.E. Morgan, M. Verkhovskii, J.W. Thomas, R.B. Gennis, M. Wikstrom, The low-spin heme site of cytochrome *o* from *Escherichia coli* is promiscuous with respect to heme type, *Biochemistry* 31 (1992) 10363–10369.
- [124] M. Contreras-Zentella, G. Mendoza, J. Membrillo-Hernández, J.E. Escamilla, A novel double heme substitution produces a functional bo_3 variant of the quinol oxidase aa_3 of *Bacillus cereus*, *J. Biol. Chem.* 278 (2003) 31473–31478.
- [125] R.S. Pitcher, N.J. Watmough, The bacterial cytochrome cbb_3 oxidases, *Biochim. Biophys. Acta Bioenerg.* 1655 (2004) 388–399.
- [126] M.M. Pereira, F.L. Sousa, M. Teixeira, R.M. Nyquist, J. Heberle, A tyrosine residue deprotonates during oxygen reduction by the caa_3 reductase from *Rhodothermus marinus*, *FEBS Lett.* 580 (2006) 1350–1354.
- [127] A.F. Veríssimo, M.M. Pereira, A.M.P. Melo, G.O. Hreggvidsson, J.K. Kristjansson, M. Teixeira, A ba_3 oxygen reductase from the thermohalophilic bacterium *Rhodothermus marinus*, *FEMS Microbiol. Lett.* 269 (2007) 41–47.
- [128] C.S. Bond, TopDraw: a sketchpad for protein structure topology cartoons, *Bioinformatics* 19 (2003) 311–312.
- [129] G. Deckert, P.V. Warren, T. Gaasterland, W.G. Young, A.L. Lenox, D.E. Graham, R. Overbeek, M.A. Snead, M. Keller, M. Aujay, R. Huber, R.A. Feldman, J.M. Short, G.J. Olsen, R.V. Swanson, The complete genome of the hyperthermophilic bacterium *Aquifex aeolicus*, *Nature* 392 (1998) 353–358.
- [130] L. Potterton, S. McNicholas, E. Krissinel, J. Gruber, K. Cowtan, P. Emsley, G.N. Murshudov, S. Cohen, A. Perrakis, M. Noble, Developments in the CCP4 molecular-graphics project, *Acta Crystallogr. D* 60 (2004) 2288–2294.
- [131] M.A. Larkin, G. Blackshields, N.P. Brown, R. Chenna, P.A. McGettigan, H. McWilliam, F. Valentin, I.M. Wallace, A. Wilm, R. Lopez, J.D. Thompson, T.J. Gibson, D.G. Higgins, Clustal W and Clustal X version 2.0, *Bioinformatics* 23 (2007) 2947–2948.

1 **CYTOCHROME C₅₅₂ MEDIATES ELECTRON TRANSFER BETWEEN**
2 **COMPLEXES III AND IV OF *THERMUS THERMOPHILUS***

3
4 Tewfik Soulimane^{a,*}, Mohamed Radzi Noor^a, Marzia Arese^b, Elena Forte^b, Marguerita
5 McCarthy^a, Paolo Sarti^{b,c} and Alessandro Giuffrè^c

6
7 ^a Department of Chemical and Environmental Sciences & Materials and Surface
8 Science Institute (MSSI), University of Limerick, Limerick, Ireland

9 ^b Department of Biochemical Sciences and Istituto Pasteur–Fondazione Cenci
10 Bolognetti, Sapienza University of Rome, Italy.

11 ^c CNR Institute of Molecular Biology and Pathology, Rome, Italy.

12
13 * Corresponding author

14 Tewfik Soulimane

15 L2-009 Lonsdale Building

16 Department of Chemical and Environmental Sciences

17 University of Limerick

18 Limerick, Ireland

19 Phone: +353 61 234133

20 Fax: +353 61 202568

21 Email: tewfik.soulimane@ul.ie

22
23 Running title: Electron transfer between Complexes III and IV

24

25

ABSTRACT

26

27

28

29

30

31

32

33

34

35

36

37

38

39

40

41

42

43

44

45

Under reduced oxygen tension, the extremely-thermophilic eubacterium *Thermus thermophilus* expresses, along with the *bc* complex (Complex III) and cytochrome *c*₅₅₂, two cytochrome *c* oxidases, *ba*₃- and *caa*₃-oxidase, the latter having a covalently-bound cytochrome *c*. Direct electron transfer between *bc* complex and *caa*₃-oxidase was postulated in a previous study involving only the water soluble domains of each protein. At variance, it is shown here that the electron transfer between *bc* complex and the whole *caa*₃- (or *ba*₃-) oxidase is slow, unless mediated by cytochrome *c*₅₅₂. Computational analyses indicate differential docking modes of cytochrome *c*₅₅₂ to both oxidases and their dynamics to accommodate protein-protein interaction.

Keywords: *Thermus thermophilus*; respiratory complex; terminal oxidase; *caa*₃-oxidase; *ba*₃-oxidase

Abbreviations: ANM, anisotropic network model; CcO, cytochrome *c* oxidase; *c*₅₅₂, *T. thermophilus* cytochrome *c*₅₅₂; *c*_{bc}, C-terminal soluble domain of the cytochrome *c*_{549/554} subunit of *T. thermophilus* *bc* complex; *c*_{caa3}, cytochrome *c* domain of *caa*₃-oxidase; LCP, lipidic cubic phase; VD, vapor diffusion.

Highlights

- Electron transfer between Complexes III and IV of *T. thermophilus* is described.
- Cytochrome c_{552} is a prerequisite for efficient transfer between the complexes.
- Interaction between Complex III and c_{552} is dependent on the ionic strength.
- Molecular modeling suggests cytochrome *c* of *caa*₃-oxidase holds the c_{552} .

1. INTRODUCTION

1
2 In *T. thermophilus* HB8, the respiratory chain consists of the four canonical protein
3 complexes (Complexes I-IV) for aerobic respiration and two additional membrane-
4 bound complexes for nitrate respiration (see [1] and references therein). The quinol
5 generated by Complex I (NADH:quinone oxidoreductase) and Complex II
6 (succinate:quinone oxidoreductase) [2] is reoxidized by the four-subunit Complex III
7 (quinol:cytochrome *c* oxidoreductase; *bc* complex) [3]. The exact electron transfer
8 pathway from Complex III to Complex IV (cytochrome *c* oxidase, CcO) [4] highly
9 depends on the available oxygen tension and, therefore, has been a subject of
10 intense discussion. Depending on O₂ availability, *T. thermophilus* indeed expresses
11 along with a soluble cytochrome *c*₅₅₂ (*c*₅₅₂) two CcO, termed *ba*₃- and *caa*₃-
12 oxidases, the latter possessing a covalently-bound cytochrome *c*. The crystal
13 structures of both CcO have been determined, greatly facilitating our understanding
14 of their mechanism of action [5],[6].

15 Under non-limiting oxygen tension, the *caa*₃-oxidase is the only CcO being
16 expressed [7],[8] along with the electron carrier *c*₅₅₂. In the context relevant to the
17 present study, electrons from the *bc* complex have been postulated by Janzon *et al.*
18 [9] to be directly transferred to the cytochrome *c* domain of *caa*₃-oxidase (*c*_{*caa*3}). In
19 contrast, under reduced oxygen tension the high-oxygen affinity *ba*₃-oxidase is
20 expressed together with the *caa*₃-oxidase [10],[11], resulting in a branched electron
21 transfer pathway between the *bc* complex and the two CcO. The *ba*₃-oxidase itself
22 can indeed only receive electrons through *c*₅₅₂ [12]. As long as the *caa*₃-oxidase is
23 capable of binding oxygen at low tension, following the proposal in [9], electrons
24 should be preferentially transferred from *bc* complex directly to *c*_{*caa*3} rather than to
25 *ba*₃-oxidase via *c*₅₅₂. A fraction of electrons is anyway expected to be transferred to

26 c_{552} , that incidentally was previously shown to react with c_{caa3} much more quickly
27 than to ba_3 -oxidase ($k \sim 10^{10} \text{ M}^{-1} \text{ s}^{-1}$ vs. $10^6 \text{ M}^{-1} \text{ s}^{-1}$) [9]. Therefore, depending on O_2
28 availability and in turn on the expression levels of the two CcO (and c_{552}), the fate of
29 electrons leaving the bc complex may vary and this should have an impact on
30 energy transduction, as the proton pumping efficiency of caa_3 -oxidase is $1 \text{ H}^+/\text{e}^-$
31 [13],[14], while that of ba_3 -oxidase is $0.5 \text{ H}^+/\text{e}^-$ [15].

32 In contrast to Janzon *et al.* [9], we show here that electrons are transferred from
33 the C-terminal soluble domain of the cytochrome $c_{549/554}$ subunit of bc complex (c_{bc})
34 to either of the two CcO through c_{552} , thus precluding any direct transfer between the
35 Complexes III and IV. The key difference between this study and the previous one
36 [9] is the use of the whole CcO complexes here, compared to only soluble domain
37 fragments in the latter. Furthermore, we report computational analyses revealing the
38 binding mode of c_{552} to both CcO as well as their overall conformational dynamics.
39 These results, while contributing to a better definition of the electron transfer
40 pathway along the respiratory chain of *T. thermophilus*, raise questions on our
41 current understanding of the bioenergetics of this thermophile.

42

43

44

2. MATERIALS AND METHODS

45

46 The proteins c_{552} [12], caa_3 - [6] and ba_3 -oxidases [16], and c_{bc} [17] were purified
47 according to the previously published methods. Electron transfer reactions were
48 investigated by time-resolved absorption spectroscopy, using a thermostated
49 stopped-flow instrument (DX.17MV; Applied Photophysics, Leatherhead, United
50 Kingdom) equipped with a 1 cm pathlength observation chamber. Measurements
51 were carried out in 5 mM bis-Tris pH 7.0, supplemented with 0.1 % *n*-dodecyl- β -D-
52 maltopyranoside in experiments with ba_3 - or caa_3 -oxidase.

53 Reaction of c_{bc} with either of the two oxidases was investigated at 25 °C. Briefly,
54 c_{bc} was degassed and reduced with 300 μ M ascorbate prior to mixing with ba_3 - or
55 caa_3 -oxidase in air-equilibrated buffer, in the absence or presence of c_{552} at
56 increasing concentrations. Oxidation of c_{bc} was followed at 418 nm. Reaction of
57 ascorbate-reduced c_{bc} with oxidized c_{552} was investigated anaerobically by multi-
58 wavelength spectrophotometry at 5 °C. Ionic strength was adjusted by the addition of
59 KCl.

60 In these experiments, the stopped-flow instrument was used as interfaced with a
61 diode-array that allows absorption spectra collection as a function of time, with an
62 acquisition time of 1 ms/spectrum. Noise filtering and global analysis of the acquired
63 time-resolved spectral changes was performed by singular value decomposition
64 (SVD) [18] using the MATLAB software (Mathworks, South Natick, MA). As the
65 reaction was assayed under non-pseudo-first order conditions, *i.e.*, at comparable
66 concentrations of the two proteins, observed rate constants (k_{obs}) were obtained by
67 fitting the experimental time courses to the equations described in [19]. In agreement

68 with Mooser *et al.* [3], the number of charges involved in the reaction was estimated
69 from the ionic strength dependence of the observed rate constant, by using the
70 Brønstedt equation [20].

71 Docking simulations were performed using *Global Range Molecular Matching*
72 (GRAMM-X) webserver
73 (<http://vakser.bioinformatics.ku.edu/resources/gramm/grammx/>) [21],[22]. PDB files
74 of the corresponding crystal structures (PDB ID: 1C52, 1XME, 3S8F and 2YEV)
75 [23],[24],[25],[6] were prepared with the DockPrep module of UCSF Chimera 1.7
76 alpha version [26]. Solvent molecules, all heteroatoms and all but the highest
77 occupancy alternate conformations were deleted. Hydrogen atoms were added by
78 considering steric and hydrogen bonds while charges were added using AMBER
79 ff12SB algorithm for standard residues. For *caa*₃-oxidase, chains D-F were removed
80 as they form a crystallographic dimer. Docking models were built by running blind
81 simulations with default parameters; 10, 20 and 30 models were set as the outputs
82 for *c*₅₅₂/*caa*₃-oxidase, *c*₅₅₂/*ba*₃-oxidase (PDB ID: 3S8F) and *c*₅₅₂/*ba*₃-oxidase (PDB
83 ID: 1XME), respectively. For the network model analyses, the anisotropic network
84 model webserver (<http://ignmtest.ccbb.pitt.edu/cgi-bin/anm/anm1.cgi>) was used [27],
85 with a 15-Å cutoff for interaction between C α atoms. Input files were prepared similar
86 to that used in docking simulations. Figures for presentation were prepared with
87 UCSF Chimera.

88

89

90

3. RESULTS AND DISCUSSION

91

92 **3.1 Cytochrome $c_{549/554}$**

93 The *T. thermophilus* *bc* complex consists of four individual subunits, the
94 cytochrome $c_{549/554}$, cytochrome b_{562} , Rieske iron-sulfur protein and cryptic FbcX
95 subunit [3],[28] (Table S1). During *bc* complex purification, cytochromes b_{562} and
96 $c_{549/554}$ readily dissociate. This could result from the relatively high ionic strength
97 conditions (100 mM Tris-HCl pH 7.6 and 100 mM NaCl) and/or membrane
98 solubilization with 5 % Triton X-100 detergent, both not affecting the stability of the
99 two CcO or Complex II [2]. Perhaps the inter-subunit interactions in *bc* complex are
100 more labile so that, similarly to *P. denitrificans* CcO [29], Triton X-100 induces the
101 subunit dissociation. Following to the purification protocol detailed elsewhere [17],
102 Edman degradation coupled with MALDI- and ESI-mass spectrometry showed that,
103 of the 243 predicted residues, the purified subunit $c_{549/554}$ contained only the last 102
104 residues (residues 142-243) corresponding to the soluble C-terminal domain of the
105 subunit (c_{bc}). The N-terminal region is presumably cleaved *in vivo* to form this mature
106 protein.

107

108

109 **3.2 Electrons are transferred from Complexes III to IV via cytochrome c_{552}**

110 Two electron transfer reactions were studied by stopped-flow spectroscopy: (i)
111 from reduced c_{bc} to whole CcO complexes in the absence or presence of c_{552} , and
112 (ii) from reduced c_{bc} to oxidized c_{552} . Fig. 1 illustrates that under aerobic conditions
113 c_{bc} is very slowly (several tens of seconds) oxidized by either of the two CcO, unless
114 c_{552} is present acting as an electron shuttle. This argues against the hypothesis by
115 Janzon *et al.* [9] that electrons are directly transferred from bc complex to caa_3 -
116 oxidase.

117 Further experiments were performed to investigate the reaction between reduced
118 c_{bc} and oxidized c_{552} . Due to the remarkable similarity between the reduced-*minus*-
119 oxidized spectra of the two proteins, these experiments were technically more
120 challenging and required multi-wavelength data acquisition, combined with noise-
121 filtering and global analysis by singular value decomposition [18]. As shown in Fig.
122 S1, the reaction is fast, proceeding at high rate ($\sim 65 \text{ s}^{-1}$) even under non-optimal
123 conditions, i.e., low temperature (5 °C) and high ionic strength ($\sim 300 \text{ mM}$); under
124 these conditions a second order rate constant in the order of magnitude of $10^7 \text{ M}^{-1} \text{ s}^{-1}$
125 was estimated, consistent with [3]. As expected, when the temperature was
126 increased from 5 °C to 25 °C, keeping ionic strength constant at $\sim 300 \text{ mM}$, the
127 measured rate constant increased by a factor of 4 and, at temperatures higher than
128 25 °C most of the reaction occurred in the dead time of the stopped-flow instrument
129 (not shown). While the reaction of c_{552} with ba_3 -oxidase was previously suggested to
130 be mainly driven by apolar interactions [30],[31],[32], in agreement with [3] the
131 reaction between c_{bc} and c_{552} displayed an ionic strength dependence consistent
132 with the involvement of ~ 1.5 charges (Fig. 2).

133

134 **3.3 *caa*₃-oxidase displays high flexibility**

135 Docking experiments were performed using *c*₅₅₂ as the ligand (PDB ID: 1C52) and
136 each of the two CcO in separate simulations, with the coordinates of LCP- (PDB ID:
137 3S8F) and VD-crystallized (PDB ID: 1XME) *ba*₃-oxidase, as well as those of the
138 LCP- crystallized *caa*₃-oxidase (PDB ID: 2YEV). Notably, both LCP-crystallized
139 protein crystals diffracted much better than VD crystals (2.3 Å vs. 1.8 Å and 3.8 Å vs.
140 2.4 Å for *ba*₃- and *caa*₃-oxidases, respectively). The simulations for *c*₅₅₂ and *caa*₃-
141 oxidase, as shown in Fig. 3A, indicate a binding site at the interface between
142 subunits I/III and II/c. Of the ten predicted models, only one is actually biologically
143 plausible in that the binding site is mostly on hydrophilic regions.

144 Given that there are multiple crystal structures of *ba*₃-oxidase available, one each
145 of the best available structures obtained by VD or LCP method were selected to
146 minimize possible crystal packing-induced artifacts. Docking of *c*₅₅₂ to either of the
147 two *ba*₃-oxidase structures is illustrated in Fig. 3B and C. While the docking sites for
148 both structures were the same, only one plausible solution was obtained with the VD
149 crystal structure compared to three with the LCP structure. Interestingly, no model
150 predicted *c*₅₅₂ binding to *ba*₃-oxidase to the same side as in *caa*₃-oxidase.

151 Calculating the edge-to-edge distances between *c*₅₅₂ heme and Cu_A in either of *ba*₃-
152 oxidase docking models (VD and LCP structures), a distance of ~ 32 Å was obtained
153 (not shown). More remarkably, the distance from *c*₅₅₂ heme to heme *c* and to Cu_A in
154 *caa*₃-oxidase is 16.3 and 16.8 Å, respectively. Two conclusions can be drawn,
155 assuming that the docking simulations represent at least near physiological
156 interactions – (i) the electron transfer between *c*₅₅₂ and *ba*₃-oxidase is mediated by
157 protein residues (through-bond transfer), keeping the limit to 14 Å [33], and (ii)
158 electrons from *c*₅₅₂ could theoretically bypass *c*_{caa3}.

159 It is being increasingly realized that crystal structures do not necessarily represent
160 the physiological conformations, as demonstrated by the differences between
161 crystallography- and NMR-derived structures [34],[35]. Furthermore, crystal
162 structures lack dynamics data except with the assistance of time-resolved
163 crystallography. As such, computational techniques at atomic level such as
164 molecular dynamics simulation and normal mode analysis can be used to model
165 potential structural changes. However, both are computationally very expensive and
166 are not practicable for longer simulations especially exceeding the microsecond
167 scale. Elastic network model, in conjunction with normal mode analysis, represents a
168 more suitable alternative with both the isotropic Gaussian network model and
169 anisotropic network model (ANM) being available as methods for proteins (see [36]
170 and references therein).

171 In this study, we investigated the dynamics of all three proteins using ANM. Fig. 4
172 and the Movies SF8-11 show a rather limited dynamics of the electron carrier c_{552}
173 (Fig. 4A) and ba_3 -oxidase (Fig. 4C and 4D), but larger movements in the cytochrome
174 c -cupredoxin domain of caa_3 -oxidase. It is tempting to speculate that this remarkable
175 flexibility may be of mechanistic relevance, by contributing to 'hold' c_{552} in place once
176 bound to caa_3 -oxidase and/or promote its release upon changes in the redox state of
177 the oxidase metal centers.

178

179

180

4. CONCLUSION

181 Using whole ba_3 - and caa_3 -complexes, it is shown that electrons are transferred
182 from bc complex to either of the two oxidases at high rates only via cytochrome c_{552} ,
183 contrary to previous proposals [9]. In agreement with Mooser *et al.* [3], reaction of bc
184 complex with c_{552} is confirmed to be fast ($> 10^7 \text{ M}^{-1} \text{ s}^{-1}$ at 5°C) and characterized by
185 a significant ionic strength dependence. Moreover, *in silico* docking simulations
186 revealed differential binding modes of c_{552} to the oxidase complexes, with an
187 unprecedented large-scale movement observed only for caa_3 -oxidase that may be of
188 mechanistic relevance.

189 That no electron transfer occurs directly between the bc complex and the two
190 terminal oxidases calls for a fundamental rethinking of the putative role of the
191 additional cytochrome c domain in caa_3 -oxidase, as well as of the critical function
192 presumably played by c_{552} in the bioenergetics of *T. thermophilus*. Moreover, if
193 respiratory supercomplexes form in *T. thermophilus* and are required for cellular
194 function, it would be interesting to assay whether cytochrome c_{552} takes part in their
195 formation. Finally, in light of the critical role of c_{552} unveiled in the present study, it
196 would be of relevance to evaluate the effects on the bioenergetics of *T. thermophilus*
197 resulting from deletion of the c_{552} gene or modulation of c_{552} expression by RNA
198 interference.

199

200

ACKNOWLEDGMENTS

201 MRN is a recipient of the Irish Research Council EMBARK Scholarship while TS
202 was funded by the Science Foundation Ireland (BICF685). Work partially supported
203 by MIUR of Italy (FIRB RBF08F41U_001 to AG and FIRB RBIN06E9Z8 to PS).

204

205

REFERENCES

206 [1] Cava, F., Zafra, O., Da Costa, M.S. and Berenguer, J. (2008). The role of the
207 nitrate respiration element of *Thermus thermophilus* in the control and activity
208 of the denitrification apparatus. *Environ. Microbiol.* 10, 522–533.

209 [2] Kolaj-Robin, O., O’Kane, S.R., Nitschke, W., Léger, C., Baymann, F. and
210 Soulimane, T. (2011). Biochemical and biophysical characterization of
211 succinate: quinone reductase from *Thermus thermophilus*. *Biochim. Biophys.*
212 *Acta - Bioenergetics* 1807, 68–79.

213 [3] Mooser, D., Maneg, O., Corvey, C., Steiner, T., Malatesta, F., Karas, M.,
214 Soulimane, T. and Ludwig, B. (2005). A four-subunit cytochrome *bc*₁ complex
215 complements the respiratory chain of *Thermus thermophilus*. *Biochim.*
216 *Biophys. Acta - Bioenergetics* 1708, 262–274.

217 [4] Noor, M.R. and Soulimane, T. (2012). Bioenergetics at extreme temperature:
218 *Thermus thermophilus* *ba*₃- and *caa*₃-type cytochrome *c* oxidases. *Biochim.*
219 *Biophys. Acta - Bioenergetics* 1817, 638–649.

220 [5] Soulimane, T., Buse, G., Bourenkov, G.P., Bartunik, H.D., Huber, R. and Than,
221 M.E. (2000). Structure and mechanism of the aberrant *ba*₃-cytochrome *c*
222 oxidase from *Thermus thermophilus*. *EMBO J.* 19, 1766–1776.

223 [6] Lyons, J.A., Aragão, D., Slattery, O., Soulimane, T. and Caffrey, M. (2012).
224 Structural insights into electron transfer in *caa*₃-type cytochrome oxidase.
225 *Nature* 487, 514–518.

226 [7] Fee, J.A., Choc, M.G., Findling, K.L., Lorence, R. and Yoshida, T. (1980).
227 Properties of a copper-containing cytochrome *c*₁*aa*₃ complex: a terminal

228 oxidase of the extreme thermophile *Thermus thermophilus* HB8. Proc. Natl.
229 Acad. Sci. USA 77, 147–151.

230 [8] Hon-nami, K. and Oshima, T. (1980). Cytochrome oxidase from an extreme
231 thermophile, HB 8. Biochem. Biophys. Res. Commun. 92, 1023–1029.

232 [9] Janzon, J., Ludwig, B. and Malatesta, F. (2007). Electron transfer kinetics of
233 soluble fragments indicate a direct interaction between complex III and the
234 *caa*₃ oxidase in *Thermus thermophilus*. IUBMB Life 59, 563–569.

235 [10] Zimmermann, B.H., Nitsche, C.I., Fee, J.A., Rusnak, F. and Münck, E. (1988).
236 Properties of a copper-containing cytochrome *ba*₃: a second terminal oxidase
237 from the extreme thermophile *Thermus thermophilus*. Proc. Natl. Acad. Sci.
238 USA 85, 5779–5783.

239 [11] Keightley, J.A., Zimmermann, B.H., Mather, M.W., Springer, P., Pastuszyn, A.,
240 Lawrence, D.M. and Fee, J.A. (1995). Molecular genetic and protein chemical
241 characterization of the cytochrome *ba* from *Thermus thermophilus* HB8. J.
242 Biol. Chem. 270, 20345–20358.

243 [12] Soulimane, T., Walter, M. von, Hof, P., Than, M.E., Huber, R. and Buse, G.
244 (1997). Cytochrome-*c*₅₅₂ from *Thermus thermophilus*: A functional and
245 crystallographic investigation. Biochem. Biophys. Res. Commun. 237, 572–
246 576.

247 [13] Yoshida, T. and Fee, J.A. (1984). Studies on cytochrome *c* oxidase activity of
248 the cytochrome *c*₁*aa*₃ complex from *Thermus thermophilus*. J. Biol. Chem.
249 259, 1031–1036.

250 [14] Fee, J.A., Yoshida, T., Surerus, K.K. and Mather, M.W. (1993). Cytochrome
251 *caa*₃ from the thermophilic bacterium *Thermus thermophilus*: a member of the
252 heme-copper oxidase superfamily. J. Bioenerg. Biomembr. 25, 103–114.

- 253 [15] Kannt, A., Soulimane, T., Buse, G., Becker, A., Bamberg, E. and Michel, H.
254 (1998). Electrical current generation and proton pumping catalyzed by the
255 *ba*₃-type cytochrome *c* oxidase from *Thermus thermophilus*. FEBS Lett.
256 434, 17–22.
- 257 [16] Soulimane, T., Buse, G., Dewor, M., Than, M.E. and Huber, R. (2000). Primary
258 structure of a novel subunit in *ba*₃-cytochrome oxidase from *Thermus*
259 *thermophilus*. Protein Sci. 9, 2068–2073.
- 260 [17] Schell, A. (2000) Proteinchemische charakterisierung und kristallisation der
261 *caa*₃-cytochrom-*c*-oxidase aus *Thermus thermophilus*. Rheinisch-
262 Westfälische Technische Hochschule Aachen, Aachen, Germany.
- 263 [18] Henry, E.R. and Hofrichter, J. (1992) Singular value decomposition: application
264 to analysis of experimental data. Methods Enzymol. 210, 129-192.
- 265 [19] Malatesta, F. (2005). The study of bimolecular reactions under non-pseudo-first
266 order conditions. Biophys. Chem. 116, 251–256.
- 267 [20] Brønsted, J.N. and Mer, V.K.L. (1924). The activity coefficients of ions in very
268 dilute solutions. J. Am. Chem. Soc. 46, 555–573.
- 269 [21] Tovchigrechko, A. and Vakser, I.A. (2005). Development and testing of an
270 automated approach to protein docking. Proteins 60, 296–301.
- 271 [22] Tovchigrechko, A. and Vakser, I.A. (2006). GRAMM-X public web server for
272 protein-protein docking. Nucl. Acids Res. 34, W310–W314.
- 273 [23] Than, M.E., Hof, P., Huber, R., Bourenkov, G.P., Bartunik, H.D., Buse, G. and
274 Soulimane, T. (1997). *Thermus thermophilus* cytochrome-*c*₅₅₂: a new highly
275 thermostable cytochrome-*c* structure obtained by MAD phasing. J. Mol. Biol.
276 271, 629–644.

- 277 [24] Hunsicker-Wang, L.M., Pacoma, R.L., Chen, Y., Fee, J.A. and Stout, C.D.
278 (2005). A novel cryoprotection scheme for enhancing the diffraction of crystals
279 of recombinant cytochrome *ba*₃ oxidase from *Thermus thermophilus*. *Acta*
280 *Crystallogr. D* 61, 340–343.
- 281 [25] Tiefenbrunn, T., Liu, W., Chen, Y., Katritch, V., Stout, C.D., Fee, J.A. and
282 Cherezov, V. (2011). High resolution structure of the *ba*₃ cytochrome *c*
283 oxidase from *Thermus thermophilus* in a lipidic environment. *PLoS ONE*
284 6, e22348.
- 285 [26] Pettersen, E.F., Goddard, T.D., Huang, C.C., Couch, G.S., Greenblatt, D.M.,
286 Meng, E.C. and Ferrin, T.E. (2004). UCSF Chimera--a visualization system for
287 exploratory research and analysis. *J. Comput. Chem.* 25, 1605–1612.
- 288 [27] Eyal, E., Yang, L.-W. and Bahar, I. (2006). Anisotropic network model:
289 systematic evaluation and a new web interface. *Bioinformatics* 22, 2619–
290 2627.
- 291 [28] Mooser, D., Maneg, O., MacMillan, F., Malatesta, F., Soulimane, T. and Ludwig,
292 B. (2006). The menaquinol-oxidizing cytochrome *bc* complex from *Thermus*
293 *thermophilus*: Protein domains and subunits. *Biochim. Biophys. Acta -*
294 *Bioenergetics* 1757, 1084–1095.
- 295 [29] Nicoletti, F., Witt, H., Ludwig, B., Brunori, M. and Malatesta, F. (1998).
296 *Paracoccus denitrificans* cytochrome *c* oxidase: a kinetic study on the two-
297 and four-subunit complexes. *Biochim. Biophys. Acta - Bioenergetics*
298 1365, 393–403.
- 299 [30] Maneg, O., Ludwig, B. and Malatesta, F. (2003). Different interaction modes of
300 two cytochrome-*c* oxidase soluble Cu_A fragments with their substrates. *J. Biol.*
301 *Chem.* 278, 46734–46740.

- 302 [31] Maneg, O., Malatesta, F., Ludwig, B. and Drosou, V. (2004). Interaction of
303 cytochrome *c* with cytochrome oxidase: two different docking scenarios.
304 Biochim. Biophys. Acta - Bioenergetics 1655, 274–281.
- 305 [32] Muresanu, L., Pristovsek, P., Löhr, F., Maneg, O., Mukrasch, M.D., Rüterjans,
306 H., Ludwig, B. and Lücke, C. (2006). The electron transfer complex between
307 cytochrome *c*₅₅₂ and the Cu_A domain of the *Thermus thermophilus* *ba*₃
308 oxidase. J. Biol. Chem. 281, 14503–14513.
- 309 [33] Page, C.C., Moser, C.C. and Dutton, P.L. (2003). Mechanism for electron
310 transfer within and between proteins. Curr. Opin. Chem. Biol. 7, 551–556.
- 311 [34] Andrec, M., Snyder, D.A., Zhou, Z., Young, J., Montelione, G.T. and Levy, R.M.
312 (2007). A large data set comparison of protein structures determined by
313 crystallography and NMR: Statistical test for structural differences and the
314 effect of crystal packing. Proteins 69, 449–465.
- 315 [35] Sikic, K., Tomic, S. and Carugo, O. (2010). Systematic comparison of crystal
316 and NMR protein structures deposited in the Protein Data Bank. Open
317 Biochem. J. 4, 83–95.
- 318 [36] Yang, L., Song, G. and Jernigan, R.L. (2009). Protein elastic network models
319 and the ranges of cooperativity. Proc. Natl. Acad. Sci. USA 106, 12347–
320 12352.
- 321
- 322

FIGURE LEGENDS

323

324

325 **Fig. 1. Electron transfer between c_{bc} and CcO.** Aerobic oxidation of 700 nM
326 reduced c_{bc} by 100 nM ba_3 - (A) or caa_3 -oxidase (B) is slow (dashed) unless c_{552} at
327 increasing concentration is added (right to left solid lines), the effect being
328 proportional to c_{552} concentration (inset). The absorbance change was followed at
329 418 nm and 25 °C.

330

331 **Fig. 2. Effect of ionic strength in electron transfer between c_{bc} and c_{552} .** (A)
332 Time courses obtained by global analysis of the data collected after mixing 3.8 μ M
333 reduced c_{bc} with 8 μ M oxidized c_{552} at increasing ionic strength (left to right) at 5 °C.
334 (B) Ionic strength dependence of the observed rate constant.

335

336 **Fig. 3. Docking of cytochrome c_{552} to CcO complexes.** (A) Docking to caa_3 -
337 complex. The subunits I/III, II/c and IV are shown in yellow, blue and red,
338 respectively, while c_{552} is in dark grey. (B) Docking to VD-crystallized ba_3 -oxidase.
339 The subunits I, II and IIa are colored in yellow, blue and red, respectively. This
340 docking is similar in the LCP crystal structure of ba_3 -oxidase (C).

341

342 **Fig. 4. ANM models of cytochrome c_{552} (A), caa_3 -oxidase (B), and VD- and LCP-**
343 **crystallized ba_3 -oxidase (C and D, respectively).** Color code is as in Fig. 3.
344 Compared to the other proteins here, caa_3 -oxidase clearly displays the highest
345 structural dynamics.

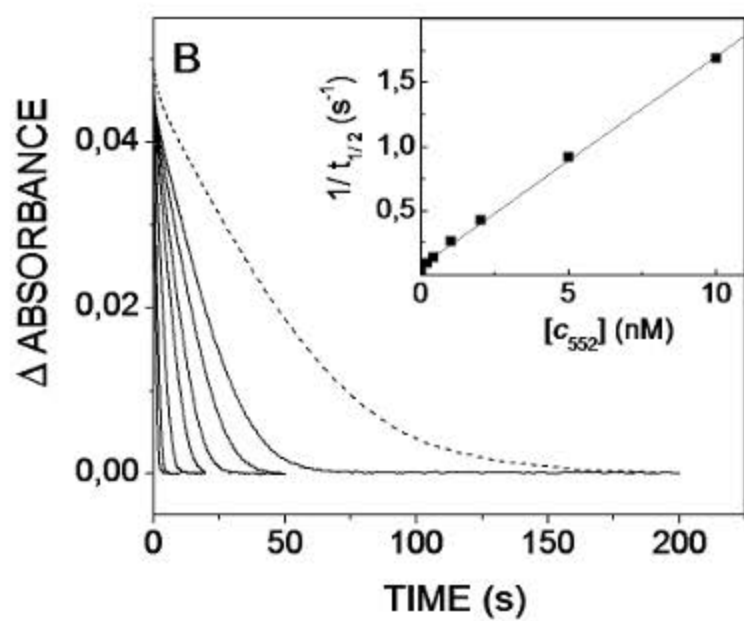
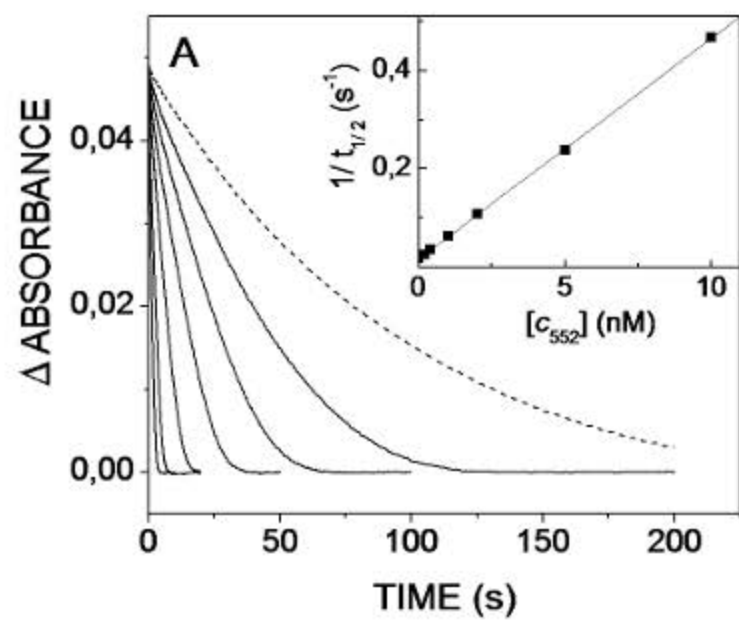


Fig.1

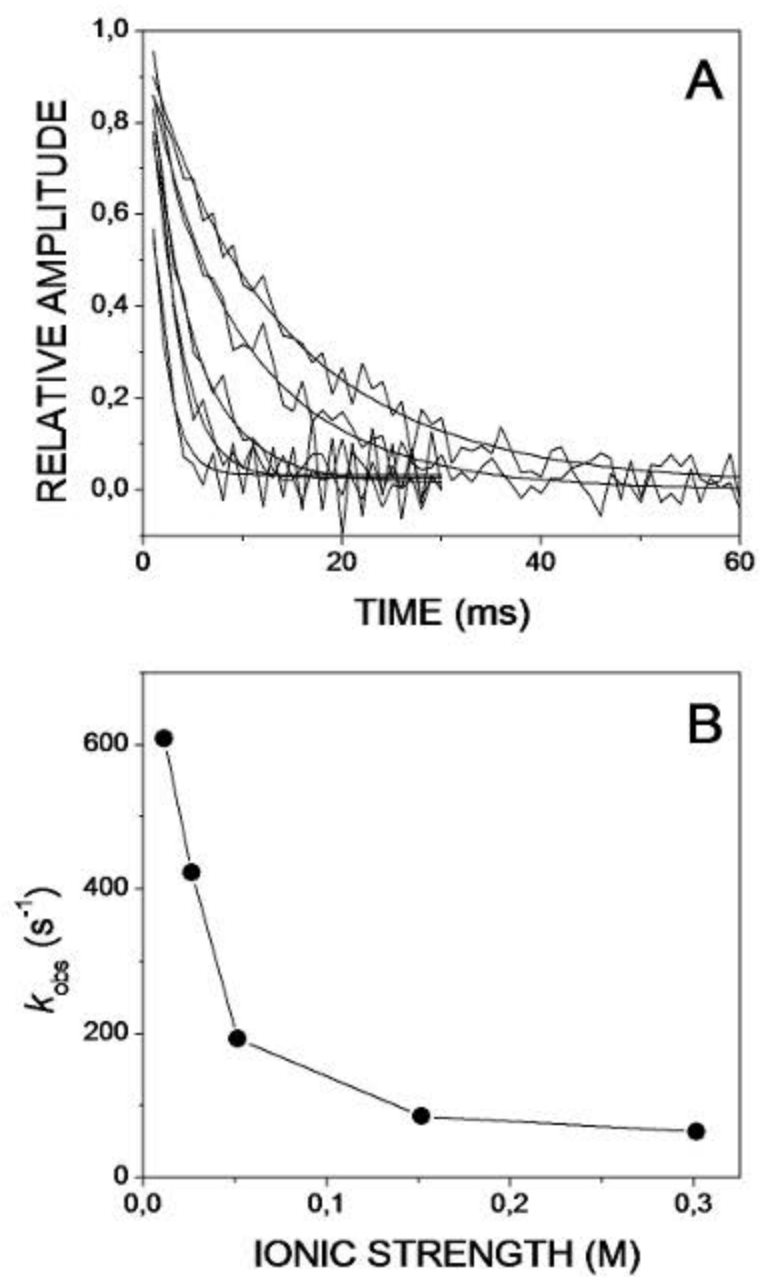
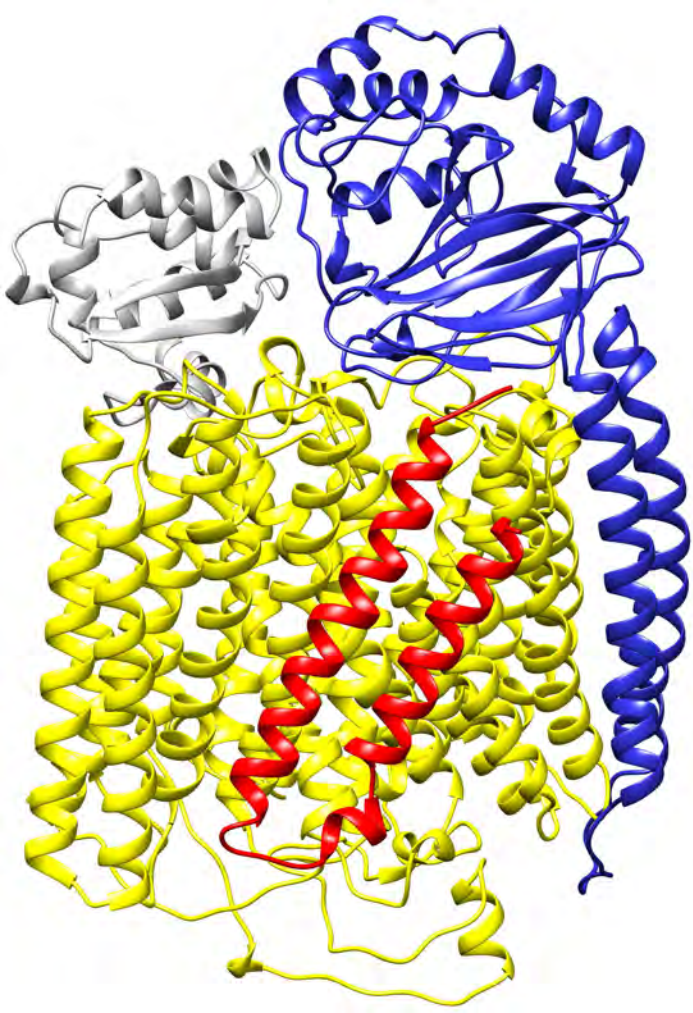
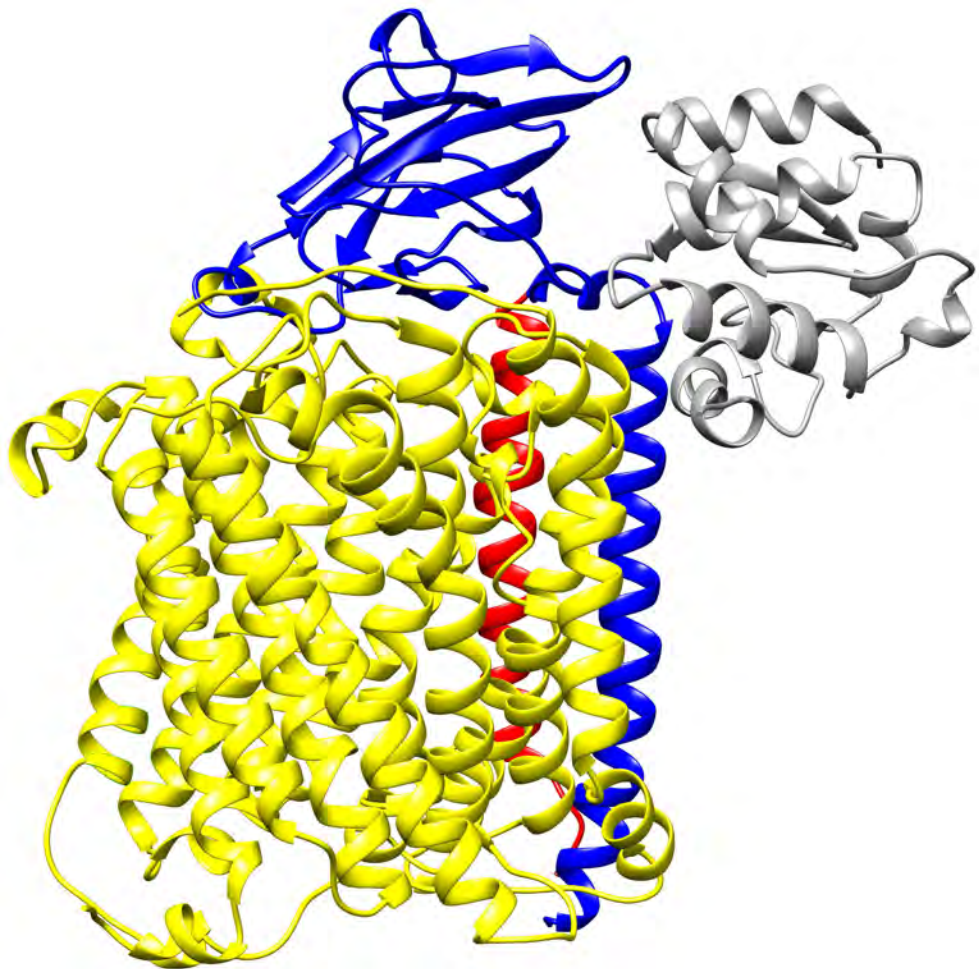
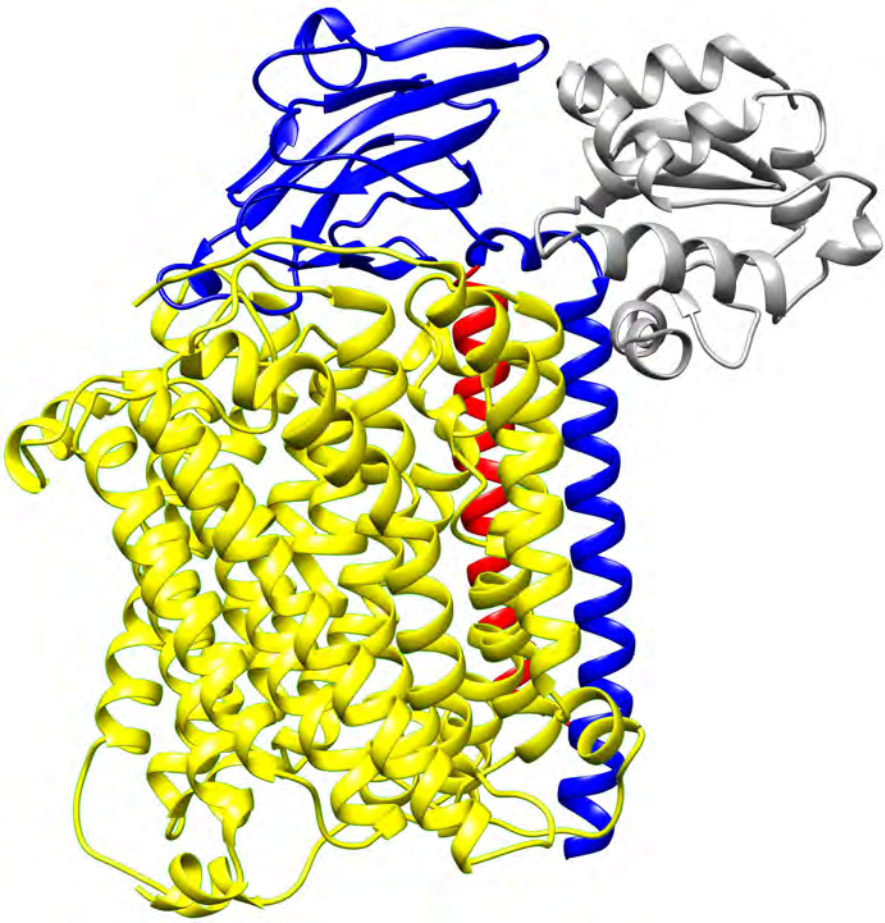
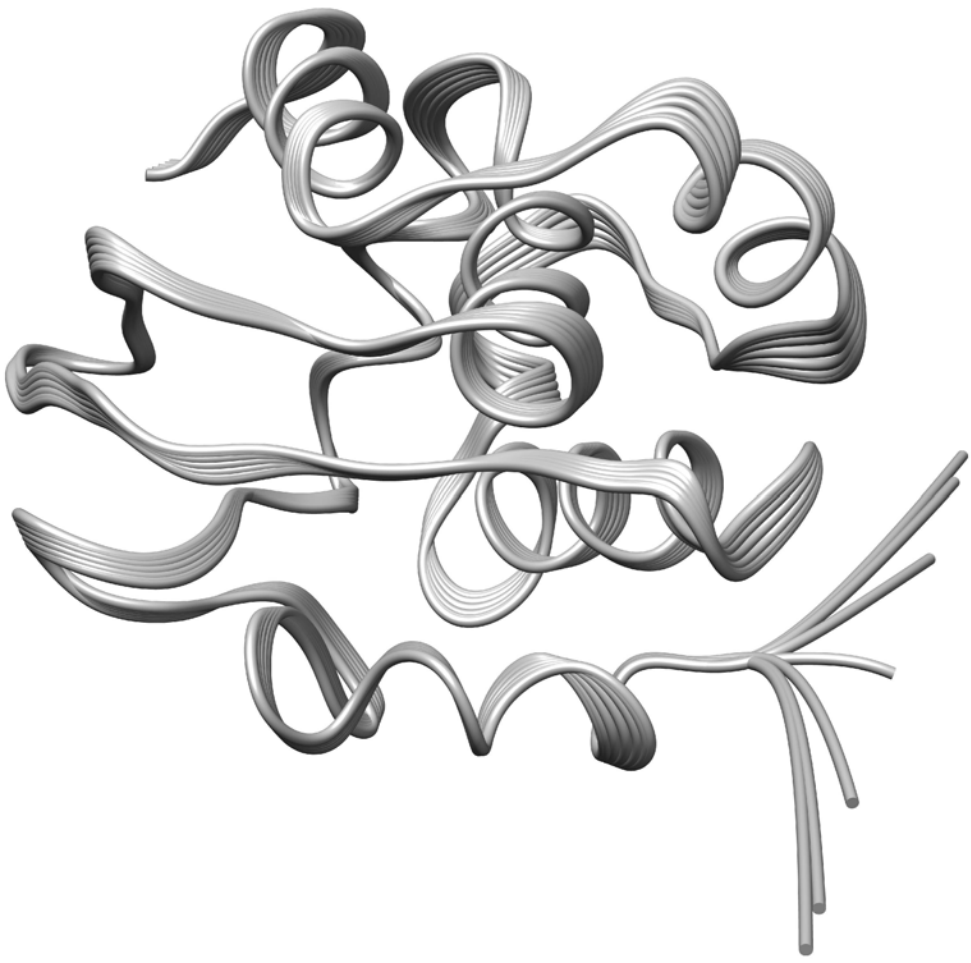


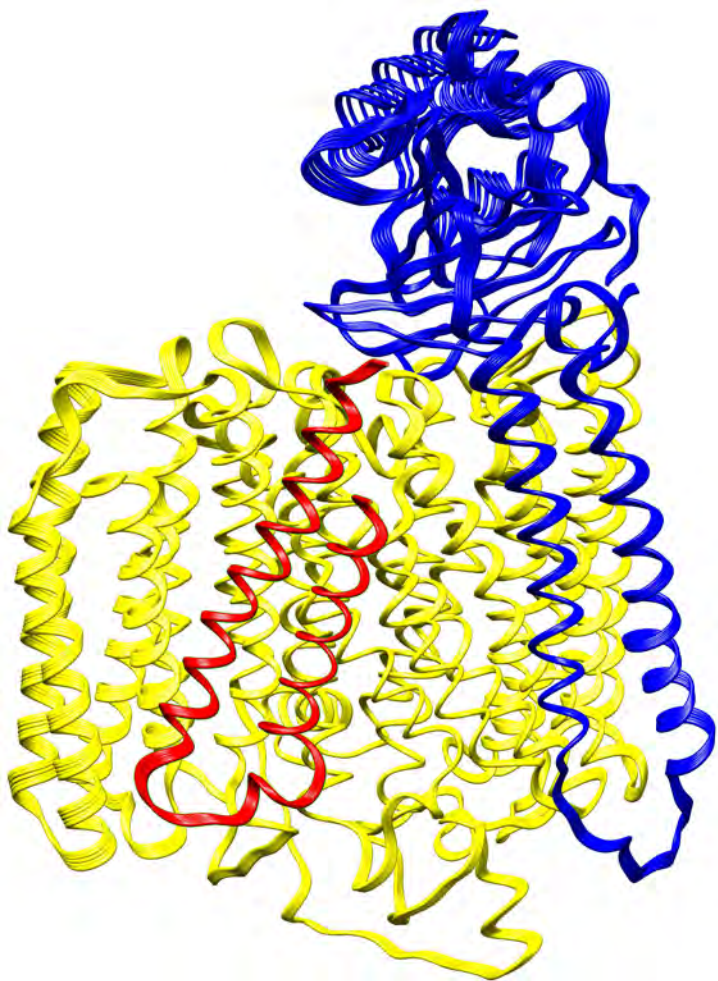
Fig. 2

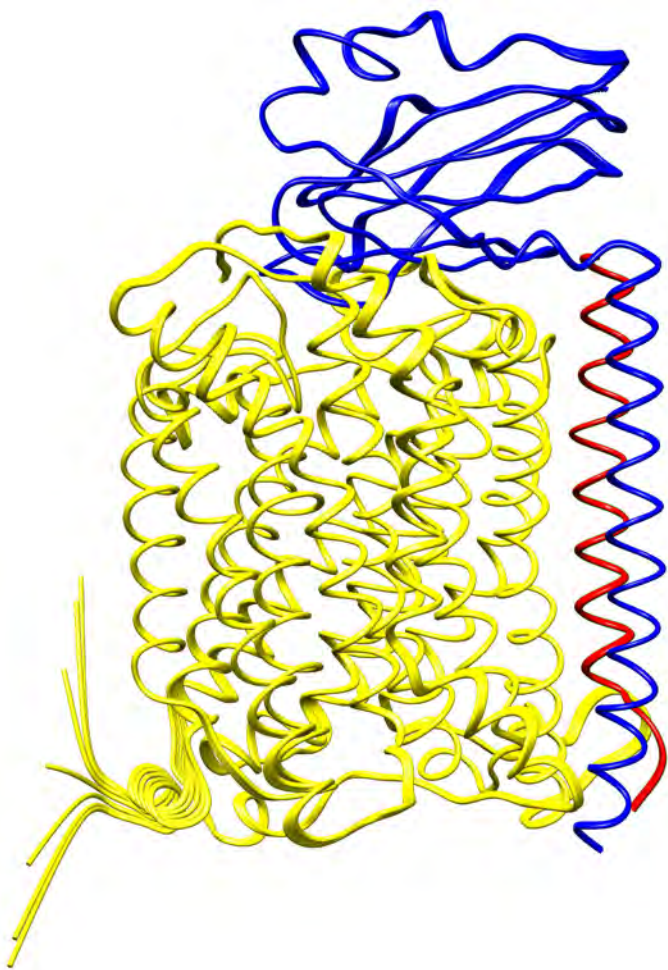


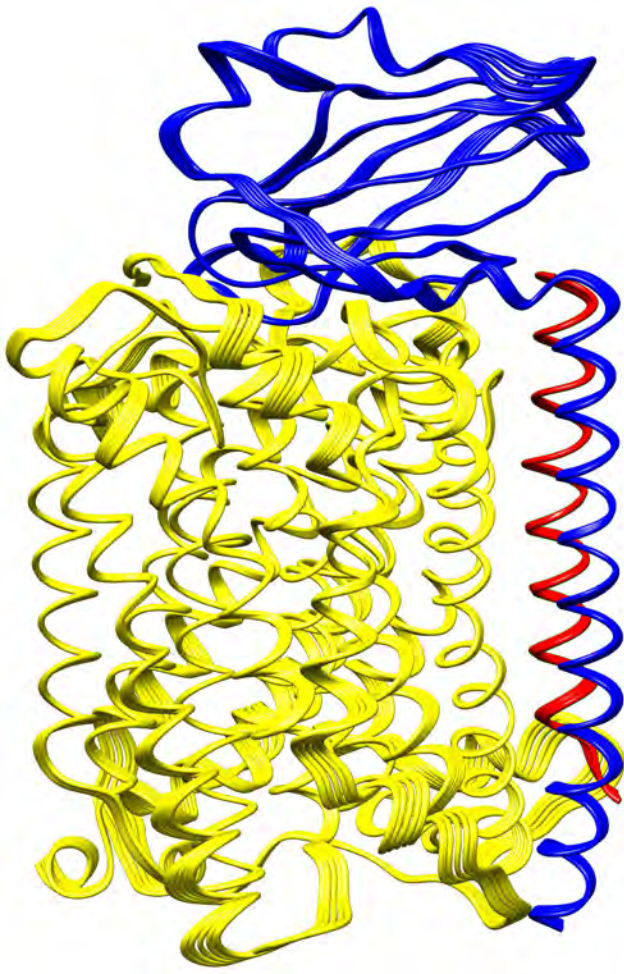












1 **CYTOCHROME C₅₅₂ MEDIATES ELECTRON TRANSFER BETWEEN**
2 **COMPLEXES III AND IV OF *THERMUS THERMOPHILUS***

3

4

SUPPLEMENTARY ONLINE MATERIAL

5

6

7

SUPPLEMENTARY TABLE

8

Table S1. Molecular weight and subunit composition of the isolated

9

cytochromes. The locus tags and UniProt accession ID refer to the *T. thermophilus*

10

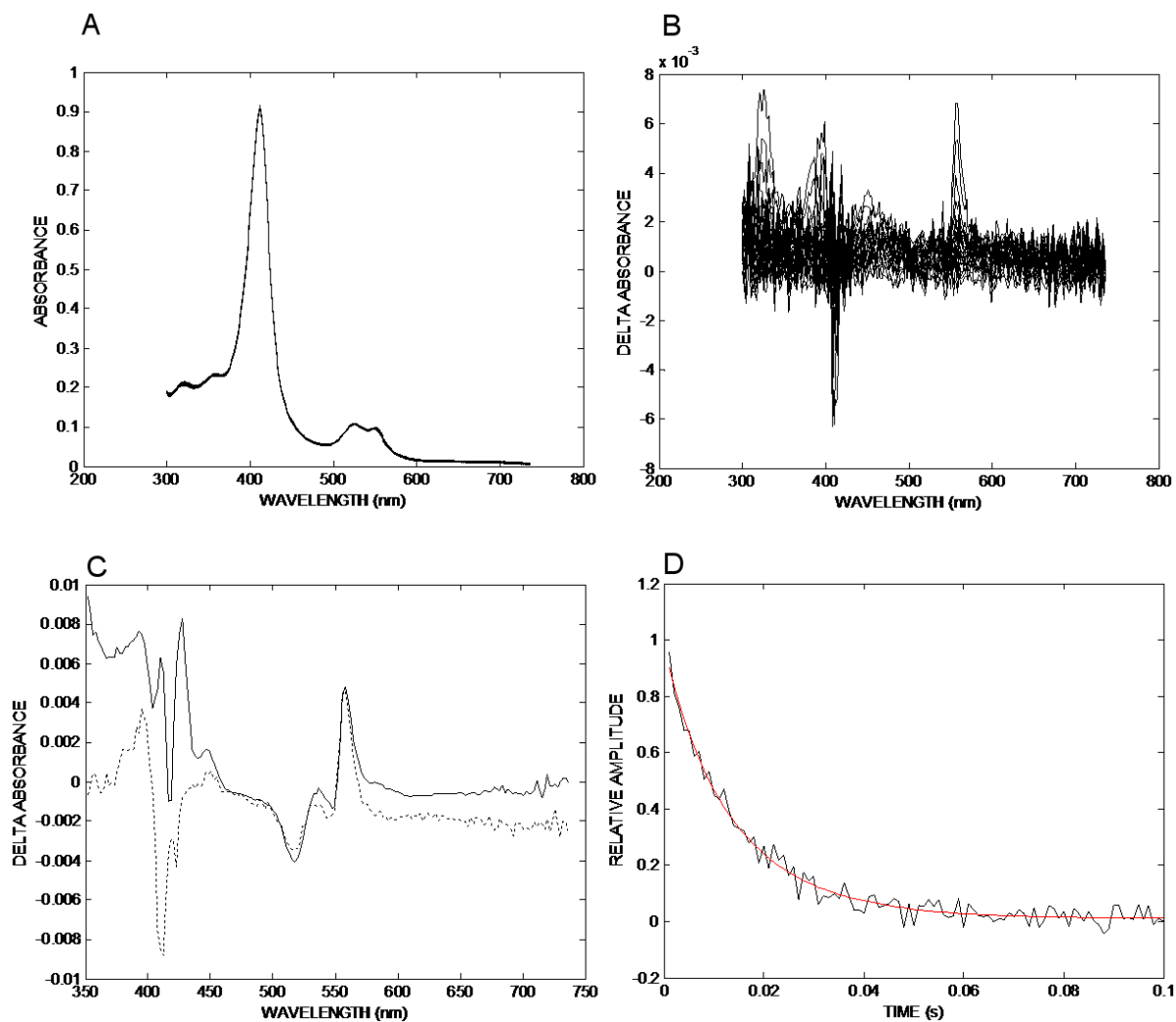
strain HB8. The molecular weights are theoretically predicted from sequences.

Protein	Subunit	Locus tag	UniProt	Molecular weight (kDa)
Cytochrome <i>c</i>₅₅₂		TTHA1235	Q5SIX9	14.2
<i>ba</i>₃-oxidase	I	TTHA1135	Q5SJ79	62.5
	II	TTHA1134	Q5SJ80	18.6
	Ila	TTHA1133	P82543	3.8
	Total			84.9
<i>caa</i>₃-oxidase	I/III	TTHA0312	P98005	89.2
	II/c	TTHA0311	Q5SLI2	37.3
	IV	TTHA1863	Q5SH67	7.3
	Total			133.8
<i>bc</i> complex	<i>b</i> ₅₆₂	TTHA1930	Q5SH00	46.7
	<i>C</i> _{549/554}	TTHA1933	Q5SGZ7	26.0
	Rieske	TTHA1931	Q5SGZ9	22.6
	FbcX	TTHA1932	Q5SGZ8	17.6
	Total			112.9

11

12
13
14

SUPPLEMENTARY FIGURE



15
16

17 **Fig. S1. Reaction of reduced c_{bc} with oxidized cytochrome c_{552} .** Absolute
18 spectra (A) and corresponding absorption changes (B) acquired over the first 100
19 ms after anaerobically mixing reduced c_{bc} ($\sim 3.8 \mu\text{M}$, reduced with $100 \mu\text{M}$
20 ascorbate) with oxidized c_{552} ($\sim 8 \mu\text{M}$) at 5°C and ionic strength $\sim 300 \text{ mM}$. In panel
21 C, the kinetic optical species (dotted), obtained by SVD analysis of the spectral
22 changes in B, is shown together with its best fit to a linear combination of the
23 reduced-*minus*-oxidized spectra of both proteins (solid), independently acquired. The

24 good match between the spectra (particularly in the α and β regions) confirms that
25 the measured absorption changes are those expected for the reaction between c_{bc}
26 and c_{552} . As shown in panel **D**, despite the relatively low temperature and the high
27 ionic strength, electrons are transferred efficiently at $\sim 65 \text{ s}^{-1}$.
28

29

30

SUPPLEMENTARY FILES

31 SF1. PDB file of cytochrome *c*₅₅₂ docked to *caa*₃-oxidase.

32 SF2. PDB file of cytochrome *c*₅₅₂ docked to *ba*₃-oxidase (VD crystal structure).

33 SF3. PDB file of cytochrome *c*₅₅₂ docked to *ba*₃-oxidase (LCP crystal structure).

34 SF4. PDB file containing ANM of cytochrome *c*₅₅₂.

35 SF5. PDB file containing ANM of *caa*₃-oxidase.

36 SF6. PDB file containing ANM of *ba*₃-oxidase (VD crystal structure).

37 SF7. PDB file containing ANM of *ba*₃-oxidase (LCP crystal structure).

38 SF8. Movie file showing structural dynamics of cytochrome *c*₅₅₂.

39 SF9. Movie file showing structural dynamics of *caa*₃-oxidase.

40 SF10. Movie file showing structural dynamics of *ba*₃-oxidase (VD crystal structure).

41 SF11. Movie file showing structural dynamics of *ba*₃-oxidase (LCP crystal structure).

42

43 Notes for movie files: All movies are encoded in the open Theora format and can be

44 viewed with the open source Media Player Classic – Home Cinema (<http://mpc->

45 hc.sourceforge.net/).

Due to copyright restrictions the full text of the following article is not included in the electronic version of this Ph.D.

The Journal of Physical Chemistry B

2012, 116, 8955–8960

Observation of Ligand Transfer in ba3 Oxidase from *Thermus thermophilus*: Simultaneous FTIR Detection of Photolabile Heme a₃²⁺-CN and Transient CuB₂⁺-CN Complexes

Andreas Loullis, Mohamed Radzi Noor, Tewfik Soulimane, and Eftychia Pinakoulaki,

<http://dx.doi.org/10.1021/jp305096y>